

# **Synthesis of Prenyl Transferase Inhibitors and Histone Deacetylase Inhibitors**

by

ALPHONSO S. RIOJA



**UNIVERSITY COLLEGE LONDON**

A thesis presented to the University of London for the degree of  
Doctor of Philosophy

UCL Chemistry Department  
Christopher Ingold Laboratories  
20 Gordon Street  
London WC1H 0AJ

April 2002



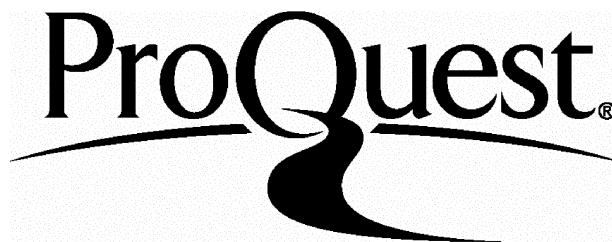
ProQuest Number: U643953

All rights reserved

INFORMATION TO ALL USERS

The quality of this reproduction is dependent upon the quality of the copy submitted.

In the unlikely event that the author did not send a complete manuscript and there are missing pages, these will be noted. Also, if material had to be removed, a note will indicate the deletion.



ProQuest U643953

Published by ProQuest LLC(2016). Copyright of the Dissertation is held by the Author.

All rights reserved.

This work is protected against unauthorized copying under Title 17, United States Code.  
Microform Edition © ProQuest LLC.

ProQuest LLC  
789 East Eisenhower Parkway  
P.O. Box 1346  
Ann Arbor, MI 48106-1346

*For my mother and father and the chance that they never had*

## Acknowledgements

I would like to thank Dr. Charles M. Marson for all his helpful support, encouragement, advice and friendship throughout the course of the PhD. A huge debt of gratitude must go to Dr. N. Shaun Thomas and Arnold Pizzey for all their support, advice and friendship over the last few years. Special thanks are owed to Dr. David M. Vigushin, Dr. Greg Brooke and Prof. R. C. Coombes for the use of their time, expertise and instrumentation. I also would like to thank Mr. Robert Mandeville for making this work possible through his trust fund.

I am indebted to Dr. C. Marson and Dr. N. S. Thomas for proof reading the final draft of this manuscript.

To all members of the Marson group, former and current, I would like to express my appreciation, especially Alex Cobb for his constant companionship. Many thanks to all the members of the chemistry staff at both University College London and Queen Mary and Westfield College London for all their kind help and expertise.

Finally, I would like to thank my parents (Sergio and Nili), my friends, (especially Darryn and Stephen) and Paula (my ursa) for their constant support, help and ever readiness to make my life more enjoyable.



## Abstract

Simple monoterpenes and terpenoids such as limonene and perillyl alcohol have been reported to confer significant chemopreventive activity in rat and human carcinomas. A clinical study at Charing Cross Hospital highlighted a possible correlation between the isoprenoids ability to prevent protein-prenylation of small G-proteins (Ras) by inhibiting prenyl-protein transferase (enzyme) and their anti-cancer activity. An investigation into the family of terpenes and terpenoids (isoprenoids) with their correlation to chemoprevention was conducted.

Since the inhibition of prenyl-protein transferase enzyme was believed to be integral to the anti-cancer activity of isoprenoids, a thorough examination of enzyme activity and different types of enzyme inhibition was performed.

An in-depth analysis of farnesyl-protein transferase and geranylgeranyl (type I and II)-protein transferase was carried out, as these are the enzymes inhibited by terpenes and terpenoids, believed to result in their anti-cancer activity. A look at the known inhibitors of these enzymes in literature is assessed, and the production of a model designed to produce synthetic 'terpenoid' compounds capable of significant prenyl-protein transferase inhibition was created. From the model, a range of compounds encompassing short-chain monocyclic, long-chain mono- and bicyclic, and medium- to long-chain structures with a strongly polar terminus was produced, and evaluated with an *in vitro* enzyme inhibition assay to determine the potency of the compounds.

Farnesol has been reported to cause apoptosis of cancerous cell lines, an investigation was performed with farnesol and two more compounds, (structurally similar to farnesol) to see whether these compounds could induce preferential apoptosis of various leukaemic cells.

Histone deacetylation (HDAC) inhibition as a potential cancer therapy has been a recent discovery. Validation of a non-isotopic HDAC assay (HPLC) to determine HDAC inhibition for different compounds was conducted. The production of possible HDAC inhibitors based on the structure of trichostatin A was performed and the potency evaluated with an *in vitro* isotopic HDAC assay and a cancerous cell line proliferation assay.

## Contents

Acknowledgements	iii
Abstract	iv
Contents	v
List of figures	x
List of schemes	xiv
List of tables	xvi
Glossary	xiii

<b>The Role of Terpenes and Terpenoids in Chemoprevention</b>	<b>1</b>
1.0 Introduction	1
1.1 Chemoprevention	1
1.2 Carcinogenesis	1
1.3 Limonene and perillyl alcohol cancer therapy	2
1.4 The family of terpenes and terpenoids (isoprenoids)	3
1.5 Biosynthesis of 3-methyl-3-butenyl pyrophosphate	5
1.6 Monoterpenes and terpenoids (C <sub>10</sub> structures)	6
1.7 Sesquiterpenes and terpenoids (C <sub>15</sub> structures)	7
1.8 Diterpenes and terpenoids (C <sub>20</sub> structures)	9
1.9 Sesterterpenes and terpenoids (C <sub>25</sub> structures)	10
1.10 Triterpenes and terpenoids (C <sub>30</sub> structures)	11
1.11 Possible modes of action of terpenes and terpenoids chemopreventive properties	12
1.11.1 Isoprenoid-mediated inhibition of mevalonate synthesis	13
1.11.2 Inhibition of phosphatidylcholine biosynthesis	15
1.11.3 Anti-oxidation role played by isoprenoids	15
1.12 References	18
<b>Enzyme Inhibition</b>	<b>21</b>
2.0 Aims of chapter	21
2.1 Introduction	21

2.2	<b>Classification of enzymes</b>	21
2.3	<b>Protein structure of enzymes</b>	22
2.3.1	Primary structure	22
2.3.2	Secondary structure	22
2.3.3	Tertiary structure	23
2.3.4	Quaternary structure	24
2.4	<b>Cofactors</b>	24
2.5	<b>Catalytic properties of enzymes</b>	25
2.6	<b>Mechanism of enzyme action</b>	26
2.7	<b>Reaction profile of an enzymatic reaction</b>	27
2.8	<b>Factors affecting enzymatic reactions</b>	28
2.8.1	Temperature	28
2.8.2	pH	28
2.9	<b>Definition of enzyme activity</b>	28
2.10	<b>Enzyme kinetics</b>	29
2.11	<b>Treatment of kinetic data from enzyme inhibition</b>	31
2.12	<b>Inhibitors</b>	34
2.12.1	Irreversible inhibition	34
2.12.2	Reversible inhibition	35
2.13	<b>Allosteric enzymes</b>	39
2.13.1	Allosteric regulation	40
2.14	<b>References</b>	43

## **Prenyl-Protein Transferase Inhibitors and a Potential**

<b>Cancer Therapy</b>	44
3.0 <b>Introduction</b>	44
3.1 <b><i>Ras</i> genes and Ras proteins</b>	45
3.2 <b>Ras pathway</b>	46
3.2.1    The importance of prenyl-protein transferases to the Ras pathway	48
3.3 <b>Farnesyl-protein transferase (FPTase)</b>	49
3.4 <b>Geranylgeranyl-protein transferase (GGPTase)</b>	51
3.5 <b>Design of prenyl-protein transferase inhibitors</b>	52

3.5.1	Peptidomimetics	53
3.5.2	Non-peptidomimetics	56
3.5.3	Competitive prenyl pyrophosphate substrate inhibitors	58
3.5.4	Bisubstrate analogues	60
3.5.5	Natural products	61
3.6	<b>Selectivity for tumorous cells</b>	62
3.7	<b>The rationale for designing new synthetic terpenoid inhibitors of prenyl-protein transferase</b>	63
3.8	<b>Determining the potency of new chemopreventive compounds</b>	65
3.8.1	Non-linear regression analysis of enzyme isotope-labelled kinetic data	66
3.8.2	Determination of $IC_{50}$ from sigmoidal dose-response curves	67
3.8.3	The importance of the $IC_{50}$ value	68
3.9	<b>Preparation of potential prenyl-protein transferase inhibitors</b>	71
3.10	Short-chain monocyclic analysis of perillyl alcohol	73
3.10.1	Evaluation of short-chain monocyclic compounds	76
3.11	<b>Long-chain mono- and bicyclic compounds</b>	78
3.11.1	Evaluation of long-chain mono- and bicyclic compounds	82
3.12	<b>Medium- to long-chain compounds with strongly polar terminus</b>	83
3.12.1	Evaluation of medium- to long-chain compounds with a strongly polar terminus	89
3.13	<b>Conclusion</b>	92
3.14	<b>References</b>	93

## **Preferential Induction of Apoptosis by Farnesol and Two Terpenoid-Type analogues on Various Leukaemic Cells**

4.0	<b>Introduction</b>	100
4.1	<b>Action of isoprenoid on tumorous cells</b>	100
4.2	<b>Conducting a leukaemic cell line assay</b>	101
4.3	<b>The apoptotic action of farnesol on leukaemic cells</b>	104
4.4	<b>The apoptotic action of farnesol on primary T-lymphocytes and monocytes</b>	108

4.5	<b>The apoptotic action of farnesol on proliferating T-lymphocytes</b>	110
4.6	<b>The action of farnesol on primary leukaemic cells</b>	111
4.7	<b>The action of diethyl ester 23 and ketone 24 on leukaemic cell lines</b>	112
4.8	<b>The action of diethyl ester 23 and ketone 24 on primary T-lymphocytes</b>	115
4.9	<b>Conclusion</b>	116
4.10	<b>References</b>	118
<b>Appendix I</b>		119
1.0	<b>The cell cycle</b>	119
1.1	<b>Cell cycle analysis by flow cytometry</b>	121
<b>Histone Deacetylase Inhibitors and a Potential Cancer Therapy</b>		123
5.0	<b>Introduction</b>	123
5.1	<b>Importance of histone acetylation and deacetylation</b>	123
5.2	<b>Histones</b>	124
5.3	<b>Acetylation of histones</b>	124
5.4	<b>Histone deacetylases</b>	125
5.4.1	Class I histone deacetylases	126
5.4.2	Class II histone deacetylases	126
5.4.3	Class III histone deacetylases	127
5.5	<b>Histone deacetylases and cancer</b>	128
5.5.1	Interference of Mad/Sin3/HDAC	128
5.5.2	HDACs interaction with leukaemia	129
5.5.3	HDAC containing complexes and transcriptional restraint of tumour-suppressing genes	130
5.6	<b>Histone deacetylase inhibitors</b>	131
5.7	<b><i>In vitro</i> activity of histone deacetylase inhibitors</b>	136
5.8	<b><i>In vivo</i> activity of histone deacetylase inhibitors</b>	137
5.9	<b>Histone deacetylase inhibitors prepared for a non-isotopic enzyme activity (HPLC assay)</b>	138

5.10	<b>HDAC inhibitors produced with structural features of trichostatin A (TSA)</b>	140
5.11	<b>HPLC assay for determining HDAC inhibition</b>	144
5.11.1	Data analysis of non-isotopic enzyme activity HDAC assay	144
5.12	<b>Evaluation of HPLC assay for determining potential inhibitors of HDAC</b>	145
5.13	<b><i>In vitro</i> [<sup>3</sup>H]-labelled HDAC assay</b>	147
5.13.1	Determination of IC <sub>50</sub> values	147
5.14	<b>Evaluation of HDAC inhibitors 36 and 45 in an <i>in vitro</i> HDAC assay</b>	150
5.15	<b>Breast cancer cell line proliferation assay of HDAC inhibitors</b>	151
5.16	<b>Evaluation of the cytotoxic effects of HDAC inhibitor 36 and TSA on various breast cancer cell lines</b>	152
5.17	<b>Conclusion</b>	153
5.18	<b>References</b>	155
<b>Experimental</b>		159
6.0	<b>Instrumentation and experimental techniques</b>	159
6.1	<b>Experimental procedures</b>	160
6.2	<b><i>In vitro</i> [<sup>3</sup>H]-labelled prenyl-protein transferase enzyme inhibition assay methodology</b>	211
6.3	<b><i>In vitro</i> [<sup>3</sup>H]-labelled HDAC assay methodology</b>	214
6.4	<b>Methodology for the non-isotopic HDAC enzyme activity assay (HPLC)</b>	214
6.5	<b>Methodology for sulforhodamine B cell proliferation assay</b>	215
6.6	<b>References</b>	217

## List of Figures

### Chapter 1

<b>Figure 1</b>	Structure of limonene and perillyl alcohol.....	3
<b>Figure 2</b>	Structure of perillic acid and dihydroperillic acid.....	3
<b>Figure 3</b>	Isoprene.....	4
<b>Figure 4</b>	‘Head-to-tail’ connections of limonene and $\alpha$ -farnesene....	4
<b>Figure 5</b>	Farnesol.....	8
<b>Figure 6</b>	All <i>trans</i> -retinoic acid.....	8
<b>Figure 7</b>	Linear diterpenoids.....	9
<b>Figure 8</b>	Formation of taxol.....	10

### Chapter 2

<b>Figure 1</b>	Diagrammatic representation of an $\alpha$ -helix.....	23
<b>Figure 2</b>	Fischer’s ‘lock and key’ hypothesis.....	26
<b>Figure 3</b>	Reaction profile for enzymatic and non-enzymatic reactions	27
<b>Figure 4</b>	Michaelis-Menten plot.....	31
<b>Figure 5</b>	Lineweaver-Burk plot.....	32
<b>Figure 6</b>	Eadie-Hofstee plot.....	32
<b>Figure 7</b>	(a)Direct linear plot with one set of experimental values, (b)Direct linear plot with a number of sets of experimental values.....	33
<b>Figure 8</b>	Structure of penicillin.....	35
<b>Figure 9</b>	Competitive inhibition.....	36
<b>Figure 10</b>	Lineweaver-Burk plot of competitive inhibition.....	36
<b>Figure 11</b>	Non-competitive inhibition.....	37
<b>Figure 12</b>	Lineweaver-Burk plot of non-competitive inhibition.....	37
<b>Figure 13</b>	Uncompetitive inhibition.....	38
<b>Figure 14</b>	Lineweaver-Burk plot of uncompetitive inhibition.....	39
<b>Figure 15</b>	Allosteric regulation of ATCase.....	39

**Chapter 3**

<b>Figure 1</b>	Structure of FPTase heterodimer.....	50
<b>Figure 2</b>	The amino acid methionine.....	51
<b>Figure 3</b>	Compounds based on pseudo-peptide strategy.....	53
<b>Figure 4</b>	Peptidomimetic inhibitors using stable hydrophobic Spacers.....	54
<b>Figure 5</b>	Peptidomimetics using alkane and alkene hydrophobic spacers.....	55
<b>Figure 6</b>	Peptidomimetics incorporating a benzodiazepine subunit...	55
<b>Figure 7</b>	Analogues of CVFM tetrapeptide.....	56
<b>Figure 8</b>	Non-peptidomimetics.....	57
<b>Figure 9</b>	Tri-cyclic non-peptidomimetic inhibitor.....	58
<b>Figure 10</b>	Farnesyl pyrophosphate and two analogues.....	59
<b>Figure 11</b>	FPP analogues with amide bonds.....	59
<b>Figure 12</b>	Oreganic acid and its analogues.....	60
<b>Figure 13</b>	Bisubstrate analogue inhibitors.....	61
<b>Figure 14</b>	Natural product inhibitors.....	62
<b>Figure 15</b>	Binding of farnesyl pyrophosphate in enzyme pocket of FPTase and rationale for binding of new synthetic isoprenoid.....	64
<b>Figure 16</b>	<i>In vivo</i> inhibition concentrations of natural occurring isoprenoids of human MIA PaCa2 pancreatic tumour cells.....	64
<b>Figure 17</b>	Sigmoidal dose-response curve.....	67
<b>Figure 18</b>	GGPTase-I assay for PTase 9.....	70
<b>Figure 19</b>	Compounds submitted for PTase enzyme assay determination.....	72
<b>Figure 20</b>	Comparison of farnesol with diethyl ester <b>23</b> and ketone <b>24</b> .....	82



**Chapter 4**

<b>Figure 1</b>	Comparison of the structure of farnesol, diethyl ester <b>23</b> and ketone <b>24</b> .....	101
<b>Figure 2</b>	Flow cytometric analysis of Jurkat cells.....	106
<b>Figure 3</b>	Slides showing TF1 cells after 72 hours.....	107
<b>Figure 4</b>	Cell slides of primary T-lymphocytes taken after 72 hours cultured with DMSO and farnesol.....	109
<b>Figure 5</b>	Three AML-patient samples cultured with DMSO and farnesol after 72 hours.....	112
<b>Figure 6</b>	Structure of compounds <b>23</b> , <b>24</b> and their key features.....	113

**Appendix I**

<b>Figure 1</b>	The stages of the cell cycle.....	120
<b>Figure 2</b>	The cell cycle profile of Jurkat cells cultured with DMSO and farnesol.....	122

**Chapter 5**

<b>Figure 1</b>	A nucleosome octamer.....	124
<b>Figure 2</b>	The amino acid lysine.....	125
<b>Figure 3</b>	Model of histone deacetylase complex.....	127
<b>Figure 4</b>	APML HDAC repressor complexes.....	130
<b>Figure 5</b>	Action of HDAC and HDAC inhibitors.....	131
<b>Figure 6</b>	Histone deacetylase inhibitors.....	132
<b>Figure 7</b>	Diagrammatic representation of TSA interactions with HDAC.....	133
<b>Figure 8</b>	Key characteristics of hydroxamic acid-based HDAC inhibitors.....	134
<b>Figure 9</b>	SAHA binding to HDLP.....	136
<b>Figure 10</b>	Histology of carcinogen-induced rat mammary carcinomas	138
<b>Figure 11</b>	MAL structure.....	144
<b>Figure 12</b>	Concentration-response curves for HDAC inhibitors.....	146

<b>Figure 13</b>	Space-filling model of TSA in the active-site pocket of HDLP.....	147
<b>Figure 14</b>	Dose-response curve for HDAC inhibition for TSA.....	149
<b>Figure 15</b>	Proposed catalytic mechanisms for the deacetylation of an acetylated lysine in HDLP enzyme protein.....	151
<b>Figure 16</b>	Calibration of the SRB and Lowry cell proliferation assay <i>versus</i> number of cells.....	152

## List of Schemes

### Chapter 1

<b>Scheme 1</b>	Pathway to five-carbon units.....	5
<b>Scheme 2</b>	Isomerisation of C <sub>5</sub> unit.....	5
<b>Scheme 3</b>	Formation of Geranyl pyrophosphate from two C <sub>5</sub> units.	6
<b>Scheme 4</b>	Formation of monoterpenoid from Geranyl pyrophosphate.....	6
<b>Scheme 5</b>	Biosynthetic pathway for terpenes and steroids.....	7
<b>Scheme 6</b>	Formation to precursor of sesquiterpenoids.....	8
<b>Scheme 7</b>	Formation of diterpene precursor.....	9
<b>Scheme 8</b>	Biosynthesis of ophiobolins from sesterterpenes.....	10
<b>Scheme 9</b>	Formation of a triterpene.....	11
<b>Scheme 10</b>	Cholesterol biosynthesis.....	12
<b>Scheme 11</b>	The role of isoprenoids on the mevalonate pathway.....	13
<b>Scheme 12</b>	Oxidation and reduction of ( <i>R</i> )-perillaldehyde.....	16

### Chapter 2

<b>Scheme 1</b>	Concerted and sequential allosteric regulation.....	42
-----------------	---	----

### Chapter 3

<b>Scheme 1</b>	Ras pathway.....	47
<b>Scheme 2</b>	Farnesylation of Ras protein.....	49
<b>Scheme 3</b>	Preparation of all short-chain compounds.....	74
<b>Scheme 4</b>	Formation of compound <b>5</b> by a Williamson ether synthesis	75
<b>Scheme 5</b>	Preparation of all long-chain mono- and bicyclic compounds.....	79
<b>Scheme 6</b>	Preparation of diethyl ether <b>23</b> and ketone <b>24</b> .....	80
<b>Scheme 7</b>	Synthesis of compound <b>28</b> <i>via</i> a Wittig reaction.....	81
<b>Scheme 8</b>	Preparation of medium-chain chaetomelic acid analogues.	84
<b>Scheme 9</b>	Preparation of various polar $\alpha$ -myrcene derived inhibitors.	85

<b>Scheme 10</b>	Mechanism of formation of an <i>N</i> -hydroximide.....	86
<b>Scheme 11</b>	Preparation of anhydrides incorporating a sesquiterpenoid lipophilic unit.....	86
<b>Scheme 12</b>	The E2 mechanism for the formation of $\beta$ -farnesene.....	87
<b>Scheme 13</b>	Preparation of long-chain compounds with strongly polar terminus.....	87
<b>Scheme 14</b>	Preparation of various long-chain saturated lipophilic compounds.....	88
<b>Scheme 15</b>	Formation of tricarboxylic acid <b>70</b> .....	89

## Chapter 5

<b>Scheme 1</b>	Preparation of known and potential HDAC inhibitors for HPLC assay.....	139
<b>Scheme 2</b>	Mechanism of formation of acid chloride.....	139
<b>Scheme 3</b>	Synthesis of HDAC inhibitors <b>36</b> and <b>40</b> .....	140
<b>Scheme 4</b>	Mechanism of formation of hydroxamic acids.....	141
<b>Scheme 5</b>	Attempted synthesis of HDAC inhibitor <b>40</b> .....	142
<b>Scheme 6</b>	Attempted synthesis of HDAC inhibitor <b>42a</b> .....	143
<b>Scheme 7</b>	Attempted synthesis of HDAC inhibitor <b>80</b> .....	144

## List of Tables

### Chapter 1

<b>Table 1</b>	Chemopreventive agents and their modes of action.....	2
<b>Table 2</b>	Classification of terpene types.....	4

### Chapter 2

<b>Table 1</b>	Classification of enzymes by reactions.....	21
<b>Table 2</b>	Enzymes and their metal ions.....	25

### Chapter 3

<b>Table 1</b>	The scintillation values obtained for the amount of [ <sup>3</sup> H]-labelled Ras in the presence of inhibitor PTase 9.....	69
<b>Table 2</b>	Table of results obtained from the non-linear regression analysis of a sigmoidal dose-response curve for PTase 9...	71
<b>Table 3</b>	Enzyme inhibition assay values for short-chain mono-cyclic compounds.....	76
<b>Table 4</b>	Enzyme inhibition assay values for long-chain mono- and bicyclic analogues.....	82
<b>Table 5</b>	Enzyme inhibition assay values for medium to long-chain compounds with strongly polar terminus.....	90

### Chapter 4

<b>Table 1</b>	Contents of flasks used for cell line assays.....	102
<b>Table 2</b>	The effect of farnesol on the cell cycle of Jurkat cells.....	106
<b>Table 3</b>	The effect of farnesol on the percentage of TF1 cells in each cell cycle phase.....	107
<b>Table 4</b>	The effect of compounds <b>23</b> and <b>24</b> on the Jurkat cell cycle	114
<b>Table 5</b>	The effect of diethyl ester <b>23</b> and ketone <b>24</b> on the cell cycle phase of TF1 cells.....	115

**Chapter 5**

<b>Table 1</b>	Effect of spacer group on the inhibition of HDAC 1.....	135
<b>Table 2</b>	The IC <sub>50</sub> values obtained from known HDAC inhibitors from HPLC assay.....	146
<b>Table 3</b>	The scintillation values obtained for the amount of [ <sup>3</sup> H]-labelled histone H4 peptide in the presence of trichostatin A.	148
<b>Table 4</b>	Table of results obtained from non-linear regression analysis of a sigmoidal dose-response curve for trichostatin A.....	149
<b>Table 5</b>	<i>In vitro</i> HDAC inhibition values for HDAC inhibition.....	150
<b>Table 6</b>	The cytotoxic IC <sub>50</sub> values for TSA and HDAC inhibitor <b>36</b> in various breast cancerous cell lines.....	153

**Chapter 6**

<b>Table 1</b>	The quantities of various reagents necessary for a FPTase enzyme inhibition assay.....	212
<b>Table 2</b>	The composition of X1 PFT stock buffer solution.....	213
<b>Table 3</b>	Constituents of X5 PFT stock buffer solution.....	213
<b>Table 4</b>	The quantities of the various reagents necessary for a GGPTase enzyme inhibition assay.....	213

## Glossary

Ac	acetylated
ADH	atypical ductal hyperplasia
AML	acute myeloid leukaemia
APML	acute promyelocytic leukaemia
ATP	adenosine triphosphate
ATRA	all- <i>trans</i> -retinoic acid
BPH	benign prostatic hyperplasia
CAF-1	chromatin assembly factor
cAMP	cyclic adenosine monophosphate
CDP	cytidine 5'-diphosphate
CTP	cytidine 5'-triphosphate
DCM	dichloromethane
DDT	dithiothreitol
DFMO	2-difluoromethylornithine
DMF	<i>N,N</i> -dimethylformamide
DMSO	dimethylsulfoxide
DNA	deoxyribonucleic acid
EDTA	ethylenediaminetetraacetic acid
EGF	epidermal growth factor
EGFR	epidermal growth factor receptor
EI	electron impact
FCS	fetal calf serum
FITC	fluorescein isothiocyanate
FPP	farnesyl pyrophosphate
FPTase	farnesyl-protein transferase
G <sub>0</sub>	quiescent stage
G <sub>1</sub>	gap 1
G <sub>2</sub>	gap 2
GDP	guanine diphosphate
GGPP	geranylgeranyl pyrophosphate
GGPTase	geranylgeranyl-protein transferase

GSH	glutathione
GTP	guanine triphosphate
HAT	histone acetyltransferase
HDAC	histone deacetylase
HDLP	histone deacetylase like-protein
HMG-CoA	hydroxy-3-methylglutaryl coenzyme A
HMG-SCoA	hydroxy-3-methylglutaryl-SCoA
HPLC	high performance liquid chromatography
HRE	hormone response element
IL-2	interleukin-2
KOH	potassium hydroxide
LiOH	lithium hydroxide
M	mitosis
MAL	<i>N</i> -[5-Acetylamino-1-(4-methyl-2-oxo-2 <i>H</i> -chromen-7-ylcarbamoyl)- pentyl]-2,2-dimethylpropionamide
MAPK	mitogen activated protein kinase
MAPKK	mitogen activated protein kinase kinase
MEL	murine erythroleukaemia
MeOH	methanol
mRNA	messenger ribonucleic acid
MVA	mevalonic acid
N-CoR	nuclear receptor corepressor
NMU	<i>N</i> -methylnitrosurea
NO	nitric oxide
NOS	nitric oxide synthase
NSAID	non-steroidal anti-inflammatory drug
PI	propidium iodide
PKC	protein kinase C
PLZF	promyelocytic leukaemia zinc finger
PML	promyelocytic leukaemia
PPTase	prenyl protein transferase
R <sup>2</sup>	‘goodness-of-fit’
RAR	retinoic acid receptor
RbAp48	Rb-associated protein 48



<i>rh</i>	wild-type
RPD	reduced potassium dependency
ROS	reactive oxygen species
RTK	receptor tyrosine kinase
S	synthesis
SAHA	suberoylanilide hydroxamic acid
SAP	sin3 associated proteins
SERM	selective oestrogen receptor modulator
SDS	sodium dodecyl sulfate
SMRT	silencing mediator for retinoid/thyroid hormone receptor
SOD	superoxide <i>dismutase</i>
SRB	sulforhodamine B
SS	sum-of-squares
TBHP	<i>tert</i> -butyl hydroperoxide
TCA	trichloroacetic acid
TGF	transforming growth factor
THF	tetrahydrofuran
TSA	trichostatin A
UTP	uridine 5'-triphosphate

# The Role of Terpenes and Terpenoids in Chemoprevention

## 1.0 Introduction

Limonene and perillyl alcohol have been shown to exhibit significant anti-cancer properties in rat and human carcinomas. In collaboration with a clinical group interested in anti-cancer compounds related to these terpenes and terpenoids, this project began by examining monoterpenoids and synthetic compounds derived from them, with the purpose of providing new cancer treatments. Accordingly, a brief summary of terpenes and terpenoids with their principal features in relation to cancer is given.

## 1.1 Chemoprevention

Chemoprevention of cancer has been defined as “a means of cancer control in which the occurrence of this disease is *prevented* by the administration of one or more natural or chemical properties”.<sup>1,2</sup> Common epithelial cancers such as colon, breast and prostate carcinomas remain the dominant cause of cancer deaths in the western world.<sup>3</sup> The treatments available for these tumours at the advanced stages are dominated by cytotoxic chemotherapies, which often have severe limitations in terms of success and quality of life. Consequently, chemoprevention or more specifically, *chemopreventive agents* have become a prominent force against cancer. Chemopreventive agents can be divided into two categories: (a) compounds that are effective against carcinogens, and (b) compounds that are effective against tumour promoters. There are chemopreventive agents that belong to both categories.<sup>3</sup>

## 1.2 Carcinogenesis

Carcinogenesis provides the biological basis for chemoprevention.<sup>4</sup> Carcinogenesis is abnormal differentiation and/or apoptosis. Historically this process has been divided into the three phases of *initiation*, *promotion* and *progression*.<sup>5</sup> The initiation phase

centres on the attack of carcinogens on DNA leading to damage and irreversible mutations. After this, promotion starts, in which continued mutations occur through external environmental exposures. This results in the loss of key functional cellular proliferations and the loss of regulatory proteins. Another characteristic of this phase is the clonal expansion of mutated cells. Lastly the progression phase occurs, in which the altered cells develop micro- and macroscopic changes.

In the past, chemopreventive agents were developed that prevented specifically one of the above three phases of carcinogenesis, for example *anti-initiation*. The improved understanding of molecular mechanisms of carcinogenesis has led to the production of new modes of chemoprevention. The ability to modulate one or more molecular carcinogenic events, as shown in Table 1, provides the new understanding in terms of mechanisms of action.

Mechanism of Action	Agents
Anti-oxidant	Polyphenols, vitamin E, selenium
Modulation of arachidonic acid cascade	Non-steroidal anti-inflammatories (NSAIDs), polyphenols, tamoxifen
Signal transduction modification	NSAIDs, polyphenols, tamoxifen
Modification of hormonal or growth factors	Tamoxifen, NSAIDs, retinoids
Suppression of oncogene function	Monoterpenes, NSAIDs
Suppression of mutator phenotype	NSAIDs
Promotion of cellular differentiation	Retinoids
Enhancement of apoptosis	NSAIDs, curcumin, retinoids, tamoxifen

**Table 1** Chemopreventive agents and their modes of action

It should not generally be assumed that there is a single mode of action for a chemopreventive agent and many compounds, especially natural products, have multiple modes of action.

### **1.3 Limonene and perillyl alcohol cancer therapy**

Both limonene and perillyl alcohol have shown the potential to simultaneously prevent and treat cancers, especially breast cancer, and therefore act as chemopreventive agents.<sup>6,7</sup> Limonene entered clinical trials in 1993, and clinical trials for perillyl alcohol began in 1996.<sup>8,9</sup>

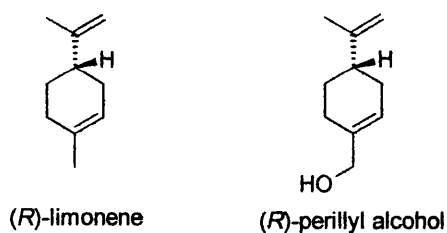


**Figure 1** Structures of limonene and perillyl alcohol

Perillyl alcohol is a hydroxylated derivative of limonene and both are metabolised to perillic acid and dihydroperillic acids, (figure 2), which themselves have been shown to be potent anti-cancer agents.<sup>10,11</sup>

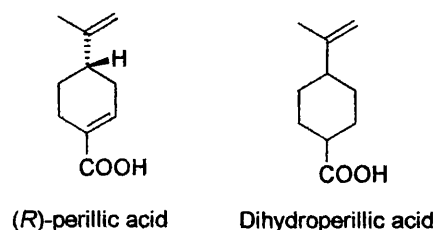


**Figure 2** Structures of perillic acid and dihydroperillic acid

Both enantiomers of limonene and perillyl alcohol are effective anti-cancer agents, the (*R*)-enantiomer being slightly more potent.<sup>12</sup> Even though limonene is now being viewed as a pro-drug of perillyl alcohol, perillic acid and dihydroperillic acid,<sup>12</sup> limonene has still been shown to inhibit the growth of mouse,<sup>13</sup> lung,<sup>13</sup> and skin tumours<sup>14</sup> as well as induce regression of established mammary tumours.<sup>15</sup> Perillyl alcohol inhibits rat liver<sup>15</sup> and hamster pancreatic<sup>16</sup> tumours and causes the regression of established rat mammary tumours.<sup>17</sup> However, the clinical potential of both limonene and perillyl alcohol is limited by the large doses required for efficacy.<sup>18</sup> For example, the minimum dietary dose for rat mammary tumour prevention is 1-5%, equivalent to 35-175 g daily for a 70 kg human being.<sup>18</sup>

#### **1.4 The family of terpenes and terpenoids (isoprenoids)**

By gently heating or steam distilling certain plant extracts, a mixture of odoriferous compounds known as the *essential oils* can be isolated. These oils have had a variety of uses, in particular as perfumes and in early medicine.<sup>19</sup> The most important constituents of these 'essential oils' are hydrocarbons, more generally known as

*terpenes*, and oxygen containing compounds, known as *terpenoids*, both of which can either be linear or cyclic compounds.

Almost all the terpenes have skeletons of 10, 15, 20, 25 and 30 carbon atoms and are classified accordingly as depicted in Table 2.

Number of carbon atoms	Class
10	Monoterpenes
15	Sesquiterpenes
20	Diterpenes
25	Sesterterpenes
30	Triterpenes

**Table 2** Classification of terpene types

The essential building blocks of terpenes are  $C_5$  blocks called *isoprene units*. Isoprene is 2-methyl-1,3-butadiene, as shown in figure 3, and though plants do not synthesis terpenes from isoprene itself, the isoprene unit is a great aid in illuminating terpene structures. This has led to both terpenes and terpenoids being grouped as isoprenoids.



**Figure 3** Isoprene

Indeed, the isoprene rule was devised, which states that all terpenes are multiples of the  $C_5$  units, and that the structural formation of such compounds occurs almost exclusively in 'head-to-tail' connections.<sup>20</sup> Examples of this are shown in figure 4, for limonene (a monoterpene) isolated from oranges or lemons, and  $\alpha$ -farnesene (a sesquiterpene) isolated from the natural coating of apples.<sup>19</sup>

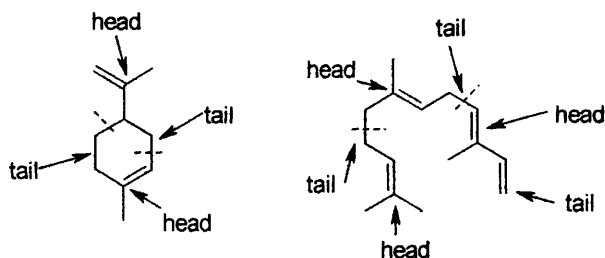
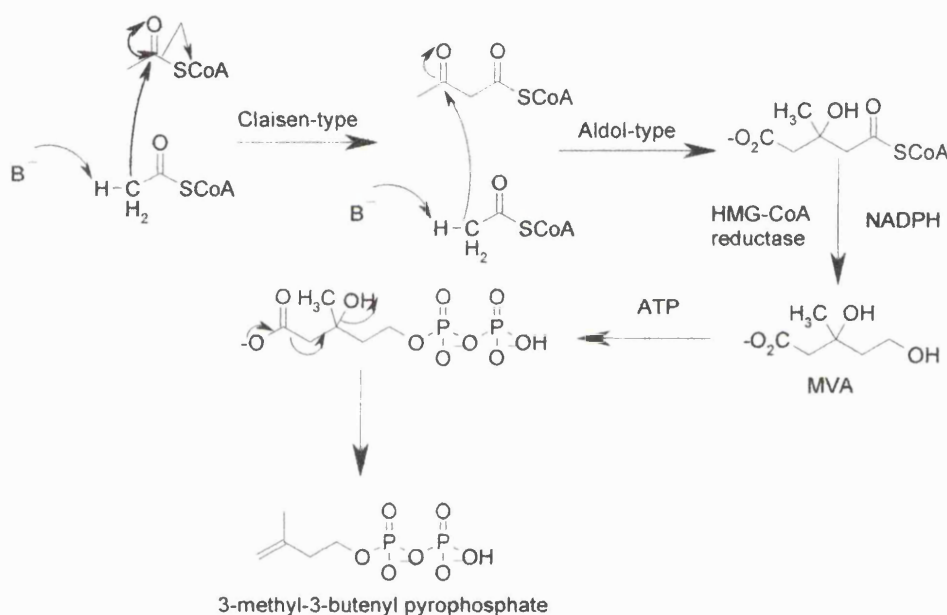


**Figure 4** 'Head-to-tail' connections of limonene and  $\alpha$ -farnesene, respectively

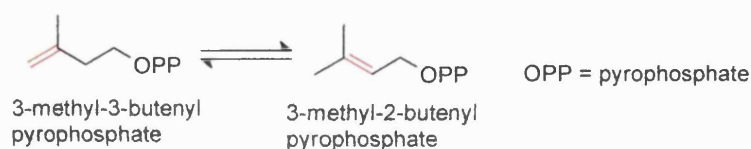
### 1.5 Biosynthesis of 3-methyl-3-butenyl pyrophosphate

In the 1960s, Bloch and co-workers discovered the pathway to this key isoprenoid unit, the basic building block of terpenes and terpenoids.<sup>21</sup> The synthesis is shown in Scheme 1, and the first step is catalysed by acetoacetyl-SCoA thiolase and involves a Claisen ester condensation between two acetyl-SCoA units. The second step is an Aldol reaction catalysed by hydroxymethylglutaryl-SCoA (HMG-SCoA) synthase, leading into a reduction of HMG-SCoA to produce mevalonic acid (MVA). This process utilises two moles of NADPH, catalysed by HMG-CoA reductase. MVA is phosphorylated producing MVA-5-pyrophosphate, which after decarboxylation yields 3-methyl-3-butenyl pyrophosphate, the biogenetic isoprene unit.



**Scheme 1** Pathway to five-carbon units

An isomerisation of 3-methyl-3-butenyl pyrophosphate to 3-methyl-2-butenyl pyrophosphate. This isomerisation (shown in scheme 2) achieves an equilibrium that makes both compounds available to the cell.<sup>19</sup>

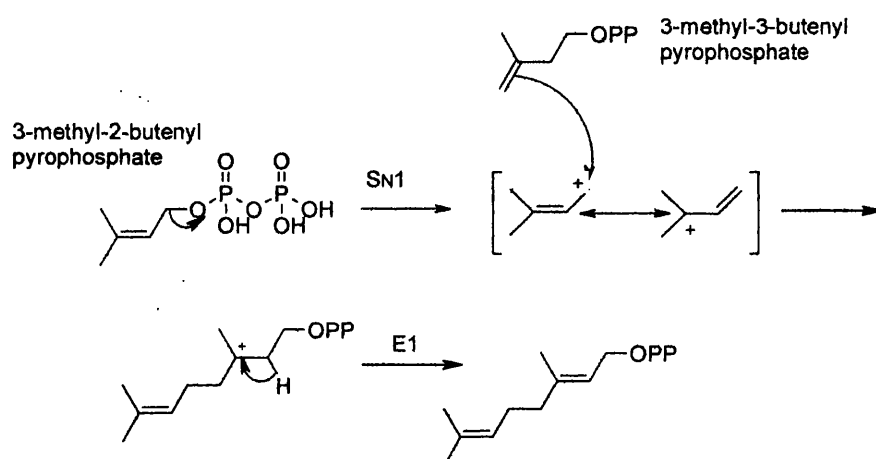


**Scheme 2** Isomerisation of C<sub>5</sub> unit

Nature employs the pyrophosphate group for a vast number of biochemical processes. In the reactions for the formation of different terpenes and terpenoids, the pyrophosphate group acts as a 'natural' leaving group.<sup>19</sup>

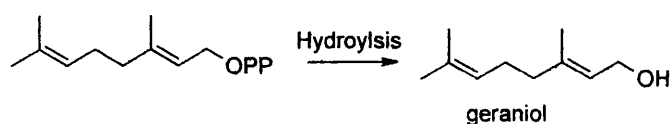
### 1.6 Monoterpenes and terpenoids ( $C_{10}$ structures)

The formation of monoterpenes and subsequent terpenoids involves the condensation of two isoprene pyrophosphate groups. 3-Methyl-2-butenyl pyrophosphate now has the pyrophosphate group in an *allylic* position. This contributes to easy ionisation, producing an allyl cation that is attacked by the 3-methyl-3-butenyl pyrophosphate to give a  $C_{10}$  compound, geranyl pyrophosphate.<sup>22</sup> The reaction as shown in scheme 3, proceeds *via* a  $S_N1$  mechanism followed by an  $E1$  type mechanism.<sup>22</sup>



**Scheme 3** Formation of geranyl pyrophosphate from two  $C_5$  units

Geranyl pyrophosphate is the precursor of many monoterpenes and terpenoids, for example hydrolysis of geranyl pyrophosphate gives geraniol (a monoterpene), as shown in scheme 4.

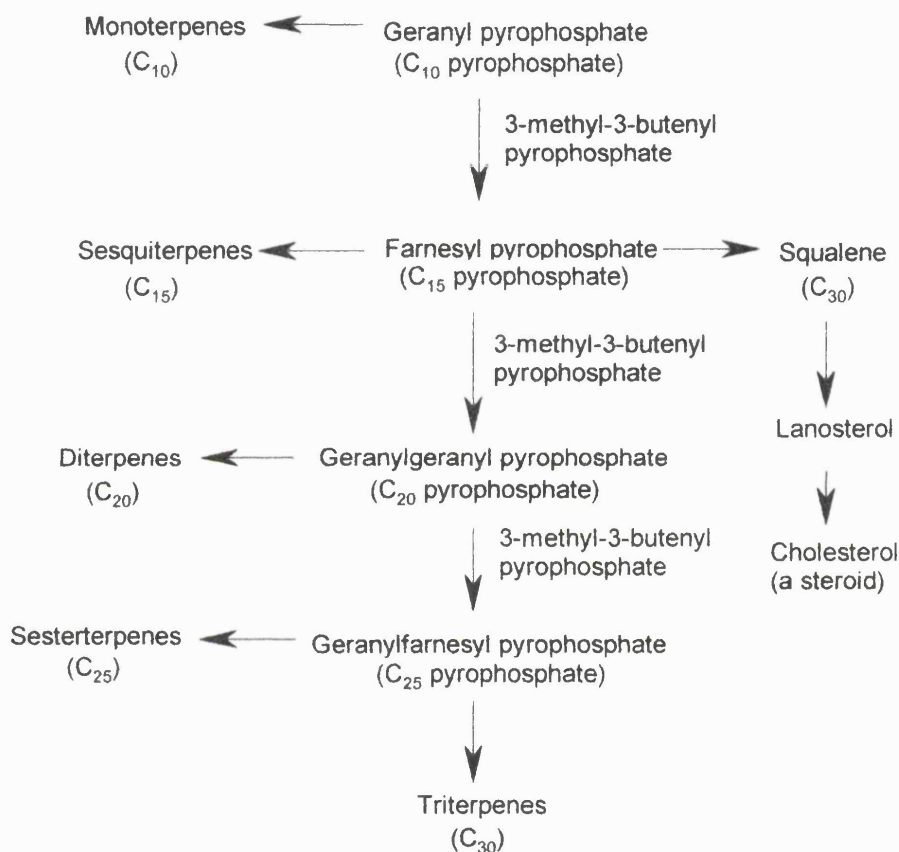


**Scheme 4** Formation of monoterpene from geranyl pyrophosphate

Two more examples of monoterpenes and terpenoids are obviously limonene and perillyl alcohol. As stated above in section 1.3, both compounds have therapeutic

value. (*R*)-(+)-Limonene has an odour of oranges whilst the opposite enantiomer, (*S*)-(-)-limonene, smells of lemons; indeed both enantiomers are found in large quantities in the respective citrus fruits.<sup>21</sup> The odour of perillyl alcohol for the (*S*)-(-)- and (*R*)-(+)-perillyl alcohol enantiomers is cherry and spearmint respectively.

Condensation of geranyl pyrophosphate with more 3-methyl-3-butenyl pyrophosphate leads to the formation of precursors of almost all other terpenes and terpenoids, including an important set of terpenoids known as *steroids*, as shown in scheme 5.<sup>19</sup>

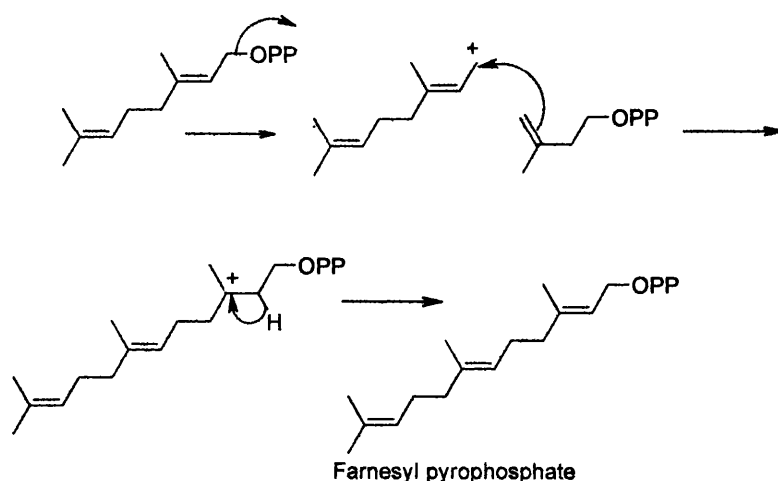


**Scheme 5** Biosynthetic pathway for terpenes and steroids

### 1.7 Sesquiterpenes and terpenoids (C<sub>15</sub> structures)

Geranyl pyrophosphate condenses with 3-methyl-3-butenyl pyrophosphate to form the C<sub>15</sub> precursor of sesquiterpenes; farnesyl pyrophosphate, (shown in scheme 6).





**Scheme 6** Formation to precursor of sesquiterpenes

As with geranyl pyrophosphate, farnesyl pyrophosphate can be hydrolysed and gives farnesol, shown in figure 5.

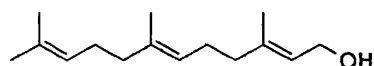


**Figure 5** Farnesol (a sesquiterpenoid)

Farnesol has the odour of lily of the valley, and is isolated from ambrette oil.<sup>19</sup> In certain insects, farnesol functions as a hormone and also initiates the conversion of a caterpillar to pupa and then to butterfly.<sup>19</sup> Along with farnesol, there are other sesquiterpenoids capable of chemoprevention, one such example is all *trans*-retinoic acid (figure 6).

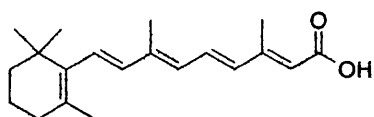
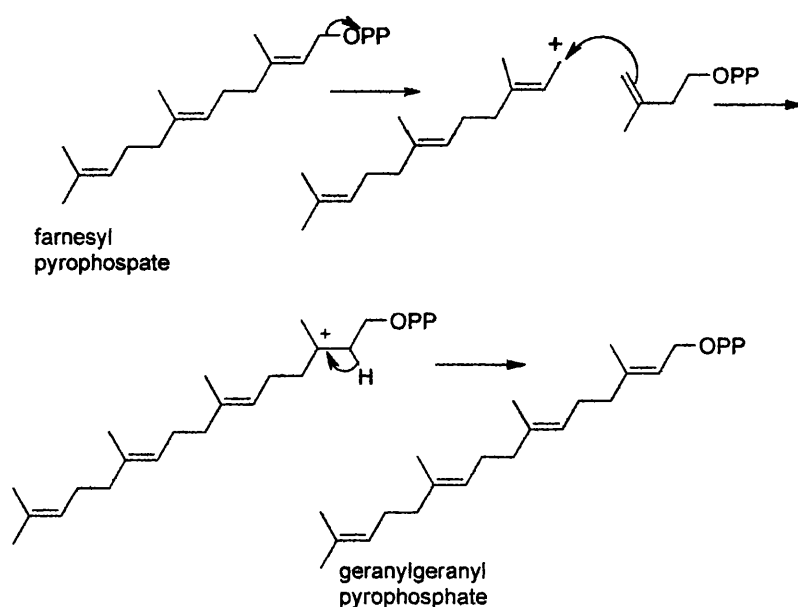


**Figure 6** All *trans*-retinoic acid

All *trans*-retinoic acid is a signal transduction modulator, and acts by inhibiting proliferation and inducing differentiation.<sup>23,24</sup> The retinoid receptors function as transcription factors which regulate the expression of certain genes. Changes in gene transcription caused by all *trans*-retinoic acid leads to its chemopreventive capabilities; the acid has a strong affinity for the retinoid receptors.<sup>23</sup>

## 1.8 Diterpenes and terpenoids ( $C_{20}$ structures)

The precursor of diterpenes is geranylgeranyl pyrophosphate, which is formed in the same manner as for monoterpenes and sesquiterpenes, essentially a condensation of farnesyl pyrophosphate with 3-methyl-3-butenyl pyrophosphate, (scheme 7).



**Scheme 7** Formation of diterpene precursor

Again, as with the geranyl pyrophosphate and farnesyl pyrophosphate, the geranylgeranyl pyrophosphate is hydrolysed, to form geranylgeraniol. Another linear diterpenoid is phytol; both compounds are shown in figure 7.

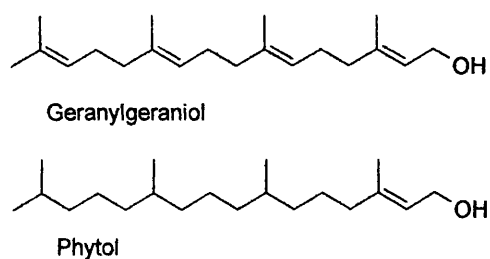


**Figure 7** Linear diterpenoids

One diterpenoid of great contemporary interest is taxol, (figure 8) which is extremely potent and has a broad spectrum of anti-cancer activity, and is undergoing advanced

clinical trials in the USA and Europe. Most supplies of the complex diterpenoid come from the bark of the pacific yew, *Taxus brevifolia*.

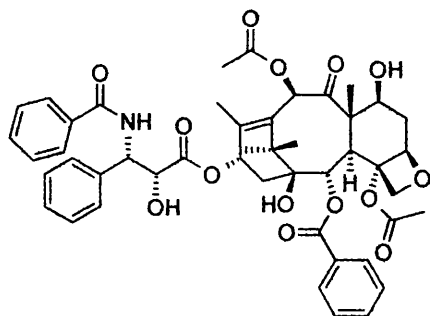
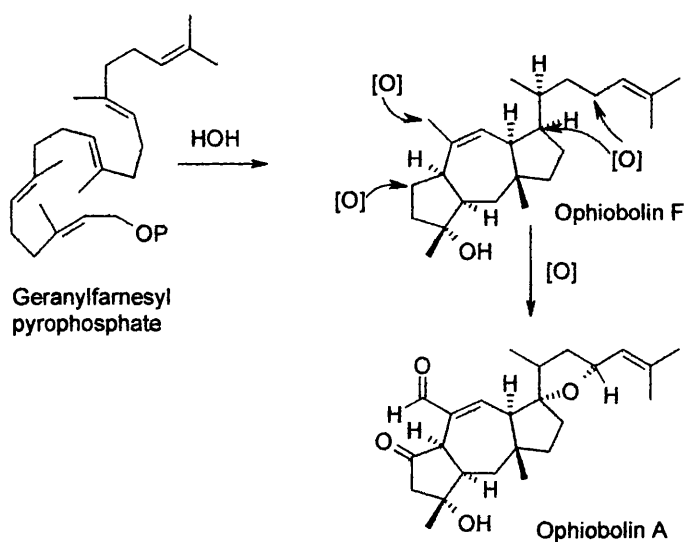


**Figure 8** Formation of taxol (a complex diterpenoid)

### 1.9 Sesterterpenes and terpenoids ( $C_{25}$ structures)

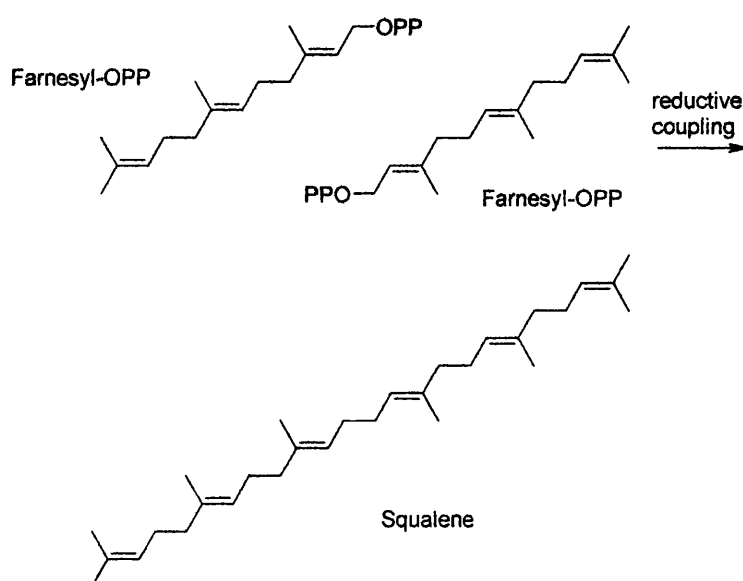
The members of this terpene family originate from geranylfarnesol and are rare.<sup>25</sup> The ophiobolines, a group of tricyclic terpenes were isolated from phytopathogenic fungi; they all have a 5-8-5 ring system. The biosynthesis of ophiobolin A from all *trans*-geranylfarnesyl pyrophosphate is outlined in scheme 8.<sup>26</sup> Ophiobolin A is a fungal toxin that affects rice and maize. It interferes with the protein calmodulin by reacting with its lysine residues.<sup>27</sup>



**Scheme 8** Biosynthesis of ophiobolins from sesterterpenes

### 1.10 Triterpenes and terpenoids ( $C_{30}$ structures)

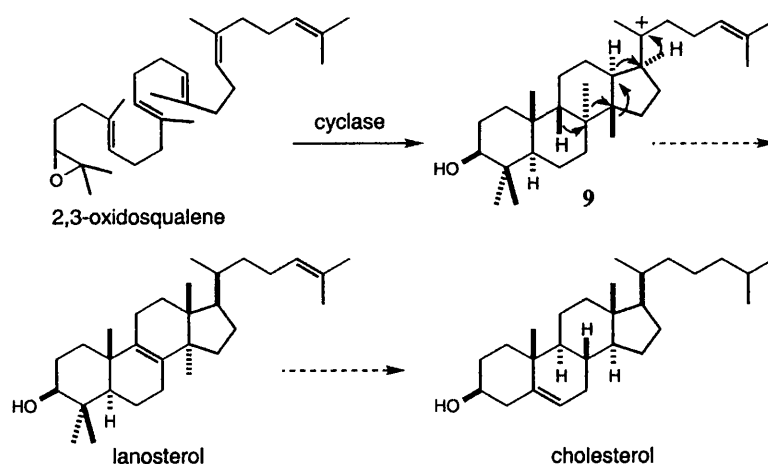
The formation of triterpenes is unlike that of other terpenes; rather than a long chain pyrophosphate condensing with 3-methyl-3-butenyl pyrophosphate, the triterpenes and terpenoids are formed in a different manner.<sup>21</sup> The first  $C_{30}$  compound to be discovered was squalene (in shark oil). The structure of squalene consists of two farnesyl pyrophosphate units; however rather than the head-to-tail connection between the two units, a tail-to-tail bond exists through a reductive condensation.<sup>19,26</sup>



**Scheme 9** Formation of a triterpene

Squalene is an important triterpene, as it is a mandatory biosynthetic precursor of cholesterol, in a biosynthetic pathway, using the enzyme squalene synthase. Squalene is then epoxidised and subsequently cyclised to yield lanosterol,<sup>26</sup> which after several more steps is converted into cholesterol, as shown in scheme 10.<sup>27</sup> (Squalene synthase is discussed in chapter three in connection with farnesyl pyrophosphate inhibitors).

Triterpenes are the gateway to many steroids since a  $C_{30}$  chain length is very susceptible to cyclase enzymes, which stereospecifically cyclise long-chain terpenes into steroids, the major example being epoxysqualene cyclase.<sup>28</sup>



**Scheme 10** Cholesterol biosynthesis<sup>27</sup>

### **1.11 Possible modes of action of terpenes and terpenoids chemopreventive properties**

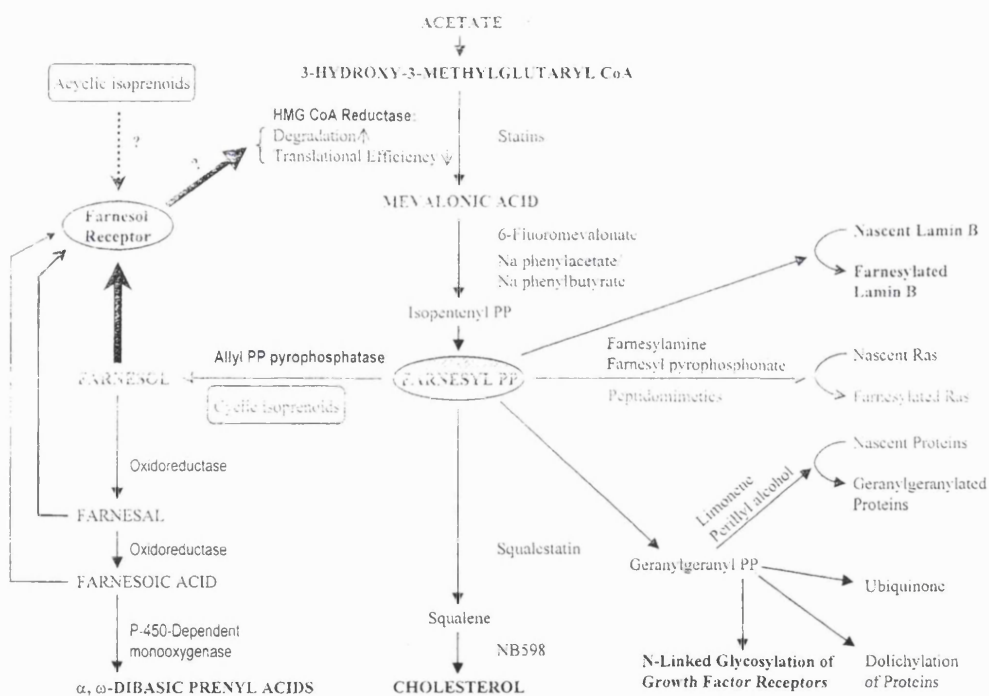
It might seem that there are numerous means by which terpenes such as limonene and terpenoids (perillyl alcohol) could impart their therapeutic action. However, there are four mechanisms that have undergone and are still receiving intense research.

- Limonene, perillyl alcohol and other terpenes/terpenoids inhibit the post-translational isoprenylation of small G proteins.<sup>29</sup> This is investigated in chapter three.
- As terpenes and terpenoids are synthesised from a component of the mevalonate metabolism pathway, the effects of isoprenoids on the mevalonate pathway could impart anti-cancer properties.
- It was observed that isoprenoids affect choline phosphotransferase (an enzyme) which regulates cell proliferation and apoptosis.<sup>30</sup>
- Oxidative metabolites of limonene and perillyl alcohol would suggest that such terpenes/terpenoids (isoprenoids) may play an anti-oxidant role within the body.<sup>31</sup>

### 1.11.1 Isoprenoid-mediated inhibition of mevalonate synthesis

The blocking and suppressing activities conferred by secondary products (*i.e.* isoprenoids) of the mevalonate plant metabolism have now been recognised.<sup>32</sup> Blocking agents act at the initiation phase of carcinogenesis by inhibiting the formation of carcinogens from precursor compounds and also by preventing carcinogenic agents from reaching or reacting with target sites.<sup>33</sup>

It was reported that a diet augmented with 10% *d*-limonene (735 mmol/kg) caused regression of chemically initiated primary human mammary tumours.<sup>34</sup> Diets supplemented with 2% perillyl alcohol (130 mmol/kg) were shown to cause tumour regression.<sup>35</sup> A possible mechanism by which these isoprenoids possess anti-carcinogenic activity is owing to the effect on the feedback resistant 3-hydroxy-3-methylglutaryl coenzyme A (HMG-CoA), by isoprenoid-modulated downregulation, as shown in scheme 11.<sup>33</sup> The mevalonate pathway and the various sites of isoprenoid-mediated actions is shown in the scheme below.



**Scheme 11** The role of isoprenoids on the mevalonate pathway<sup>33</sup>

In animal cells, a finely tuned metabolic feedback mechanism that involves transcription and post-transcription control of HMG-CoA reductase, maintains a

certain amount of mevalonate intermediates necessary for cell survival and cholesterol homeostasis.<sup>36</sup> Cholesterol, the end product of the pathway in sterologenic tissues, exerts transcriptional control on sequential activities in the mevalonate pathway,<sup>33</sup> especially those catalysed by HMG-CoA reductase and farnesyl pyrophosphate synthase. The multivalent regulation of HMG-CoA reductase integrates activities at the transcriptional, post-transcriptional and post-translational levels.<sup>36</sup> The post-translational control of HMG-CoA reductase is controlled by nonlysosomal cysteine protease only when isoprenoid requirements are satisfied.<sup>37</sup> This protease activity (accelerated by a mevalonate derived nonsterol product) has a high specificity for HMG-CoA reductase.<sup>38</sup> The mevalonate derived nonsterol product is a vital component to the regulation of HMG-CoA reductase, and its identity is believed to be farnesol (a terpenoid).<sup>37</sup> Supporting this belief is the detection and subsequent characterisation of hepatic microsomal allyl pyrophosphate pyrophosphatase, an enzyme that has a high affinity for farnesyl pyrophosphate.<sup>39</sup> Therefore, farnesol is a key terpenoid in the post-translational control of HMG-CoA reductase, since farnesol accelerates specific proteases which regulates HMG-CoA reductase. There is also evidence that farnesol (or a similar type of isoprenoid) can mediate translational control of the synthesis of HMG-CoA reductase.<sup>37</sup>

A sterol (any group of natural steroid alcohols, such as cholesterol) feedback-resistant HMG-CoA reductase enzyme is an anomaly associated with tumour growth. It creates an extensive store of sterologenic pathway intermediates and such intermediates provide lipophilic anchors essential for membrane attachment and biological activity of growth hormone receptors and *oncogenic ras*.<sup>40,41</sup> However, tumorous HMG-CoA reductase retains its high sensitivity to this isoprenoid-mediated secondary regulation,<sup>37</sup> and thus the repression of mevalonate synthesis by down-regulation of HMG-CoA reductase reduces oncogenic ras processing, arrests cells in the G<sub>1</sub> phase of the cell cycle and initiates cell apoptosis.<sup>42,43,44</sup> It is this tumour specific anomaly that allows isoprenoids to be used for chemoprevention and to be free of any side-effects.<sup>33</sup>

### 1.11.2 Inhibition of phosphatidylcholine biosynthesis

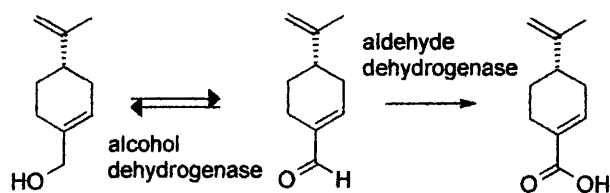
Phosphatidylcholine (PC) is the most abundant phospholipid in mammalian cells, comprising up to 50 % of the membrane phospholipids.<sup>30</sup> PC is synthesised mainly through the CDP-choline pathway regulated by CTP (cytidine 5'-triphosphate): phosphocholine cytidyltransferase (CT).<sup>30</sup> PC and the CDP (cytidine 5'-diphosphate)-choline pathway have been implicated as an important component in the control of cell proliferation and cell death.<sup>30</sup> An increase in biosynthesis of PC is required for normal progression through the cell cycle; without it accumulation in the G<sub>1</sub> phase occurs, as shown in cell mediums which are choline-deficient.<sup>30</sup> Inhibition of CT in cells treated with anti-tumour phospholipid analogues induces apoptosis.<sup>45</sup>

There is evidence that farnesol and geranylgeraniol (terpenoids) rapidly and competitively inhibit phosphatidylcholine biosynthesis, and that this is the cause of induction of apoptosis, at least in human lung adenocarcinoma A549 cells.<sup>30</sup> The last step of the CDP-choline pathway, also known as the Kennedy pathway, which is controlled by choline phosphotransferase, is affected.<sup>30</sup> *In vitro* assays on microsomal fractions clearly showed that farnesol and geranylgeraniol act by *competitive* inhibition with diacylglycerol (DAG) binding.<sup>30</sup> It is important to note that inhibition does not occur at the points in the CDP-choline pathway which are regulated by CTP: phosphocholine cytidyltransferase, the key enzyme of the pathway.<sup>30</sup> It was shown that the isoprenoid-induced apoptosis was preceded by an arrest in the G<sub>0</sub>/G<sub>1</sub> cell cycle phase and that these effects were *independent* of protein prenylation and MAP kinase.<sup>30</sup>

### 1.11.3 Anti-oxidation role played by isoprenoids

Limonene and its metabolite perillyl alcohol have cancer preventing and therapeutic properties.<sup>46</sup> In mammalian cells perillyl alcohol is rapidly metabolised to perillic acid and dihydroperillic acid.<sup>11</sup> The oxidation of perillyl alcohol to perillic acid presumably proceeds through perillaldehyde. Perillaldehyde is oxidised to perillic acid by aldehyde dehydrogenase and reduced to perillyl alcohol by alcohol dehydrogenase (scheme 12).<sup>47</sup>





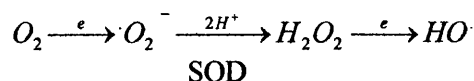
**Scheme 12** Oxidation and reduction of (*R*)-perillaldehyde

It is possible that perillaldehyde is an active metabolite, since compounds containing conjugated aldehyde-double bond structure are very reactive, especially to thiol groups in proteins.<sup>31</sup> This could lead to the possibility of perillaldehyde being a potential glutathione conjugate (*i.e.* scavenging reactive electrophiles, or consuming oxygen radicals).<sup>31</sup> It is also well known that many plant derivatives possess anti-oxidant properties.

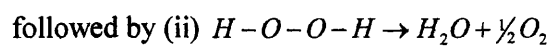
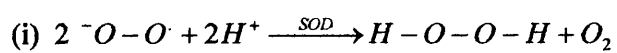
Reactive oxygen species (ROS) are produced by the reduction of molecular oxygen ( $O_2$ ). Oxidative phosphorylation occurs throughout the body, leading to the processing of about  $10^{12}$  oxygen molecules per cell per day. About 1% of these oxygen molecules are not consumed and result in the formation of ROS. The major ROS are:

Superoxide	$\cdot\text{O}-\text{O}\cdot$	(R = lipid)
Singlet oxygen	$^1\text{O}_2$	
Hydrogen peroxide	$\text{H}-\text{O}-\text{O}-\text{H}$	
Hydroxyl radical	$\text{H}-\text{O}\cdot$	
Alkanoyl radical	$\text{R}-\text{O}\cdot$	
Alkylperoxy radical	$\text{R}-\text{O}-\text{O}\cdot$	
Alkyl hydroperoxide	$\text{R}-\text{O}-\text{O}-\text{H}$	

Superoxide, hydroxyl radicals and hydrogen peroxide are the main ROS from mitochondrial oxidation, with superoxide *dismutase* (SOD) catalysing the formation of hydrogen peroxide:



*In vivo*, the initial step is usually the reduction of molecular oxygen to superoxide. Despite its name, superoxide is not a powerful oxidising agent and undergoes a relatively slow disproportionation to hydrogen peroxide and oxygen:



The above is a crucial pathway for the removal of radical oxidants in the body. In mammals, an increased lifespan is associated with higher levels of SOD.

## 1.12 References

- 1] Wattenberg, L. W. *Cancer Res.*, **1985**, *45*, 1
- 2] Greenwold, P.; Kellof, G. in 'The role of chemoprevention in cancer control', Prentice Hall, New York, 2<sup>nd</sup> ed. **1996**, *139*, 13
- 3] Landis, S.; Murry, T.; Bolden, S.; Wingo, P. *Cancer Statistics*, **1999**, *49*, 8
- 4] Shureigu, I. *Critical Reviews in Oncology/Hematology*, **2000**, *35*, 157
- 5] Gescher, A.; Pastorino, U.; Plummer, S. M.; Manson, M. M. *Br. J. Clin. Pharmacol.*, **1998**, *45*, 1
- 6] Crowell, P. L.; Gould, M. N. *Crit. Rev. Oncogenesis*, **1994**, *5*, 1
- 7] Gould, M. N. *J. Cell. Biochem.*, **1995**, *22*, 139
- 8] McNamee, D. *Lancet*, **1993**, *342*, 801
- 9] Seachrist, L. *NIH. Res.*, **1996**, *8*, 43
- 10] Crowell, P. L.; Lin, S.; Vedejs, E.; Gould, M. N. *Cancer Chemother. Pharmacol.*, **1992**, *31*, 205
- 11] Crowell, P. L.; Chang, R. R.; Ren, Z.; Elson, C. E.; Gould, M. N. *J. Biol. Chem.*, **1991**, *266*, 17679
- 12] Hardcastle, I. R.; Rowlands, M. G.; Barber, A. M.; Grimshaw, R. M.; Mohan, M. K.; Nutley, B. P.; Jarman, M. *Biochem. Pharmacol.*, **1999**, *57*, 801
- 13] Newman, A. A. in 'The Chemistry of Terpenes and Terpenoids', Academic Press, London, 1<sup>st</sup> ed. **1972**, vol 1, 20
- 14] van Duuren, B. L.; Goldschmidt, B. M. *J. Natl. Cancer Inst.*, **1976**, *56*, 1237
- 15] Elegbebe, J. A.; Elson, C. E.; Tanner, M. A.; Qureshi, A.; Gould, M. N. *J. Natl. Cancer Inst.*, **1986**, *76*, 323
- 16] Mills, J. J.; Chari, R. S.; Boyer, I. J.; Gould, M. N.; Jirtle, R. L. *Cancer Res.*, **1995**, *55*, 979
- 17] Stark, M. J.; Burke, Y. D.; McKinzie, J. H.; Ayoubi, A. S.; Crowell, P. L. *Cancer Lett.*, **1995**, *96*, 15
- 18] Jirtle, R. L.; Haag, J. D.; Ariazi, E. A.; Gould, M. N. *Cancer Res.*, **1993**, *53*, 3849

- 19] Solomons, T. W. G. in 'Organic Chemistry', Wiley, New York, **1996**, vol 23, 1106
- 20] Loudon, G. M. in 'Organic Chemistry', Addison-Wesley, New York, **1995**, vol 17, 806
- 21] Ruzicka, L. *Experientia*, **1953**, 9, 357
- 22] Jones, M. in 'Organic Chemistry', Norton, New York, **1997**, vol 12, 553
- 23] Verma, A. K. in 'Vitamins and Cancer Prevention', Wiley-Liss, New York, 2<sup>nd</sup> ed. **1991**, 21
- 24] Ionnides, C.; Ayrton, A. D.; Keele, A.; Lewis, D. F. V.; Flatt, P. R.; Walker, R. *Mutagenesis*, **1990**, 5, 257
- 25] Gudas, L. J.; Sporn, M. B.; Roberts, A. B. in 'Retinoids: Biology, Chemistry and Medicine', Raven, New York, ed. **1994**, vol 7, 443
- 26] Torrsell, K. B. G. in 'Natural product chemistry – a mechanistic and biosynthetic approach to secondary metabolism', Wiley, Chichester, 2<sup>nd</sup> ed. **1983**, 167
- 27] Corey, E. J.; Russey, W. E.; Ortiz de Montellano, P. R. *J. Am. Chem. Soc.*, **1966**, 88, 4751
- 28] Cordell, G. A. *Phytochemistry*, **1974**, 13, 2343
- 29] Crowell, P. L.; Chang, R. R.; Ren, Z. B.; Elson, C. E.; Gould, M. N. *J. Biol. Chem.*, **1991**, 266, 17679
- 30] Miguel, K.; Pradines, A.; Terce, F.; Selmi, S.; Favre, G. *J. Biol. Chem.*, **1998**, 273, 26179
- 31] Boon, P. J. M.; van der Boon, D.; Mulder, G. J. *Toxicol. Appl. Pharm.*, **2000**, 167, 55
- 32] Elson, C. E.; Maltzman, T. H.; Boston, J. L.; Tanner, M. A.; Gould, M. N. *Carcinogenesis*, **1988**, 9, 331
- 33] Elson, C. E.; Peffley, D. M.; Hentosh, P.; Mo, H. *Soc. Exp. Biol. Med.*, **1999**, 221, 294
- 34] Elegbede, J. A.; Elson, C. E.; Tanner, M. A.; Qureshi, A. A.; Gould, M. N. *J. Natl. Cancer Inst.*, **1986**, 76, 323
- 35] Haag, J. D.; Gould, M. N. *Cancer Chemother. Pharmacol.*, **1994**, 34, 477
- 36] Goldstein, J. L.; Brown, M. S. *Nature*, **1990**, 343, 425
- 37] Meigs, T. E.; Simoni, R. D. *Arch. Biochem. Biophys.*, **1997**, 345, 1

- 38] Tam, S. P.; Brissette, L.; Ramharack, R. Deeley, R. G. *J. Biol. Chem.*, **1991**, 266, 16764
- 39] Bansal, V. S.; Vaidya, S. *Arch. Biochem. Biophys.*, **1994**, 315, 393
- 40] Schmidt, R. A.; Schneider, C. J. Glomset, J. A. *J. Biol. Chem.*, **1984**, 259, 10175
- 41] Shafer, W. R.; Kim, R.; Sterne, R.; Thorner, J. Kim, S. H.; Rine, J. *Science*, **1989**, 245, 379
- 42] DeClue, J. E.; Vass, W. C.; Papageorge, A. G.; Lowy, D. R.; Willumsen, B. M. *Cancer Res.*, **1991**, 51, 712
- 43] Sinenski, M.; Logel, J. *Natl. Acad. Sci. USA*, **1985**, 82, 3257
- 44] Perez-Sala, D.; Mollinedo, F. *Biochem. Biophys. Res. Commun.*, **1994**, 199, 1209
- 45] Boggs, K. P.; Rock, C. O.; Jackowski, S. *J. Biol. Chem.*, **1995**, 270, 7757
- 46] Elegbede, J. A.; Elson, C. E.; Qureshi, A.; Tanner, M. A.; Gould, M. N. *Carcinogenesis*, **1984**, 5, 661
- 47] Ishida, T.; Toyota, M.; Asakawa, Y. *Xenobiotica*, **1989**, 19, 843

## Enzyme Inhibition

### 2.0 Aims of chapter

Since much of the work within this thesis centres on the inhibition of enzymes (*prenyl-protein transferase* and *histone deacetylase*), this chapter explores the principal features of enzymes and the various different types of inhibition that can occur.

### 2.1 Introduction

Almost all biological functions are supported by chemical reactions catalysed by enzymes, biological catalysts.<sup>1</sup> Enzymes speed up the rates of reaction without themselves being consumed. Enzymes accelerate chemical reactions under physiological conditions, 37 °C and neutral pH.<sup>1</sup> Enzymes increase the reaction rate by lowering the activation energy of the reaction but do not alter the equilibrium position of the process. Most forms of metabolism involve enzymes and regulation of their activities allows metabolism to adapt to rapidly changing conditions.<sup>1</sup>

### 2.2 Classification of enzymes

The classification of enzymes is either according to the *type* of reaction they catalyse, or the *composition* of the active enzyme. There are six major types of reaction, as shown in Table 1.<sup>2</sup>

Enzyme type	Reaction catalysed
Oxidoreductases	Oxidation – reduction reactions (transfer of hydrogen between substrates).
Transferases	Transfer of functional group containing C, N or P.
Hydrolases	Cleavage of bonds by the addition of water.
Lyases	Cleavage of C-C, C-O or C-N bonds other than by hydrolysis or oxidation-reduction reactions.
Isomerases	Conversion between <i>cis</i> - and <i>trans</i> -isomers, D- and L-isomers, or aldoses and ketoses.
Ligases	ATP-dependent condensation reactions.

Table 1 Classification of enzymes by reactions

According to the composition of active enzymes, there are two types:<sup>3</sup>

- Simple – enzymatic activity achieved by the structure of the enzyme alone.
- Complex – the enzyme requires additional cofactors for full enzymatic activity. An enzyme with its cofactor forming the fully active enzyme is known as a *holoenzyme*.

## **2.3 Protein structure of enzymes**

In proteins that consist of one polypeptide chain, there are three levels of organisation, primary, secondary and tertiary. Where two or more polypeptide chains are involved, each chain is a subunit and there is a quaternary level of structure.

### **2.3.1 Primary structure**

The primary structure is the sequence and type of covalently linked amino acids in a polypeptide chain.<sup>3</sup> Each primary structure is unique to each polypeptide chain and governs which higher structure it assumes. The biological, chemical and physical properties of the protein depend upon its primary structure.

### **2.3.2 Secondary structure**

This entails the interaction of the  $\text{--C=O}$  and  $\text{--NH}$  functional groups within the polypeptide chain *via* the formation of *intermolecular* and *intramolecular* hydrogen bonds. This allows the protein to fold in a stable conformation. Common types of secondary structure include the  $\alpha$ -helix,  $\beta$ -pleated sheets and  $\beta$ -turns.

The  $\alpha$ -helix (figure 1) consists of an *intrachain* hydrogen bond usually between the  $\text{--C=O}$  and  $\text{--NH}$  groups within the same polypeptide chain. These bonds are parallel to the axis of the helix.<sup>3</sup> Most  $\alpha$ -helixes contains about 12 amino acid residues (although the number can vary from 4 –50) with 3-6 residues per turn.

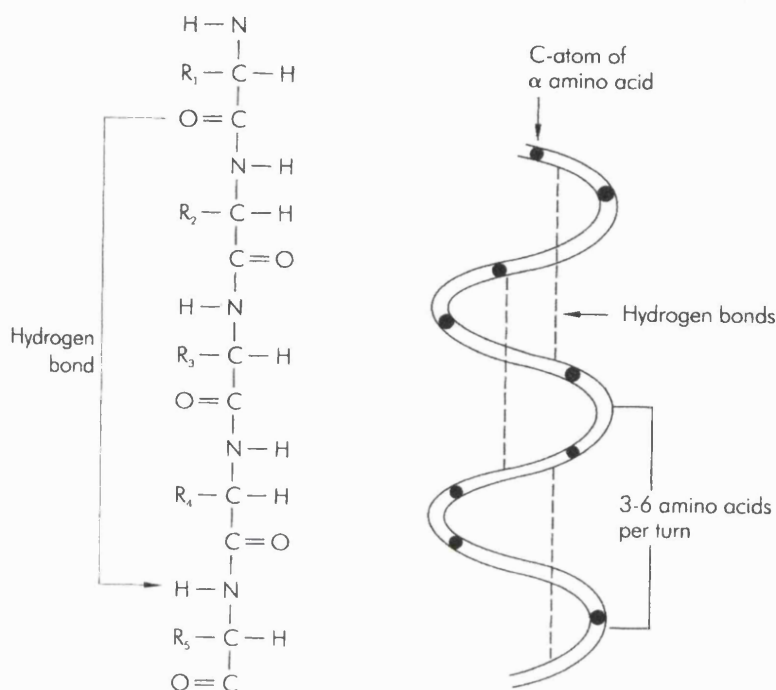


**Figure 1** Diagrammatic representation of an  $\alpha$ -helix<sup>3</sup>

$\beta$ -pleated sheet structures are formed by *interchain* hydrogen bonds between  $\text{--C=O}$  and  $\text{--NH}$  groups on adjacent polypeptide chains. Certain amino acids such as glycine and alanine in the polypeptide chain promote the formation of such secondary structures. The hydrogen bonds are perpendicular to the axis of the chain with the chain being almost fully extended.

A reversal in direction of the polypeptide chain usually results in a  $\beta$ -turn. A loop is formed in which the  $\text{--C=O}$  group forms a hydrogen bond with the  $\text{--NH}$  group of the amino acid residue three positions along in the polypeptide chain. Such turns lead the chain to become compact molecules, for example globular proteins with ellipsoidal or spherical shapes.<sup>3</sup>

### 2.3.3 Tertiary structure

This describes the orientation of the protein molecule caused by its various secondary structures interactions with the R-groups of the amino acid residues to give a three-dimensional shape. In general there are two forms, *globular* and *fibrous*.



The bond formations that preserve the tertiary structure include hydrogen bonding between amino acid side chains, hydrophobic bonds formed between amino acids containing hydrophobic R-groups (*e.g.* alanine, leucine and phenylalanine), ionic (electrostatic) bonds between amino acids containing oppositely charged side chains and covalent bonds, the most common type being a disulfide bond (bridge) between cysteine residues.

#### 2.3.4 Quaternary structure

The spatial arrangement of polypeptide chains in relation to one another in a multi-changed protein is the quaternary structure. Many enzymes as well as insulin and haemoglobin are examples of proteins where numerous subunits interact non-covalently to form the active protein molecule.<sup>3</sup>

### 2.4 Cofactors

As stated in section 2.2, the *complex* classification of an enzyme requires the presence of a cofactor for the full enzymatic catalysis to occur. There are two significant types of cofactor.

- inorganic molecules (metal ions),
- organic molecules (mostly derivatives of vitamins), known as coenzymes.

Cofactors are generally linked to enzymes by non-covalent bonds. A cofactor that is covalently bound is referred to as a prosthetic group.<sup>3</sup>

As the enzymes covered in chapter 3 and 5 require metal ions (zinc), only the inorganic cofactor type will be discussed here. Metal ions essentially assist enzyme activity by forming part of the catalytic subunit. An example of this is carboxypeptidase, (hydrolysis of proteins), which requires zinc for its activity in catalysing. Removal of the zinc metal ion by EDTA (ethylenediamine tetraacetic acid) causes a cessation in enzyme activity; when zinc is re-introduced, enzyme activity resumes.<sup>4</sup> In Table 2 are a few examples of metal ions (inorganic cofactors) required by several enzymes, giving some idea how important these inorganic cofactors are.<sup>4</sup>

Metal ion (inorganic cofactor)	Enzyme
Na <sup>+</sup>	Sucrose $\alpha$ -D-glucosidase
K <sup>+</sup>	Pyruvate kinase
Mg <sup>2+</sup>	Myosin adenosinetriphosphatase
Fe <sup>2+</sup>	Nitrogenase
Cu <sup>+2+</sup>	Cytochrome <i>c</i> oxidase

Table 2 Enzymes and their metal ions

## 2.5 Catalytic properties of enzymes

There are three main features to enzyme catalysis:

a) *Catalytic power*: enzymes greatly increase the rates of reaction,<sup>5</sup> in some cases by  $10^{17}$ . Since enzymes mostly operate at specific pH and temperature, there are not many direct comparisons with synthetic catalysts. Where such comparisons do occur, enzymes have no equals in the synthetic world.<sup>5</sup>

b) *Specificity*: this is derived from the nature of substrate(s) utilised and the reaction that is catalysed. Since enzymes has a relatively low specificity, in that they are not specific to the substrate as a whole but are specific to the cleavage or formation of a given bond. Such enzymes encompass a wide range of substrates (which all contain the particular chemical bond). Other enzymes exhibit *group specificity*; for instance, a hexokinase will catalyse the phosphorylation of a number of different sugars so long as they are aldohexoses. Most enzymes display *absolute* or *near-absolute* specificity and so will only catalyse a specific reaction with a specific substrate.

c) *Regulation*: this is the process by which the production of the enzyme is controlled. There are generally five processes by which such regulation can occur.

- The expression of the enzyme by its gene changes due to the cell's changing environment and demands.
- Proteolytic enzymes can irreversibly activate or inactivate the enzyme.
- Covalent modification, such as phosphorylation can reversibly activate or inactivate an enzyme.
- The reversible binding of small molecules to sites on the enzyme distant from the active site (allosteric regulation) is a rapid and usually first response of cells to the changing environment.

- The degradation of enzymes by intracellular proteases in the lysosome or by proteosomes in the cytosol determine the lifetime of the enzyme and consequently its activity.<sup>1</sup>

It is these last two features (specificity and regulation) of enzymes that really separate the biological catalysts from their synthetic ‘cousins’ and give enzymes a huge advantage.

## 2.6 Mechanism of enzyme action

The region of the enzyme that contains the binding catalytic region is known as the *active site*. This is only a small proportion of the enzyme compared to the total volume and is usually near or at the surface of the enzyme for accessibility to substrate molecules. The amino acid residues in the active site that do not play a role in catalysis may contribute to the specificity of the enzyme. Their side chains must be of appropriate size and shape as not to interfere with the binding of the substrate, but to hinder with chemically similar structures that do not exactly match.

The active site often contains both polar and non-polar amino acid residues creating hydrophobic and hydrophilic environments, which are not replicated elsewhere on the enzyme. Such microenvironments found in the active site usually play a big role in the enzyme’s specificity.

In 1894, Emil Fischer performed experiments that demonstrated enzyme specificity for substrates. On the basis of this work, he proposed the ‘*lock and key*’ hypothesis.<sup>4</sup> This postulation applies the role of the enzyme and substrate to that of a lock and key, where the enzyme is the lock and the substrate is the key. In figure 2, a pictorial representation of the ‘lock and key’ model is shown.<sup>4</sup>

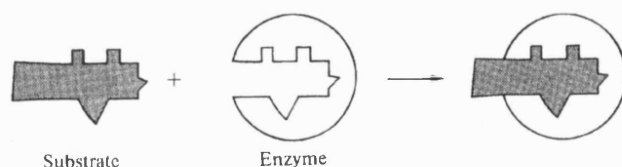


**Figure 2** Fischer’s ‘lock and key’ hypothesis

During the latter part of the 1950s, numerous experiments suggested that enzymes are considerably more flexible than expected from Fischer's 'lock and key' hypothesis. In 1958, Koshland introduced the 'induced fit' theory; which states that the enzyme undergoes structural changes as it interacts with the desired substrate. This requires the active site to be flexible and the substrate to be rigid structurally, allowing the enzyme to 'wrap' itself around the substrate, exactly as a glove fits onto a hand. Additionally, this theory explains how the binding of small molecules (other than the substrate) to the enzyme causes enzymatic activity and also how the enzyme works within a cell.<sup>4</sup>

## 2.7 Reaction profile of an enzymatic reaction

For a typical reaction, an energy profile shows the process from reactant(s) to product(s). To do this, an activation energy ( $\Delta G$ ) barrier must be overcome, as shown in figure 3.<sup>1</sup> For each molecule undergoing transformation, a point is reached along the reaction co-ordinate called the *transition state*, at which the energy level is at a maximum.<sup>1</sup> Since the transition state of the enzyme catalysed reaction is lower than that of the uncatalysed reaction, the enzyme catalysed reaction proceeds faster.

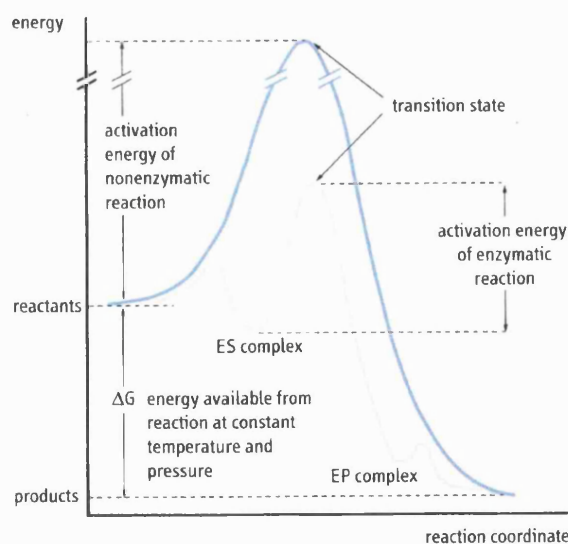


**Figure 3** Reaction profile for enzymatic and non-enzymatic reactions

Enzyme catalysis increases the rate at which the equilibrium between reactants and products is formed, but does not alter the ratio of reactants to products.

## **2.8 Factors affecting enzymatic reactions**

There are various factors that affect the rate of enzymatic reactions including substrates, products, intermediates and regulatory molecules. Two better-known factors are temperature and pH.

### **2.8.1 Temperature**

With a synthetic (inorganic) catalyst, increasing temperature would increase the rate of the reaction. As enzymes function within the body, only a limited range of temperature is viable, because the three-dimensional structure of the enzyme is held together by weak bonding interactions, for example hydrogen bonds. Such bonds can easily be broken by high temperature.

### **2.8.2 pH**

The pH in the body is in the range of 6.8-7.4 at which many enzymes function optimally. Since there are ionisable amino acids in enzymes, such as histidine, glutamate and cysteine, every enzyme has an optimum pH value. A few enzymes operate outside the normal pH range in the body, for example pepsin, which has a pH optimum of 1.5-2.0 (secreted by gastric cells and functions in gastric juice).<sup>1</sup> Changes in pH affect the ionic charge of the amino acids in the enzyme and can also greatly affect its catalytic activity.

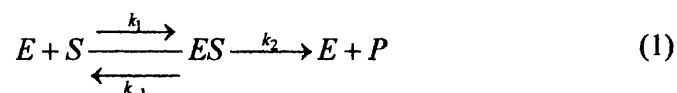
## **2.9 Definition of enzyme activity**

The activity of an enzyme is measured by determining the rate of an enzyme-catalysed reaction under defined conditions.<sup>1</sup> The reaction rate or velocity ( $v$ ) is usually expressed as the rate of conversion of substrate to product per minute, *i.e.* mol/min. Since the catalytic activity of an enzyme is normally independent of reaction volume, substrate turnover per unit of time under defined conditions (pH, temperature) is often used as the 'yardstick' definition of enzyme activity.<sup>1</sup> The amount of enzyme activity that catalyses the conversion of one mole of substrate into one mole of product per second is expressed as a katal (1 kat = 1 mol/s). However, such a unit is inconvenient for expressing actual enzyme activity, because it is usually

a very small number. A more common and convenient unit used is the international unit (IU), which is equal to 1  $\mu\text{mol}/\text{min}$ .<sup>1</sup>

## 2.10 Enzyme kinetics

In the beginning of the last century, (1913) long before advances in the knowledge of enzymology, Michaelis and Menten created a simple model (equation 1) for examining the kinetics of enzyme catalysed reactions. The primary assumption of the Michaelis-Menten model is that the substrate (S) binds reversibly to enzyme (E), forming an essential intermediate known as the enzyme-substrate complex (ES), which consequently decomposes to form product (P) and the enzyme.<sup>1</sup> In most cases, the reversible formation of ES cannot be measured, however, the second reaction (production of product) can be measured.



From the model (equation 1), an equation must be derived that describes the rate of enzyme activity (amount of product formed per time interval) as a function of substrate concentration. The rate of product formation equals the rate at which ES turns into E + P, which equals  $k_2$  times [ES]. This is especially helpful, because ES is unknown, therefore ES must be solved in terms of other quantities. This calculation is simplified by two assumptions. First, the concentration of ES is steady during the time intervals used for enzyme kinetic work. This implies that the rate of ES formation is equal to the rate of ES dissociation (either back to E + S or forward to E + P), as shown in equation 2. Second, the reverse reaction (formation of ES from E + P) is negligible, because the kinetics are derived at early time points where the concentration of product is very small.

Rate of ES formation = Rate of ES dissolution

$$k_1[S][E_{\text{free}}] = k_{-1}[ES] + k_2[ES] \quad (2)$$

The total concentration of enzyme,  $E_{\text{total}}$ , equals ES plus E. Therefore equation 2 can be re-written as:

$$k_1[S]([E_{total}] - [ES]) = k_{-1}[ES] + k_2[ES] \quad (3)$$

Solving for ES:

$$[ES] = \frac{k_1[E_{total}][S]}{k_1[S] + k_2 + k_{-1}} = \frac{[E_{total}][S]}{[S] + \frac{k_2 + k_{-1}}{k_1}} \quad (4)$$

The velocity (V) of the enzyme reaction therefore is:

$$V = k_2[ES] = \frac{k_2[E_{total}][S]}{[S] + \frac{k_2 + k_{-1}}{k_1}} \quad (5)$$

Finally, define  $V_{max}$  (the velocity at maximal concentrations of substrate) as  $k_2$  times  $E_{total}$ , and  $K_M$  (the Michaelis-Menten constant, as  $(k_2 + k_{-1})/k_1$ ). Giving the Michaelis-Menten equation (6):

$$V = \frac{V_{max}[S]}{[S] + K_M} \quad (6)$$

Analysis of the Michaelis-Menten equation implies that the Michaelis constant,  $K_M$ , has units of concentration and also corresponds to the substrate concentration at which  $v$  is 50 % of the maximum velocity, *i.e.* set  $[S]$  equal to  $K_M$  in equation 6, cancel the terms giving  $V = V_{max}/2$ .

A low  $K_M$  value indicates that the enzyme has a high affinity for the substrate and *vice versa*.<sup>3</sup>  $K_M$  is not a binding constant that measures the strength of binding between the enzyme and substrate. Its value includes the affinity of substrate for enzyme, but also the rate at which the substrate bound to the enzyme is converted to product, (only if  $k_2$  is much smaller than  $k_{-1}$  will  $K_M$  be equal to binding affinity).

The assumptions can hinder the validity of the Michaelis-Menten model, and thus assumptions below must always be borne in mind:<sup>1</sup>

- E, S and ES are in rapid equilibrium.
- There are no forms of enzyme present other than E and ES.

- The conversion of ES into E + P is irreversible.

## 2.11 Treatment of kinetic data from enzyme inhibition

It is very difficult to determine the limiting value of  $V$ , (*i.e.*  $V_{\max}$ ) from a plot of  $V$  (velocity) against  $[S]$  (substrate concentration), as shown in figure 4, (also known as the Michaelis-Menten plot),<sup>1</sup> nor can  $K_m$  values be readily extrapolated. To overcome this difficulty, the Michaelis-Menten equation (6) can be rearranged in a number of different ways to give suitable graphical representations. Three of the most commonly rearranged forms are described.

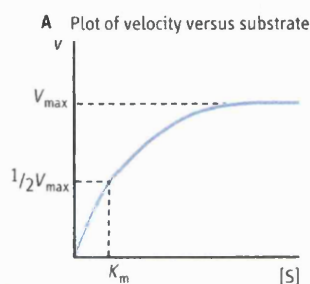


Figure 4 Michaelis-Menten plot

### 1. The Lineweaver-Burk equation

This equation is derived by taking reciprocals of the two sides from equation (6) to give:

$$\frac{1}{V} = \frac{K_M}{V_{\max}} \cdot \frac{1}{[S]} + \frac{1}{V_{\max}} \quad (7)$$

A plot of  $1/V$  against  $1/[S]$  gives a straight line of slope  $K_M/V_{\max}$  and intercepts on the x- and y-axis of  $-1/K_M$  and  $1/V_{\max}$  respectively.<sup>6</sup> The graphical form of the Lineweaver-Burk equation, shown in figure 5,<sup>1</sup> is still the most commonly used form for deriving kinetic data; it has the advantage that both  $V$  and  $[S]$  reciprocals are plotted on separate axes. However, analysis of the errors involved in the collection of data and the subsequent  $K_M$  and  $V_{\max}$  values, show a highly non-uniform distribution



of errors over the range (*i.e.* points in the line drawn), causing the intercept on the X-axis not to be ‘truly’ representative for the  $1/V_{\max}$  value.

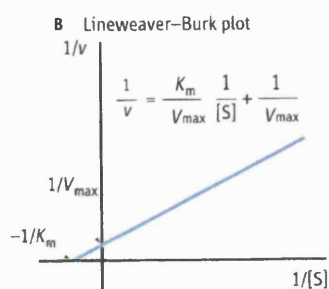


**Figure 5** Lineweaver-Burk plot

## 2. The Eadie-Hofstee equation

In this case the Michaelis-Menten equation is rearranged to give the following equation.<sup>7</sup>

$$V = V_{\max} - K_M \frac{v}{[S]} \quad (8)$$

Thus a plot of  $V/[S]$  against  $V$  gives a straight line of slope  $-K_M$  and an x-axis intercept of  $V_{\max}$ , as shown in figure 6.<sup>1</sup> Although less common than the Lineweaver-Burk plot, the Eadie-Hofstee plot is recommended because the data over the whole concentration range are more even weighted, therefore allowing the  $V_{\max}$  and  $K_M$  values to be more accurately obtained.

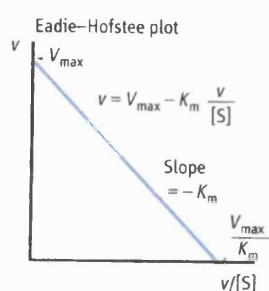


**Figure 6** Eadie-Hofstee plot

### 3. The direct linear plot

This method uses a different approach compared to either of the first two.<sup>8</sup> Once again equation (6) is rearranged to give:

$$V_{\max} = V + \frac{V}{[S]} K_M \quad (9)$$

Here  $V$  and  $[S]$  are the constants and  $V_{\max}$  and  $K_M$  are now treated as variables. If the first pair of observed values of  $V$  and  $[S]$  ( $V_1$  and  $[S]_1$ ) are plotted as shown in figure 7a,<sup>4</sup> the straight line connecting them describes the pairs of values of  $V_{\max}$  and  $K_M$  that are consistent with the observed values of  $V$  and  $[S]$ .<sup>4</sup> A straight line is drawn through the one set of experimental values; the dashed lines indicate pairs of values of  $V_{\max}$  and  $K_M$  that are consistent with the values obtained experimentally.<sup>4</sup>

If a second set of values of  $V$  and  $[S]$ , ( $V_2$  and  $[S]_2$ ) are drawn, a new line can be designated, as shown in figure 7b.<sup>4</sup> The point of intersection specifically defines the values for  $K_M$  and  $V_{\max}$  that comply with the two sets of data. This procedure can be repeated for further data points, (shown in figure 7b). Theory shows that the various lines should intersect at a common point, but owing to experimental error, several points of intersection may be observed.<sup>4</sup> In such cases the procedure is to use the median of the values of  $V_{\max}$  and  $K_M$  as the best-fit values.<sup>8</sup>

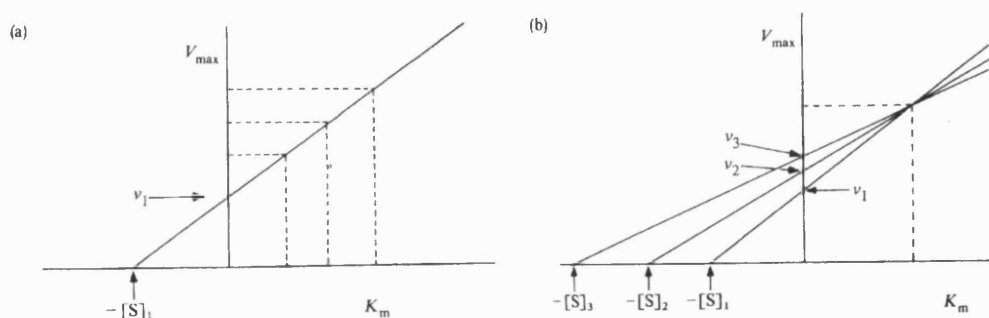


**Figure 7** (a) Direct linear plot with one set of experimental value, (b) direct linear plot with a number of sets of experimental values

Advantages of the linear plot over the Lineweaver-Burk and Eadie-Hofstee are:<sup>4</sup>

(a) the values of  $V$  and  $[S]$  are plotted directly, thus  $V_{\max}$  and  $K_M$  can be determined without further calculations, and (b) it is statistically sound (the use of median values of  $K_M$  and  $V_{\max}$  minimises the influence of extreme values of  $V$  and  $[S]$  on these

parameters). However, disadvantages of using the direct linear plot are that it can make analysis of multi-substrate reactions far too complex, with too many lines needed on the graph and secondly, it is not easy to detect deviations from the Michaelis-Menten equation.<sup>4</sup>

It has now become common to use 'best fit' values of  $V_{\max}$  and  $K_M$  by the use of non-linear regression computer programs<sup>9</sup> in which data are fitted directly to the Michaelis-Menten equation. Indeed, the kinetic data extrapolated for the results in chapters 3 and 5 were obtained using a 'best fit' computer package.<sup>10</sup>

## 2.12 Inhibitors

Compounds that decrease the rate of an enzyme catalysed reaction are called inhibitors.<sup>5</sup> There are two main types of inhibition; irreversible and reversible. Within these two main sections there are also many subdivisions. These are listed as below:

### *Irreversible inhibition*

- suicide inhibition
- transition state inhibition

### *Reversible inhibition*

- competitive inhibition
- non-competitive inhibition
- uncompetitive inhibition

#### 2.12.1 Irreversible inhibition

An irreversible inhibitor binds to the active site of the enzyme by an *irreversible* reaction and hence cannot consequently dissociate from it. A covalent bond is usually formed between the enzyme and the inhibitor. The inhibitor acts by either destroying a component of the active site in the enzyme or by preventing substrate binding. Irreversible inhibition is progressive and will increase with time until the enzyme present has been effectively used up in the enzyme-inhibitor complex. One type of

irreversible inhibitor is *suicide inhibition*, which operate by the enzyme trying to carry out normal bio-transformations on the inhibitor (believing it to be the substrate) and subsequently forms a covalent bond to the inhibitor that deactivates the enzyme.

A *transition state inhibitor* mimics the conformation of the active site when the substrate is bound to the enzyme. The transition states themselves cannot be isolated, because they are not a stable molecular assembly. However for some enzymes, analogues can be produced which have some structural features of the transition state. Penicillin is a famous example of a transition state inhibitor.<sup>1</sup> Penicillin contains a strained 4-membered lactam ring that mimics the transition state of the normal substrate. When penicillin binds to the active site of the enzyme, the lactam ring opens forming a covalent bond with a serine residue at the active site. The reactive peptide bond of penicillin is shown in figure 8. Penicillin is a potent irreversible inhibitor of bacterial cell-wall synthesis, making bacteria osmotically fragile and unable to survive in the body.<sup>1</sup>

**Structure of penicillin showing the reactive peptide bond**

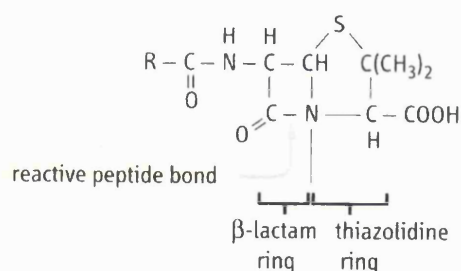


**Figure 8** Structure of penicillin showing reactive peptide bond in the  $\beta$ -lactam ring<sup>1</sup>

### 2.12.2 Reversible inhibition

The three main types of reversible inhibition are:

#### (a) *Competitive inhibition*

This is the most common type of inhibition. It occurs when the substrate and the inhibitor are both in *competition* for the same active site of the enzyme, as shown in figure 9.

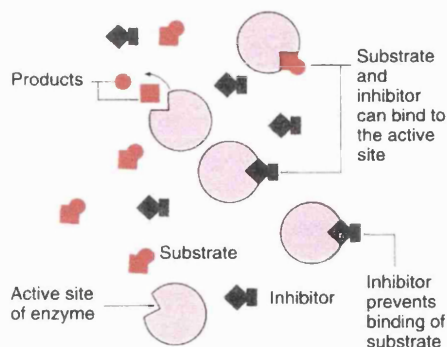
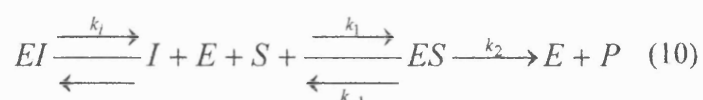


**Figure 9** Competitive inhibition<sup>11</sup>

The kinetic model for competitive inhibition is:



The inhibition constant ( $K_i$ ) is the dissociation constant of the enzyme-inhibitor complex (EI).<sup>1</sup> The lower the value of  $K_i$ , the more effective is the enzyme inhibitor. A characteristic of competitive inhibition, as shown in the Lineweaver-Burk plot below, is the apparent increase in  $K_M$  without changing  $V_{max}$ . This characteristic arises because the enzyme can bind to both the substrate and inhibitor forming both complexes, thus  $V_{max}$  remains unchanged. Since a higher concentration of substrate is required to obtain half the maximum rate in the presence of the inhibitor, the value of  $K_M$  increases.

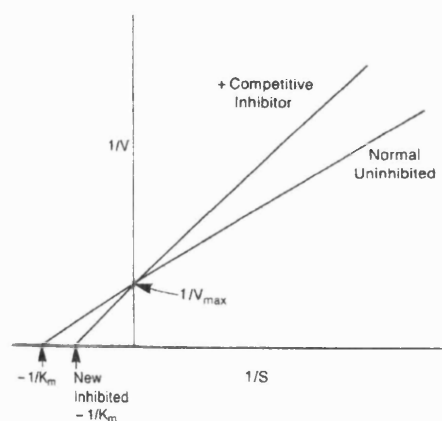


**Figure 10** Lineweaver-Burk plot of competitive inhibition<sup>12</sup>

*(b) Non-competitive inhibition*

With this type of inhibition, the inhibitor binds either to the free enzyme or the enzyme-substrate complex. However, whichever of these sites the inhibitor binds to is different from the active site where the substrate joins to the enzyme (hence the name). A pictorial representation of this particular inhibition is shown in figure 11.

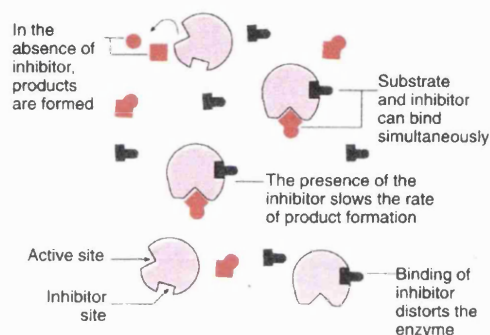


**Figure 11** Non-competitive inhibition<sup>11</sup>

Non-competitive inhibition has a more complex kinetic model (equation 11) than the other types of inhibition described in this chapter.



Addition of a non-competitive inhibitor, shown in a Lineweaver-Burk plot (figure 12), results in the lowering of  $V_{\max}$ , whilst the value of  $K_m$  remains unchanged. This is because the effect of the inhibitor is the same as completely blocking a percentage of the active site, thus equivalent to reducing the effective concentration of the enzyme, hence a lower value for  $V_{\max}$  is observed.

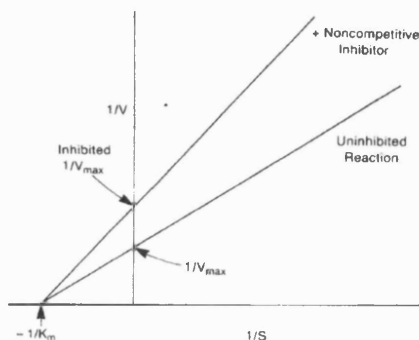


**Figure 12** Lineweaver-Burk plot of non-competitive inhibition<sup>12</sup>

*(c) Uncompetitive inhibition*

The term uncompetitive arises from the inhibitor that neither competes with the enzyme nor the substrate, but instead ‘attacks’ the enzyme-substrate complex [ES]. As shown in figure 13, the inhibitor cannot bind to the enzyme unless the substrate is first attached to the enzyme.

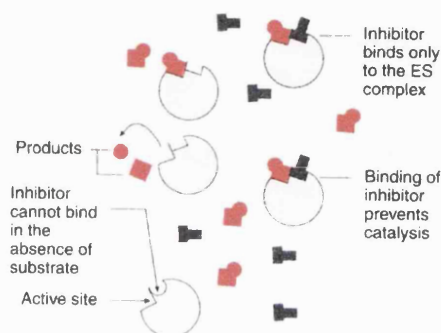


**Figure 13** Uncompetitive inhibition<sup>11</sup>

The kinetic equation for uncompetitive inhibition is shown below:



The characteristic of uncompetitive inhibition is the decrease for both  $V_{\max}$  and  $K_M$  values. The uncompetitive inhibitor diverts a percentage of the enzyme-substrate complex [ES] to the enzyme-substrate-inhibitor complex [ESI], causing a decrease in the amount of enzyme-substrate complex, consequently decreasing the amount of product formed, hence the value of  $V_{\max}$  decreases. The enzyme-substrate-inhibitor complex also increases the affinity between the enzyme and the substrate. Thus, dissociation of the substrate from the complex to form the product is reduced, causing a sequential reduction in the  $K_M$  value, (shown with a Lineweaver-Burk plot in figure 14).

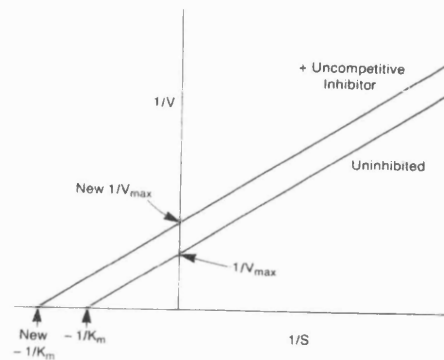


**Figure 14** Lineweaver-Burk plot of uncompetitive inhibition<sup>12</sup>

### 2.13 Allosteric enzymes

Although Michaelis-Menten kinetics have significantly explained many facets of enzyme inhibition, there are examples for which it is unsatisfactory. One such case is allosteric regulation. As shown in figure 4, the substrate saturation curve is hyperbolic. However for allosteric enzymes, a sigmoidal plot is often observed on a plot of reaction velocity and substrate concentration. An example of an enzyme exhibiting allosteric regulation is *aspartate transcarbamoylase* (ATCase). A graph showing ATCase's allosteric activity in producing sigmoidal curves is shown in figure 15.<sup>1</sup>

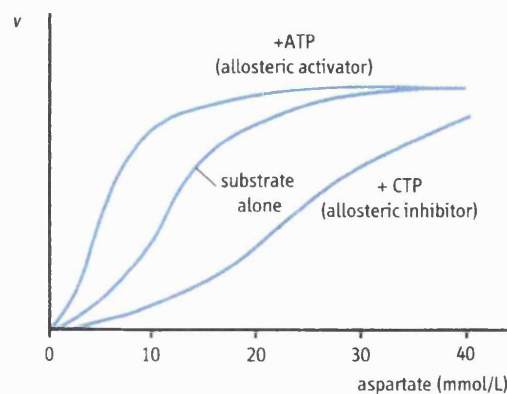


**Figure 15** Allosteric regulation of ATCase



When the substrate itself is the effector molecule, this is known as the *homotropic* effect. When the effector molecule is not the substrate, this is referred to as the *heterotropic* effect. A heterotropic effector molecule binds to the enzyme at a separate site than where the substrate would join, but affects the overall substrate binding and consequently reaction velocity.<sup>1</sup>

Homotropic effects are observed when the reaction of one substrate with an enzyme affects the reaction of a second substrate on a different active site of a multi-site enzyme. The interaction between the effector molecules makes the binding of successive substrates positive (*cooperative*) or negative, both of which result in the sigmoidal curves in the plot of reaction velocity and concentration of substrate.<sup>1</sup> In the case of figure 15, the aspartate (substrate) homotropically regulates ATCase activity, providing the sigmoidal kinetics. The end product of the enzyme-catalysed reaction, CTP, heterotropically inhibits the activity of ATCase leading to the decreased reaction velocity (allosteric inhibition). The precursor to the reaction, ATP, heterotropically activates ATCase, thereby increasing the reaction velocity, and is therefore an allosteric activator (cooperative effect).<sup>1</sup>

### 2.13.1 Allosteric regulation

The affect the allosteric effector molecule has on overall substrate binding and reaction velocity is known as allosteric regulation. There are both positive and negative forms of regulation.<sup>1,4,11</sup> Positive regulation (cooperativity) indicates the reaction of a substrate with one active site makes it easier for another substrate to react at another active site on the enzyme.<sup>1</sup> Negative regulation means that the reaction of a substrate with an active site makes subsequent substrate interaction at a different active site within the enzyme harder.<sup>1</sup>

Since the affinity for substrates by the enzyme changes with substrate concentration, Michaelis-Menten kinetics cannot be used. Instead allosteric regulation is described with the use of the Hill coefficient. This is based on an equilibrium expression as follows:

$$K = \frac{[R][L]^n}{[RL_n]} \quad (11)$$

where  $[RL_n]$  is the concentration of receptor with n bound ligands:

$$\therefore y = \frac{[RL_n]}{[R_{tot}]} \quad (12)$$

$$\text{Since } [RL_n] = [R_{tot}] - [R] \quad (13)$$

$$\text{Then } 1 - y = \frac{[R]}{[R_{tot}]} \quad (14)$$

Which gives the derivation of:

$$\frac{y}{(1-y)} = \frac{[RL_n]}{[R]} \quad (15)$$

$$\text{but } [RL_n] = \frac{[R][L]^n}{K} \quad (16)$$

$$\text{giving } \frac{y}{(1-y)} = \frac{[L]^n}{K} \quad (17)$$

Therefore, the Hill equation:

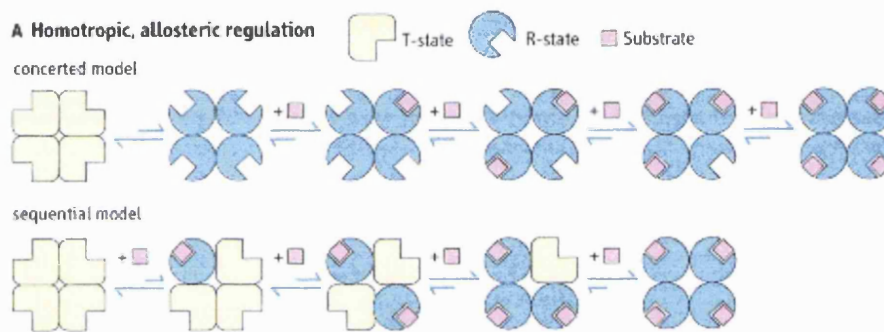
$$\log\left[\frac{y}{(1-y)}\right] = n \log[L] - \log k \quad (18)$$

where n is known as the Hill coefficient and y is the fractional saturation.<sup>11</sup>

In the derivation of the Hill equation, various assumptions are made about the binding of the ligand to the enzyme that may not occur in practice. Consequently, the Hill coefficient is used only as a conventional indicator as to the nature of the ligand-binding interaction.<sup>11</sup> If  $n=1$ , there is no regulation, as in the case of myoglobin.<sup>11</sup> If  $n > 1$ , cooperativity occurs, if  $n < 1$ , negative regulation is occurring.<sup>11</sup>

The most common model used to explain allosteric regulation was described by Monod, Wyman and Changeaux, and called the concerted model (scheme 1).<sup>1</sup> In the absence of substrate, the enzyme has a low affinity for substrate, and is in a T-state (tense state).<sup>1</sup> The other conformation of the enzyme is the R-state (relaxed state). The binding of the allosteric effector molecules shifts a fraction of the enzyme from

one state to the other. The enzyme is shifted to the R-state by the binding of positive allosteric effector molecules (cooperativity), whilst the enzyme is stabilised in the T-state by the binding of negative allosteric effector molecules.<sup>1</sup> In scheme 1, all active sites in the R-state are the same and have increased substrate affinities than in the T-state, and it is called the concerted model because the transition between the T- and R-states occurs at the same time for all subunits. The sequential model (scheme 1) proposes that each active site changes to the different conformation (T- to R-state or *vice versa*) one at a time, (*i.e.* sequentially), as opposed to all at once, as described above in the concerted model.<sup>1</sup> Both the concerted and sequential models are shown in scheme 1 with the substrate being the allosteric effector molecule, and are therefore examples of homotropic allosteric regulation.



**Scheme 1** Concerted and sequential allosteric regulation<sup>1</sup>

## 2.14 References

- 1] Baynes, J.; Dominiczak, M. H. in 'Medical Biochemistry', Mosby, New York, 3<sup>rd</sup> ed. 1999, vol. 5, 43
- 2] Palmer, T. in 'Understanding Enzymes', Prentice Hall, New York, 1995, 3
- 3] Thabrew, I.; Ayling, R. M.; Wicks, C. in 'Biochemistry For Clinical Medicine', Greenwich, London, 2001, vol 9, 111
- 4] Price, N. C.; Stevens, L. in 'Fundamentals Of Enzymology', Oxford, University Press, 1999, vol 1 and 4, 1 and 118
- 5] Holbrook, J. J.; Liljas, A.; Steindel, S. J.; Rossmann, M. G. in 'The Enzymes', Prentice Hall, New York, 1975, vol 11, 191
- 6] Lineweaver, H.; Burk, D. *J. Am. Chem. Soc.*, 1934, 56, 658
- 7] Hofstee, B. H. J. *J. Biol. Chem.*, 1952, 199, 357
- 8] Cornish-Bowden, A. C.; Eisenthal, R. *J. Biochem.*, 1974, 139, 721
- 9] Duggleby, R. G. *Methods Enzymol.*, 1995, 249, 61
- 10] Motulsky, H. in 'Analyzing data with GraphPad Prism', 1999, GraphPad Software Inc., San Diego CA, [www.graphpad.com](http://www.graphpad.com)
- 11] Campbell, P. N.; Smith, A. D. in 'Biochemistry Illustrated', Churchill Livingstone, New York, 2000, vol 6, 75
- 12] Schumm, D. E. in 'Essentials of Biochemistry', Little Brown and Co., Boston, 1995, vol 11, 117

## Prenyl-Protein Transferase Inhibitors and a Potential Cancer Therapy

### 3.0 Introduction

(+)-Limonene, the major monoterpene found in orange peel oil, has substantial chemopreventive and chemotherapeutic activity against chemically induced mammary, lung and stomach cancers in rodents;<sup>1</sup> it was the first selective inhibitor of protein-isoprenylation to be shown to have *in vivo* chemotherapeutic activity.<sup>1</sup> A study at Charing Cross Hospital showed that limonene at high dosage could be an effective treatment of female breast cancer. Limonene, or more likely its metabolites,<sup>1</sup> selectively inhibit protein-prenylation of a class of G-proteins, including Ras proteins. The post-translational modification of the *Ras* gene is integrally connected with mammalian cancers, and inhibitors of the functioning of Ras have advantages over existing chemotherapeutic agents on account of their greater selectivity.<sup>2</sup> It seems remarkable that limonene (a simple hydrocarbon) can show any anti-cancer activity. A mechanism of action quite distinct from conventional anti-cancer drugs (*e.g.* alkylation of DNA) appears probable. Moreover, terpenoid agents would have major advantages such as high dosage tolerance, very low toxicity and importantly, be cost-effective. The mechanism by which the chemotherapeutic properties of monoterpenoids is conferred (as discussed in Chapter 1) is uncertain; however, a study at Charing Cross Hospital was consistent with inhibition of protein-prenylation of Ras proteins being a key mechanism. Consequently, the aim was to create a model for the design of *terpenoid inhibitors* of prenyl-protein transferase for the chemoprevention of cancer. This model would hopefully provide a rational and mechanistic basis for the design of new inhibitors of farnesyl-protein transferase (FPTase) and geranylgeranyl-protein transferase (GGPTase); a new approach to cancer chemotherapy.<sup>3</sup> A detailed section now follows on the mechanism of prenylation of Ras proteins and the various inhibitors reported in the literature. A model for the new protein-prenylation transferase inhibitors (based on terpenoids) is then discussed, and also the compounds prepared in this work and their subsequent evaluation.

### 3.1 *Ras* genes and *Ras* proteins

*Ras* proteins are small guanine-triphosphate (GTP) proteins that are essential for cell signalling and proliferation. It is this function of cell signalling and proliferation that is so significant, especially when considered that in 30% of all human cancers, *mutated Ras* genes have been detected. This indicates an important role of abnormal *Ras* function in cancer activation or sustainment.

In different types of cancer, the percentage of mutated *Ras* genes varies. The highest incidence occurring for pancreatic (90%), colorectal (50%) and lung (40%) cancer, whilst only 5% for ovarian, cervical and breast cancer.<sup>4</sup> This variation suggests that mutation of *Ras* genes and subsequent *Ras* protein production do not directly result in either instigating or promoting cancerous tumours. Nevertheless, as *Ras* proteins are known to be essential in signalling pathways that regulate cell proliferation, differentiation and apoptosis, it may be another cellular component involved with *Ras* in these processes that causes abnormal function of *Ras*. Therefore the presence of mutated *Ras* genes and subsequent proteins may not be necessary for carcinogenesis to occur.<sup>5,6,7</sup> One example of this is the over-expression of epidermal growth factor (EGF) on cell surface receptor tyrosine kinases (RTKs), a fundamental cause of breast cancer. For this to take effect, the transforming properties of RTKs are dependent on cell signalling and gene amplification *via* *Ras* proteins.<sup>8</sup> Also important are the abnormalities that arise from the loss of *Ras* regulators. For example, the deficit of tumour suppressor genes *via* malignant schwannomas (type 1 neurofibromatosis) causes up-regulation of *Ras* functions leading to abnormalities.<sup>9,10</sup> Consequently, the connection of *Ras* genes with cancer is more widespread than first thought, and not just confined to cancer growths containing the mutated *Ras* genes.

*Ras* genes are not only present in humans but in other mammals, insects, plants and fungi. Indeed, the term *Ras* arose from the detection in rats of a sarcoma found to contain the mutated G-protein, hence *Ras* (Rat) and (sarcoma).<sup>4</sup> In mammals, four types of *Ras* genes have been identified. They are known as H-*Ras*, K-*Ras*-4A, K-*Ras*-4B and N-*Ras*. All four possess high amino acid homology (~90%) and exhibit the same transforming action in experimental animal studies and cell cultures.<sup>11</sup> Accordingly, the assumption was made that all four would have similar biochemical

and biological properties.<sup>12,13</sup> However, this appears not to be the case and indeed *essential* differences can be ascertained.

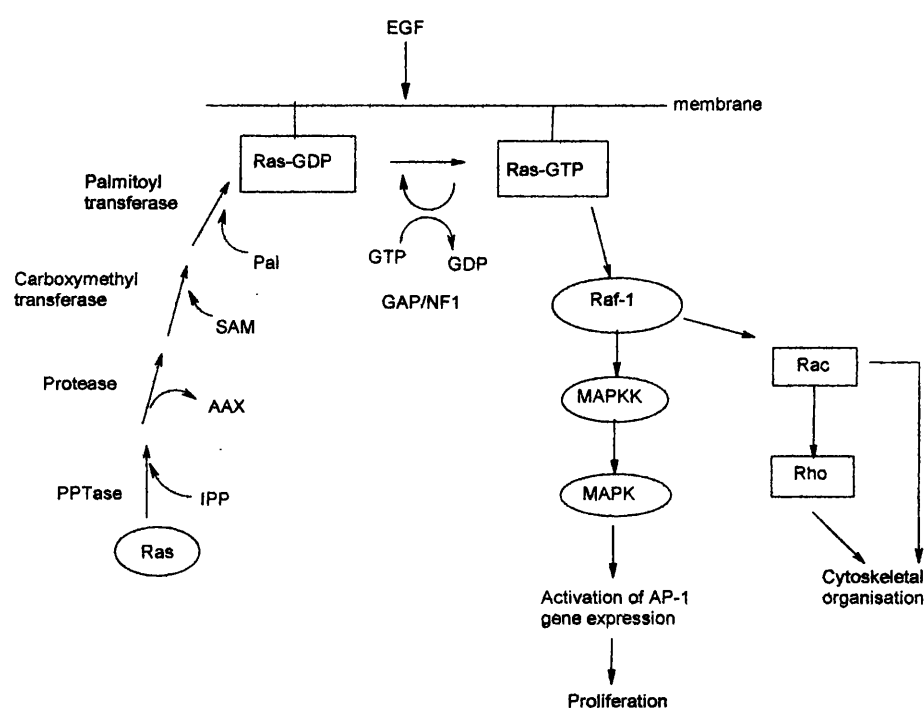
The first gene whose mutation was identified was *H-Ras*; consequently, the greatest amount of research was conducted on the *H-Ras* gene. However, the *H-Ras* mutation is the least commonly associated with cancerous growths.<sup>14</sup> Mutations in the *K-Ras* and *N-Ras* genes are most frequent. *K-Ras* is often discovered in pancreatic, colorectal and lung cancer,<sup>14</sup> whilst *N-Ras* is associated with the haematopoietic varieties of cancerous growths. However, the level of study into the *K-* and *N-Ras* mutations are considerably less than compared with the *H-Ras* gene, and as such any conclusions inferred from the study into *H-Ras* may not be applicable to either of the other (more important) mutations.

While the evidence *suggests* abnormal Ras function contributes to certain aspects of malignant tumours, Ras mutations *alone* do not possess the capability of transforming ‘normal’ cells into malignant ones.<sup>4</sup> This implies that an overall effect obtained from two or more oncogenic sources, such as mutated Ras and either a loss of a tumour suppressing gene or mutated EGF-RTKs are needed for such a malignancy to grow.<sup>15,16,17</sup> This multi-step nature of cancerous growths perhaps explains the diverse effects observed from the consequences of mutated *Ras* genes.

### 3.2 The Ras pathway

To be able to produce compounds that are effective against isoprenoid protein-prenylation, an understanding of the Ras signalling pathway is vital. The binding of different growth factors, such as epidermal growth factor (EGF) to the membrane-bound receptor tyrosine kinases (RTKs) effects a dimerisation and autophosphorylation of the tyrosine residues on the protein surface.<sup>18</sup> This is recognised by src-homology 2 domain (SHC) on the growth factor receptor binding protein (GRB2), which is complexed to a guanine nucleotide exchange protein, known as m-SOS-1.<sup>19</sup> This in turn activates the membrane-bound Ras protein by catalysing the formation of Ras GTP (guanine triphosphate) from the Ras GDP (guanine diphosphate) form.<sup>20</sup> A conformational change occurs when becomes GTP activated, allowing several effector molecules to bind, one of which is Raf-1 (a

serine/threonine kinase), and has been thoroughly investigated.<sup>21</sup> Translocation of Raf (an effector molecule) to the membrane results in DNA (deoxyribonucleic acid) synthesis *via* activation of mitogen activated protein kinase kinase (MAPKK) and commencement of a number of steps through mitogen activated protein kinase (MAPK), leading to the activation of transcription factors, eventually causing DNA production.<sup>22</sup> Therefore, the action of all four Ras proteins (H, K-4A, K-4B and N) resemble *biological switches* and all four Ras proteins are regulated by GDP to GTP exchange, as shown in Scheme 1.



**Scheme 1** Ras pathway<sup>23</sup>

From the pathway of Ras proteins, four main approaches can be postulated for inhibition strategies. The first two methods centre on the exchanging GDP/GTP forms of the Ras proteins.<sup>24</sup> The creation of 'super' Ras-GAPs that are able to return the GTP-bound Ras to the non-active GDP state. Also, as conformational changes occur on the Ras protein to form the active GTP-form, allows the creation of agents that can specifically target the GTP-Ras protein.<sup>25,26,27</sup>

The third approach is to block mutated Ras protein signalling going 'downstream' the Ras pathway by interfering with the effector molecules (Raf) and MAPKK, thereby

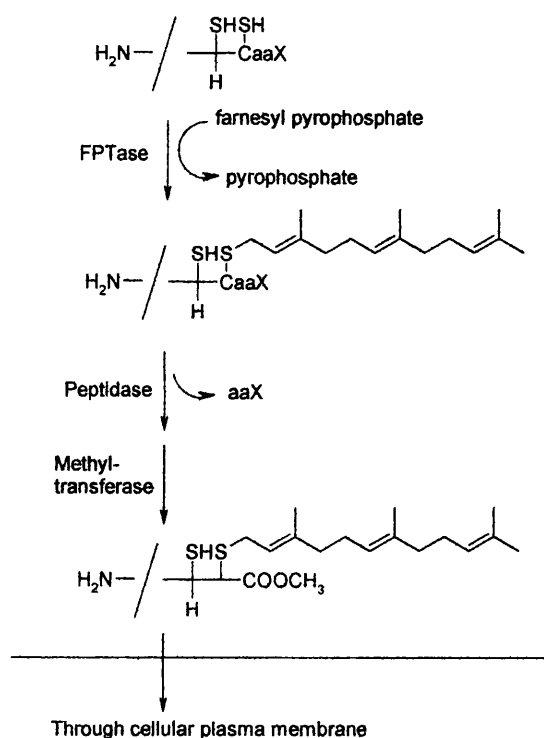


preventing activated Ras signals from transforming cells and leading to growth or differentiation.<sup>28,29,30</sup>

The fourth and final approach induces inhibition of Ras proteins by the non-activation of prenyl-protein transferases.

### 3.2.1 The importance of prenyl-protein transferases to the Ras pathway

Ras proteins require lipid modification for association with the plasma membrane and resulting activation.<sup>31,32,33</sup> To begin with, Ras proteins are inactive *cytoplasmic* proteins, however post-translation modification of the COOH-terminal tetrapeptide causes the translocation of the Ras protein to the inner surface of the plasma membrane. This terminal tetrapeptide is commonly referred to as the CaaX box or motif (a structural domain).<sup>18</sup> The CaaX box consists of a cysteine amino acid (C) two aliphatic amino acids (aa) and any terminal amino acid (X). It is this structural domain where farnesyl-protein transferase (FPTase) or a geranylgeranyl-protein transferase (GGPTase) are involved. Such enzymes catalyse the addition of a farnesyl- or geranylgeranyl-isoprenoid unit to the cysteine amino acid of the CaaX box from either farnesyl pyrophosphate (FPP) or geranylgeranyl pyrophosphate (GGPP) donor.<sup>32</sup> As shown in Scheme 2, the isoprenoid unit is attached *via* a sulfur linkage, followed by the removal of the aaX amino acid residues. Carboxymethylation occurs to the now farnesylated or geranylgeranylated cysteine residue, and subsequent additional modifications by palmitate (a fatty acid). This additional modification by palmitate allows greater binding of the Ras protein to the plasma membrane, but the initial addition of the isoprenoid unit followed by the carboxymethylation of the cysteine amino acid residue is enough to allow plasma membrane association of the Ras protein and subsequent activation.



**Scheme 2** Farnesylation of Ras protein allowing plasma membrane association

### 3.3 Farnesyl-protein transferase (FPTase)

FPTase was first identified from rat cytosol samples and was purified by a CaaX peptide affinity column.<sup>34,35</sup> The enzyme consists of a heterodimer, with  $\alpha$ - and  $\beta$ -subunits totalling 48 and 46 kD respectively,<sup>35</sup> as shown in figure 1. FPTase binds to FPP in a *non-covalent* manner forming a stable complex that can be isolated from gel filtration. The binding of enzyme to substrate is known to be non-covalent because when enzyme denaturation occurs, FPP is released.<sup>36</sup> From various cross-linking experiments the active binding site has been shown to be on the  $\beta$ -subunit of FPTase, to which both the Ras protein and FPP were bound.<sup>37</sup> However, neither the  $\alpha$ - or  $\beta$ -subunits are capable of catalytic activity on their own, thus the active site of the FPTase enzyme is thought to be close to the interface between the two subunits.<sup>38,39</sup>

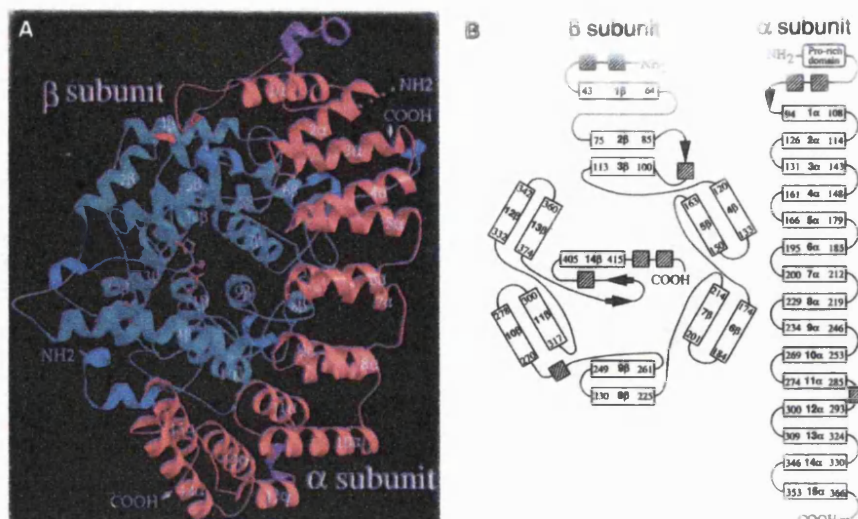


**Figure 1** Structure of FPTase heterodimer<sup>40</sup>

FPTase is a zinc heterodimer,<sup>42</sup> as shown with the H-Ras protein in which the enzyme was treated with EDTA, its binding ability was reduced. However with the addition of  $\text{Zn}^{2+}$ , the binding ability was restored to its full activity, thus it would seem that FPTase requires  $\text{Zn}^{2+}$  cations to function to its full potential.<sup>43</sup> A hypothesis states that at the active site of the enzyme, the  $\text{Zn}^{2+}$  cation is required to increase the nucleophilicity of the enzyme by coordinating to the cysteine sulfhydryl group present in the substrate.<sup>40</sup> An examination of the  $\beta$ -subunit revealed that within the 437 amino acid sequence there was no obvious metal-binding site, even though it is known that  $\text{Zn}^{2+}$  is required for FPTase function.<sup>39</sup> Thus, the question of whether the cysteine sulfhydryl group of the terminal tetrapeptide of the Ras protein binds to the zinc ion is still unclear, but it maybe that the metal plays a structural role or is involved in the actual catalysis.<sup>40</sup>

Initial results from steady-state kinetics suggested that the farnesylation process proceeded *via* an ordered sequential mechanism, with FPP and the Ras protein binding independently to the enzyme.<sup>44</sup> This mechanism was latter confirmed from various substrate-binding experiments.<sup>45</sup> However, in later experiments involving isotope partitioning studies, the results indicated that the catalytic pathway contains an enzyme-FPP binary complex. This was confirmed with pre-steady-state kinetic experiments that showed the first step in the catalytic pathway is the formation of the FPTase-FPP complex.<sup>46</sup> The same study indicated that conformational changes

occurred within the binary complex before farnesyl group transfer, and consequently the product release would be the rate-limiting step.<sup>46</sup>

Small peptides as short as four amino acids which are similar to the C-terminal box of the Ras proteins have shown similar activities compared to the Ras proteins themselves, indicating the structural requirement for FPTase from the Ras proteins is contained within the CaaX amino acid residues of the carboxy-terminus.<sup>47</sup> A systematic study of the Ca<sub>1</sub>a<sub>2</sub>X tetrapeptide using many different amino acids showed strong preference by the FPTase enzyme for specific amino acids at the a<sub>1</sub>a<sub>2</sub>X positions.<sup>48</sup> While the cysteine amino acid is essential in the CaaX box, the a<sub>1</sub>a<sub>2</sub> positions are normally occupied by *non-polar hydrophobic aliphatic* amino acids. This is of more importance for the a<sub>2</sub> position within the Ca<sub>1</sub>a<sub>2</sub>X box. Charged amino acids at the a<sub>1</sub> position reduce enzyme affinity, and charged amino acid residues at the a<sub>2</sub> position virtually nullify enzyme preference. It is the terminal amino acid of the CaaX box that showed the greatest effect when varied, and thus has the highest selectivity for the FPTase enzyme. When the first three amino acids are cysteine-valine-isoleucine, methionine shows the greatest selectivity for FPTase at position X.<sup>4</sup> To a lesser extent, serine and phenylalanine are also good amino acids at the X position, while glutamic acid, lysine and glycine all show greatly reduced affinity for the FPTase enzyme.<sup>4</sup> Consequently, FPTase enzymes are *selective to methionine* ending carboxy-terminus Ras proteins (structure of methionine displayed in figure 2).

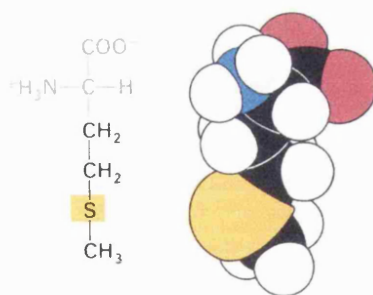


**Figure 2** The amino acid methionine and its space-filler model<sup>49</sup>

### 3.4 Geranylgeranyl-protein transferase (GGPTase)

There are two types of GGPTase enzymes, geranylgeranyl-protein transferase type-1 (GGPTase-I) and geranylgeranyl-protein transferase type-2 (GGPTase-II).<sup>50</sup>

GGPTase-I is very similar to FPTase as they both contain the same  $\alpha$ -subunit and their  $\beta$ -subunits contain 30% amino acid homology.<sup>50</sup> Also GGPTase-I utilises the same CaaX structural motif as FPTase. However, leucine is terminal amino acid favoured by GGPTase-I rather than methionine as preferred by FPTase.<sup>50</sup> Latterly, the greatest amount of research has centred on GGPTase-I as it was discovered that mutated K-Ras protein signalling was geranylgeranylated, and therefore a GGPTase-I inhibitor would be able to block K-Ras protein signalling. This is a very important aspect as the most frequently discovered mutated Ras protein in human cancers is *K-Ras*.<sup>51</sup> Another reason why GGPTase function is important is because Ras proteins which have been unable to utilise the FPTase transfer mechanism due to inhibition or any other reason can still effect protein prenylation through up-regulating geranylgeranylation, as even potent FPTase inhibitors do not affect the GGPTase enzymes.<sup>51</sup>

GGPTase-II has different  $\alpha$ - and  $\beta$ -subunits from either GGPTase-I and FPTase enzymes and complexes to a protein called the Rab escort protein (REP) which directs the protein substrate to the catalytic active site.<sup>45</sup> GGPTase-II also favours a different carboxy-terminus in Ras proteins, while both FPTase and GGPTase 'attack' CaaX motifs, GGPTase-II prefers tetrapeptides in the manner of xxCC and xCxC form, where x is any aliphatic amino acid and C is the cysteine amino acid residue.<sup>45</sup> Finally, the interactions between GGPTase-II and the Ras protein are much more complex than its counterparts, GGPTase-I and FPTase and require various protein sequences in addition to the carboxy-terminal tetrapeptide for recognition.<sup>45</sup>

### **3.5 Design of prenyl-protein transferase inhibitors**

The primary strategies for farnesyl-protein transferase inhibitors (FPTIs) and geranylgeranyl-protein transferase inhibitors (GGPTIs) are divided into five main areas:

1. *Peptidomimetics*
2. *Non-peptidomimetics*
3. *Competitive prenyl pyrophosphate substrate inhibitors*
4. *Bisubstrate analogues*
5. *Natural products*

### 3.5.1 Peptidomimetics

This class of FPTIs and GGPTIs utilise the CaaX tetrapeptide found in Ras proteins and mimics the carboxy-terminal ending to function as a potent competitive inhibitor.<sup>52</sup> Several groups have utilised the pseudo peptide strategy in which the peptide bonds in the CaaX box are reduced to their methylamino forms.<sup>53</sup> The examples shown in figure three are specific for FPTase inhibition. Compound **L731735** is specific to inhibiting FPTase for the H-Ras protein, with an inhibition value of 20 nanomolar (nM). **L731734**, the corresponding lactone, has greater cellular uptake due to the masking of the negative charge of the carboxy-group, however the potency was reduced to 100 micromolar ( $\mu$ M).<sup>54</sup> This approach led to the development of an methyleneoxy isotere **L739750**, a very potent FPTase inhibitor ( $IC_{50}$  value of 1.8 nM). The pro-drug version **L739749T** inhibits FPTase in H-Ras at a concentration of 0.5  $\mu$ M and also suppressed the growth of *mutated* H-Ras tumours in nude mice.<sup>55</sup> Another similar pro-drug **L744832** inhibited the growth in 70% of all tumour cell lines tested at concentrations as low as 2  $\mu$ M.<sup>56</sup> The pro-drug also instigated regression of mammary carcinomas in transgenic mice infected with mutated H-Ras proteins.

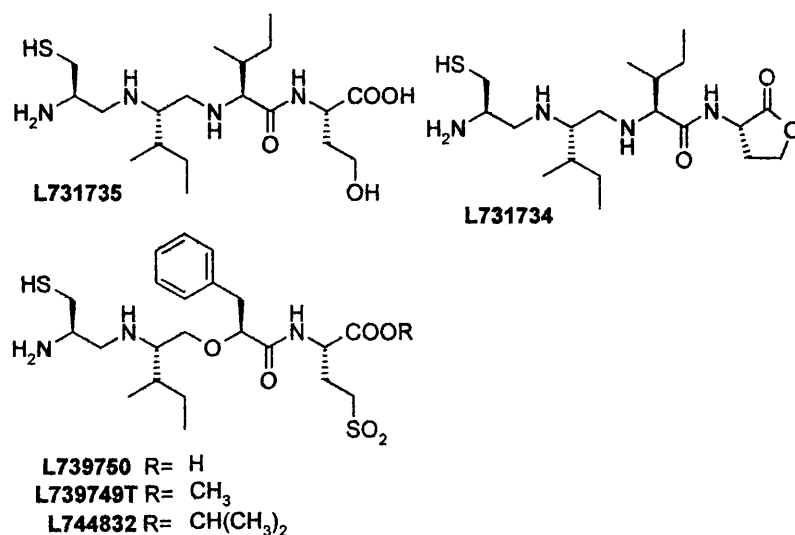


**Figure 3** Compounds based on pseudo-peptide strategy

Another approach is to replace the peptidic features of the a<sub>1</sub>a<sub>2</sub> region within the tetrapeptide carboxy-terminus by stable components. The reasoning being that the aliphatic amino acids would bind to the hydrophobic pocket of the enzyme and thus

can be replaced by a simple hydrophobic spacer based on the substituted 4-aminobenzoic acid derivatives as shown in figure 4.<sup>58</sup>

Peptidomimetic inhibitor **FTI276** inhibited FPTase *in vitro* with an  $IC_{50}$  value of 0.5 nM, while the pro-drug version **FTI277** inhibited FPTase at an impressive 100 nM concentration.<sup>58</sup> Importantly, **FTI277** resulted in the accumulation of non-mutated Ras proteins which were able to complex with Raf proteins (effector molecules) to form *active* Ras-Raf complexes. As a consequence, **FTI277** can selectively block activation of MAPK by oncogenic Ras but not Raf.<sup>58</sup> **FTI276** inhibits human lung tumours in nude mice without any sign of toxicity.<sup>59</sup> The same approach of introducing a hydrophobic spacer was studied in relation to GGPTase-I. This recognises leucine as the preferred terminal amino acid in the CaaX box, therefore incorporation of leucine into the design of peptidomimetic compounds created a new class of inhibitors. One such compound **GGT1287** has selectivity for GGPTase-I over FPTase at a 5:1 ratio, with an  $IC_{50}$  value of 5 nM for GGPTase-I enzyme.

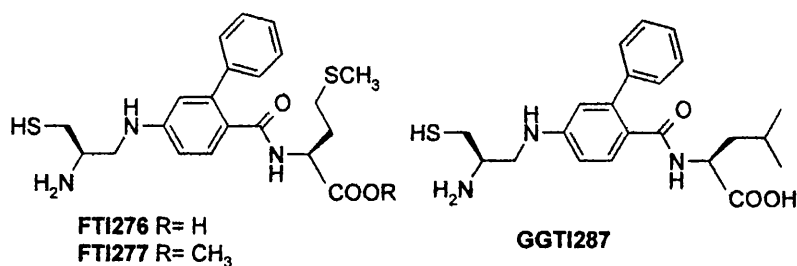


**Figure 4** Peptidomimetic inhibitors using stable hydrophobic components

A group based at Eisai used the same hydrophobic spacer principle, but rather than use derivatives of aminobenzoic acid, alkane spacers were utilised instead, as shown in figure 5.<sup>61</sup> Substitution of a benzyl group at the 2-position of 5-aminopentanoic acid produced highly potent inhibitors (**1** and **2**), achieving  $IC_{50}$  values of 20 and 18 nM respectively.<sup>58</sup> The absolute stereochemistry had very little effect with FPTase enzyme specificity.<sup>61</sup> Peptidomimetic compound **B956** was based on utilising the CVFM (cysteine, valine, phenylalanine, methionine) tetrapeptide where the cysteine amide bonds is replaced by a *trans*-alkene isostere, and a *cis*-alkene isostere replaces the central amide bond.<sup>62</sup> **B956** inhibits both H- and K-Ras for FPTase at 0.5 and 25  $\mu$ M concentrations respectively and also prevents tumour growth in nude mice.<sup>62</sup>

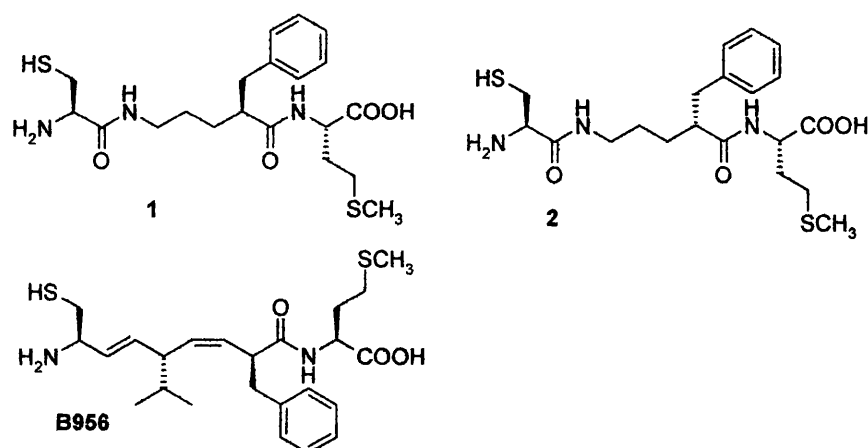


**Figure 5** Peptidomimetics using alkane and alkene hydrophobic spacers

A different approach was used to develop FPTase inhibitors **BZA2B** and **BZA5B**, shown in figure 6.<sup>63</sup> Originating from Genentech, a benzodiazepine subunit caused a turn of conformation in peptidomimetic inhibitors, with the possibility of both the thiol group and the terminal carboxy-group coordinating to a metal ion ( $\text{Zn}^{2+}$ ). 3-Amino-1-carboxymethyl-5-phenylbenzodiazepine-2-one (**BZA2B**) and its methyl ester derivative (**BZA5B**) both show potent inhibitory values for FPTase (0.85 and 10  $\mu\text{M}$  respectively).<sup>64,65</sup>

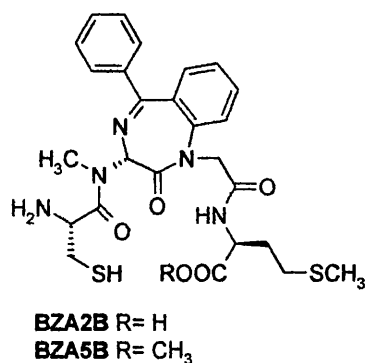


**Figure 6** Peptidomimetics incorporating a benzodiazepine subunit

The idea of using the **CVFM** tetrapeptide structure as used for compound **B956** in figure 5 was also used by another group at the Eisai research institute, however instead of using alkene spacers, a more direct comparison was used to produce further peptidomimetic compounds **B515** and **B581**, as shown in figure 7.<sup>66</sup> **CVFM** is a potent FPTase inhibitor *in vitro* ( $\text{IC}_{50}$  value of 60 nM) and is very selective to FPTase



compared to GGPTase-I by an order of magnitude.<sup>67</sup> CVFM is not modified by FPTase due to both the aromatic residue and a free amino terminus. However its peptides are not stable or permeable enough to enter through the cell membrane to be used for *in vivo* inhibition of FPTase. Compounds **B515** and **B581** are designed to be both more stable and permeable and thus more suitable as *in vivo* inhibitors.<sup>66</sup> Both **B515** and **B581** showed an increase in potency as inhibitors of FPTase with  $IC_{50}$  values of 23 and 21 nM respectively compared to CVFM. The selectivity of both compounds for FPTase over GGPTase-I were reduced compared to CVFM, with **B581** being the more selective for FPTase over GGPTase (21 nM for FPTase compared to 790 nM for GGPTase-I). Thus **B581** was used for *in vivo* inhibition studies. The inhibition value achieved by **B581** *in vivo* was 50  $\mu$ M, similar to that of lovastatin.<sup>66</sup> So although more than a 1000-fold increased concentration is required for *in vivo* inhibition, it is still an improvement on CVFM, the original tetrapeptide.<sup>67</sup>

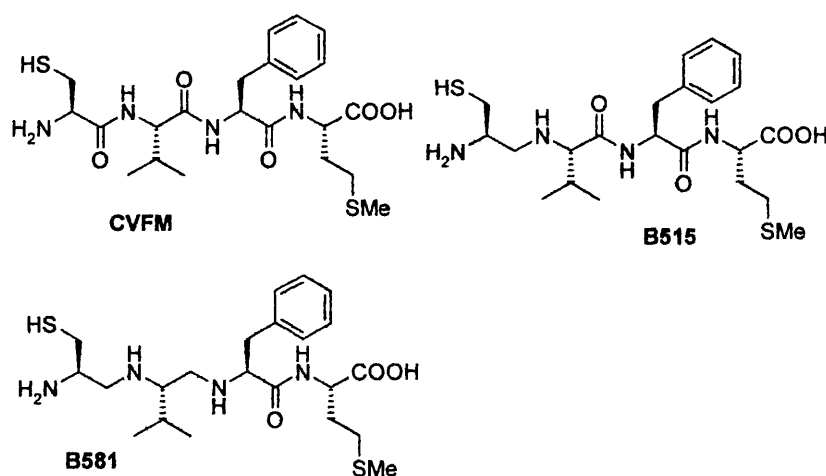


**Figure 7** Analogues of CVFM tetrapeptide

### 3.5.2 Non-peptidomimetics

Non-peptidomimetics were developed to operate in much the same way as peptidomimetics by mimicking the CaaX motif of Ras proteins, yet not suffer from their disadvantages, namely lack of stability and permeability, both of which are necessary for potent FPTase and GGPTase inhibition.<sup>70</sup>

Compound **3** utilises the same hydrophobic spacer strategy present in compounds **FTI276** and **FTI277** (figure 4). Compound **3** achieves an inhibition value of 114 nM, which is a similar  $IC_{50}$  value to CVIM, (cysteine, valine, isoleucine and methionine), a tetrapeptide found on H-Ras proteins.<sup>71</sup> This despite the structural differences caused by the substitution of 4-amino-3-carboxybiphenyl group for the VIM segments of the carboxy-terminal.<sup>71</sup> A more potent version, compound **4**, produced by the substitution on the biphenyl spacer with a hydrophobic group such as a methoxy, has an  $IC_{50}$  value of 30 nM, as shown in figure 8.<sup>72</sup> Although both **3** and **4** both lack the methionine residue, they both have over a 1,000-fold selectivity for FPTase inhibition compared to GGPTase-I. This is surprising as the methionine amino acid usually confers the specificity of the inhibitor towards FPTase.<sup>72</sup>

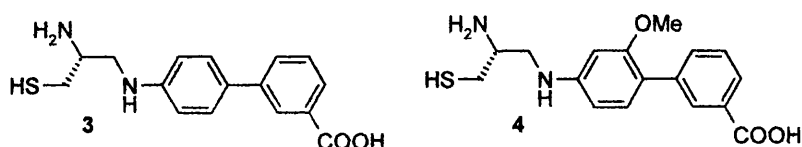


**Figure 8** Non-peptidomimetics (replacement of peptides with more stable units)

A group at Schering-Plough discovered a novel class of non-peptidomimetics for FPTase. These compounds contain a substituted tri-cyclic ring system and are represented by **SCH 44342** (shown in figure 9).<sup>73</sup> **SCH 44342** inhibits FPTase at 0.28  $\mu$ M concentration and is structurally similar to tri-cyclic compounds containing histamine (H1) and platelet activating factors (antagonist activity).<sup>74</sup> Most of the substituted tri-cyclic ring systems have poor potency against GGPTase enzymes, indeed **SCH 44342** has a 400-fold selectivity for *in vitro* inhibition of FPTase *versus* GGPTase-I.<sup>73</sup> The tri-cyclic non-peptidomimetics are of considerable significance owing to the absence of a cysteine sulfhydryl moiety. Such a feature may impart favourable pharmacokinetic and stability properties on such compounds. This is observed by increased  $IC_{50}$  values for inhibition of FPTase in cell assays as compared to enzyme assays, whereas for peptidomimetics, the reverse is usually true.<sup>73</sup>

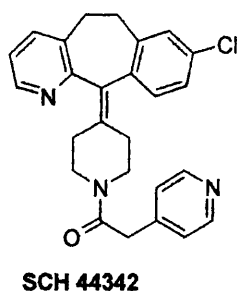


**Figure 9** Tri-cyclic non-peptidomimetic inhibitor

### 3.5.3 Competitive prenyl pyrophosphate substrate inhibitors

Ras prenylation involves two substrates, the Ras protein and either farnesyl pyrophosphate (FPP) or geranylgeranyl pyrophosphate (GGPP), both of which are required by their respective enzyme (FPTase or GGPTase). Therefore, one possible mode of inhibition for either enzyme is the mimicking the pyrophosphate substrate. Unlike the inhibition strategies mentioned above (peptidomimetics and non-peptidomimetics), such prenyl pyrophosphate analogues have one inherent disadvantage as prenyl-protein transferase inhibitors. The problem centres on specificity for the prenyl-protein transferase enzymes compared to other enzymes, which also utilises pyrophosphate substrates, such as squalene synthase. This is important, as non-specific binding by prenyl pyrophosphate substrates will cause unwanted side effects, especially as the cholesterol biosynthesis will be interrupted, (Chapter 1, scheme 10).<sup>75</sup>

In the region of competitive prenyl pyrophosphate substrate inhibitors, the majority of compounds are based on farnesyl pyrophosphate (FPP), and as such, the remainder of this section will concentrate on FPTase inhibition.

In figure 10, two FPP analogues are shown, both of which are very similar to farnesyl pyrophosphate, except that the pyrophosphate group is replaced with a moiety which is far less hydrolysable. Compound **5** ( $\alpha$ -hydroxyfarnesylphosphonic acid) has a monophosphate unit replace the pyrophosphate group in FPP, whereas compound **6** utilises a methylene group as a replacement for the diphosphate oxygen in FPP, making **5** and **6** less susceptible to hydrolysis.<sup>18</sup> These two compounds are competitive inhibitors of FPP, but are non-competitive with respect to the Ras protein

in FPTase inhibition, with inhibition  $IC_{50}$  values of 30 and 830 nM respectively.<sup>45</sup> However,  $\alpha$ -hydroxyfarnesylphosphonic acid inhibits squalene synthase *in vitro* at 630 nM concentration, which causes side effects.<sup>45</sup>

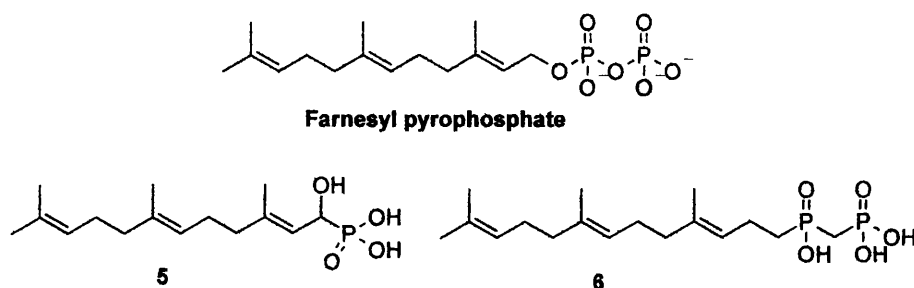


**Figure 10** Farnesyl pyrophosphate and two analogues

Another method of creating analogues of pyrophosphate group is the use of  $\beta$ -carboxyphosphonic acid. This can be linked to a farnesyl group *via* an amide bond, as shown in compound 7 in figure 11.<sup>18</sup> Compound 7 inhibits FPTase with an  $IC_{50}$  value of 75 nM, however the lack of specificity means that squalene synthase is also inhibited (516  $\mu$ M), which is an improvement compared to compound 5 (figure 10).<sup>18</sup> Retro-amide analogues of compound 7 can be produced, one such compound 8, is a slightly more potent FPTase inhibitor ( $IC_{50}$  value of 50 nM).

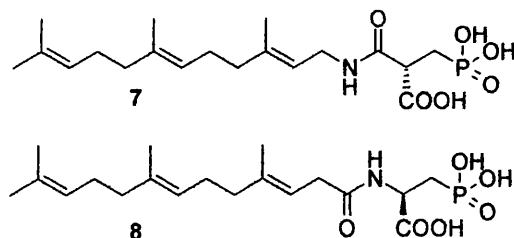


**Figure 11** FPP analogues with amide bonds

FPP analogues have also been obtained from microbial sources. One such compound is oreganic acid.<sup>77</sup> This contains a polar tri-carboxylic acid 'head' and a long fatty chain 'tail' terminating with a hydroxyl group which is sulphated. Oreganic acid and its analogues (figure 12) are potent FPTase inhibitors.<sup>77</sup> Oreganic acid exhibits an  $IC_{50}$  value of 14 nM for FPTase inhibition. Such inhibitory activity is independent of Ras substrate, suggesting that oreganic acid is purely FPP competitive.<sup>78</sup>

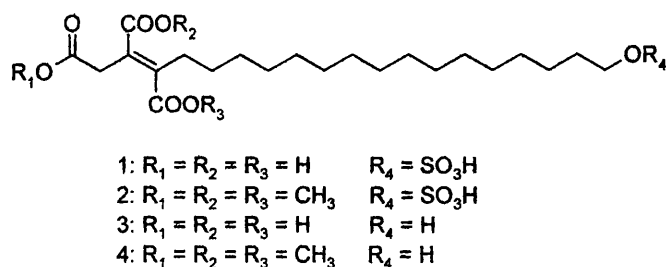


**Figure 12** Organic acid and its analogues

### 3.5.4 Bisubstrate analogues

Bisubstrate analogues are based on the dual nature of the substrate complex in which the carboxy-terminal region (the CaaX box) is joined to the prenyl pyrophosphate.<sup>52</sup> The bisubstrate analogue binds to the prenyl-protein transferase enzyme, and so can achieve inhibition in two ways, either by the tetrapeptide portion of the compound acting as an peptidomimetic, or *via* its prenyl chain segment, acting as a competitive prenyl pyrophosphate inhibitor; hence the term *bisubstrate analogues*.

An example of a bisubstrate analogue is peptide **9**, (shown in figure 13). This was designed to contain both the FPP and the tripeptide VVS (valine, valine, serine) components.<sup>79</sup> Therefore compound **9** contains the hydrophobic part of the farnesyl chain and the mimics the tetrapeptide carboxy-terminus, allowing protein recognition to occur. Usually a linking group, often an ester or a phosphonate connects these two segments.<sup>79</sup> Bisubstrate analogue **9** achieves an inhibition of FPTase with an  $IC_{50}$  value of 33 nM. Such activity arises from the glutamyl carboxylic acid moiety.<sup>77</sup> The D-isomer of the glutamate-derived inhibitor showed a decrease (100-fold) in FPTase inhibition potency.<sup>80</sup>

Four more examples of bisubstrate analogues are also shown in figure 13. They are unlike compound **9**, in the sense that none has a stereogenic centre in the connecting region linking the tripeptide VVM (valine, valine and methionine) with the farnesyl group.<sup>79</sup> Both **BMS-185878** and **BMS-184467** achieved potent FPTase inhibition, both attaining an  $IC_{50}$  value of 6 nM. These two compounds are also very selective for FPTase inhibition compared to the inhibition achieved for GGPTase ( $>10,000 \mu M$ ).<sup>79</sup> The pro-drug versions, **BMS-186511** and **BMS-184382** have demonstrated inhibition

(70-85 %) of growth for transformed *foci* cells at concentrations as low as 100  $\mu$ M, without any toxic side effects manifesting in the untransformed cells.<sup>80</sup>

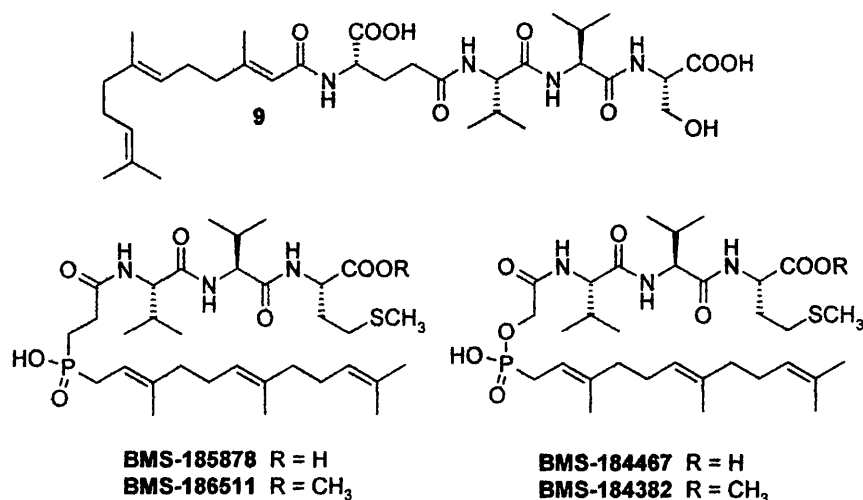


**Figure 13** Bisubstrate analogue inhibitors

### 3.5.5 Natural products

Random screening can disclose the potency of natural products. Unlike the above classes of inhibitors, these natural products often share no structural similarity to either prenyl pyrophosphate or the CaaX tetrapeptide region of Ras proteins. Such compounds inhibit FPTase and GGPTase by a variety of mechanisms ranging from competitive with respect to prenyl pyrophosphate and the Ras protein, to non-competitive with respect to either of the substrates.

Three examples of natural products that are FPP competitive are compounds **20**, **21** and **22**, (shown in figure 14).<sup>81</sup> All three compounds contain multiple carboxylic acids and it is these negatively charged carboxylate groups that mimic the diphosphate moiety in FPP, hence the FPP competitive inhibition. Natural products **20-22** also contain long hydrophobic chains that 'copy' the farnesyl chain unit. All three compounds are potent FPTase inhibitors, achieving 55, 12, and 50 nM IC<sub>50</sub> values respectively.<sup>82,83,84</sup> Carboxylic acids **20**, **21**, and **22** are also selective for FPTase inhibition, with GGPTase-I inhibition values of at least two orders of magnitude less potent.<sup>83</sup> However, chaetomelic acid (**21**) is a competitive FPP inhibitor, and as is

often the case, it is also a potent inhibitor of squalene synthase, with an  $IC_{50}$  value of 78 picomolar (pM).<sup>83</sup>

Also shown in figure 14 are three more examples of natural products (**25**, **26**, and **27**) which inhibit prenyl-protein transferase enzymes, however, their mode of action is non-competitive with respect to both FPP and Ras protein. This is interesting, especially for gliotoxin (**27**) since it contains two thiol groups, which are known key functional groups for many peptidomimetic inhibitors.<sup>85</sup> The potency of compounds **25**, **26** and **27** do not reach the levels obtained by the three carboxylic acid containing natural products (2,200, 300 and 1,100 nM respectively) but also do not have the disadvantages of being potent squalene synthase inhibitors.<sup>86</sup>

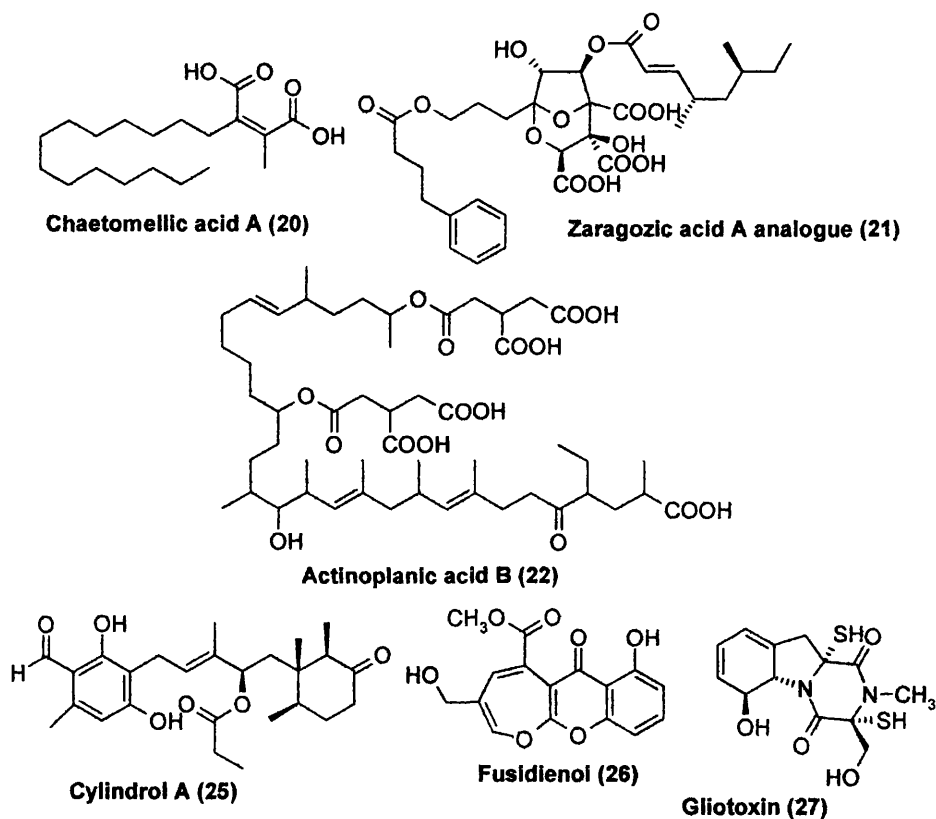


**Figure 14** Natural product inhibitors

### 3.6 Selectivity for tumorous cells

For all the above strategies utilised to design potent prenyl transferase inhibitors, all the results obtained were very good in regressing tumorous cells. More significantly,

chemoprevention was evident and yet there was little or no sign of toxicity to 'normal' cells. Possible explanations are:

- a) Not all prenylated proteins have the same sensitivity to either FPTase or GGPTase inhibition in cells. For example, H-Ras protein is potently inhibited by low concentration of FPTIs (farnesyl-protein transferase inhibitors), but lamin proteins A and B (which require farnesylation) are only affected by a ten-fold increase in concentration.<sup>87,88,89</sup>
- b) In the absence of FPTase, some Ras proteins utilise GGPTase-I,<sup>90</sup> thus some proteins become geranylgeranylated if farnesylation is not possible, so permitting the signalling of the Ras pathway.
- c) Redundant pathways in 'normal' cells are activated to counterbalance the functional loss of Ras proteins, such as H-Ras, an example of which is the MAPK pathway involving EGF receptor signalling.<sup>91</sup>

### ***3.7 The rationale for designing new synthetic terpenoid inhibitors of prenyl-protein transferase***

FPTase and GGPTase inhibitors restrain the addition of an isoprenoid unit onto an inactive form of Ras protein, and as a result not allowing association with the plasma cell membrane, where it can be transformed into its active state. Consequently, proliferation of malignant cells and transformation is significantly reduced.<sup>93</sup>

The structure of Ras proteins is homologous to G-proteins in general and the 'lock-and-key' hypothesis for the action of enzymes is an important consideration. The crystal structure of farnesyl-protein transferase reveals that one region of FPTase is lined with aromatic residues, which have the function of binding to farnesyl pyrophosphate, as shown in figure 15. This aromatic region of FPTase is where the 'tail' portion of farnesyl pyrophosphate would reside, as the 'tail' is non-polar. Contrastingly, the 'head' of the FPP (the pyrophosphate portion) would occupy the polar region of the enzyme, forming hydrogen bonds to various amino acid residues as well as a zinc ion contained within the enzyme structure.<sup>40</sup> Therefore from this crystal structure, a model (shown in figure 15) will be designed to incorporate not



only the features of prenyl pyrophosphate association but also the starting point of this thesis, the monoterpenoids such as limonene and perillyl alcohol, (see figure 1, Chapter 1) to create a new class of synthetic terpenoids which could have potent prenyl-protein transferase inhibitory action.

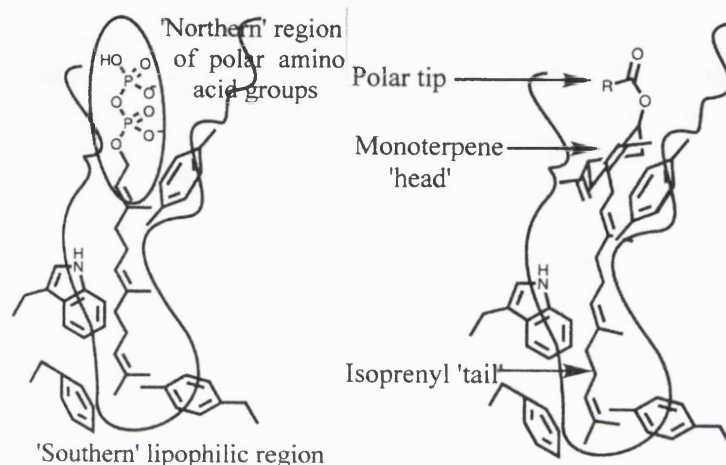


**Figure 15** Binding of farnesyl pyrophosphate in enzyme pocket of FPTase (left) and rationale for binding of new synthetic terpenoid (right)

From the crystal structure of the FPTase enzyme and the general structure of monoterpenoids (shown in figure 16), it would seem that three chemical features must be addressed to design a compound that would possess optimum inhibition for prenyl-protein transferase, as shown in figure 15 (right hand side). These are:

1. A polar tip,
2. a monoterpene head ('lipophilic spacer'), and
3. an isoprenyl chain ('lipophilic tail').

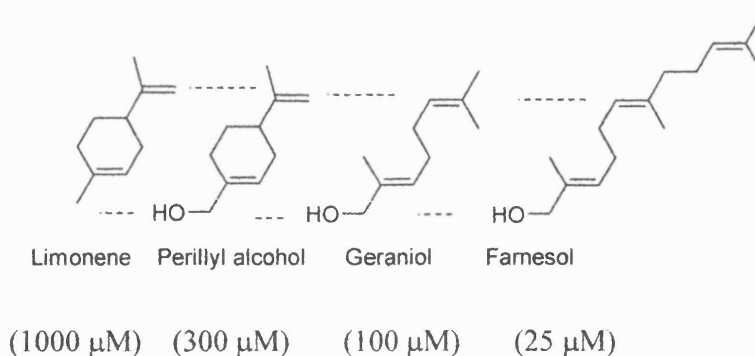


**Figure 16** *In vivo* inhibition concentrations of naturally occurring isoprenoids of human MIA PaCa2 pancreatic tumour cells

Compounds such as limonene possess a lack of reactive chemical functionality, with the exception of the double bonds, so the mode of action could be consistent with enzyme inhibition. However, the *modus operandi* may be simply steric bulk, causing a blocking action, most likely at the cell membrane surface, causing interference with cell signalling and even cell death. It must also be considered that there may be more than one mechanism at work, indeed the metabolites of limonene (perillic acid and dihydroperillic acid, figure 2, Chapter 1) are more potent at FPTase inhibition than limonene itself.<sup>94</sup>

### **3.8 Determining the potency of new chemopreventive compounds**

The main method for determining the potency of compounds in terms of FPTase and GGPTase-I inhibition is through enzyme assays. The procedures used to conduct the enzyme inhibition assays are described in the experimental chapter (section 6.2).

The enzyme inhibition assay is possible because both FPTase and GGPTase-I enzymes possess a prenyl pyrophosphate carrier function. This forms a stable complex with the prenyl pyrophosphate substrate and on binding there is a direct transfer of the isoprenoid moiety from the enzyme-bound prenyl pyrophosphate to the carboxy-terminal residue of the Ras protein. It is this complex which is formed between the enzyme and the [<sup>3</sup>H]-pyrophosphate substrate and the extent of this transfer which is measured.

The transfer of [<sup>3</sup>H] farnesyl to H-Ras protein from enzyme-bound [<sup>3</sup>H] farnesyl pyrophosphate is much quicker than the [<sup>3</sup>H] farnesyl pyrophosphate dissociation from the enzyme. The [<sup>3</sup>H] farnesyl moiety is covalently bound to Ras and is trichloroacetic acid (TCA) precipitable, whereas the enzyme-bound [<sup>3</sup>H] farnesyl pyrophosphate is dissociated by TCA. Therefore only [<sup>3</sup>H]-labelled Ras (and not enzyme-bound [<sup>3</sup>H] farnesyl pyrophosphate) is trapped on the filter paper when TCA is added to the transfer mixture.<sup>95</sup> In the present study, two controls are utilised to confirm the validity of the results obtained. For each enzyme assay conducted, three sample tubes do not contain any compound, just the radio-labelled prenyl pyrophosphate and the respective enzyme, thereby allowing the comparison of the

enzyme solutions containing potential inhibitor compounds. Another tube contains chaetomelic acid A (a known potent protein-prenylation transferase inhibitor), which acts as a positive control, thus the accuracy of enzyme inhibition can be validated.

### **3.8.1 Non-linear regression analysis of enzyme isotope-labelled kinetic data**

The use of “a mathematical model is neither a hypothesis nor a theory. Unlike scientific hypotheses, a model is not verifiable directly by an experiment. For all models are both true and false, and the validation of a model is not true that it is ‘true’ but that it generates good testable hypotheses relevant to important problems”.<sup>96</sup> The use of linear regression fits data to a model of a linear relationship between x and y in the manner of the following equation:

$$y = \text{slope} \cdot x + \text{intercept} \quad (1)$$

Thus a line is described by the above simple equation to calculate y from x and the slope and intercept. The purpose of which is to obtain values for the slope and intercept that define a line that minimises the sum of the square of the vertical distances of the points from the line.<sup>97</sup> The problem with linear regression is the distortion of experimental error; the assumption that the scatter of points around the line follows a Gaussian distribution, with the standard deviation the same at every value of x.<sup>97</sup> Such an assumption results in the values derived from the slope and intercept of the line drawn not being the most accurate determinations of the variables in the model. It is computer powered non-linear regression that produces the most accurate results.<sup>97</sup>

Non-linear regression is a more general model than its linear counterpart, and can fit data to any equation that defines y as a function of x and one or more parameters.<sup>97</sup> It finds the values of those variables that generate the curve that most closely fits the data.<sup>97</sup> A measure of the accuracy of the graph drawn can be determined by the sum-of-squares (SS) analysis from non-linear regression. The sum-of-squares (SS) is the sum of the vertical distances of the points from the curve. Non-linear regression varies the value of the variables to minimise the sum-of-squares. It is expressed in the square

of the units used for the y values.<sup>97</sup> An indication to the accuracy of the values derived from the non-linear regression curve graph is known as the ‘goodness of fit’ ( $R^2$ ).<sup>97</sup> It is a fraction between 0.0 and 1.0 and has no units; when  $R^2 = 1.0$ , all the data points in the graph lie exactly on the curve, with no scatter, meaning that if you know x exactly, then y can be calculated exactly.<sup>97</sup> The equation to derive  $R^2$  is as follows:

$$R^2 = 1.0 - \frac{SS_{reg}}{SS_{tot}} \quad (2)$$

where  $SS_{reg}$  is the sum-of-squares of the points from the non-linear regression curve, and  $SS_{tot}$  is the sum-of-squares of the distances of the points from a horizontal line through the mean of all y values. If the curve fits the data, the value of  $SS_{reg}$  will be much smaller than for the value of  $SS_{tot}$ .<sup>97</sup>

### 3.8.2 Determination of $IC_{50}$ from sigmoidal dose-response curves

The experiments conducted in Charing Cross and Hammersmith Hospitals were a measure of the transfer of [ $^3H$ ]-labelled ligand (prenyl pyrophosphate) to an enzyme (prenyl-protein transferase) in the presence of various concentrations of unlabelled ‘drug’ inhibitor. The concentrations of the ‘drug’ used should vary over a minimum of 3 orders of magnitude, to produce a sigmoidal dose-response curve which follows almost exactly the receptor-binding curve, showing the isotope-ligand binding (y-axis) as a function of the logarithm of concentration of ‘drug’ (x-axis) (figure 17).

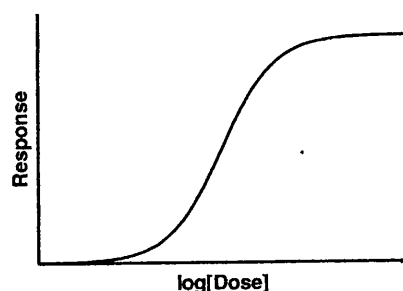


**Figure 17** Sigmoidal dose-response curve<sup>97</sup>

Such dose-response curves can be used to display data from many kinds of experiments. The x-axis plots the concentration of a drug, and the y-axis plots the response, whatever the response may be.<sup>97</sup> The term dose-response curve is used loosely to describe *in vitro* experiments where you apply known concentrations of

drugs. Therefore the term, concentration-response curve, would be a more accurate description for the results of such experiments.<sup>97</sup> An agonist is a drug that causes a response, if various concentrations of an agonist is used, the dose-response curve will go uphill as you go from low concentration (left-side) to high concentration (right-side). An antagonist is a drug that does not provoke a response itself, but blocks agonist-mediated responses, therefore if the concentration of an antagonist is varied in the presence of a fixed concentration of agonist, the dose-response curve will go downhill.<sup>97</sup>

From a dose-response curve concentrating on antagonistic activity, the top of the curve is a plateau that equals the value obtained for binding of substrate in the absence of a 'drug' inhibitor and the bottom of the curve is a plateau equivalent to non-specific binding. Therefore the concentration of 'drug' inhibitor that produces response halfway between the top and bottom plateaus, is the called the IC<sub>50</sub> (inhibitory concentration 50%).

The general equation for this type of sigmoidal dose-response curve is as follows:

$$y = y_b + \frac{(y^t - y_b)}{1 + 10^{\text{LogIC}_{50} - x}} \quad (3)$$

where  $y^t$  and  $y_b$  are the y values at the top and bottom plateau of the curve.<sup>97</sup>

### 3.8.3 The importance of the IC<sub>50</sub> value

Since the IC<sub>50</sub> is defined as the concentration of inhibitor that triggers a response halfway between the baseline and maximum values (*i.e.* blocks 50% binding), it is impossible to have an IC<sub>50</sub> value without first defining the baseline and maximum response. In the assays conducted, the wide range of concentrations used for the 'drug' inhibitor allow definition for the top and bottom plateaus of the receptor-binding curve.

The value of the IC<sub>50</sub> is determined by two factors:<sup>97</sup>

(a) the affinity of the enzyme for the inhibitor; if the affinity is high, the IC<sub>50</sub> value will be low. The affinity of the enzyme is shown by the K<sub>i</sub> value (with is used to indicate inhibited enzyme activity). Thus, it is the concentration of the 'drug' required

to bind to half the binding sites at equilibrium, in the absence of substrate or other inhibitors. So if  $K_i$  value is low, the affinity for the inhibitor by the enzyme is high, thus the  $IC_{50}$  value is low,

(b) the  $K_M$  value, (*i.e.* the affinity of the substrate for the enzyme), therefore it takes more inhibitor to compete with a substrate with a low  $K_M$  value for an enzyme.

The value of  $K_i$  can be calculated from a sigmoidal dose-response curve using the equation obtained from Cheng and Prusoff as shown below:<sup>98</sup>

$$K_i = \frac{IC_{50}}{1 + \frac{[substrate]}{K_M}} \quad (4)$$

The calculations of the data collected from the scintillation counts concerning the transfer of the [<sup>3</sup>H]-prenyl pyrophosphate to the substrate (Ras protein) *via* the enzyme to obtain the  $IC_{50}$  value for each ‘drug’ inhibitor was conducted at the Charing Cross and Hammersmith Hospitals by Dr. D. M. Vigushin and Mr. G. Brooke. The  $IC_{50}$  values obtained were subsequently reported to Dr. C. M. Marson and Mr. A. S. Rioja. The example below illustrates how the  $IC_{50}$  values were determined; in this instance, the  $IC_{50}$  value for inhibitor (PTase 9) was calculated for geranylgeranyl-protein transferase enzyme inhibition.

Tube	Inhibitor concentration	Sample	CPM (counts per minute)	CPM minus substrate blank (A)	Percentage of control experiment (mean n=3)
1	0	Substrate Blank	989	-----	
2	0	Inhibitor Blank 1	4189	3200	
3	0	Inhibitor Blank 2	6281	5292	
4	0	Inhibitor Blank 3	5928	4939	
5	1 $\mu$ M	PTase 9	7610	6621	147.9
6	10 $\mu$ M	PTase 9	6056	5067	113.2
7	100 $\mu$ M	PTase 9	2667	1678	37.5
8	1 mM	PTase 9	2265	1276	28.5

**Table 1** The scintillation values obtained for the amount of [<sup>3</sup>H]-labelled Ras in the presence of inhibitor PTase 9

Mean  $\pm$ SD 100% of negative substrate control CPM(B):  $4477 \pm 914.4$

The amount of [ $^3$ H] FPP or [ $^3$ H] GGPP transferred to native or chimaeric H-Ras, respectively, for each concentration of inhibitor was expressed as a percentage of control incubations without inhibitor, as shown in the formula below:

$$\frac{CPM(A)}{CPM(B)} \times 100\% \quad (5)$$

A sigmoidal dose-response curve plot is drawn with the percentage (obtained as shown above) of the control values as the y-axis, and the log concentrations of inhibitor (PTase 9) used as the x-axis, (for example if the inhibitor concentration varied from 1  $\mu$ M to 1 mM, x values of -6 to -3 were entered), from which the log  $IC_{50}$  value can be determined (figure 18).

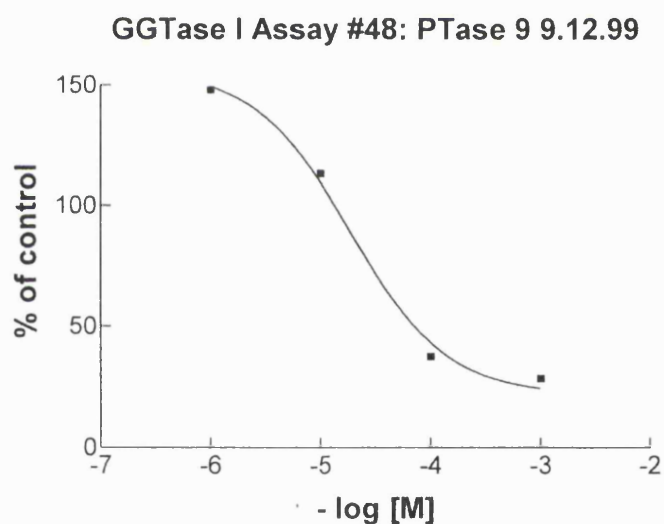


**Figure 18** A sigmoidal dose-response curve of the percentage of CPM for [ $^3$ H]-labelled Ras protein obtained with various concentrations of PTase 9

From the graph above, the following values were obtained (Table 2).

X values	Y values
Variables	
Bottom	156.1
Top	22.11
LOG IC <sub>50</sub>	-4.724
IC <sub>50</sub>	1.888 x 10 <sup>-5</sup>
Std. Error	
Bottom	9.766
Top	7.603
LOG IC <sub>50</sub>	0.1637
Goodness of Fit	
R <sup>2</sup>	0.9937
Absolute sum of squares	64.30

**Table 2** Table of results obtained from the non-linear regression analysis of a sigmoidal dose-response curve for PTase 9

The results show that the IC<sub>50</sub> value for PTase 9 in terms of geranylgeranyl-protein transferase inhibition was 18.9  $\mu$ M. The accuracy of the IC<sub>50</sub> value was ascertained by the 'goodness of fit' R<sup>2</sup> value (0.9937), where if R<sup>2</sup> = 1.0, then all data points lie exactly on the curve of the graph, with no scatter (section 3.8.1). The x-axis is expressed in terms of log of concentration, as this would mean the concentrations of the inhibitor used are equally spaced in a log scale, thus the uncertainty of the log IC<sub>50</sub> value is symmetrical (*i.e.* a Gaussian curve distribution), with the IC<sub>50</sub> value obtained simply by taking the anti-log value; whereas the uncertainty of IC<sub>50</sub> values obtained directly from the value of concentration, and not logs of concentration, is unsymmetrical, therefore less Gaussian and more likely to contain larger errors.<sup>97</sup>

### 3.9 Preparation of potential prenyl-protein transferase inhibitors

In the design of prenyl-protein transferase inhibitors, the starting point was limonene and perillyl alcohol (monoterpenes). Therefore, the first step is to vary the functionality around perillyl alcohol, (*i.e.* short chain monocyclic analysis) and in that way identify which functional group is important in conferring prenyl-protein transferase inhibition. The second stage is to take the results obtained from the first phase and combine it with the new model for designing potent terpenoid-type inhibitors of prenyl-protein transferase (long chain mono- and bicyclic analogues). The third stage is to produce medium- to long-chain analogues with a strongly polar terminus, again in concert with the model designed to create potent prenyl-protein



transferase inhibitors. Figure 19 shows all the compounds sent for enzyme assay testing to Charing Cross and Hammersmith Hospitals. (Where compounds can exist in racemic forms, the racemic forms were tested, unless otherwise stated).

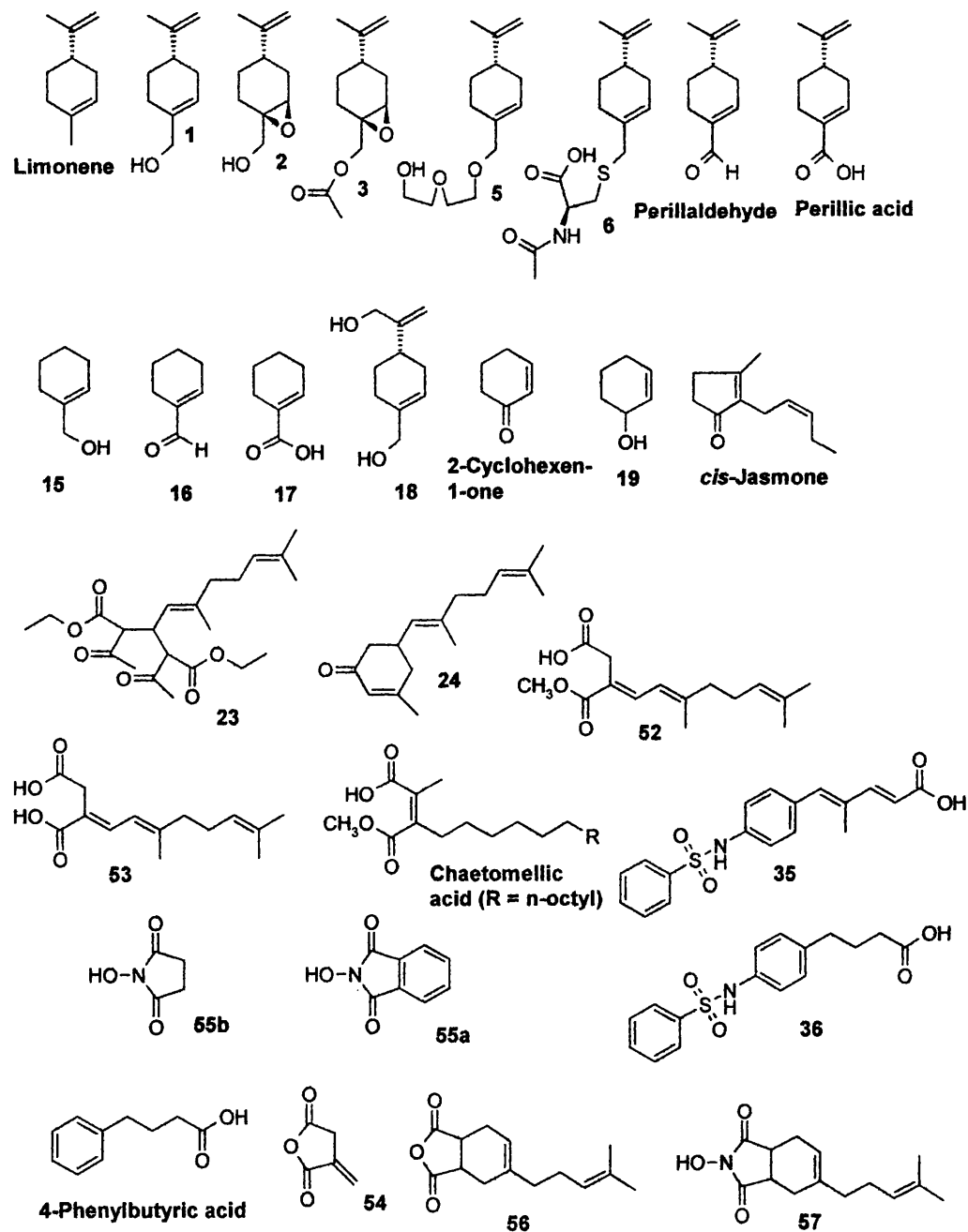


**Figure 19** Compounds submitted for PTase enzyme assay determination

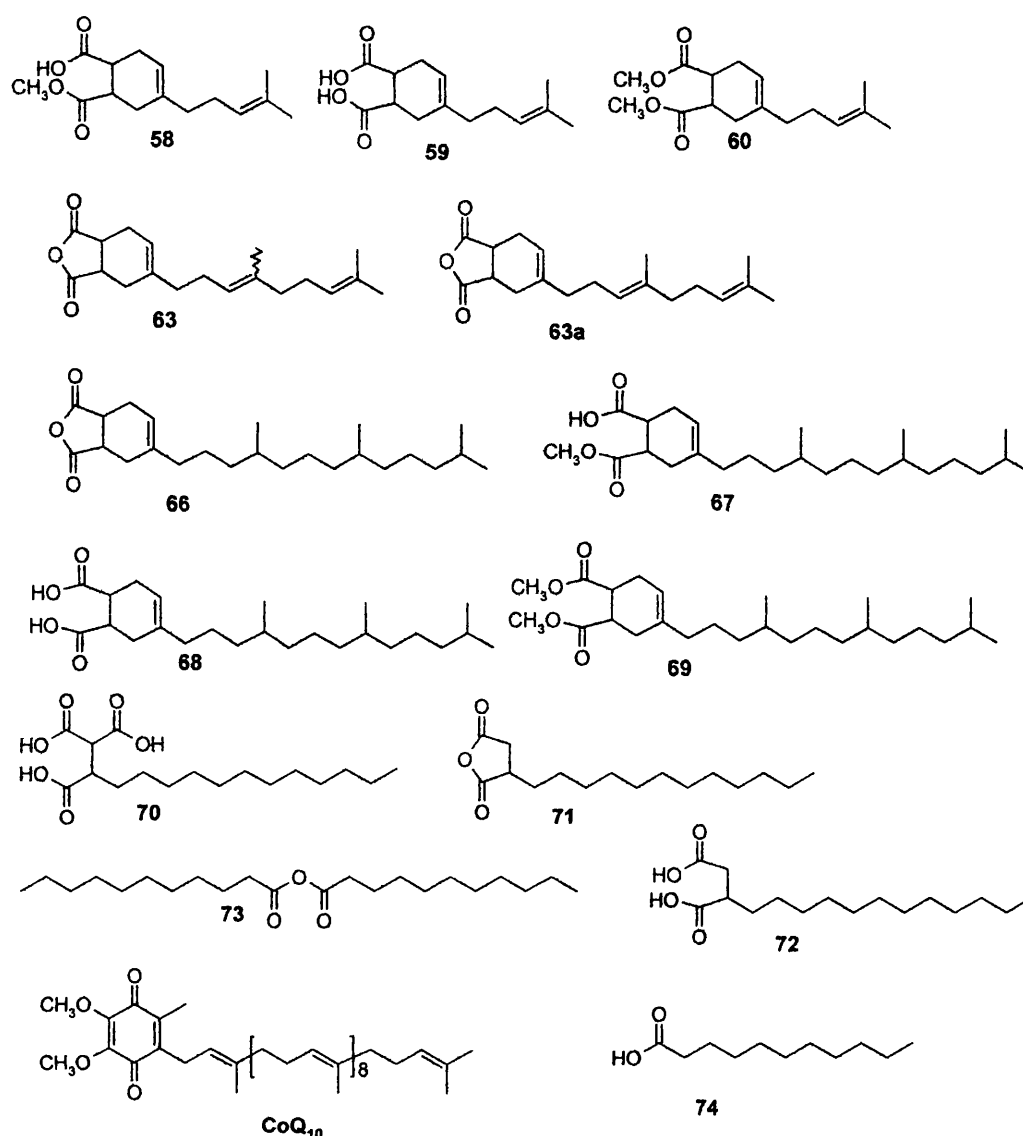
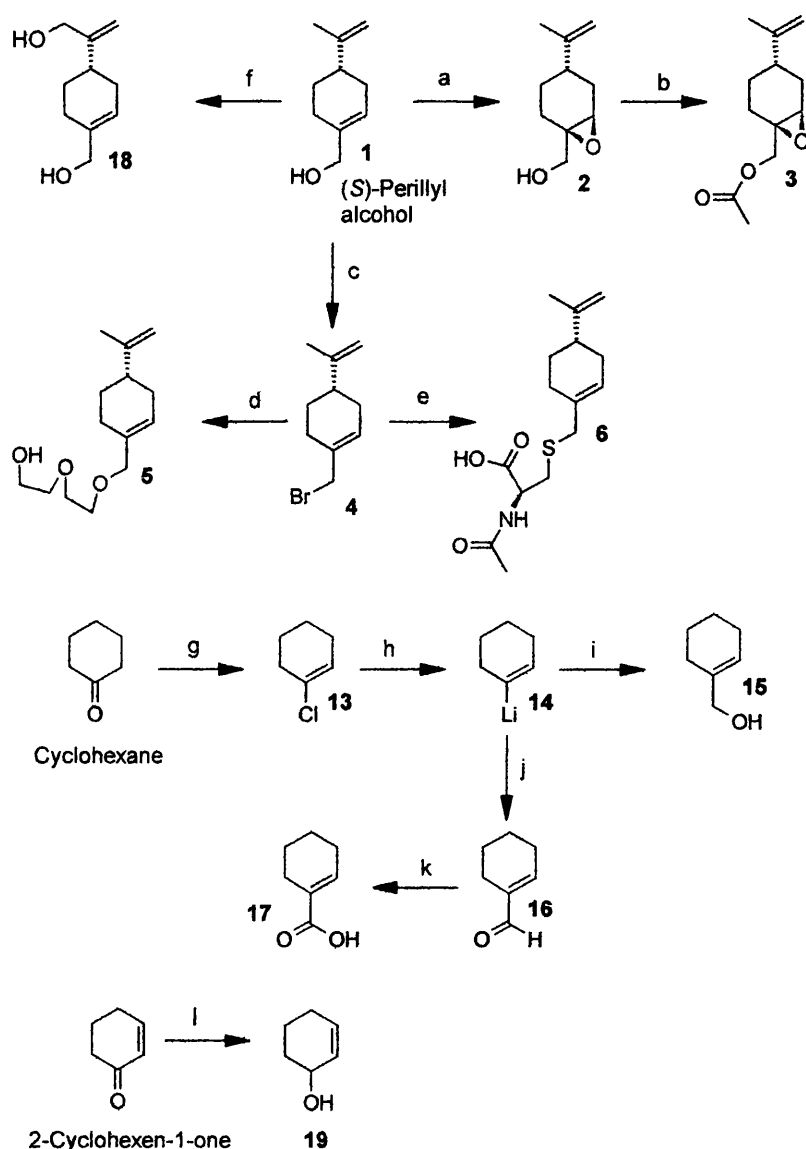


**Figure 19 continued** Compounds submitted for PTase enzyme assay determination

### 3.10 Short-chain monocyclic analysis of perillyl alcohol

The identification of key functional group(s) on perillyl alcohol that confer the anti-cancer properties is central, and it was hoped that a systematic removal and insertion of functional groups might provide some insight into what is required to design a potent prenyl-protein transferase inhibitor, and consequently a potent anti-cancer agent. In Scheme 3, the preparation of all short-chain monocyclic compounds is shown.

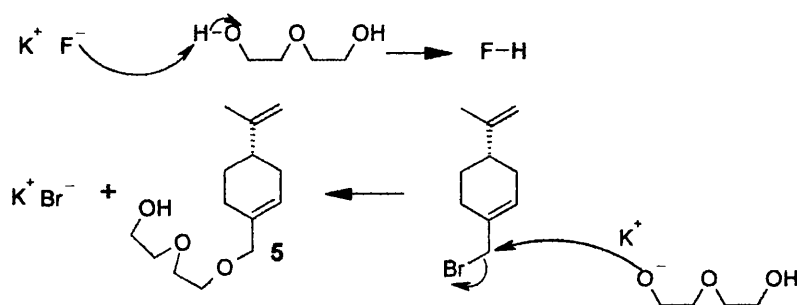


Reagents: (a) TBHP, VO(acac)<sub>2</sub>, (b) acetic anhydride, (c) PBr<sub>3</sub>, (d) KF, diethylene glycol, (e) *N*-acetyl-L-cysteine, NaOH, (f) O<sub>2</sub>, (g) PCl<sub>5</sub>, (h) Li, (i) paraformaldehyde, (j) DMF, (k) Jones' reagent, (l) sodium borohydride

**Scheme 3** Preparation of all short-chain compounds

Epoxy-alcohols **2** and **3** were prepared using *tert*-butylhydrogen peroxide (TBHP)-VO(acac)<sub>2</sub> rather than *m*-chloroperbenzoic acid (*m*-CPBA) for two reasons. Firstly, the yield of product obtained using TBHP was higher (80%), and secondly, TBHP affords only one diastereoisomer, (the  $\alpha$ -epoxide as shown in scheme 3); *m*-CPBA affords a mixture of diastereoisomers (*i.e.* both the  $\alpha$ - and  $\beta$ -epoxide products).<sup>99</sup>

The preparation of both compounds **5** and **6** proceeded *via* perillyl bromide, which was achieved in moderate yields (55%) according to the Buchecker procedure.<sup>100</sup> Product **5** was not the desired compound; originally the aim was to produce perillyl fluoride because a fluorine group has similar polarity to an alcohol moiety, yet may have better pharmaceutical potential owing to its relatively smaller size. The method was based on the procedure utilised by Pattison,<sup>101</sup> in which allylic fluorides are obtained from allylic bromides using potassium fluoride and diethylene glycol as a solvent. However, rather than producing an allylic fluoride, the resulting compound was an allylic glycol-type unit. Evidently, potassium fluoride acts as base allowing deprotonation of the glycol unit within diethylene glycol *via* a Williamson ether synthesis (shown in Scheme 4).



**Scheme 4** Formation of compound **5** by a Williamson ether synthesis

Compound **6** proceeds *via* the same mechanism, utilising sodium hydroxide as the base which deprotonates *N*-acetyl-L-cysteine and thus undergo the S<sub>N</sub>2 substitution with perillyl bromide. Diol **18** was prepared according to a procedure by Hiroshi,<sup>102</sup> in which sodium hydride is used in an oxygen atmosphere to produce in low yield (24%) compound **18**, the same yield as was reported.<sup>102</sup>

Compounds **15**, **16** and **17** mimic perillyl alcohol, perillaldehyde and perillic acid respectively, except that they all lack the isopentenyl moiety. This allowed observations as to the importance of the lipophilic 'tail unit'. Compound **13** was synthesised using phosphorus pentachloride according to Baird's procedure.<sup>103</sup> A subsequent lithiation with sheets of lithium followed by an addition with either paraformaldehyde<sup>104</sup> or dimethylformaldehyde<sup>105</sup> to give either the alcohol **15** or the aldehyde **16** respectively. The final transformation of aldehyde **16** into carboxylic acid

17 was performed *via* a Jones oxidation proceeding in a 69% yield.<sup>106</sup> Cyclohexenol 19 was prepared from 2-cyclohexen-1-one by reduction with sodium borohydride. Sodium borohydride was the reducing agent of choice because it does not really affect the carbon-carbon double bond and can also be used in polar solvents.

### 3.10.1 Evaluation of short-chain monocyclic compounds

Fifteen compounds were submitted for enzyme assay analysis of prenyl-protein transferase inhibition, including (*S*)-limonene, (*S*)-perillyl alcohol, (*S*)-perillaldehyde, (*S*)-perillic acid, 2-cyclohexen-1-one and *cis*-jasmonone. Inhibition experiments were conducted by Dr. D. M. Vigushin. The results are shown in Table 3.

Compound No./Name	FPTase inhibition (IC <sub>50</sub> )	GGPTase inhibition (IC <sub>50</sub> )
( <i>S</i> )-Limonene	>40 mM	>40 mM
( <i>S</i> )-Perillyl alcohol	1.0 mM	1.0 mM
( <i>S</i> )-Perillaldehyde	1.0 mM	5.0 mM
( <i>S</i> )-Perillic acid	1.0 mM	1.0 mM
2	4.5 mM	4.5 mM
3	4.0 mM	4.0 mM
5	7.9 mM	10 mM
6	1.0 mM	10 mM
18	1.0 mM	2.7 mM
15	10 mM	10 mM
16	3.9 mM	10 mM
17	2.1 mM	10 mM
2-cyclohexen-1-one	1.0 mM	1.0 mM
19	10 mM	10 mM
<i>cis</i> -jasmonone	10 mM	10 mM

**Table 3** Enzyme inhibition assay values for short-chain monocyclic compounds

From the comparison of values obtained from the various compounds submitted for enzyme inhibition assay testing, several inferences can be drawn. Epoxy-compounds 2 and 3 show that either the presence of the carbon-carbon double bond is important, or that the introduction of a polar group into that region of the compound causes a decrease in potency of both compounds compared with perillyl alcohol. Another important consideration is the enantiomeric forms of compounds 2 and 3. It may be that the enantiomers of 2 and 3 are the less potent, and that the opposite enantiomers of 2 and 3 are more active. The enzyme inhibition achieved by compound 5, which has a 'glycol'-type unit in place of the hydroxy moiety, was significantly less potent

than perillyl alcohol. This may suggest that either too long a polar extension may have a negative effect or that the orientation of the polar group is an important aspect that can affect the potency of inhibition. Once again, the opposite enantiomer of **5**, the (*R*)-enantiomer should be assayed to observe its potency.

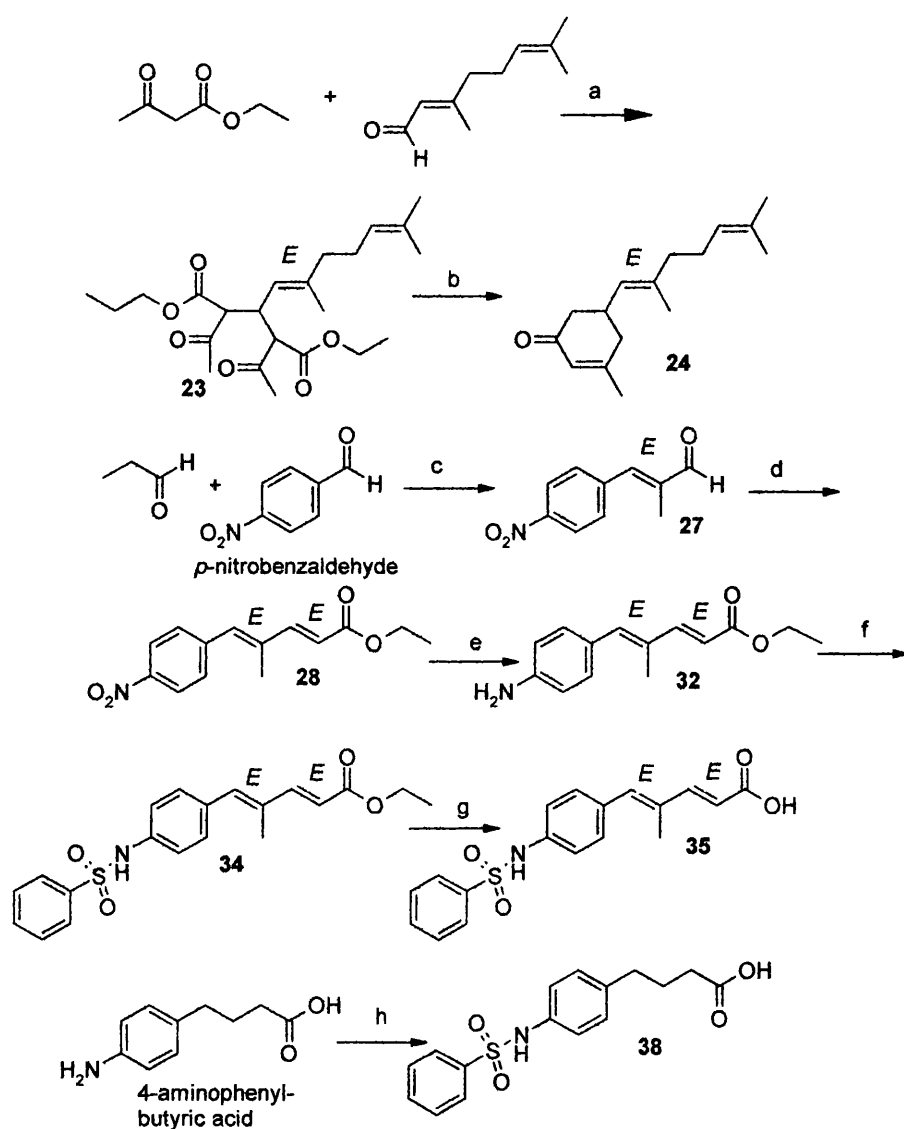
Inhibitor **6** contains an amino acid in its polar group, (as FPTase and GGPTase-I enzyme protein-prenylation occurs at the CaaX motif on the Ras protein, where C = cysteine amino acid), therefore the incorporation of a cysteine residue into a terpenoid compound could confer greater inhibitory potency. Indeed the FPTase inhibitory value of **6** is identical to perillyl alcohol; however, the value for GGPTase-I is much less potent. This suggests that the incorporation of cysteine as the amino acid of choice causes selectivity between the two prenyl-protein enzymes. A possible reason for this preference is that compound **6** may operate as a competitive Ras protein inhibitor, and that the lipophilic requirement provided by the terpenoid 'body' would most suit FPTase, since the lipophilic enzyme pocket would not be as large as that required by GGPTase-I. It would be interesting to examine the potency of **6** for GGPTase-II enzyme inhibition, because the structural motif on the Ras protein required for this particular enzyme is xCxC, (where C = cysteine). Consequently, the importance of incorporating a cysteine amino acid residue is considerably greater, since cysteine is now the terminal amino acid in the tetrapeptide structural domain, (*i.e.* act as a peptidomimetic). Examination of diol **18** deemed relevant by analogy with oreganic acid,<sup>78</sup> in which a polar group resides at the lipophilic end of the molecule. The inhibitory potency of diol **18** was similar to perillyl alcohol, suggesting little effect, either positive or negative. Once again, the opposite enantiomer of **18** (the (*R*)-enantiomer) should be tested for enzyme inhibition.

Comparison of compounds **15**, **16** and **17** with perillyl alcohol, perillaldehyde and perillic acid in terms of enzyme inhibition potency revealed that all three compounds were much less potent than their respective monoterpenoids. This suggests the importance of the isoprenyl moiety at the C<sub>4</sub> position for potent enzyme inhibition. Accordingly, the values obtained for GGPTase-I enzyme inhibition were less potent than the respective FPTase inhibitory values, owing to the necessity of a large lipophilic portion required by the GGPTase-I enzyme. 2-Cyclohexen-1-one, cyclohexenol **19** and *cis*-jasmane provided interesting inhibitory values. It was very

surprising to observe that 2-cyclohexen-1-one has the same potency as perillyl alcohol, especially as 2-cyclohexen-1-one does not contain a lipophilic segment. A possible reason may lie in conjugate addition to the electrophilic double bond, presumably by the RSH of a cysteine residue in or near the CaaX box. This is consistent with the lower inhibitory value achieved by cyclohexenol **19**, (a six-membered allylic alcohol). This shows that a ketone moiety may be a useful polar group when designing prenyl-protein transferase inhibitors. *cis*-Jasmone (a five-membered allylic ketone) is less effective as an inhibitor than 2-cyclohexen-1-one, perhaps suggesting either that a six-membered ring is structurally important or that the lipophilic segment attached one carbon position away from the ketone moiety is at an unfavourable location to confer enzyme inhibition potency. Additionally, conjugate addition at the 3-methyl substituted  $\beta$ -position would be more hindered.

### **3.11 Long-chain mono- and bicyclic compounds**

Inhibitors of prenyl-protein transferase, long-chain analogues were prepared with the aim to increasing the potency found for the short-chain compounds discussed above, scheme 5 outlines some routes.

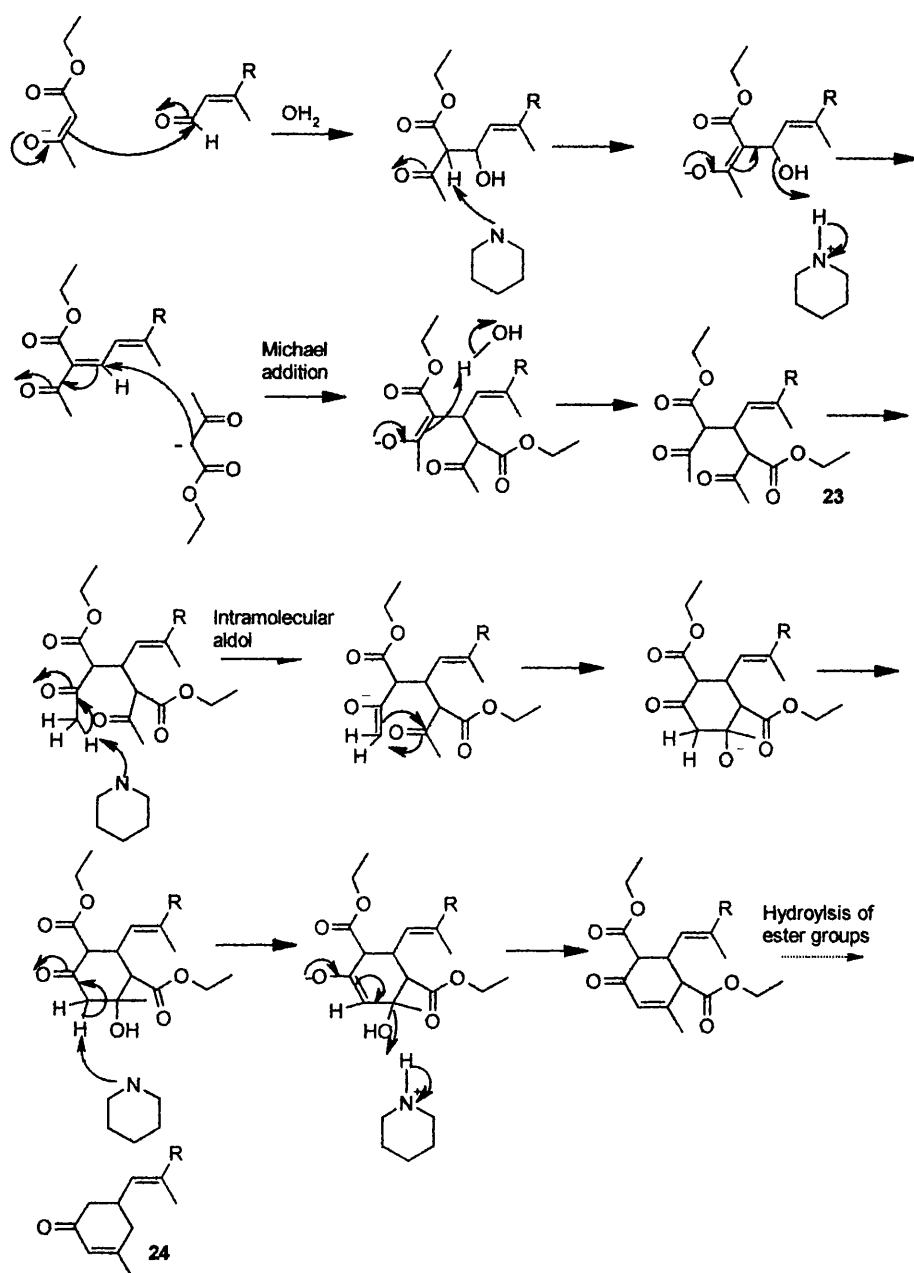


Reagents: (a) piperidine, (b) KOH, (c) NaOH, (d)  $\text{Ph}_3\text{PCHCO}_2\text{Et}$ , (e)  $\text{FeSO}_4$ , aq ammonia, (f) benzenesulfonyl chloride, pyridine, (g) LiOH, (h), benzenesulfonyl chloride, NaOH

### Scheme 5 Preparation of all long-chain mono- and bicyclic compounds

Diethyl ester **23** and ketone **24** were synthesised according to a procedure by Knoevenagel.<sup>107</sup> The mechanism by which  $\beta$ -keto diethyl ester **23** and allylic ketone **24** are formed involves a Michael addition followed by an intramolecular aldol condensation to form a six-membered ring. This combination of a Michael addition followed by an aldol condensation has the features of a Robinson annulation. The mechanism by which **23** and **24** are prepared is shown in Scheme 6.



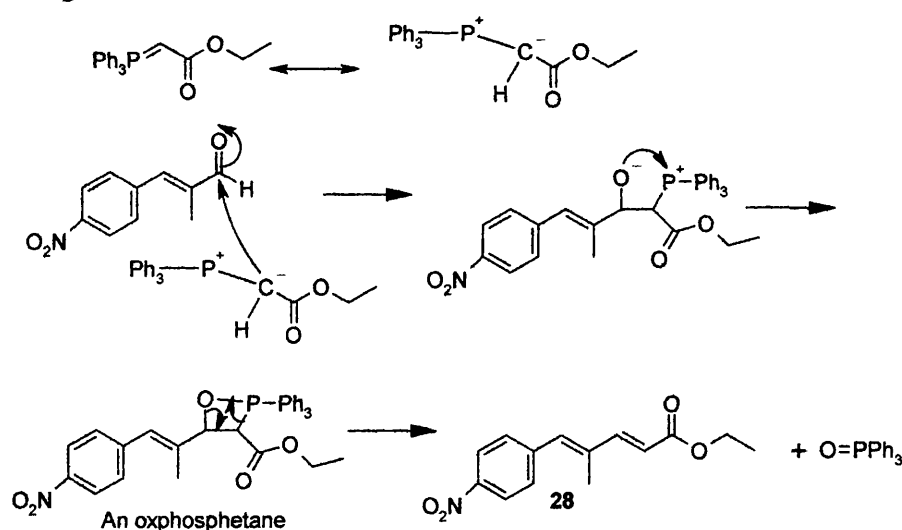


**Scheme 6** Preparation of diethyl ester **23** and ketone **24**

After a series of recrystallisations, diethyl  $\beta$ -keto ester **23** was obtained with a sharp melting point of 64 °C. The  $^{13}\text{C}$  n.m.r. was consistent with a single diastereoisomer, although Knoevenagel<sup>107</sup> did not comment upon the stereochemistry. It is inferred that compound **23** has an (*E*)-configuration about the double bond, as this is the major diastereoisomer present in the mixture of citral, the starting aldehyde. The reaction conditions necessary for synthesis of compound **23** are not sufficient to cause a

change in isomerism. Evidently, the recrystallisations led to the isolation of the pure (*E*)-isomer. Allylic ketone **24** obtained after a reflux in methanol with potassium hydroxide,<sup>107</sup> retains the (*E*)-configuration from **23**, again consistent with <sup>13</sup>C n.m.r signals for only one diastereoisomer. Both diethyl ester **23** and ketone **24** are racemates, and were submitted for enzyme inhibition testing as such.

Aldehyde **27** was prepared by an aldol condensation, giving a 9:1 mixture of (*E*):(*Z*) isomers, which upon a single recrystallisation afforded the (*E*)-isomer in pure form,<sup>108</sup> consistent with <sup>13</sup>C n.m.r signals. A subsequent Wittig reaction (shown in Scheme 7) with a stabilised ylid gave ester **28** in high yield (92%). Stabilised ylids in reaction temperatures higher than 20 °C generally lead to products of the (*E*)-configuration. This was confirmed by the coupling constants of 15 Hz for the double bonds of **28** in <sup>1</sup>H n.m.r and signals in the <sup>13</sup>C n.m.r consistent with only the (*E,E*)-isomer. Reduction of the nitro group to the amino moiety with Fe<sup>2+</sup> and ammonia proceeded smoothly, and allowed the double bonds to be retained, providing dienic ester **32**, retaining the (*E,E*)-geometry about the double bonds, again consistent with both <sup>1</sup>H and <sup>13</sup>C n.m.r data. Sulfonylation and subsequent hydrolysis afforded carboxylic acid **35**. The vicinal coupling about the double bonds in <sup>1</sup>H for compound **35** was 15 Hz, typical of *trans*-double bonds, and alkenic carbon atoms in the <sup>13</sup>C n.m.r data being consistent with a single diastereoisomer.



**Scheme 7** Synthesis of compound **28** via a Wittig reaction

Carboxylic acid **38** was prepared by a sulfonylation on 4-aminophenylbutyric acid with benzenesulfonyl chloride and sodium hydroxide in moderate yield (43%).

### 3.11.1 Evaluation of long-chain mono- and bicyclic compounds

Including (*S*)-limonene, (*S*)-perillyl alcohol and 4-phenylbutyric acid, seven compounds were submitted for enzyme assay analysis of prenyl-protein transferase inhibition, which were conducted by Dr. D. M. Vigushin. The results are shown in Table 4.

Compound No./Name	FPTase inhibition (IC <sub>50</sub> )	GGPTase inhibition (IC <sub>50</sub> )
( <i>S</i> )-Limonene	>40 mM	>40 mM
( <i>S</i> )-Perillyl alcohol	1.0 mM	1.0 mM
<b>23</b>	2.1 mM	2.1 mM
<b>24</b>	4.5 mM	4.5 mM
4-phenylbutyric acid	1.0 mM	1.0 mM
<b>35</b>	1.0 mM	1.0 mM
<b>38</b>	1.0 mM	1.0 mM

**Table 4** Enzyme inhibition assay values for long-chain mono- and bicyclic analogues

Compounds **23** and **24** were viewed with much promise as they contained all the aspects required (a polar tip, monoterpene head and lipophilic tail). Both compounds also possessed some structural similarity to farnesol, (as shown in figure 20) which itself is known to be a reasonably potent prenyl-protein transferase inhibitor.<sup>109</sup> However, the enzyme inhibition values obtained for both compounds were less potent than the values observed for perillyl alcohol. This may suggest either that the model designated as a template for potent prenyl-protein transferase inhibitors is not valid (figure 15) or that the orientation adopted by the lipophilic portion of both diethyl ester **23** and ketone **24** may not be appropriate; for example the number of C-O bonds in a ring will alter the number of directions it can adopt. Also both diethyl ester **23** and ketone **24** are racemates, and each enantiomer may show values different to the racemate used in the enzyme inhibition assay. Nevertheless, since both compounds correspond very well with the model for synthetic terpenoids capable of anti-cancer potential, diethyl ester **23** and ketone **24** were used in various leukaemic cell line assays to determine the effect on the cell cycle of various cancerous cell lines, as described in detail in Chapter four.

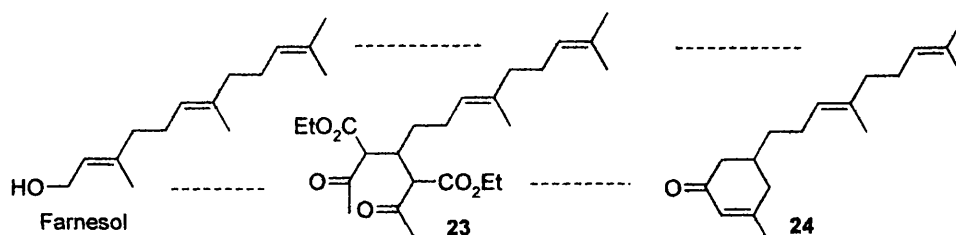


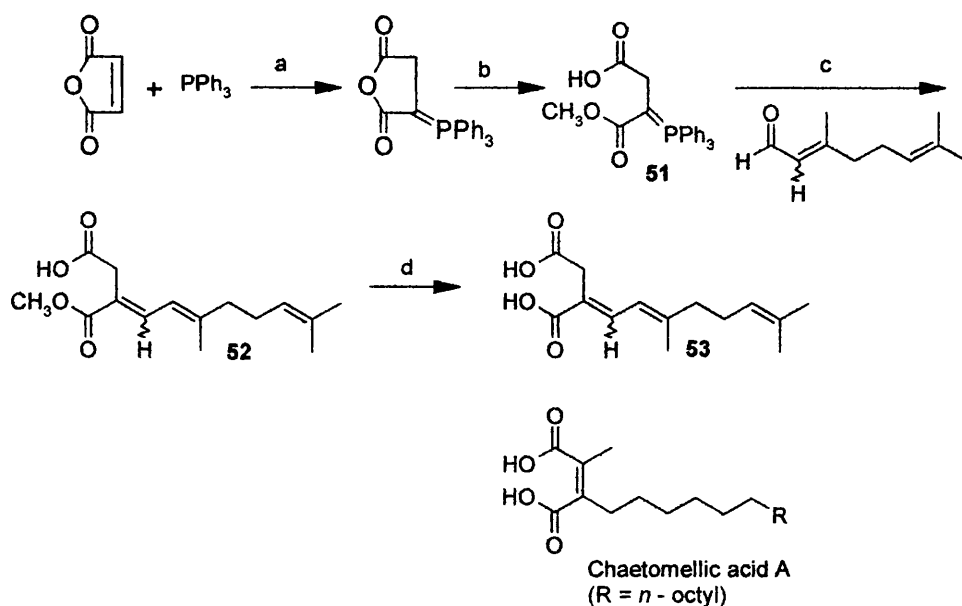
**Figure 20** Comparison of farnesol with diethyl ester **23** and ketone **24**

4-Phenylbutyric acid and compounds **35** and **38** showed the same potency for prenyl-protein transferase inhibition as did perillyl alcohol. The fact that all three compounds have similar values is interesting, since the extension of a sulfonamido unit had little effect on potency, either positive or negative. With the sulfonamido moiety, compounds **35** and **38** may show more promise if conducted with an *in vivo* enzyme inhibition assay compared with the standard *in vitro* enzyme inhibition assay, owing to the cell delivery potential of the sulfonamido group in terms of permeability. Another interesting observation is that the degree of unsaturation contained within compounds **38** and **35** had little effect on the potency of enzyme inhibition.

### **3.12 Medium- to long-chain compounds with a strongly polar terminus**

Chaetomelic acid A is a very potent FPTase inhibitor, with an  $IC_{50}$  value of 55 nM.<sup>110</sup> The dicarboxylic acid moiety is thought to be an excellent mimic of the pyrophosphate unit on farnesyl pyrophosphate, thus chaetomelic acid A could possibly be a competitive inhibitor with respect to farnesyl pyrophosphate. The fact that chaetomelic acid A (a potent FPTase inhibitor) is a dicarboxylic acid, led to the idea of modifying the rationale into the model designed as a template for producing potent synthetic terpenoid inhibitors of prenyl-protein transferase, by significantly increasing the polar terminus of future compounds. In the following schemes, the synthesis of corresponding dicarboxylic acids, dimethyl esters, monocarboxylic acid-methyl ester, and anhydrides of varying different lipophilic lengths will be shown.

In Scheme 8, the preparation of compounds **52** and **53** is shown with the structure of chaetomelic acid A as a comparison.

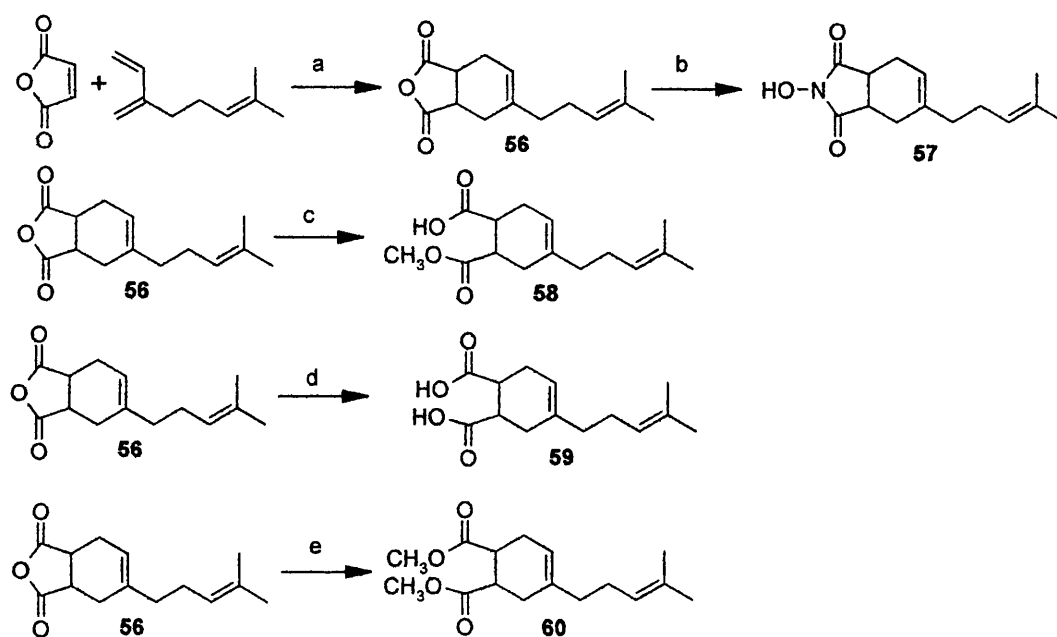


Reagents: (a) triphenylphosphine, (b) methanol, (c) citral, (d) LiOH

#### Scheme 8 Preparation of medium-chain chaetomelic acid analogues

Stirring the ylid (formed from furan-2,5-dione and triphenylphosphine) with methanol at 25 °C for 24 hours gave the half-ester **51**, as a pale yellow crystalline solid. Fulorand<sup>111</sup> postulated that the methoxy group is adjacent to the triphenylphosphine unit, and it has been assumed that this is correct structure throughout the present work. A Wittig reaction gave the monocarboxylic acid-methyl ester **52** in satisfactory yield (84%). The <sup>13</sup>C n.m.r spectrum revealed that compound **52** was a 3:1 stereoisomeric mixture, with the major isomer assigned as the (*E*)-configuration, because citral (the starting aldehyde) consists of a 3:1 stereoisomer of the (*E*)-configuration, and a Wittig reaction is not expected to alter the isomer composition of the existing double bond. Dicarboxylic acid **53**, formed by an ester hydrolysis with lithium hydroxide, also retained the 3:1 ratio of (*E*) to (*Z*) isomerism found in compound **52**.

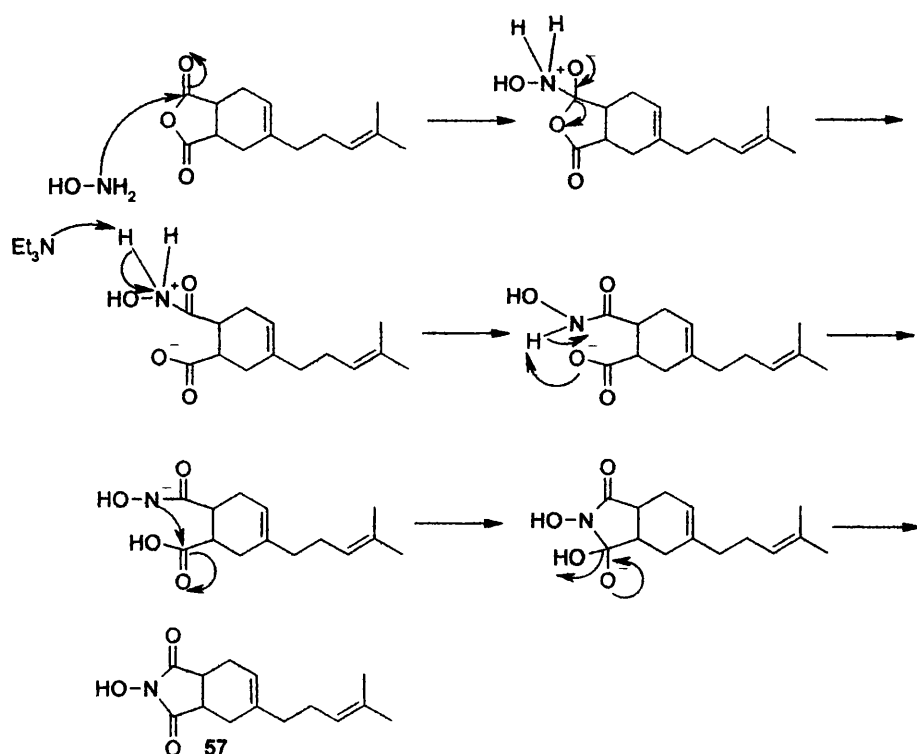
Scheme 9, depicts the synthesis of compounds with a lipophilic chain derived from  $\gamma$ -myrcene.



Reagents: (a)  $\gamma$ -myrcene, (b)  $\text{HO.NH}_3\text{Cl}$ , (c)  $\text{K}_2\text{CO}_3$ , (d)  $\text{KOH}$ , (e)  $\text{H}_2\text{SO}_4$ , methanol

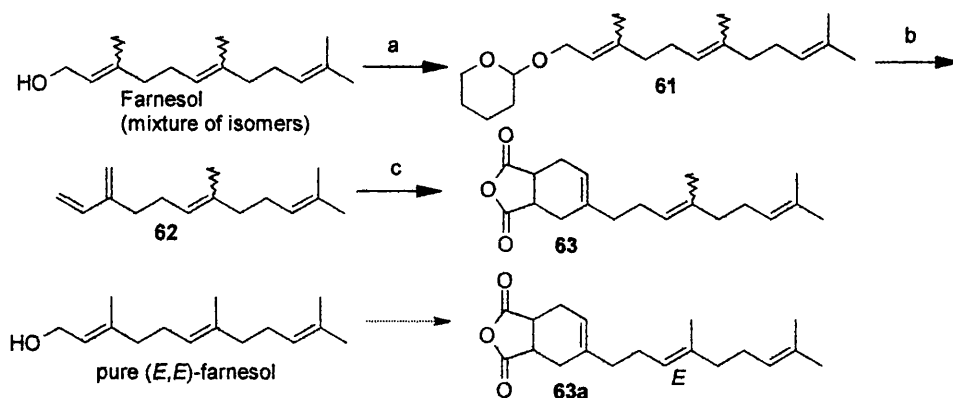
### Scheme 9 Preparation of various polar $\gamma$ -myrcene derived inhibitors

Anhydride **56** was synthesised *via* a Diels-Alder reaction and thus contains a *cis*-ring junction, following from the rules of cycloadditions.<sup>112</sup> From the  $^{13}\text{C}$  n.m.r spectra, compounds **57-60** are consistent with a single (*cis*) ring junction on the cyclohexane ring. All compounds shown in this scheme exist in racemic forms and were enzyme assayed as racemates. Anhydride **56** was hydrolysed with potassium carbonate, potassium hydroxide and sulphuric acid/methanol to give respectively the monocarboxylic acid-methyl ester **58**, dicarboxylic acid **59** and dimethyl ester **60** in yields above 65%. Preparation of *N*-hydroxy **57** was first attempted with hydroxylamine hydrochloride and pyridine (as the base), however, an undesirable adduct was formed between the anhydride **56** and pyridine. When triethylamine was used in place of pyridine as the base, the reaction occurred smoothly, the desired product **57** being formed in good yield (83%). The mechanism in the formation of compound **57** is shown in Scheme 10.



**Scheme 10** Mechanism of formation of an *N*-hydroximide

The synthesis of anhydrides with a longer unsaturated lipophilic portion (farnesol) is shown in Scheme 11.

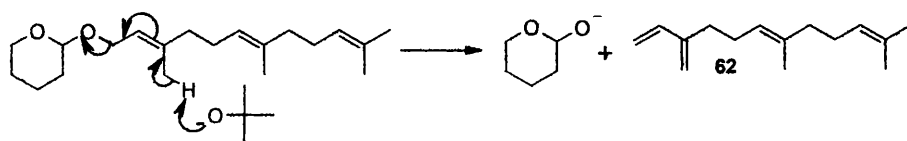


Reagents: (a) 3,4-dihydro-2H-pyran, (b) Bu<sup>t</sup>OK, 18-Crown-6, (c) maleic anhydride

**Scheme 11** Preparation of anhydrides incorporating a sesquiterpenoid lipophilic unit

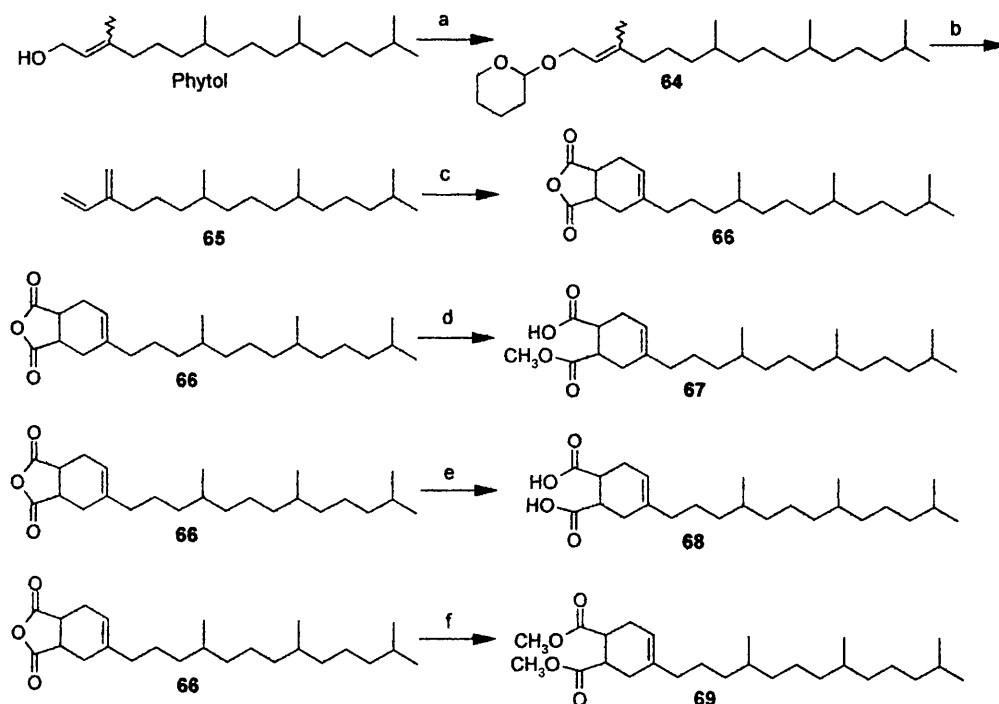
Compound **61** was prepared in high yield (78%) by protection of the alcohol moiety with 3,4-dihydro-2H-pyran. The protected pyran **61** underwent elimination using Bu<sup>t</sup>OK with 18-crown-6 to afford β-farnesene **62** in moderate yield (73%). Anhydrides **63** and **63a** were synthesised using the above cycloaddition pathway, and

they both possess a *cis*-ring junction. Once again, both anhydrides **63** and **63a** were obtained as racemates, and as such were subsequently tested for enzyme inhibition in racemic mixtures. Anhydride **63** was prepared from farnesol (2:1 (*E*):(*Z*) isomers), the same variation in isomers was exhibited in anhydride **63**. In contrast, anhydride **63a** was synthesised from stereopure (*E,E*)-farnesol, and retained the (*E*)-configuration in the end product **63a**, (isolated in 52% yield), as confirmed by  $^{13}\text{C}$  n.m.r spectrum, with only one diastereoisomer observed.



**Scheme 12** The E2 mechanism for the formation of  $\beta$ -farnesene **62**

The third lipophilic chain length used for the preparation of new compounds was obtained from phytol (a diterpenoid), as shown in Scheme 13.



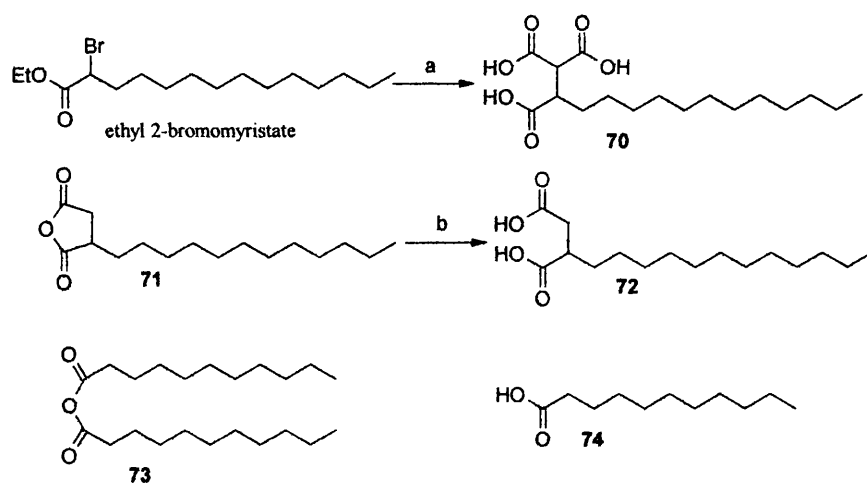
Reagents: (a) 3,4-dihydro-2*H*-pyran, (b) Bu<sup>t</sup>OK, 18-crown-6, (c) maleic anhydride, (d) K<sub>2</sub>CO<sub>3</sub>, (e) H<sub>2</sub>SO<sub>4</sub>, methanol, (f) KOH

**Scheme 13** Preparation of long-chain compounds with strongly polar terminus



As with the previous compounds in Scheme 9, the alcohol was derivatised with 3,4-tetrahydro-2*H*-pyran, which underwent elimination to give a 2-substituted buta-1,3-diene (neophytadiene, **65**),<sup>113</sup> which reacted with maleic anhydride in acetone to give the anhydride **66** *via* a Diels-Alder reaction.<sup>114</sup> Once again, the anhydride has a *cis*-ring junction following the rules of cycloaddition, and compounds **66-69** were all obtained in racemic form, and tested for enzyme inhibition as racemates. Phytol is a naturally occurring mixture of (*E*):(*Z*) isomers about the double bond, however the (*E*):(*Z*) isomerism no longer existed after formation of diene **65**. The phytol obtained from Aldrich is stated to be a mixture of isomers, without further classification. However, Rowland attained anhydride **66** using phytol obtained from tobacco plants, with an *R,R* configuration. The n.m.r data do not permit further inferences regarding the regiochemistry, although a racemic mixture of isomers at the anhydride bridge location must exist, and this mixture was tested for enzyme inhibition. Anhydride **66** was hydrolysed with potassium carbonate, potassium hydroxide and sulfuric acid/methanol to give the monocarboxylic acid-methyl ester **67**, dicarboxylic acid **68** and dimethyl ester **69** respectively, in yields above 65%.

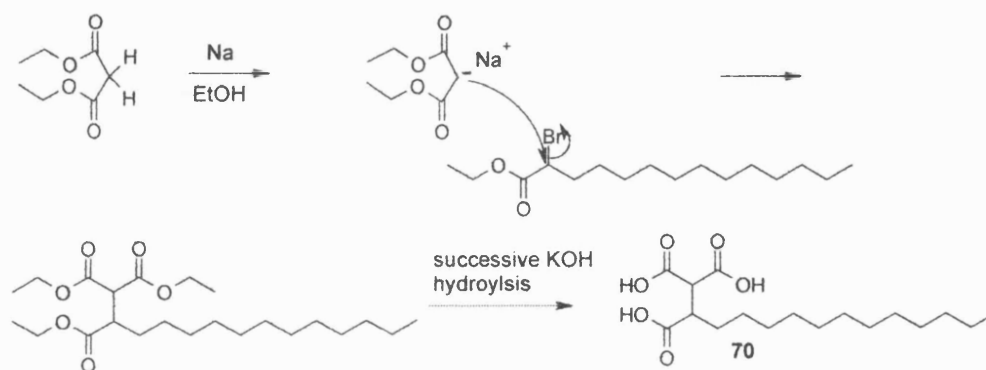
Scheme 14 shows the synthesis of a tricarboxylic acid with a long saturated lipophilic tail, with the corresponding anhydride and dicarboxylic acid and a non-cyclic anhydride with matching monocarboxylic acid.



Reagents: (a) diethyl malonate, sodium ethoxide, (b) (i) KOH, H<sub>2</sub>O, (ii) HCl

**Scheme 14** Preparation of various long-chain saturated lipophilic compounds

Tricarboxylic acid **70** was prepared by an  $S_N2$  displacement using the anion of diethyl malonate,<sup>115</sup> (shown in Scheme 15). Hydrolysis of anhydride **71** with potassium hydroxide afforded the dicarboxylic acid **72** in high yield (72%). Compounds **70**, **71** and **72** are all racemic, and were submitted for enzyme inhibition testing as racemates. Compounds **73** and **74** were examined in order to assess the importance of the cyclic ring fused to the anhydride, in terms of prenyl-protein transferase inhibition.



**Scheme 15** Formation of tricarboxylic acid **70**

### 3.12.1 Evaluation of medium- to long-chain compounds with strongly polar terminus

Including (*S*)-limonene, (*S*)-perillyl alcohol, chaetomelic acid A, CoQ<sub>10</sub>, itaconic anhydride, 2-hydroxyisoindole-1,3-dione and 1-hydroxypyrrolidine-2,5-dione, twenty-five compounds were submitted for enzyme assay analysis for prenyl-protein transferase inhibition, which was conducted by Dr. D. M. Vigushin, Dr. G. Brooke and A. S. Rioja. The results are shown in Table 5.

Compound No./Name	FPTase inhibition (IC <sub>50</sub> )	GGPTase inhibition (IC <sub>50</sub> )
(S)-Limonene	>40 mM	>40 mM
(S)-Perillyl alcohol	1.0 mM	1.0 mM
Chaetomelic acid A	55 nM	92 $\mu$ M
<b>52</b>	1.0 mM	185 $\mu$ M
<b>53</b>	1.0 mM	420 $\mu$ M
Itaconic anhydride	>1.0 mM	>1.0 mM
<b>56</b>	449 $\mu$ M	40.2 $\mu$ M
<b>58</b>	500 $\mu$ M	>1.0 mM
<b>59</b>	>1.0 mM	>1.0 mM
<b>60</b>	900 $\mu$ M	500 $\mu$ M
<b>57</b>	171 $\mu$ M	216 $\mu$ M
2-Hydroxyisoindole-1,3-dione	>1.0 mM	>1.0 mM
1-Hydroxypyrrolidine-2,5-dione	>1.0 mM	>1.0 mM
<b>63</b>	9.0 $\mu$ M	503 $\mu$ M
<b>63a</b>	190 $\mu$ M	136 $\mu$ M
<b>66</b>	>1.0 mM	20.8 $\mu$ M
<b>67</b>	>1.0 mM	>1.0 mM
<b>68</b>	>1.0 mM	>1.0 mM
<b>69</b>	>1.0 mM	>1.0 mM
<b>70</b>	166 $\mu$ M	252 $\mu$ M
<b>71</b>	854 $\mu$ M	229 $\mu$ M
<b>72</b>	402 $\mu$ M	>1.0 mM
<b>73</b>	>1.0 mM	401 $\mu$ M
<b>74</b>	>1.0 mM	>1.0 mM
CoQ <sub>10</sub>	500 $\mu$ M	>1.0 mM

**Table 5** Enzyme inhibition assay values for medium- to long-chain compounds with strongly polar terminus

Comparison of results obtained from the enzyme inhibition assays allowed several inferences. This third set of compounds proved to be the most successful batch in terms of inhibiting both FPTase and GGPTase-I. The compounds were designed on the premise that the polar group (dicarboxylic acid, monocarboxylic acid-methyl ester, dimethyl ester and anhydride) would mimic the pyrophosphate group of FPP or GGPP, and that respective FPTase and GGPTase-I inhibition can be favoured by the adjustment of lipid chain length and the degree of unsaturation of the lipid chain.

The anhydrides **56**, **63**, **63a**, **66**, **71** and **73** are much more efficient inhibitors of GGPTase-I than succinic acids **53**, **59**, **68**, **72** and **74**, implying a singular role for the anhydride moiety, and also indicating that hydrolysis to the corresponding dicarboxylic acids do not occur rapidly *in vitro*. That the anhydride unit is not acting just as a delivery system is indicated by the activity of compound **66** (an IC<sub>50</sub> value for GGPTase-I of 21  $\mu$ M) *versus* the inactivity of the corresponding dimethyl ester

**69**, ( $IC_{50}$  value for GGPTase-I  $>1000\ \mu\text{M}$ ). It may be that the activity is conferred by an acylating role of the anhydrides. As expected, the length and nature of the lipophilic chain markedly influences the prenyl-protein transferase inhibition. The lack of an alkyl (including prenyl) chain, as in itaconic anhydride (compound **54**), excludes prenyl-protein transferase inhibition, whereas the compound with the longest lipophilic chain, anhydride **66** has excellent inhibition of GGPTase-I. Also anhydrides **66** and **56** exhibited good selectivity for GGPTase-I over FPTase by 50:1 and 11:1 respectively. Interestingly, the 2:1 *E/Z* mixture of anhydride **63** shows excellent selectivity for FPTase compared to GGPTase-I by 50:1. Therefore, anhydrides **56**, **63** and **66** could be of use as probes for the selective inhibition of either FPTase or GGPTase-I.

The uniqueness of the anhydride function is shown by comparison with a variety of related functional groups including dicarboxylic acids, monocarboxylic acid-methyl ester, *N*-hydroxy anhydride compounds **57**, and **55**, the tricarboxylic acid **70** and CoQ<sub>10</sub>. Thus, FPTase  $IC_{50}$  values for the dicarboxylic acids **53**, **59** and **68** were all  $>1000\ \mu\text{M}$ , and that for dicarboxylic acid **72** was  $402\ \mu\text{M}$ . The GGPTase-I  $IC_{50}$  values for the monocarboxylic acid-methyl ester compounds **52**, **58** and **67** were each above  $>1000\ \mu\text{M}$ , and those for the dicarboxylic acid compounds **59** and **53** were 900, and  $402\ \mu\text{M}$  respectively. FPTase/GGPTase-I  $IC_{50}$  values (ratio of  $\mu\text{M}$ ) for various non-anhydride moieties are: **60** (900:500); compound **52** ( $>1000:185$ ) and compound **69** ( $>1000:>1000$ ). The *N*-hydroxy compounds **55a**, **55b** and **57** had FPTase/GGPTase-I  $IC_{50}$  values (ratio of  $\mu\text{M}$ ) of  $>1000:>1000$ ,  $>1000:>1000$  and 171:216 respectively, emphasising, once again that the lack of a lipophilic chain dramatically reduces the potency of inhibition (as observed by the  $IC_{50}$  values of **55a** and **55b**). Tricarboxylic acid **70** (the most polar compound) had FPTase/GGPTase-I inhibitory  $IC_{50}$  values of  $166:252\ \mu\text{M}$  respectively, and was thus not as potent for GGPTase-I enzyme inhibition as anhydrides **56** and **66**. CoenzymeQ<sub>10</sub> had an  $IC_{50}$  value for FPTase of  $500\ \mu\text{M}$ , whilst for GGPTase-I, the  $IC_{50}$  value was  $>1000\ \mu\text{M}$ . Perhaps suprisingly, despite the lengthy prenylated chain of CoQ<sub>10</sub>, and the possibility of it acting as a Michael acceptor or participating in redox processes, CoQ<sub>10</sub> was not found to be a significant GGPTase-I inhibitor.

### 3.13 Conclusion

The results obtained from the compounds prepared as potential prenyl-protein transferase inhibitors; provide some validation of the model created of a polar tip, monoterpene ring and long lipophilic chain. However, it is the choice of polar 'tip' that has been the most surprising aspect. Carboxylic acids, ketones and alcohols are often the common polar groups for prenyl-protein transferase inhibitors. Thus, the emergence of anhydrides as conferring moderately potent GGPTase inhibition was unexpected. Indeed, in contrast to chaetomelic acid A (a potent FPTase inhibitor) cyclic, fused anhydrides have been shown to be much *more* active than their corresponding dicarboxylic acids or methyl ester derivatives. For instance, anhydride **66** is over 50 times more potent than either the corresponding dicarboxylic acid **68** or dimethyl ester **69** as an inhibitor of GGPTase-I. Indeed, the synthetic GGPTase-I inhibitors **56** and **66** are more *potent* than the naturally occurring chaetomelic acid A (GGPTase-I  $IC_{50} = 92 \mu M$  and GGPTase-II  $IC_{50} = 34 \mu M$ ), and are among the most potent non-peptidic inhibitors of GGPTase-I known.<sup>116</sup> They possess the advantage over peptidic enzyme inhibitors because anhydrides **56** and **66** lack the peptide bonds that could be degraded by peptidases, and when placed in solution, the structures remain intact for at least 24 hours, confirmed by  $^1H$  n.m.r spectroscopy. Although a peptidic GGPTase-I inhibitor with an  $IC_{50}$  value of 55 nM has been reported, the effect on whole cells requires micromolar concentrations.<sup>117</sup> Whether an anhydride could act as a neutral analogue of the pyrophosphate group of FPP or GGPP is an important matter, which needs further investigation. It is known that certain GGPTase-I inhibitors are thought to prevent hyperplastic remodelling and act on vascular lesions by inducing apoptotic regression.<sup>118</sup> Consequently, the emergence of these anhydride inhibitors of GGPTase-I, whose activity can be varied by altering the lipid chain length and type, point towards a potential therapeutic value and use as biochemical probes.<sup>118</sup>

### 3.14 References

- 1] Crowell, P. L.; Chang, R. R.; Ren, Z.; Elson, C. E.; Gould, M. N. *J. Biol. Chem.*, **1991**, *266*, 17679
- 2] Gibbs, J. B. *Semin. Can. Biol.*, **1992**, *3*, 383
- 3] Graham, S. L. *Exp. Opin. Ther. Patents*, **1995**, *5*, 1269
- 4] Fiorucci, G.; Hall, A. *Biochimica et Biophysica Acta*, **1988**, *1*, 81
- 5] Satoh, T.; Nakafuku, M.; Kaziro, Y. *J. Biol. Chem.*, **1992**, *267*, 24149
- 6] Khosravifar, R.; Der, C. J. *Cancer Metastasis Rev.*, **1994**, *13*, 67
- 7] Clark, G. J.; Der, C. J. *Breast Cancer Res. Treat.*, **1995**, *35*, 133
- 8] Pazin, M. J.; Williams, L. T. *Trends Biochem. Sci.*, **1992**, *17*, 374
- 9] DeClue, J. E.; Papageprge, A. G.; Fletcher, J. A.; Deihl, S. R.; Ratner, N.; Lowy, D. R. *Cell*, **1992**, *69*, 265
- 10] Basu, T. N.; Gutmann, D. H.; Fletcher, J. A.; Glover, T. W.; Collins, F. S.; Downward, J. *Nature*, **1992**, *356*, 713
- 11] Gibbs, J. B.; Oliff, A. *Cell*, **1994**, *79*, 193
- 12] Barbacid, M. *Annu. Rev. Biochem.*, **1987**, *56*, 779
- 13] Bos, J. L. *Cancer Res.*, **1989**, *49*, 4682
- 14] Clark, G. J.; Der, C. J. *GTPases in Biology I*, Springer Verlag, Berlin, **1992**, 259
- 15] Fearon, E. R.; Vogelstein, B. *Cell*, **1990**, *61*, 759
- 16] Hunter, T. *Cell*, **1991**, *64*, 249
- 17] Kinzler, K. W.; Vogelstein, B. *Cell*, **1996**, *87*, 159
- 18] Sebt, M.; Hamilton, A. D. *Drug Design Today*, **1998**, *3*, 26
- 19] Fantl, W. J.; Escobedo, J. A.; Martin, G. A.; Turok, C. W.; Delrosario, M.; McCormick, F.; Williams, L. T. *Cell*, **1992**, *69*, 413
- 20] Egan, S. E.; Giddings, B. W.; Brooks, M. W.; Buday, L.; Sreland, A. M.; Weinberg, R. A. *Nature*, **1993**, *363*, 45
- 21] Prive, G. G.; Milburn, M. V.; Tong, L.; Devos, A. M.; Yamaizumi, Z.; Nishimura, S.; Kim, S. H. *Proc. Natl. Acad. Sci. USA*, **1992**, *89*, 3649
- 22] Langercarter, C. A.; Pleiman, C. M.; Gardner, A. M.; Blumer, K. J.; Johnson, G. L. *Science*, **1993**, *260*, 315
- 23] Gibbs, J. B.; Kohl, N. E.; Koblan, K. S.; Omer, C. A.; Rosen, N.; Anthony, N. J.; Conner, M. W.; deSolms, S. J.; Williams, T. M.; Graham, S. L.; Hartman, G. D.; Oliff, A., *Breast Cancer Res. Treat.*, **1996**, *38*, 375

- 24] Boguski, M. S.; McCormick, F. *Nature*, **1993**, 366, 643
- 25] Tong, L.; deVos, A. M.; Milburn, M. V.; Jancarik, J.; Noguchi, S.; Nishimura, S.; Miura, K.; Outsuka, E.; Kim, S. H. *Nature*, **1989**, 337, 90
- 26] Krenzel, U.; Schlichting, I.; Scherer, A.; Schumann, R.; Frech, M.; John, J.; Kabsoh, W.; Pai, E. F.; Wittinghofer, A. *Cell*, **1990**, 62, 539
- 27] Clark, G. J.; Drugan, J. K.; Terrell, R. S.; Bradham, C.; Der, C. J.; Bell, R. M.; Campbell-Burk, S. *Proc. Natl. Acad. Sci. USA*, **1995**, 93, 1577
- 28] Davis, R. J. *J. Biol. Chem.*, **1993**, 286, 14553
- 29] Egan, S. E.; Weinberg, R. A. *Nature*, **1993**, 365, 781
- 30] Marshall, C. J. *Cell*, **1995**, 80, 179
- 31] Maltese, W. A.; Sheridan, K. M.; Repko, E. M.; Erdman, R. A. *J. Biol. Chem.*, **1990**, 265, 2148
- 32] Cox, A. D. *Curr. Op. Cell Biol.*, **1992**, 4, 1008
- 33] Magee, A. I.; Newman, C. M.; Giannakouros, T.; Hancock, J. F.; Fawell, E.; Armstrong, J. *Biochem. Soc. Trans.*, **1992**, 20, 497
- 34] Reiss, Y.; Goldstein, J. L.; Seabra, M. C.; Casey, P. J.; Brown, M. S. *Cell*, **1990**, 62, 81
- 35] Moores, S. L.; Schaber, M. D.; Rands, E.; O'Hara, M. B.; Garsky, V. M.; Pompliano, D. L.; Gibbs, J. B. *J. Biol. Chem.*, **1991**, 266, 14603
- 36] Reiss, Y.; Seabra, M. C.; Armstrong, S. A.; Goldstein, J. L.; Brown, M. S. *J. Biol. Chem.*, **1991**, 266, 10672
- 37] Chen, W. J.; Andres, D. A.; Goldstein, J. L.; Russel, D. W.; Brown, M. S. *Cell*, **1991**, 66, 327
- 38] Chen, W. J.; Andres, D. A.; Goldstein, J. L.; Brown, M. S. *Proc. Natl. Acad. Sci. USA*, **1991**, 88, 11368
- 39] Ying, W.; Sepp-Lorenzino, L.; Cai, K.; Coleman, P. S. *J. Biol. Chem.*, **1994**, 269, 470
- 40] Park, H. W.; Boduluri, S. R.; Moomain, J. F.; Casey, P. J.; Beese, L. S. *Science*, **1997**, 275, 1800
- 41] Chen, W. J.; Moomaw, J. F.; Overton, L.; Kost, T. A.; Casey, P. J. *J. Biol. Chem.*, **1993**, 268, 9675
- 42] Gutierrez, L.; Magnee, A. I.; Marshall, C. J.; Hancock, J. F. *EMBO J.*, **1989**, 8, 1093
- 43] Casey, P. J.; Seabra, M. C. *J. Biol. Chem.*, **1996**, 271, 5289

- 44] Pompliano, D. L.; Rounds, E.; Schaber, M. D.; Mosser, S. D.; Anthony, N. J.; Gibbs, J. B. *Biochemistry*, **1993**, *31*, 3800
- 45] Reiss, Y.; Seabra, M. C.; Armstrong, S. A.; Slaughter, C. A.; Goldstein, J. L.; Brown, M. S. *J. Biol. Chem.*, **1991**, *266*, 10672
- 46] Furfine, E. S.; Leban, J. J.; Landavazo, A.; Moomaw, J. F.; Casey, P. J. *Biochemistry*, **1995**, *34*, 6857
- 47] Reiss, Y.; Goldstein, J. L.; Seabra, M. C.; Casey, P. J.; Brown, M. S. *Cell*, **1990**, *62*, 81
- 48] Reiss, Y.; Stradley, S. J.; Gierasch, L. M.; Brown, M. S.; Goldstein, J. L. *Proc. Natl. Acad. Sci. USA*, **1991**, *88*, 735
- 49] Stryer, L. in 'Biochemistry', 4<sup>th</sup> ed. Freeman, New York, **1995**, 21
- 50] Gibbs, J. B.; Oliff, A. *Annu. Rev. Pharmacol. Toxicol.*, **1997**, *37*, 143
- 51] Schaber, M. D.; O'Hara, M. B.; Garsky, V. M.; Mosser, S. D.; Bergstrom, J. D. *J. Biol. Chem.*, **1990**, *265*, 14701
- 52] Qian, Y. M.; Sebti, S. M.; Hamilton, A. D. *Biopolymers*, **1997**, *43*, 25
- 53] Graham, S. L.; Desolms, S. D.; Oliff, A.; Pompliano, D. L.; Rands, E.; Breslin, M. J.; Deana, A. A.; Garsky, V. M.; Scholz, T. H.; Gibbs, J. B.; Smith, R. L. *J. Med. Chem.*, **1994**, *37*, 725
- 54] Kohl, N. E.; Mosser, S. D.; Desolms, S. J.; Giuliani, E. A.; Pompliano, D. L.; Graham, S. L.; Smith, R. L.; Scolnick, E. M.; Oliff, A.; Gibbs, J. B. *Science*, **1993**, *260*, 1934
- 55] Kohl, N. E.; Wilson, F. R.; Mosser, S. D.; Giuliani, E.; Desolms, S. J.; Lonner, M. W.; Anthony, N. J.; Holtz, W. J.; Gomez, R. P.; Lee, T. J.; Smith, R. L.; Graham, S. L.; Hartman, G. D.; Gibbs, J. B.; Oliff, A. *Proc. Natl. Acad. Sci. USA*, **1994**, *91*, 9141
- 56] Sepplorezzino, L.; Ma, Z. P.; Bands, E.; Kohl, N. E.; Gibbs, J. B.; Oliff, A.; Rosen, N. *Cancer Res.*, **1995**, *55*, 5302
- 57] Kohl, N. E.; Omer, C. A.; Conner, M. W.; Anthony, N. J.; Davide, J. P.; Desolms, S. J.; Giuliani, E. A.; Gomez, R. P.; Graham, S. L.; Hamilton, K.; Handt, L. K.; Hartman, G. D.; Koblan, K. S.; Kral, A. M.; Miller, P. J.; Mosser, S. D.; O'Neill, T. J.; Rands, E.; Schaber, M. D.; Gibbs, J. B.; Oliff, A. *Nat. Med.*, **1995**, *1*, 792
- 58] Lerner, E. C.; Qian, Y. M.; Blaskovich, M. A.; Fossum, R. D.; Vogt, A.; Sun, J. Z.; Cox, A. D.; Der, C. J.; Hamilton, A. D.; Sebti, S. M. *J. Biol. Chem.*, **1995**, *270*, 26082



- 59] Sun, J. Z.; Qian, Y. M.; Hamilton, A. D.; Sebtì, S. M. *Cancer Res.*, **1995**, *55*, 4243
- 60] Lerner, E. C.; Qian, Y. M.; Hamilton, A. D.; Sebtì, S. M. *J. Biol. Chem.*, **1995**, *270*, 26770
- 61] Harrington, E. M.; Kowalczyk, J. J.; Pinnow, S. L.; Ackermann, K.; Garcia, A. M.; Lewis, M. D. *Bioorg. Med. Chem. Lett.*, **1994**, *4*, 2775
- 62] Nagasu, T.; Yoshimatsu, K.; Rowell, C.; Lewis, M. D.; Garcia, A. M. *Cancer Res.*, **1995**, *55*, 5310
- 63] James, G. L.; Goldstein, J. L.; Brown, M. S.; Rawson, T. E.; Somers, T. C.; McDowell, R. S.; Marsters, J. C.; Paris, K.; Burdick, D. J.; Oare, D. A.; Xue, Y. C.; Reynolds, M. E. *Abstr. Pap. Am. Chem. S.*, **1994**, *201*, 278
- 64] James, G. L.; Goldstein, J. L.; Brown, M. S.; Rawson, T. E.; Somers, T. C.; McDowell, R. S.; Crowley, C. W.; Lucas, B. K.; Levinson, A. D.; Marsters, J. C. *Science*, **1993**, *260*, 1937
- 65] James, G. L.; Brown, M. S.; Cobb, M. H.; Goldstein, J. L. *J. Biol. Chem.*, **1994**, *269*, 27705
- 66] Garcia, A. M.; Rowell, C.; Ackerman, K.; Kowalczyk, J. J.; Lewis, M. D. *J. Biol. Chem.*, **1993**, *268*, 18415
- 67] Brown, S. M.; Goldstein, J. L.; Paris, K. J.; Burnier, J. P.; Marsters, J. C. *Proc. Natl. Acad. Sci. USA*, **1992**, *89*, 8813
- 68] Kohl, N. E.; Mosser, S. D.; Desolms, S. J.; Giuliani, E. A.; Pompliano, D. L.; Graham, S. L.; Smith, R. L.; Scolnick, E. M.; Oliff, A.; Gibbs, J. B. *Science*, **1993**, *260*, 1934
- 69] Heimbrook, D. unpublished data
- 70] Vogt, A.; Qian, Y.; Blaskovich, M. A.; Fossum, R. D.; Sebtì, S. M.; Hamilton, A. D. *J. Biol. Chem.*, **1995**, *270*, 660
- 71] Vogt, A.; Qian, Y. M.; Blaskovich, M. A.; Fossum, R. D.; Hamilton, A. D.; Sebtì, S. M. *J. Biol. Chem.*, **1995**, *270*, 660
- 72] Qian, Y. M.; Vogt, A.; Sebtì, S. M.; Hamilton, A. D. *J. Med. Chem.*, **1996**, *39*, 217
- 73] Bishop, W. R.; Bond, R.; Wang, L.; Doll, R.; Njoroge, G.; Catino, J.; Windsor, W.; Syto, R.; Carr, D.; Kirschmeier, P. *J. Biol. Chem.*, **1995**, *270*, 30611
- 74] Tamanoi, F. *Trends. Biol. Sci.*, **1993**, *18*, 349

- 75] Valentijn, A. R. M.; Vanderberg, O.; Vandermarel, G. A.; Cohen, L. H.; Vanboom, J. H. *Tetrahedron*, **1995**, *51*, 2099
- 76] Patel, D. V.; Schmidt, R. J.; Biller, S. A.; Gordon, E. M.; Robinson, S. S.; Manne, V. *J. Med. Chem.*, **1995**, *38*, 2906
- 77] Silverman, K. C.; Jayasuriya, H.; Cascales, C.; Vilella, D.; Bills, G. F.; Singh, S. B.; Lingham, R. B. *Biochem. Biophys. Res. Commun.*, **1997**, *232*, 478
- 78] Lingham, R. B.; Silverman, K. C.; Cascales, G. F.; Jenkins, M.; Martin, S. E.; Pelaez, F.; Kong, Y. L.; Meinz, M. S.; Nallin-Omstead, M.; Schaber, M. D.; Pompliano, D. L.; Gibbs, J. B.; Singh, S. B. *Appl. Microbiol. Biotechnol.*, **1993**, *40*, 370
- 79] Bhide, R. S.; Patel, D. V.; Patel, M. M.; Robinson, S. P.; Hunihan, L. W.; Gordon, E. M. *Bioorg. Med. Chem. Lett.*, **1994**, *4*, 2107
- 80] Manne, V.; Carboni, J. M.; Ricca, C. S.; Andahazy, M. L.; Patel, D.; Weinmann, R.; Cox, A. D.; Gordon, E. M.; Seizinger, B. R. *Oncogene*, **1995**, *10*, 1763
- 81] Gibbs, J. B.; Pompliano, D. L.; Mosser, S. D.; Lingham, R. B.; Singh, S. B.; Kohl, N. E.; Oliff, A. *J. Biol. Chem.*, **1993**, *268*, 7617
- 82] Sidebottom, P. J.; Highcock, R. M.; Lane, S. J.; Procopiou, P. A.; Watson, N. S. *J. Antibiot.*, **1992**, *45*, 648
- 83] Singh, S. B.; Hiesch, J. M.; Lingham, R. B.; Silverman, K. C.; Sigmund, J. M.; Goetz, M. A. *J. Org. Chem.*, **1995**, *60*, 7896
- 84] Singh, S. B.; Zink, D. L.; Goetz, M. A.; Jenkins, R. G.; Silverman, K. C.; Mosley, R. T.; Albers-Schonberg, G.; Lingham, R. B. *Tetrahedron*, **1993**, *49*, 5917
- 85] Pyl, D. V. D.; Inokoshi, J.; Shiomi, K.; Yang, H.; Takeshima, H.; Omura, S. *J. Antibiot.*, **1992**, *45*, 1802
- 86] Singh, S. B.; Jones, E. T.; Goetz, M. A.; Bills, G. F.; Nallinomstead, M.; Jenkins, R. G.; Lingham, R. B.; Silverman, K. C.; Gibbs, J. B. *Tetrahedron Lett.*, **1994**, *35*, 4693
- 87] Dalton, M. B.; Fantle, K. S.; DeMaio, L.; Evans, R. M. *Cancer Res.*, **1995**, *55*, 3295
- 88] James G. L.; Goldstein, J. L.; Brown, M. S.; Rawson, T. E.; Somers, T. C. *Science*, **1993**, *266*, 1937
- 89] Garcia, A. M.; Rowell, C.; Ackerman, K.; Kowalczyk, J. J.; Lewis, M. D. *J. Biol. Chem.*, **1993**, *268*, 18415
- 90] Trueblood, C. E.; Ohya, Y.; Rine, J. *Mol. Cell Biol.*, **1993**, *13*, 4260

- 91] James, G. L.; Brown, M. S.; Cobb, H. M.; Goldstein, J. L. *J. Biol. Chem.*, **1994**, 269, 27705
- 92] Stacey, D. W.; Feig, L. A.; Gibbs, J. B. *Mol. Cell Biol.*, **1991**, 11, 4053
- 93] Boguski, M. S.; McCormick, F. *Nature*, **1993**, 366, 643
- 94] Ren, Z. B.; Gould, M. N. *Cancer Lett.*, **1994**, 76, 185
- 95] Reiss, Y.; Seabra, M. C.; Goldstein, J. L.; Brawn, M. S. 'Methods', **1991**, 1, 241, San Diego
- 96] Levins, R. *Scientist*, **1996**, 54, 421
- 97] Motulsky, H. J. in 'Analyzing data with GraphPad', **1999**, GraphPad Software Inc., San Diego CA, [www.graphpad.com](http://www.graphpad.com)
- 98] Cheng, Y.; Prusoff, W. H. *Biochem. Pharmacol.*, **1973**, 22, 3099
- 99] Carman, R. M.; Garner, A. C. *Aust. J. Chem.*, **1996**, 49, 741
- 100] Buchecker, R.; Marti, U.; Eugster, C. H. *Helv. Chim. Acta.*, **1982**, 3, 896
- 101] Pattison, F. *Chem. and Ind.*, **1955**, 740
- 102] Suemune, H.; Iwasaki, G.; Ueno, K.; Sakai, K. *Chem. Pharm. Bull.*, **1984**, 32, 4632
- 103] Baird, M. S.; Nethercott, W.; Slawey, P. D. *J. Chem. Res. Miniprint*, **1985**, 12, 3815
- 104] Arnold, L. *J. Am. Chem. Soc.*, **1953**, 75, 5396
- 105] Braude, E. *J. Chem. Soc.*, **1955**, 3334
- 106] Hayashi, M.; Terashima, S.; Koga, K. *Tetrahedron*, **1981**, 16, 2797
- 107] Knoevengel, E. *J. Prakt. Chem.*, **1918**, 97, 288
- 108] Shizuri, Y.; Uchida, K.; Yamamara, S. *Chem. Lett.*, **1987**, 1381
- 94] Burke, Y. D.; Stark, M. J.; Roach, S. L.; Sen, S. E.; Crowell, P. L. *Lipids*, **1997**, 32, 151
- 109] Gould, M. N. *Environ. Health Perspect.*, **1997**, 105, 977
- 110] McGuire, T. F.; Qian, Y.; Vogt, A.; Hamilton, A. D.; Sebt, S. M. *J. Biol. Chem.*, **1996**, 271, 27402
- 111] Doulut, S.; Dubuc, I.; Rodriguez, M.; Vecchini, F.; Fulcrand, H. *J. Med. Chem.*, **1993**, 10, 1369
- 112] *Justus Liebigs Ann. Chem.*, **1929**, 81
- 113] Grossi, V.; Rontani, J-F. *Tetrahedron Lett.*, **1995**, 18, 3141
- 114] Rowland. *J. Am. Chem. Soc.*, **1957**, 79, 5007
- 115] Nargund, K. S.; Prasad, K.; Thakur, M. M. *J. Indian Chem. Soc.*, **1978**, LV, 479

- 116] McGuire, T. F.; Qian, Y.; Vogt, A.; Hamilton, A. D.; Sebt, S. M. *J. Biol. Chem.*, **1996**, *271*, 27402
- 117] Lerner, E. C.; Qian, Y.; Hamilton, A. D.; Sebt, S. M.; *J. Biol. Chem.*, **1995**, *270*, 26770
- 118] Stark, W. W., Jr.; Blaskovich, M. A.; Johnson, B. A.; Qian, Y.; Vasudevan, A.; Pitt, B.; Hamilton, A. D.; Sebt, S. M.; Davies, P. *Am. J. Physiol.*, **1998**, *275*, L55
- 119] Marson, C. M.; Rioja, A. S.; Brooke, G.; Coombes, R. C.; Vigushin, D. M. *Bioorg. Med. Chem. Lett.*, **2002**, *12*, 255

## Preferential Induction of Apoptosis by Farnesol and Two Terpenoid-Type analogues on various leukaemic cells

### 4.0 Introduction

In chapter three, two compounds, diethyl ester **23** and ketone **24**, were shown to have poor *in vitro* prenyl-protein transferase inhibition, both compounds being less potent than (*S*)-perillyl alcohol (1.0 mM). However, these two carbonyl compounds fitted the model (shown in figure 15, Chapter 3) that implies significant anti-cancer properties. Inhibition of prenyl-protein transferase inhibition is only one mechanism by which such terpenoids may confer their chemotherapeutic action. In order to assess the anti-cancer activity of these compounds, it was seen whether both diethyl ester **23** and ketone **24**, and also farnesol (a sesquiterpenoid natural product) would kill leukaemic cells. Their specificity as anti-cancer agents was assessed by whether they would also kill normal, non-leukaemic haemopoietic cells at the same concentration used for the leukaemic cells. This allows the effect of the three compounds on whole cells to be investigated, rather than merely their potency in inhibiting prenyl-protein transferase enzymes.

### 4.1 Action of isoprenoids on tumorous cells

Sterol and non-sterol isoprenoids are natural products that are required for cellular functions, including cell signalling, protein synthesis, cell proliferation and apoptosis.<sup>1</sup> Such cellular functions are regulated by a number of compounds including cholesterol, ubiquinone, farnesyl and geranylgeranyl isoprenoids and retinoic acid precursors.<sup>2</sup> Cancer chemoprevention using natural products such as limonene, carvone, perillyl alcohol and farnesol is an active area.<sup>3</sup> Examples of such chemopreventive ability is shown by the inhibition of human MIA PaCa2 pancreatic tumour cells by terpenoid alcohols; perillyl alcohol, geraniol and farnesol show inhibitory activity *in vivo* at concentrations of 300, 100 and 25  $\mu$ M respectively.<sup>4</sup>

Farnesol arrests the proliferation of several tumour-derived cell lines, and has also been shown to induce apoptosis.<sup>4,5</sup> In a recent study, it was observed that farnesol induced G<sub>0</sub>/G<sub>1</sub> cell cycle arrest and apoptosis of a human lung adenocarcinoma cell line and that this was independent of protein-prenylation.<sup>6</sup> Several studies have indicated that inhibition of choline phosphotransferase by farnesol and other terpenoids may be the reason for their activity.<sup>7</sup> Farnesol also induces apoptosis in lymphoma, cervical carcinoma and other cell types.<sup>6</sup> In view of its anti-carcinogenic activity it was of interest to study whether farnesol could cause cell cycle arrest and apoptosis of leukaemic cell lines and leukaemic blast cells from patients with acute myeloid leukaemia (AML). Furthermore, its specificity was assessed by whether similar concentrations affected normal, primary haemopoietic cells isolated from the peripheral blood.

Together with pure *trans*, *trans*-farnesol, two more compounds (both of which are racemic but single diastereoisomers), were tested for the induction of apoptosis preferentially in leukaemic cell lines. The two compounds chosen were 2,4-diacetyl-3-((*E*)-2,6-dimethylhepta-1,5-dienyl)-pentanedioic acid diethyl ester (**23**) and 5-((*E*)-4,8-dimethylnona-3,7-dienyl)-3-methylcyclohex-2-enone (**24**), (which for the purposes of this chapter are referred to as diethyl ester **23** and ketone **24** respectively). They allow the characteristics of the chemopreventive synthetic terpenoid model revealed in chapter 3 (figure 15) to be investigated. Thus both compounds possess: (a) a polar tip, (b) a monoterpene head (lipophilic spacer) and (c) an isoprenyl chain (tail) that could induce apoptosis of cancerous cells without necessarily being potent prenyl-protein transferase inhibitors (see figure 1).

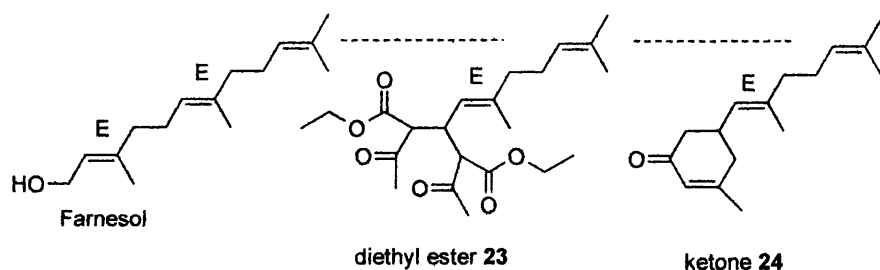


**Figure 1** Comparison of the structure of farnesol, diethyl ester **23** and ketone **24**

## 4.2 Leukaemic cell line assays of synthetic compounds 23, 24 and farnesol

Assays were conducted using various leukaemic cell lines, including Jurkat (acute T-cell leukaemia), Daudi (B-lymphocyte from a patient with Burkitt's lymphoma), HL-60 (acute pro-myelocytic leukaemia) and TF-1 (erythro-leukaemic cell line derived from bone marrow). These cell lines were obtained from Dr N. S. B. Thomas, (Dept. of Haematology, UCL), and all experiments were carried out in his laboratory. Each cell line was cultured in RPMI-1640/10% (v/v) fetal calf serum (FCS) at 37 °C in a fully humidified atmosphere containing 5% CO<sub>2</sub>. The number of viable cells present each day was determined by staining with Trypan blue and manual counting with an improved Neubauer chamber. Cells were used for an experiment when they were >95% viable (*i.e.* <5% Trypan blue positive) and were proliferating exponentially.

In a typical experiment, cells were seeded the day before at  $2 \times 10^5$  cells/mL; the following morning, equal aliquots were placed in separate flasks. For a typical experiment, additions were made as shown in Table 1.

Flask number	Compound added
1	Control - cell culture (no DMSO)
2	Control - cell culture and DMSO*
3	Farnesol (30 µM)
4	Farnesol (45 µM)
5	Farnesol (60 µM)
6	Farnesol (75 µM)
7	Taxol (2 µM)
8	Taxol (1 µM)
9	Taxol (0.5 µM)
10	Taxol (0.2 µM)

\* The same final concentration as present in flask 6.

**Table 1** Contents of flasks used for cell line assay

The cells in each flask were cultured for (a) 24 hours, and (b) 48 hours. A sample from each flask was removed at each of the above time points and the percentage of viable cells present was determined by manual counting, as described above. Samples of the cells ( $\sim 5 \times 10^5$ ) were also fixed in 80% (v/v) ethanol at -20 °C, so that cell cycle analysis could be carried out. Cell cycle analysis enabled the determination of the percentage of cells present in each phase of the cell cycle and the percentage that

had died by *apoptosis*. Cells double their DNA content during S-phase and this has led to the development of several methods for determining the phase a cell is in, within the cell cycle. DNA can be stained quantitatively with one of a number of stains *e.g.* propidium iodide (PI), TOTO3, 4,6-diamidino-2-phenylindole (DAPI) or Hoechst 33342. Flow cytometry, fluorescence microscopy or laser scanning microscopy are used to determine cellular DNA content. The flow cytometric method used in this study is the best of these methods for determining the percentage of cells in each cell cycle phase because thousands of cells (typically 5000-10,000) are analysed per sample. DNA stained with PI was combined with an analysis of total cell protein content (stained with fluorescein isothiocyanate (FITC)). This enables the determination of the percentage of cells in early and late G<sub>1</sub> (G<sub>1A</sub> and G<sub>1B</sub>) as well as in S and G<sub>2</sub>/M phases of the cell cycle. Since apoptotic cells have a decreased protein content as well as a decreased DNA content, this dual-staining method shows whether cells are dying in S and G<sub>2</sub>/M cell cycle phases as well as in G<sub>1</sub>. The analysis was carried out with an EPICS Elite flow cytometer (Coulter Electronics) excited with a blue laser (488 nm) and with filter sets to detect PI (585 nm) and FITC (530nm). Doublets of cells in G<sub>1</sub> can appear to be in the G<sub>2</sub>/M phase and as there are usually many more cells in G<sub>1</sub>, this can substantially affect the data. These doublets were excluded from the analysis by only including cells that were within linear gates for forward scatter *versus* forward scatter peak, for FITC staining *versus* FITC peak and also for PI staining *versus* PI peak. The percentage of cells in each cell cycle phase was determined by setting linear gates, as shown in Appendix I.

The cell lines that were analysed in this study were derived from leukaemic cells that were originally obtained from patients. The cells have adapted to grow in culture and have been maintained *in vitro* for many generations and are thus different from their original precursors. However, they remain good models for determining how each compound would affect leukaemic (cancerous) cells prior to confirming the findings with leukaemic cells obtained from a patient. Controls used consisted of (a) the cell culture on its own and (b) the cell culture with DMSO. These were the negative controls, ensuring that if apoptosis was observed, it was due solely to the synthetic compounds added, rather than the cells simply dying of their own accord or through the introduction of DMSO (the solvent of choice to solubilise the compounds used). The third control was taxol (~1.0  $\mu$ M), utilised as a positive control, thereby



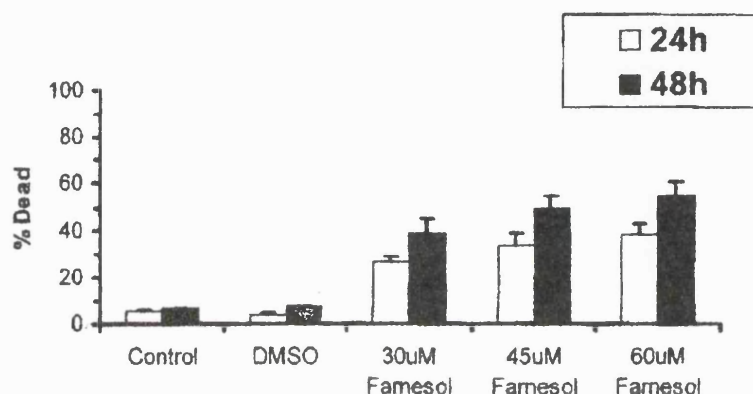
confirming that apoptosis could be induced for any of the cell cultures used, and to show where the apoptotic cells appear in a cell cycle profile, as assessed by flow cytometry.

In order to test whether the compounds killed all cells or were selective for killing leukaemic cells, tests on normal, non-leukaemic cells (T-lymphocytes and monocytes isolated from peripheral blood) were conducted. Isolation and culture of haemopoietic cells was performed as described by N. S. B. Thomas.<sup>8</sup> In each case standard immunophenotyping and morphology was used to verify the purity of each preparation. In order to obtain a population of proliferating T lymphocytes, the T-cells were cultured at  $1 \times 10^6$  cells/ml in RPMI-1640/10% (v/v) (FCS). They were stimulated with  $1 \mu\text{g/ml}$  phytohaemagglutinin (PHA) (Glaxo Wellcome, Greenford, Middlesex, UK) for three days and, after extensive washing with RPMI-1640/10% (v/v) FCS, interleukin-2 (IL-2) (R & D Systems, Abingdon, Oxfordshire, UK) was added to a final concentration of  $20 \text{ ng/mL}$  and the culture was continued for 3-5 days. Primary T lymphocytes were kept between  $0.5\text{--}2 \times 10^6$  cell/ml in by adding fresh medium containing IL-2. They were only used for an experiment if they were growing exponentially and  $>95\%$  (assessed by Trypan blue staining). The results obtained indicate how the compounds would affect the human body's normal white blood cells.

### ***4.3 The apoptotic action of farnesol on leukaemic cells***

The action of farnesol on Jurkat, Daudi, HL-60 and TF-1 cell lines was investigated. The concentrations of farnesol used varied from  $30\text{--}75 \mu\text{M}$ . After 24 and 48 hours, the numbers of live and dead cells were determined by manual counting with Trypan blue staining. Samples of the cell lines were stained for flow cytometric analysis of DNA and protein content in order to determine the percentage of cells in the different cell cycle phases, and also those that have undergone apoptosis. The cell cycle phases, which cells undergo as they divide and the graphical representation displayed by the flow cytometer that is used to determine the number of cells in each phase of the cell cycle are outlined in Appendix 1.

The results from Jurkat cell line cultures containing farnesol (30  $\mu$ M concentration or higher) showed a significant number of dead cells after both 24 and 48 hours, based on manual counting. The proportion of cells in the population that had died (*i.e.* Trypan blue-positive) increased with the concentration of farnesol. Graph 1 depicts the average number of dead cells at both 24 and 48 hours for three Jurkat cell line cultures containing various concentrations of farnesol.



**Graph 1** Cell death of Jurkat cells at varying concentrations of farnesol

Cells that are not dividing have two sets of chromosomes and are termed diploid. Cells in  $G_0$  and  $G_1$  cell cycle phases contain this amount of DNA. The flow-cytometric cell cycle analysis of Jurkat cells indicates that farnesol causes an increase in cells with a sub-diploid DNA and low protein content, characteristics of apoptotic cells. The effect of farnesol on the percentage of Jurkat cells in each cell cycle phase is shown in Table 2. These data show that the percentage of cells with sub-diploid DNA content (labelled sub- $G_1$ ) is substantially higher in the cell cultures (containing farnesol with a concentration of 30  $\mu$ M or higher) *compared* with the two control cell cultures.

Time	Cell cycle phase	Control	Control + DMSO	Farn* 15 $\mu$ M	Farn* 30 $\mu$ M	Farn* 45 $\mu$ M	Farn* 60 $\mu$ M	Farn* 75 $\mu$ M
24 h	Sub G <sub>1</sub>	5.6	4.5	7.4	26.3	37.5	41.8	41.0
	G <sub>1</sub>	50.6	51.0	49.0	39.9	33.6	23.6	25.1
	S	31.3	31.4	33.2	26.0	23.0	25.7	24.7
	G <sub>2</sub> /M	12.3	13.1	10.4	7.8	5.9	8.9	9.2
48h	Sub G <sub>1</sub>	6.9	7.7	9.5	29.5	53.1	63.7	70.8
	G <sub>1</sub>	52.0	52.3	54.5	41.8	24.6	19.1	15.4
	S	30.1	29.2	26.9	21.4	16.8	14.0	11.2
	G <sub>2</sub> /M	11.0	10.8	9.1	7.3	5.5	3.2	2.6

(Farn\* = farnesol)

**Table 2** The effect of farnesol on the percentage of Jurkat cells in each cell cycle phase (results taken from the average of four experiments)

A visual representation of the above data is shown in Figure 2. Each dot corresponds to the DNA and protein content of a set number of cells analysed (*e.g.* 10 cells per dot). The different cell cycle phases as well as those cells that have died by apoptosis are indicated. It is noticeable that the number of apoptotic cells increases and so appears darker with increasing concentrations of farnesol. From these experiments, it was concluded that farnesol induces apoptosis of Jurkat (leukaemic) T-cells at a concentration of 30  $\mu$ M.

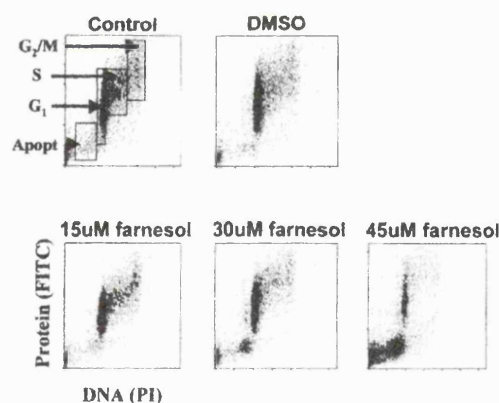


**Figure 2** Flow cytometric analysis of Jurkat cells

The data from the other three leukaemic cell lines (TF-1, HL-60 and Daudi) all showed significant cell death at 45  $\mu$ M concentration of farnesol. The results are very similar, Table 3 displaying the data (obtained from the average of three experiments) for TF-1 cells.

Time	Cell cycle phase	Control	Control + DMSO	Farnesol (45 $\mu$ M)
24 h	Sub G <sub>1</sub>	32.0	27.2	68.2
	G <sub>1</sub>	42.5	44.4	23.2
	S	20.3	22.3	6.2
	G <sub>2</sub> /M	5.2	6.1	2.4
48 h	Sub G <sub>1</sub>	19.1	39.8	90.1
	G <sub>1</sub>	54.8	43.7	8.2
	S	18.8	11.9	1.2
	G <sub>2</sub> /M	7.3	4.6	0.5

**Table 3** The effect of farnesol on the percentage of TF1 cells in each cell cycle phase

From the results, it is seen that farnesol (at 45  $\mu$ M) achieves potent apoptosis; at 48 hours, 90% of TF1 cells are in the sub-G<sub>1</sub> phase. Once again the amount of cells in the sub-G<sub>1</sub> (apoptosis) phase in the cell culture containing farnesol was significantly higher than the amount observed in the two controls. In order to determine visually that the culture contained dead cells, consistent with the induction of apoptosis, samples of TF1 cells ( $1 \times 10^5$  cells) cultured with and without farnesol were immobilised on a glass microscope slide by centrifugation (Cytospin 3, Shandon Southern). The slides were then treated with a histochemical stain (May Grunwald Giemsa (MGG)) that enables the analysis of cellular morphology by light microscopy. The slides in figure 3 show the effect of farnesol (30  $\mu$ M) on the cell structure of TF1 cells. On the slide that contains farnesol, cell debris and blebbing occurred, while the control (DMSO) slide did not contain any cell debris. Cell debris and blebbing are consistent with cells undergoing apoptosis.

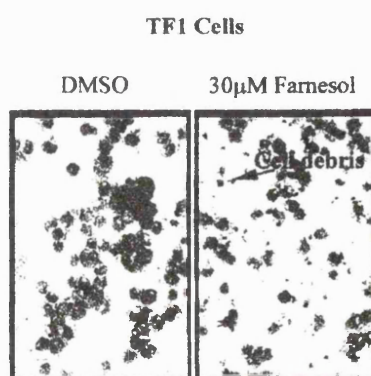
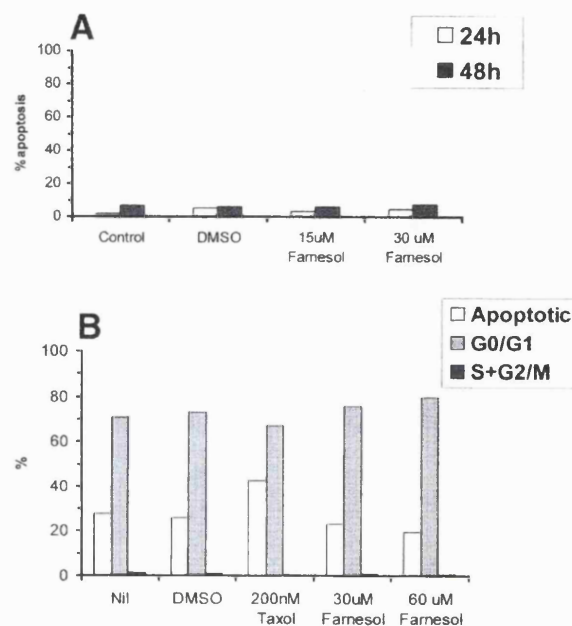


**Figure 3** Slides showing TF1 cell after 72 hours

#### **4.4 The apoptotic action of farnesol on primary T-lymphocytes and monocytes**

After observing apoptosis of various leukaemic cell lines by farnesol, it was asked whether farnesol has selective apoptotic action purely for cancerous cells or whether farnesol induces cell death for all cells. In particular, it was important to determine whether farnesol also induced apoptosis of normal haemopoietic cells. This is a crucial aspect, if farnesol is to be used as an agent to kill leukaemic cells selectively. Therefore, monocytes and primary T-lymphocytes were purified from the peripheral blood of normal donors. These are cells of the same haemopoietic lineages as HL-60 and Jurkat cells respectively. However, they are not precisely the normal counterparts of these leukaemic cell lines, but which can be used to determine whether farnesol would kill cells that comprise two of the major lineages of white cells in the blood. These purified cells were cultured *in vitro* with farnesol and manual counting with Trypan blue staining and flow cytometric analysis of the DNA and protein content of the cells was conducted. The results indicate that farnesol at 15 or 30  $\mu\text{M}$  caused little apoptosis of quiescent, primary T-lymphocytes over a 48 hour period as shown by Graph 3A, (cell cycle analysis of DNA content showed that <7% of cells had sub-G<sub>1</sub> DNA content [apoptosis]). To determine whether another primary haemopoietic cell of a different lineage was 'killed' by farnesol, monocytes from peripheral blood were isolated and were cultured with farnesol (with a concentration range of 15  $\mu\text{M}$  to 60  $\mu\text{M}$ ) for 48 hours. As with the T-lymphocytes, the proportion with sub-G<sub>1</sub> DNA and protein content was no higher than appeared in the two control experiments as judged by flow cytometry, (shown in graph 3B).



**Graph 3** A: percentage of apoptosis for primary T-lymphocytes, B: percentage of apoptotic cells with sub-G<sub>1</sub> DNA protein content

The lack of detection of apoptosis of primary T-lymphocytes and monocytes above the control levels compared with the amount detected for the leukaemic cell lines tested, indicates some preferential induction of apoptosis towards *cancerous cells only*. This inference is given further credence by the cell slides (shown in figure 4) of primary T-lymphocytes cultured with DMSO (30  $\mu$ M) and farnesol (30  $\mu$ M) which showed no sign of cell debris or blebbing, indicating that no apoptotic action had occurred.

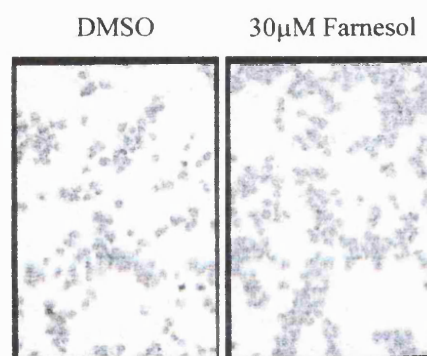
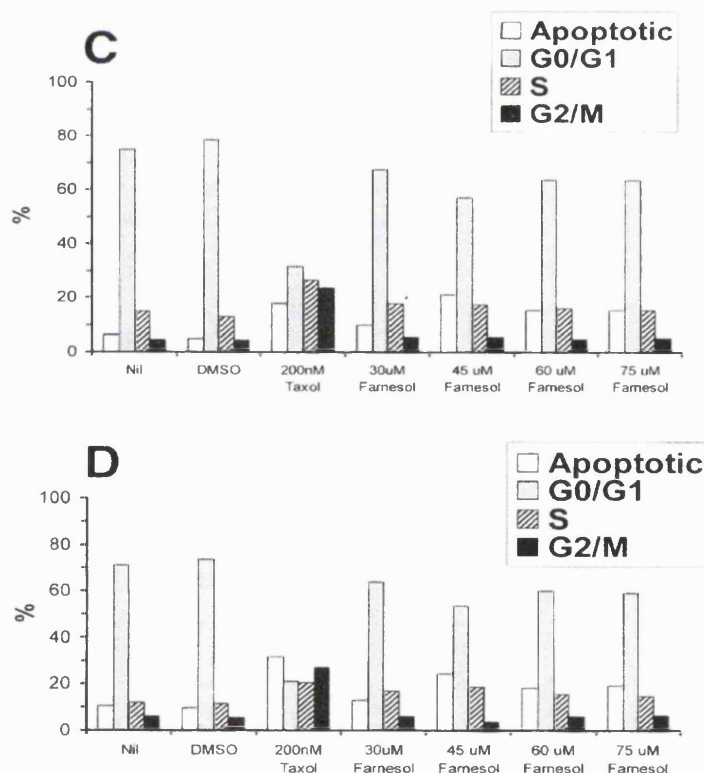


**Figure 4** Cell slides of primary T-lymphocytes taken after 72 hours cultured with DMSO and farnesol

### 4.5 The apoptotic action of farnesol on proliferating T-lymphocytes

A possible reason for the apparently selective nature of farnesol in inducing apoptosis of various leukaemic cell lines but not primary T-lymphocytes or monocytes could be that leukaemic cell lines are proliferating, whereas primary T-lymphocytes and monocytes are quiescent (non-proliferating). To determine whether farnesol acts upon proliferating cells rather than quiescent ones, primary T-lymphocytes were stimulated to proliferate by culturing with PHA followed by interleukin-2 (IL-2). These cells were then cultured with farnesol (30-70  $\mu\text{M}$  concentration range) for a period of 24 to 48 hours. The same analysis used above for the quiescent primary T-lymphocytes was utilised and the results are shown in Graph 4. The percentage of cells undergoing apoptosis in response to farnesol was not above the levels observed for the controls, even for proliferating T-lymphocytes cultured with 75  $\mu\text{M}$  of farnesol. Therefore, it would seem that farnesol does indeed *selectively induce* apoptosis of leukaemic cell lines compared with primary T-lymphocytes and monocytes, and that this does not depend on whether the cells are proliferating.

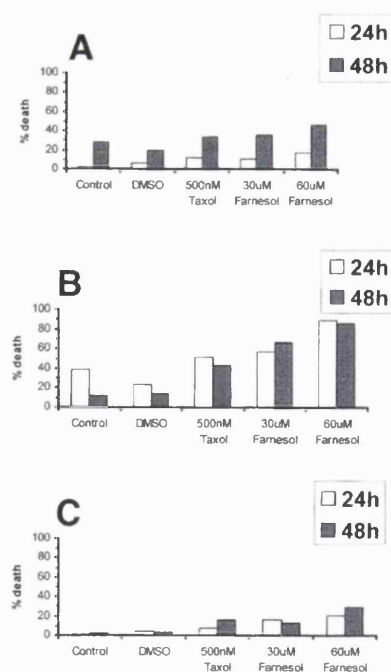


**Graph 4** C: The percentages in G<sub>0</sub>/G<sub>1</sub>, S, G<sub>2</sub>/M and undergoing apoptosis for proliferating T-lymphocytes after 24 hours, and, D: after 48 hours



#### 4.6 The action of farnesol on primary leukaemic cells

The induction of apoptosis by farnesol for various leukaemic cell lines has been demonstrated in this study, and also by another group.<sup>9</sup> The next step determined whether farnesol could cause apoptosis of primary leukaemic cells obtained from patients. Accordingly, blast cells were isolated from the peripheral blood of three patients suffering from acute myeloid leukaemia (AML) before chemotherapy. These leukaemic cells comprised >90% of the white blood cells in the circulation of these patients and they were separated from the red cells by density gradient centrifugation (Ficoll-Paque, AP Biotech). The purified cells were cultured *in vitro* in RPMI-1640, 10% (v/v) FCS, in the presence and absence of farnesol (30 to 60  $\mu$ M concentration range). Manual counting, cell cycle analysis and staining cytocentrifuge slides were used to determine the proportion of cells undergoing apoptosis. The results show (Graph 5), the amount of apoptosis observed for the AML blasts cultured with farnesol (30 – 60  $\mu$ M) was significantly higher than the levels reached in the AML cells cultured with DMSO alone. The variation in the percentage of apoptosis for each sample of AML blast occurs because the leukaemic cells were obtained from three different patients. Each will have different genetic abnormalities and so may respond differently.



**Graph 5** A, B and C: percentage of dead AML blast cells counted with Trypan blue staining for three different patients suffering from AML



As the graphs above show, apoptosis seems to be occurring for primary leukaemic cells cultured with farnesol (30-60  $\mu$ M). This is also shown by MGG staining of slides (figure 5). Cell debris and blebbing are apparent on the slides prepared from cells cultured with farnesol (30  $\mu$ M), consistent with the induction of apoptosis. For AML blast cells cultured with DMSO, no cell debris or blebbing is evident, indicating an absence of apoptosis. These data suggest that farnesol not only kills leukaemic cell lines but also causes apoptosis of leukaemic cells isolated from patients with AML.

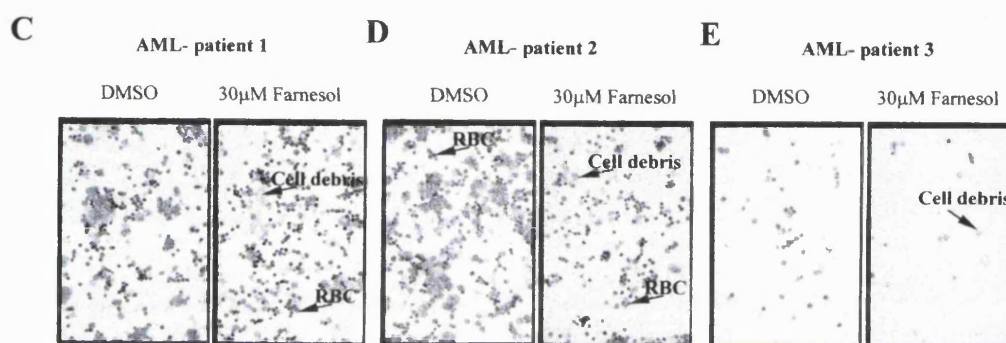


**Figure 5** Three AML-patient samples (C, D and E) cultured with DMSO (control) and farnesol (30  $\mu$ M) after 72 hours.<sup>9</sup> RBC: red blood cells

#### 4.7 The effect of diethyl ester **23** and ketone **24** on leukaemic cell lines

Since farnesol preferentially induces apoptosis of various leukaemic cell lines and primary leukaemic cells (AML blasts),<sup>9</sup> it was important to see whether compounds with similar functionality would do the same. Accordingly, synthetic diethyl ester **23** and ketone **24** (both as diastereoisomerically pure racemates) were used as they both possess the key characteristics shown in the model created to design compounds which should have potent chemotherapeutic properties (figure 15, chapter 3). Bearing in mind that both compounds **23** and **24** are less potent than (*S*)-perillyl alcohol in terms of prenyl-protein transferase inhibition, it was asked whether either compound would induce apoptosis of leukaemic cell lines.

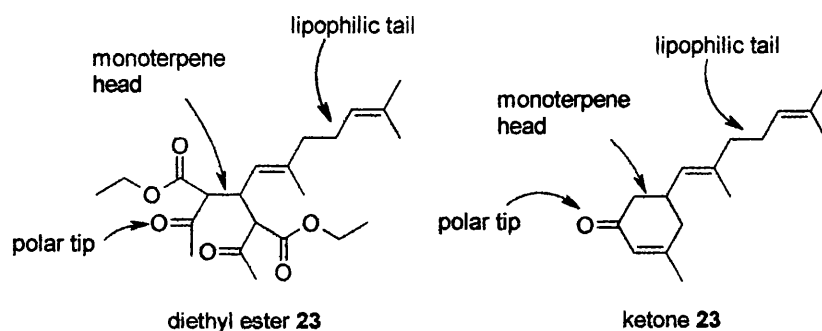
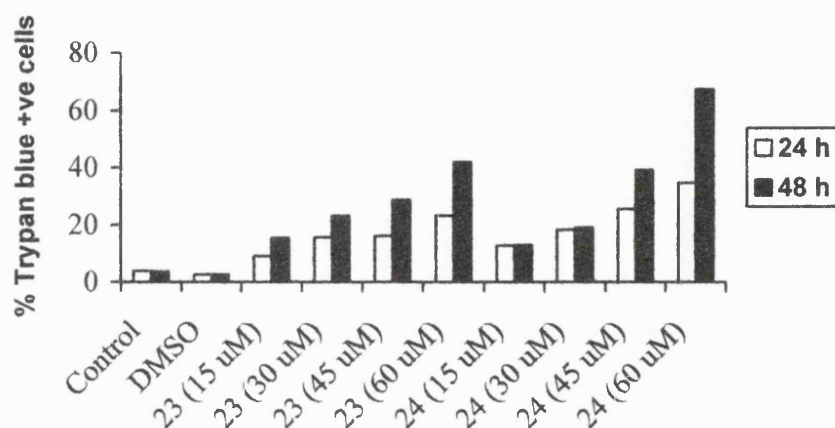


**Figure 6** Structures of compounds **23** and **24** and their key features

The  $\beta$ -keto ester moiety of diethyl ester **23** was of interest, as it provides two carbonyl groups three carbon atoms apart, which could possibly bind to certain amino acids in proteins *via* hydrogen bonding to the NH units of the amino acid residues. Such a spatial arrangement of the  $\beta$ -keto ester moiety could mimic the action of  $\beta$ -ketophosphonates.<sup>10</sup>

As with farnesol, the two compounds (diethyl ester **23** and ketone **24**) were tested on four different leukaemic cell lines; Jurkat, Daudi, HL-60 and TF-1 cell lines. The concentrations used varied from 15  $\mu$ M to 60  $\mu$ M for both compounds. After 24 and 48 hours, the numbers of live and dead cells were determined by manual counting with Trypan blue staining. Samples of the cell lines were stained for flow cytometric analysis of DNA and protein content, allowing the percentage of sub-G<sub>1</sub> phase (apoptosis) and other phases of the cell cycle to be determined.

The results from experiments with the Jurkat cell line cultured with diethyl ester **23** and ketone **24** (at 15 to 60  $\mu$ M concentrations) showed that each compound caused cell death, as judged by manual counting (Graph 6). Interestingly, ketone **24** proved to be more potent in inducing cell death of the Jurkat cell line than diethyl ester **23** (67.2% *versus* 42.0%), which is very similar to the percentage of dead Jurkat cells (71.8%) achieved by farnesol.



**Graph 6** Cell death of Jurkat cells cultured with varying concentrations of diethyl ester **23** and ketone **24**

The flow-cytometry data (Table 4) showed that a significant percentage of Jurkat cells cultured with diethyl ester **23** or ketone **24** at concentrations ranging from 45 to 75  $\mu$ M had a sub- $G_1$  DNA content. This was not the case for the two controls. The percentage of apoptotic cells (sub- $G_1$ ) evident after 48 hours for ketone **24** at 75  $\mu$ M (54.3%) was appreciably larger than the value observed for diethyl ester **23** at 75  $\mu$ M (44.0%). However, the value achieved by farnesol (75  $\mu$ M) for the same leukaemic cell line in the sub- $G_1$  phase was 70.8% after the same time period, indicating that farnesol is more potent than either diethyl ester **23** or ketone **24** for apoptosis of Jurkat cells at similar concentrations.

Time	Phase of cell cycle	Control	DMSO	23 (45 $\mu$ M)	23 (60 $\mu$ M)	23 (75 $\mu$ M)	24 (45 $\mu$ M)	24 (60 $\mu$ M)	24 (75 $\mu$ M)
24 hr	Sub $G_1$	3.13	3.86	15.50	23.15	35.70	16.56	26.36	33.17
	$G_1$	60.69	59.80	52.71	50.52	42.91	55.27	45.57	36.34
	S	21.49	21.43	20.94	15.50	11.92	16.50	14.20	18.05
	$G_2/M$	14.69	14.93	10.61	10.75	9.43	11.65	13.66	12.42
48 hr	Sub $G_1$	3.59	4.07	19.15	37.37	44.0	31.73	46.45	54.30
	$G_1$	57.74	60.34	48.63	37.93	37.06	47.52	33.77	26.08
	S	22.60	20.98	20.90	15.68	11.16	11.30	10.41	11.75
	$G_2/M$	15.82	14.41	11.28	8.02	7.78	9.45	9.37	8.87

**Table 4** The effect of compounds **23** and **24** on the Jurkat cell cycle

The data obtained with the three other leukaemic cell lines (TF-1, HL-60 and Daudi) all showed significant apoptosis at 45  $\mu$ M concentrations for both diethyl ester **23** and

ketone **24**. These other cells lines were utilised because it was possible that both compounds **23** and **24** are particularly effective (in terms of apoptosis) for the Jurkat cell line only, and not leukaemic cell lines in general. Table 5 shows the results for TF-1 leukaemic cells. It was inferred that both compounds **23** and **24** induced apoptosis and as shown in Table 5, (indicative of all three leukaemic cell lines), the more potent of the two compounds being ketone **24** which at 45  $\mu\text{M}$  caused 62.8% apoptosis (judged by sub- $G_1$  content) after 48 hours. This may imply some importance of the allylic ketone moiety of compound **24**, as opposed to the  $\beta$ -keto ester of diethyl ester **23**. Once again, comparison of both compounds with farnesol reveals that farnesol was the most potent compound with 90% in the sub- $G_1$  phase for TF-1 cells after 48 hours cultured with 45  $\mu\text{M}$  farnesol (Table 3).

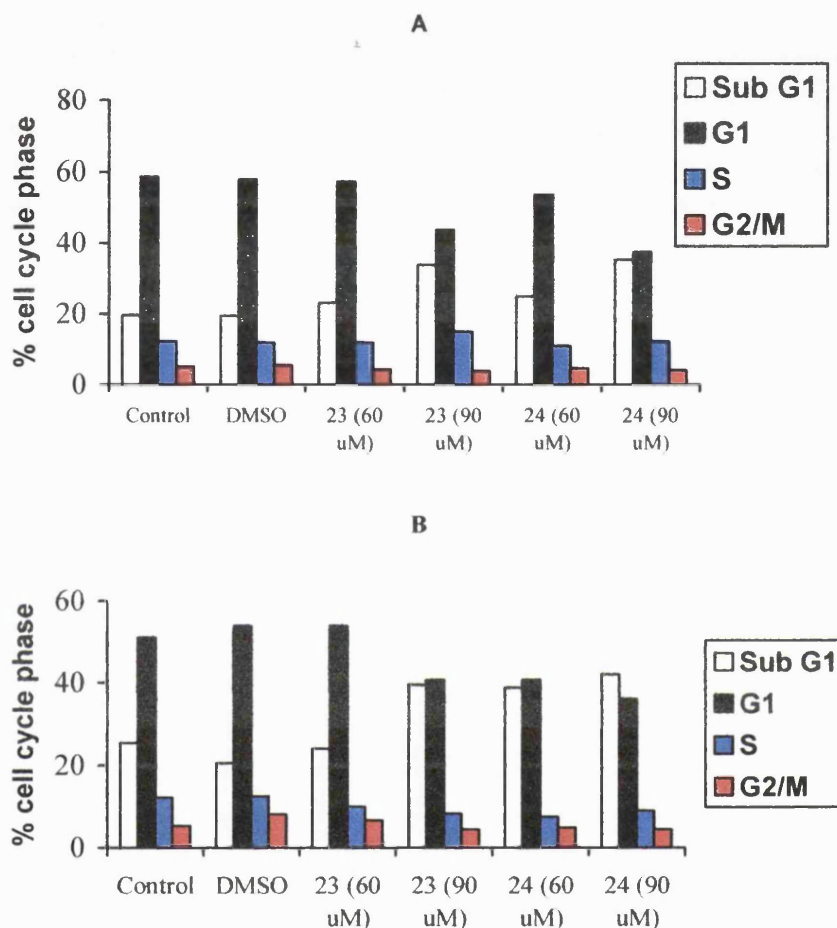
Time	Cell cycle phase	Control	DMSO	23 (45 $\mu\text{M}$ )	24 (45 $\mu\text{M}$ )
24 hr	Sub $G_1$	10.0	11.6	25.31	45.0
	$G_1$	55.75	55.56	49.38	41.85
	S	27.08	25.52	18.45	9.60
	$G_2/\text{M}$	6.95	7.06	6.86	3.73
48 hr	Sub $G_1$	18.43	21.20	28.94	62.78
	$G_1$	48.34	54.88	50.61	31.06
	S	22.18	16.59	12.27	4.85
	$G_2/\text{M}$	11.11	7.33	8.18	1.31

**Table 5** The effect of diethyl ester **23** and ketone **24** on the cell cycle phase of TF-1 cells

#### 4.8 The effect of diethyl ester **23** and ketone **24** on primary T-lymphocytes

The experiments described above showed that diethyl ester **23** and ketone **24** induced apoptosis of various proliferating leukaemic cell lines. It was asked whether these two compounds would induce apoptosis of purified, *quiescent* primary T-lymphocytes isolated from peripheral blood. Manual counting with Trypan blue staining and flow cytometric analysis of DNA and protein content of the primary T-lymphocytes was conducted. The results obtained for the effects of diethyl ester **23** and ketone **24** on primary T-lymphocytes (Graph 7), showed that the percentage of cells in the sub- $G_1$  phase for ketone **24** (42.14%) was *slightly* higher at 90  $\mu\text{M}$  concentrations, for apoptosis of primary T-lymphocytes than diethyl ester **23** (39.67%) after 48 hours

This implies that both compounds do preferentially induce apoptosis of leukaemic cell lines. However, cell studies with proliferating T-lymphocytes would need to be conducted in order to verify that the proliferating nature of the leukaemic cell lines rather than the quiescent nature of primary T-lymphocytes causes this apparent selectivity.



**Graph 7** A: Percentage of cell cycle phase for primary T-lymphocytes cultured with diethyl ester **23** and ketone **24** after 24 hours, B: after 48 hours

## 4.9 Conclusion

From the results obtained, it has been determined that farnesol at concentrations between 15 to 30  $\mu$ M selectively kills a panel of leukaemic cell lines corresponding to haemopoietic cells of different lineages. The same concentration range did not cause the cell death of normal primary T-lymphocytes and monocytes isolated from peripheral blood. It is clear that the proliferation state of the primary cells is not relevant, since farnesol did not cause significant apoptosis of either quiescent or

proliferating primary T-lymphocytes. Farnesol also causes primary AML blast cells (actual cancerous cells) to die over a period of 48 hours. It is therefore concluded that farnesol causes significant cell death of leukaemic cells without affecting normal, primary cells. However, the mechanism by which farnesol induces apoptosis of primary leukaemic cells is still not clear. Diethyl ester **23** and ketone **24** also induced apoptosis of several leukaemic cell lines whilst having a less significant effect against quiescent primary T-lymphocytes. It was observed that ketone **24** (containing the allylic ketone moiety) was the more potent of the two compounds. The reasons for this are not fully understood, although it is believed that the polar moiety may be crucial to its efficacy. Neither of the compounds achieved the same potency as farnesol in inducing apoptosis. Possible reasons may include the lack of a hydroxy group as the polar tip, or that the length of the lipophilic tail was not the same length as farnesol, or that the monocyclic ring may have restricted the movement of the isoprenyl unit, and thereby affected the potency of the compound. Comparison of the values for protein-prenylation inhibition between compounds **23**, **24** and farnesol (>1000  $\mu\text{M}$  compared with 750  $\mu\text{M}$  respectively) indicate a significant difference in potency.

Thus, it would seem that diethyl ester **23** and ketone **24**, consistent with the model shown in Chapter 3 (figure 15), are capable of selectively inducing apoptosis of leukaemic cells with moderate potency. This suggests that prenyl-protein transferase inhibition is not the most important aspect to their anti-cancer nature and that other targets by which terpenoids convey their chemotherapeutic properties must be considered.

#### 4.10 References

- 1] Goldstein, J. L.; Brown, M. S. *Nature*, **1990**, 343, 425
- 2] Britton, G. *FASEB J.*, **1995**, 9, 1551
- 3] Gould, M. N. *Environ. Health Perspect.*, **1997**, 105, 977
- 4] Burke, Y. D.; Stark, M. J.; Roach, S. L.; Sen, S. E.; Crowell, P. L. *Lipids*, **1997**, 32, 151
- 5] Adany, I.; Yazlovitskaya, E. M.; Haug, J. S.; Voziyan, P. A.; Melnykovich, G. *Cancer Lett.*, **1994**, 79, 175
- 6] Yasugi, E.; Yokoyama, Y.; Seyama, Y.; Kano, K.; Hayashi, Y.; Oshima, M. *Biochem. Biophys. Res. Commun.*, **1995**, 216, 848
- 7] Voziyan, P. A.; Goldner, C. M.; Melnykovich, G. *J. Biochem.*, **1993**, 295, 757
- 8] Devalia, V.; Thomas, N. S. B.; Roberts, P. J.; Jones, H. M.; Linch, D. C. *Blood*, **1992**, 80, 68
- 9] Rioja, A. S.; Pizzey, A. R.; Marson, C. M.; Thomas, N. S. B. *FEBS Lett.*, **2000**, 467, 291
- 10] Yasugi, E.; Yokoyama, Y.; Seyama, Y.; Kano, K.; Hayashi, Y.; Oshima, M. *Biochem. Biophys. Res. Commun.*, **1995**, 216, 848
- 11] Arends, M. in 'Expert reviews in molecular medicine', Cambridge University Press, **2001**, 4
- 12] Smith, A.; Wood, R. *Cell Biology*, 2nd ed., Prentice Hall, **1994**, 496

## Appendix I

### A1.0 The cell cycle

Proliferation of cells and programmed cell death (apoptosis) are the two of many processes that regulate the balance of cells in the human body. Cell proliferation requires duplication of DNA, and segregation of the chromosomes to each daughter cell. This process of building enough DNA and protein to produce two identical daughter cells is governed by the *cell cycle*. In a basic model (shown in figure 1), there are five main stages, known as  $G_0$  (quiescent stage),  $G_1$  (gap 1),  $S$  (synthesis),  $G_2$  (gap 2), and  $M$  (mitosis). However, most cells in the body are not dividing at a given moment in time. Many are terminally differentiated and cannot divide further. Others are in a non-dividing, quiescent state termed  $G_0$  (G zero). Quiescence does not imply that the cells are inactive, indeed cells in this state carry out a number functions in the organism, *e.g.* secretion and attacking pathogens.

Most of the lymphocytes in human blood are in  $G_0$ . However, with proper stimulation, such being stimulated *via* CD3 and CD28, they can be stimulated to re-enter the cell cycle (at the  $G_1$  phase) and proceed on to new rounds of alternating  $S$  phases and *mitosis*. Cell proliferation requires duplication of DNA, and segregation of the chromosomes to each daughter cell.

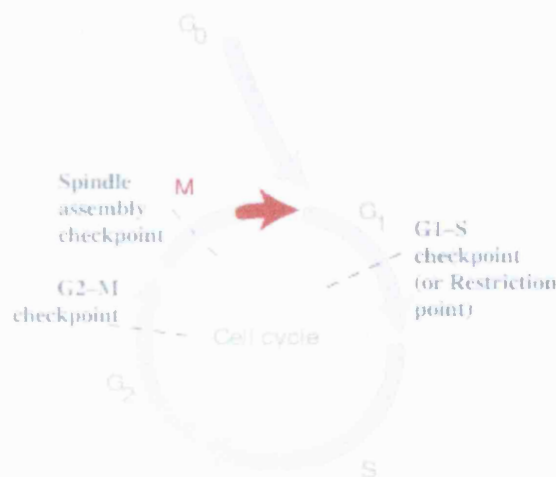


**Figure 1** The stages of the cell cycle<sup>11</sup>



In a 24 hour cell cycle (*e.g.* for Jurkat cells), the G<sub>1</sub> phase would last around 12 hours, the S phase for 6-8 hours, the G<sub>2</sub> phase for around 4 hours and Mitosis for ~1 hour. Stages G<sub>1</sub> and G<sub>2</sub> are called the 'gaps' that occur in the cell cycle between the DNA synthesis and mitosis. However, regulatory mechanisms occur in G<sub>1</sub> and G<sub>2</sub>. For example, a checkpoint in G<sub>1</sub>, known as the restriction point (figure 1), determines whether a cell responds to growth factors and enters the S phase. The cells are also thought to respond to differentiation signals whilst in the G<sub>1</sub> phase. In the G<sub>2</sub> cell cycle phase DNA repair occurs before the cell enters Mitosis and thus any DNA mutations or deletions are not propagated to the daughter cells. As the name suggests, DNA synthesis occurs in the S phase, taking a consistent length of time in most cells. While in the M phase, Mitosis causes chromosomes to separate and cytoplasmic (cytokinesis) division occurs.

To ensure that the number of cells in the body are maintained at the appropriate level, cells are killed by one of two processes; apoptosis (programmed cell death, *i.e.* suicide) or necrosis (cell death).<sup>12</sup> Apoptosis can be defined as "gene-directed cellular self-destruction" or programmed cell death. Apoptotic cells can be recognised by a characteristic pattern of morphological, biochemical and molecular changes, which may be broadly and chronologically defined as:

a) Morphological changes

- Cell shrinkage
- Cell shape change
- Condensation of cytoplasm
- Nuclear envelope changes
- Nuclear fragmentation
- Loss of cell surface structures
- Apoptotic bodies
- Cell detachment

b) Functional and biochemical changes

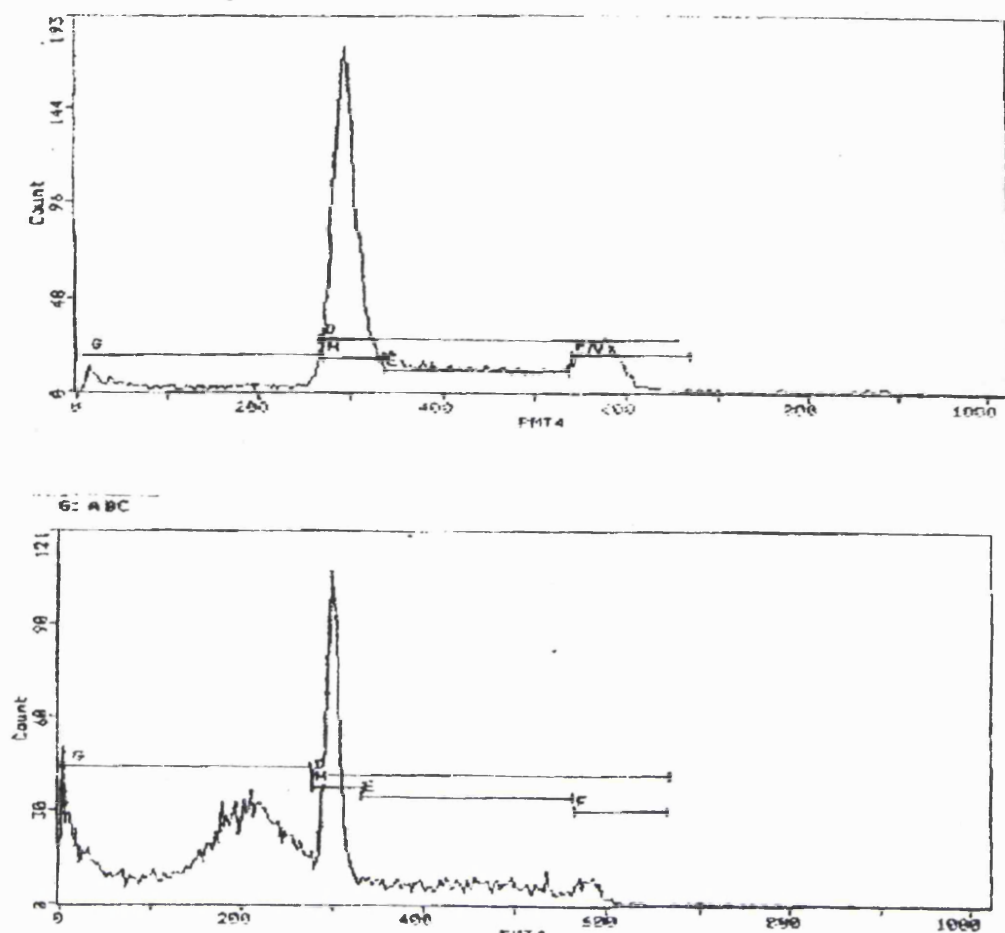
- Free calcium ion rise
- Cell dehydration
- Loss of mitochondrial membrane potential
- Proteolysis
- Phosphatidylserine externalisation

- Lamin B proteolysis
- DNA denaturation
- 50-300kb DNA cleavage
- Intranucleosomal cleavage
- Protein cross-linking.

Assays have been devised to analyse many of the changes described above. In Chapter 4, the use of an assay that quantifies DNA cleavage and a decrease in cell size and protein content is described below.

### ***A1.1 Cell cycle analysis by flow cytometry***

The graphical representations below (figure 2) show the cell cycle analyses of Jurkat cells cultured without farnesol and with farnesol (60  $\mu$ M) respectively. The flow cytometer flows a stream of cells past a laser that is tuned to emit light at a particular wavelength, *e.g.* 488 nm. In this case, propidium iodide (PI) was used to stain the cells. Propidium iodide intercalates into the DNA and the amount of PI bound per cell is proportional to the amount of DNA present. The cells then pass a detector that measures the fluorescence emitted by each cell. In this case, propidium iodide was used to stain the cells. Propidium iodide intercalates into the DNA and the amount of PI bound per cell is proportional to the amount of DNA present. The machine collects such data on a certain limit (usually about 10,000 cells), and the plots shown in the Figure 2 are representative of fluorescence (x-axis) *versus* the number of cells that emit that fluorescence (y-axis), thereby allowing a pictorial display of the results to be obtained.



(Key G = sub-G<sub>1</sub> phase, H = G<sub>1</sub> phase, E = S phase and F = G<sub>2</sub>/M phases).

**Figure 2** The cell cycle profile of Jurkat cells cultured with DMSO and Farnesol (60 μM) respectively after 48 hours

From the above figure, one can observe a normal cell cycle profile of Jurkat cells (top) and a cell cycle profile of a Jurkat cell culture in which a significant proportion of cells dying by apoptosis (bottom). During apoptosis, the DNA of the cell is cleaved and the number of cells with low DNA content can be determined. Therefore following staining by propidium iodide, these cells have a much reduced fluorescence and show a sub-G<sub>1</sub> peak, as observed in the bottom cell cycle profile.

## Histone Deacetylase Inhibitors and a Potential Cancer Therapy

### 5.0 Introduction

Originally, this was not a conceived section of the intended research area. In fact, commencement of this region only began towards the latter end of the allocated research period. The aims were two-fold; firstly produce known (and some novel) simple histone deacetylase inhibitors (hydroxamic acids) to ratify a new procedure (HPLC assay) for determining the effectiveness of compounds for histone deacetylase inhibition (performed at St. Bartholomew's Hospital), and secondly, to generate compounds with a structural similarity to trichostatin A (a potent histone deacetylase inhibitor) with a view to *in vitro* enzyme inhibition assay and cancerous cell line proliferation assay analysis (required by Hammersmith Hospital). An extensive literature survey of histones, the importance of its acetylation/deacetylation, and the key characteristics of known HDAC inhibition follow before the procedures of histone deacetylase inhibition measurement and subsequent production of potential histone deacetylase inhibitors are described.

### 5.1 Importance of histone acetylation and deacetylation

The understanding of protein phosphorylation and its consequences was one of the most important advances in the field of biology in the last few decades. The field of protein acetylation/deacetylation is believed to be the one that will follow a similar path.<sup>1</sup> For many years; studies were conducted at elucidating how DNA-bound transcription factors can affect initiation of transcription. Eventually, it was discovered that some DNA-bound transcriptional activation domains function at least in part by binding coactivator complexes that possess *histone acetyltransferase activity*. It was found that corepressor complexes, which allow transcriptional repression, possess *histone deacetylase activity*. The significance of this discovery is underlined by the fact that some human cancers are associated with malfunctions of coactivator or corepressor complexes. Thus histone deacetylases and their roles in transcriptional repression and cancer are of central importance.

## 5.2 Histones

Eukaryotic DNA is replicated into chromatin in which DNA is complexed with tightly bound proteins called histones: these proteins form disc-like structures around which DNA is wound creating a repeating unit called a nucleosome. This is the most basic element of DNA packaging.<sup>2</sup> Histones are highly conserved; indeed they are among the most highly conserved of proteins, which indicates their vital function. There are five types of histones, which are divided into two groups – the nucleosomal histones (H2A, H2B, H3 and H4) and the H1 histones. The DNA strand is wrapped twice around the central core of the histone octamer consisting of dimers of H2A, H2B, H3 and H4. Histone H1 is involved in the final formation of the nucleosome (as shown in figure 1). The nucleosomes can interact with one another forming a spiral called the solenoid structure that is 30 nm in diameter. It consists of six nucleosomes per turn and DNA packaged in such a fashion is thought to be transcriptionally inert.<sup>2</sup>

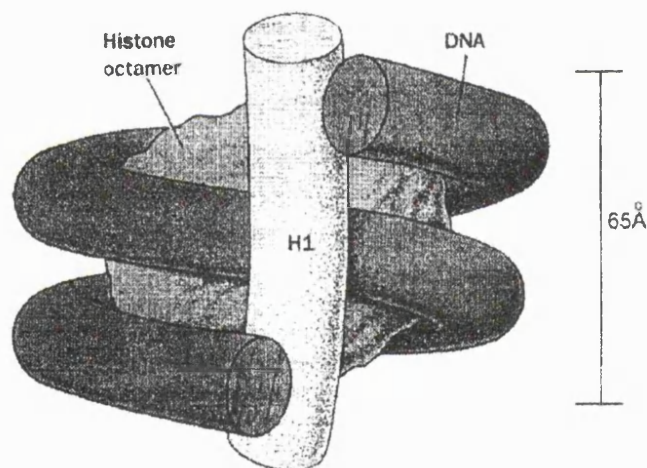


**Figure 1** A nucleosome octamer<sup>3</sup>

## 5.3 Acetylation of histones

From crystallography it was discovered that the N-terminal tails of histone proteins extend from the nucleosome.<sup>4</sup> Their purpose appears to be to allow higher-order packaging between adjacent nucleosomes. These histone protein tails contain highly

conserved lysine residues that can be acetylated on their terminal amino groups, as shown in figure 2.

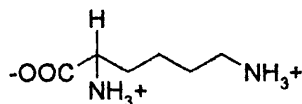


**Figure 2** The amino acid lysine

For every acetylation, a positive charge is eliminated which weakens the electrostatic interactions that bind the octamer to the negatively charged DNA phosphate backbone. Histone acetylation may affect chromatin structure by at least three different mechanisms.

- The overall reduction in positive charge could lead to the destabilisation and consequent dissociation of the nucleosomes, allowing access of transcription factors and RNA polymerase to the DNA strands.<sup>6</sup>
- Histone acetylation may prevent the stacking of nucleosomes into the solenoid structure, thus preventing the formation of a higher-order structure and allowing controlled accessibility to genes in any given region. This important concept would explain why disruption of the higher-order structure by acetylation would stimulate transcription, whereas, deacetylation would inhibit transcription by the facilitation of higher-order structures, such as the solenoid.<sup>7</sup>
- The third mechanism of histone acetylation regulation of transcription is by affecting the binding of regulatory proteins to the histones themselves. Further credence is given by the knowledge that some histone acetyltransferases and deacetylases act upon other transcription factors as well as the histones.<sup>8,9</sup>

## **5.4 Histone deacetylases**

Histone deacetylase proteins can be divided into three groups:

1. Class I RPD3-like proteins;
2. Class II HDA1-like proteins;

### 3. Class III HD2 protein.

#### 5.4.1 Class I histone deacetylases

The cloning of HDAC1 (initially called HD1) brought about the breakthrough in the identification of histone deacetylases. Along with HDAC1, associated protein RbAp48 (Rb-associated protein 48) was identified and both were co-purified in an affinity column.<sup>9</sup> Sequence analysis showed that HDAC1 homology was very similar to yeast RPD3 protein (reduced potassium dependency) which is a known yeast transcriptional regulator.<sup>10</sup> This was the first experimental evidence showing the bond between transcriptional control and histone deacetylation. At almost the same time, a second HDAC protein was discovered, HDAC2. Its was shown to bind to certain transcription factors in yeast.<sup>11</sup>

Human HDAC1 and HDAC2 are homologous in protein and DNA sequencing to the extent of 85% and 75% respectively. The third histone deacetylase protein (HDAC3) has a sequence identity of 53% and 50% for protein and DNA respectively, compared to HDAC1, and 52% and 51% for protein and DNA respectively compared to HDAC2 sequencing.<sup>12</sup>

#### 5.4.2 Class II histone deacetylases

Yeast cells contain two different histone deacetylase activities catalysed by varying enzymatic complexes.<sup>13</sup> The histone deacetylase complex A has a molecular mass of 350 kDa, and the active component is the HDA-1 catalytic subunit.<sup>13</sup> The second histone deacetylase complex (B) is 600 kDa, and its catalytic subunit belongs to RPD3 or RPD3-related proteins, such as HDA-one similar-1(HOS-1) through to HOS-3.<sup>14</sup>

Human histone deacetylases are much larger complexes (~ 2000 kDa), however they all contain highly conserved regions which are involved in the catalysis, thus any mutations within these regions would severely limit the capability to deacetylate.<sup>15</sup> Class II HAD1-like protein has at least 5 homologs in human beings: HDAC4, HDAC5, HDAC6, HDAC7 and HDAC8.<sup>16</sup>

### 5.4.3 Class III histone deacetylases

The only class III histone deacetylase is maize HD2. It does not share any sequence similarities with either class I or class II. However, maize HD2 does have similar protein and DNA sequences with acidic nucleolar phosphoproteins such as nucleolin.<sup>17</sup> Whether this means such nucleolar phosphoproteins can act as histone deacetylases is still unclear.

Thus, all histone deacetylases exist in multi-subunit complexes<sup>18</sup> (as shown in figure 3), and their role is not confined to just simple deacetylation of histones. Various serine and threonine residues on histone deacetylases (HDACs) and histone acyl transferases (HATs) have been shown to be subject to phosphorylation.<sup>1</sup>

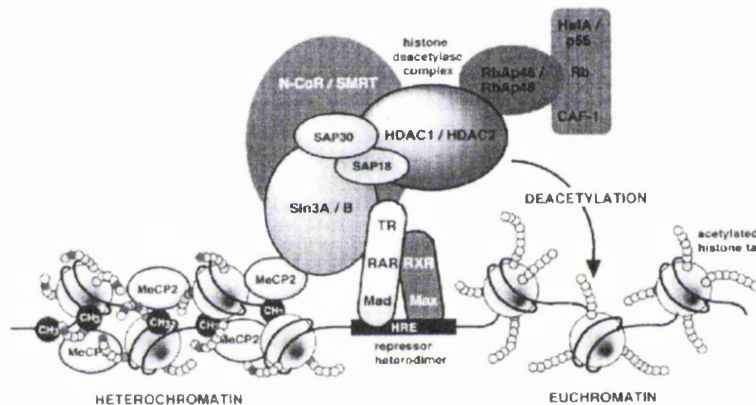


**Figure 3** Model of histone deacetylase complex<sup>1</sup>

For the hypothetical complex (shown in figure 3), either HDAC1 or HDAC2 is present. The Retinoblastoma (Rb)-associated proteins RbAp46 and RbAp48 interact with other multi-subunit complexes that mediate the metabolism of histones, such as HATs and the chromatin assembly factor (CAF-1) complex. The sin3A/B corepressor is thought to mediate the interaction with HDACs by Sin3-associated proteins (SAPs). Sin3A/B interacts with the Nuclear receptor Corepressor (N-CoR) or the related protein Silencing Mediator for Retinoid/Thyroid hormone receptors (SMRT). Consequently, N-CoR and SMRT correlate with unliganded nuclear receptor heterodimers (TR, RAR + RXR) or the Mad:Max repressor heterodimer. The Hormone Response Element (HRE) binds nuclear receptors in the absence of ligands.



The demonstration that the protein product of the *BRCA2* gene possesses HAT activity is very interesting, as *BRCA2* is also known to be a tumour suppressor gene. HDACs also regulate gene expression by deacetylating transcription factors such as p53.<sup>19</sup>

## **5.5 Histone deacetylases and cancer**

Increasing importance is now being given to the relevance of histone deacetylases to health and disease, especially as HDACs are important regulators in gene expression. It is known that HDACs are associated with a variety of well-known cellular oncogenes and tumour-suppressor genes. Consequently, HDACs represent, at least in principle, ideal targets for chemopreventive drugs and therapies. In general there are three areas in which HDACs are linked to tumourgenesis. The first area centres around the cell-cycle restraining transcriptional repressors such as the Mad/Max heterodimer.<sup>2</sup> The second area is concerned with transcriptional repressors that normally block the process of differentiation in various cell lines, for example nuclear hormone receptors such as retinoic acid receptor  $\alpha$  (RAR $\alpha$ ) in haematopoietic differentiation.<sup>2</sup> The third aspect focuses on the histone deacetylase-containing complexes and their role in genomic methylation and transcriptional silencing of various tumour-suppressor genes, such as p21<sup>WAF/CIP1</sup>.<sup>2</sup>

### **5.5.1 Interference of Mad/Sin3/HDAC (a cell-cycle retraining transcriptional repressor)**

The Mad/Sin3/HDAC complex as seen in figure 3, usually binds with *max* to form a heterodimer, however the most common alteration of this pathway that results in human cancer is the overexpression of an alternative binding partner (apart from *max*), which is *myc*. This often occurs as a result of gene amplifications, translocations or the activation of point mutations.<sup>20</sup> Expression of *myc* over *max* means Mad/Max heterodimers are excluded and consequently mad-mediated transcriptional repression is blocked.

Fifteen years ago, the oncogenic form of Ski (a cellular protein) termed v-Ski (lacking the Sin3A-binding C-terminus) was found to transform chicken embryo fibroblasts.<sup>21</sup>

The mechanism by which this occurs is not clear; however, it has been proved that Ski is a component of the Sin/NCoR/HDAC complex<sup>22</sup>, as shown in figure 3, and interacts with both Sin3A and NCoR simultaneously, thus possibly acting as a bridging protein that tethers Sin3A and NCoR. This would suggest that the transforming effects of v-Ski result from its ability to block the function and/or assembly of the Sin3A/HDAC/NCoR/Ski complex. Such disruptions to the said complex are commonly found in tumourgenesis, and also Ski can modulate RAR $\alpha$ -mediated transcriptional repression.<sup>23</sup>

### 5.5.2 HDACs interaction with leukaemia

Acute leukaemia occurs when differentiation of immature haematopoietic cells is blocked and unrestricted cell proliferation occurs. Acute promyelocytic leukaemia (APML) is often associated with chromosomal translocation between chromosome 17 and chromosome 15 or 11, and the binding of large regions of the retinoic acid receptor  $\alpha$  (RAR $\alpha$ ) to the coding sequence of a second gene, called promyelocytic leukaemia (PML), as shown in figure 4. In a minority of APML cases, the translocation of the RAR $\alpha$  region is fused to a different protein, specifically promyelocytic leukaemia zinc finger (PLZF). The role of PLZF involves development of the central nervous system development and haematopoiesis. RAR $\alpha$  also has a role in haematopoiesis, when the RAR $\alpha$  binds to DNA as a heterodimer with a retinoid-X receptor protein (RXR). This heterodimer binds to a transcriptional repressor that contains Sin3A, NCoR and HDAC.<sup>24</sup> When retinoic acid is present, the transcriptional corepressor is displaced and a coactivator complex containing HATs is substituted for patients of APML with the 15:17 chromosomal translocation. Importantly, when RAR $\alpha$  protein is present in the PLZF complex, (the 11:17 chromosomal translocation) it is no longer responsive to physiological levels of retinoic acid, because both parts of the protein recruit a HDAC complex and retinoic acid on its own is insufficient to induce differentiation, because the PLZF part of the protein is not affected by retinoic acid and continues to block transcription. Consequently RAR $\alpha$  becomes a constitutive transcriptional repressor, blocking normal differentiation and leading to leukaemia.<sup>2</sup>

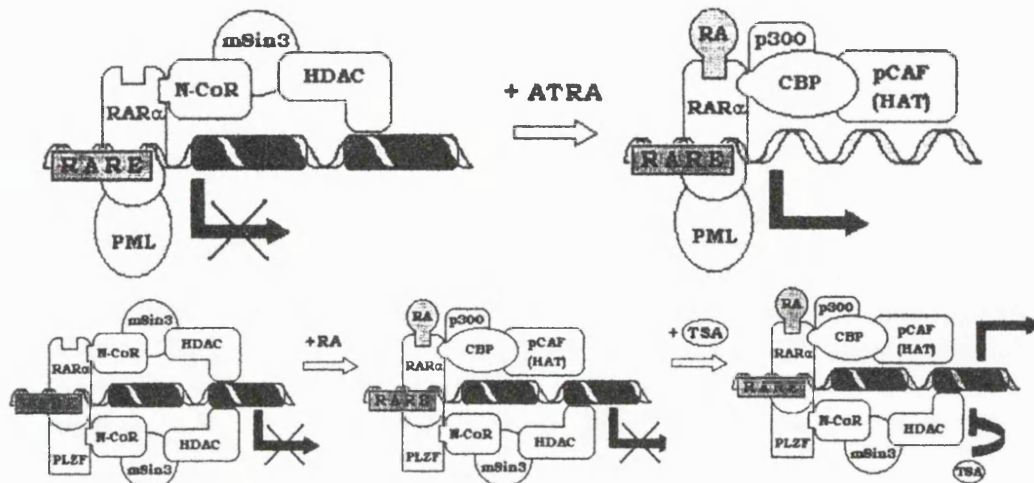


**Figure 4** APML HDAC repressor complexes - treatments with retinoic acid only and retinoic acid with another HDAC inhibitor<sup>25</sup>

### 5.5.3 HDAC-containing complexes and transcriptional restraint of tumour-suppressor genes

In recent years, many studies have shown the existence of complexes that contain histone deacetylase.<sup>26</sup> The chromatin remodelling is mediated by cellular complexes with histone deacetylase activity, and such cellular complexes bind directly to methylated genomic DNA. The methylation of the dinucleotides is closely associated with transcriptional repression.<sup>27</sup> In fact, recent studies have shown that methylation-mediated transcriptional silencing of tumour-suppressing genes may be the critical event in the formation of certain carcinomas.<sup>28</sup> Although there may be more than one mechanism involved, one possible pathway involves the recruitment of histone deacetylase to methylated dinucleotides. MeCP2 is the most well-known member of the methyl-binding proteins, and is also a transcriptional repressor that recruits HDAC via the Sin3 complex.<sup>29</sup> The role of methyl dinucleotide/HDAC complexes in human cancer is not fully understood; however, one strong postulation is the correlation between methylation and transcriptional silencing of tumour-suppressing genes. Abnormal methylation is observed in a number of tumour suppressing gene promoters, including p21<sup>WAF/CIP1</sup>. This is normally induced by p53 in response to DNA damage and is also known as WAF1 or CIP1 (wild-type p53-activated factor or cdk inhibitor protein-1).<sup>30</sup> This gene would normally express hypophosphorylated (growth-suppressing) Mad and growth arrest would then occur; however this gene is

now silenced, hence unregulated proliferation can occur. In figure 5, a simple representation shows the action of HDAC inhibitors, which allows the histone to be acetylated (Ac), causing the DNA that is tightly wrapped around the nucleosome to relax, leading to expression of specific genes and hence arrest of cell growth, differentiation and/or apoptosis, and ultimately to inhibition of tumorous growth.

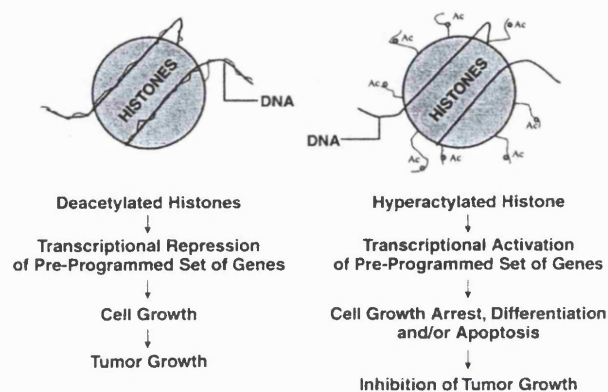


**Figure 5** Action of HDAC and HDAC inhibitors<sup>31</sup>

## 5.6 Histone deacetylase Inhibitors

The compounds shown in figure 6 allow the acetylation of histone and thereby cause cell growth arrest, differentiation, apoptosis and the all-important inhibition of tumour growth. There are five main structural divisions of HDAC inhibitors:

- Short-chain fatty acids (butyrates);
- Hydroxamic acids (trichostatin A [TSA]);
- Cyclic tetrapeptides containing a 2-amino-9,10-epoxy-8-oxodecanoyl (Aeo) moiety (trapoxin A);
- Cyclic peptides not containing the Aeo moiety (apicidin);
- Benzamides (MS-27-275)

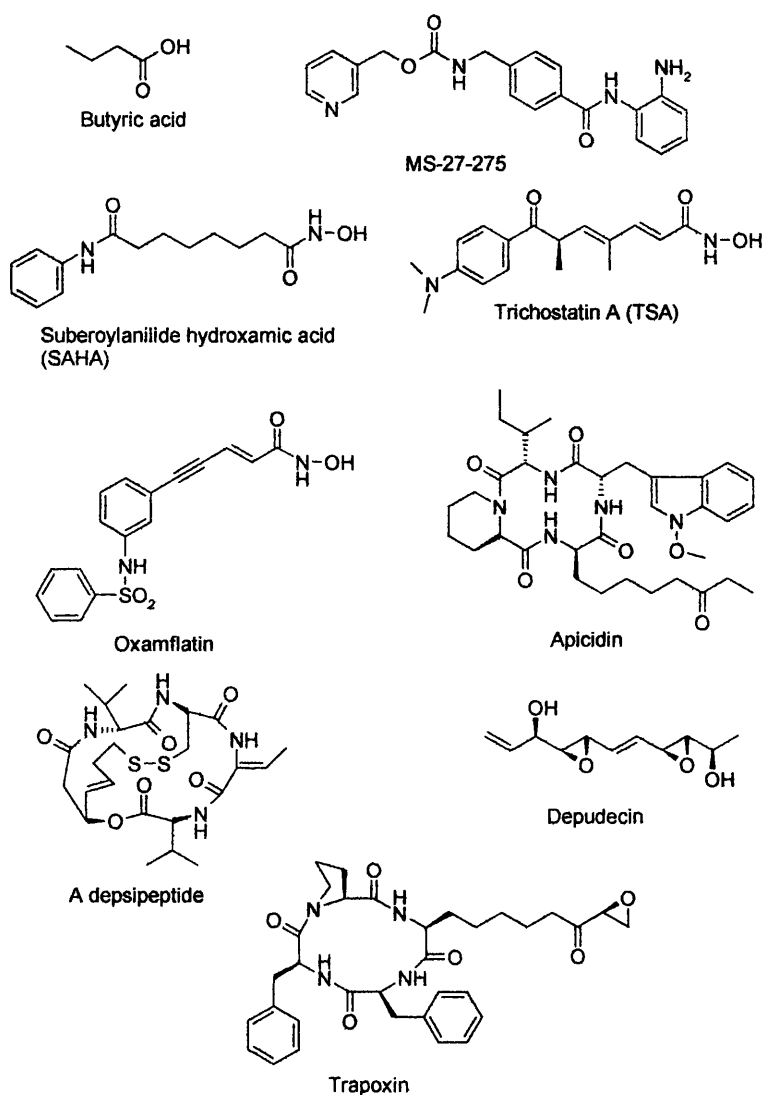
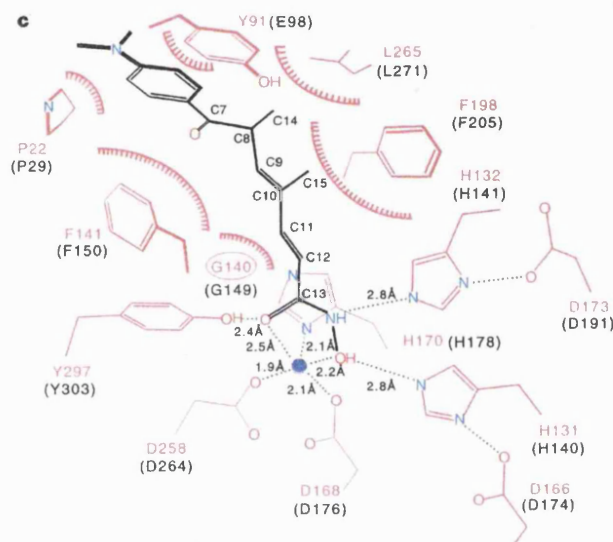


**Figure 6** Histone deacetylase inhibitors

Of all the inhibitors shown, butyrates represent the only class currently approved for use in the clinic.<sup>31</sup> However, butyrate inhibitors are *far* from ideal as high concentrations are required for just millimolar inhibition of HDAC, and their constitution means that there is limited specificity, leading to a high number of side effects experienced by the patient.<sup>32</sup>

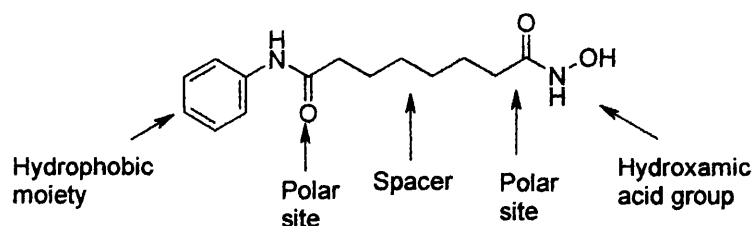
The use of hydroxamic acids is currently central to the inhibition of HDAC. Trichostatin A (TSA) was originally shown to be an anti-fungal agent but was later found to be a potent inhibitor of HDAC, active at nanomolar concentrations.<sup>33</sup> TSA

was first isolated from metabolites of *Streptomyces hygroscopicus* in 1976.<sup>33</sup> Recently the interactions of TSA with histone deacetylase have been revealed, (shown in figure 7).<sup>34</sup> It is clear that the arrangement of the hydroxamic acid moiety allows for favourable hydrogen bond interactions (dotted green lines), and also merited the long-standing belief that the enzyme contained a zinc atom in the active site.<sup>35</sup>



**Figure 7** Diagrammatic representation of TSA interactions with HDAC<sup>34</sup>

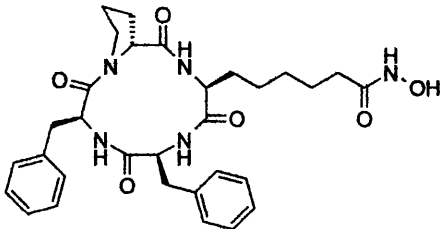
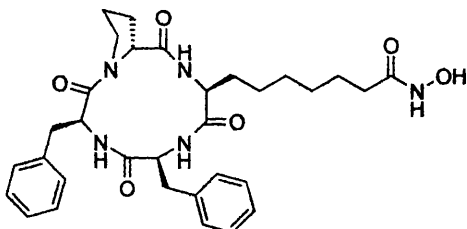
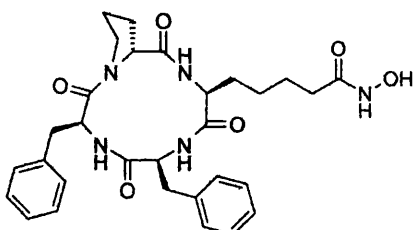
Trichostatin A has one asymmetric centre and the configuration of this has been shown to be important, as only the naturally occurring (*R*)-configuration is reported to be active.<sup>36</sup> Oxamflatin<sup>37</sup>, a hydroxamic acid-based compound, and the benzamide compound (MS-27-275)<sup>38</sup> both inhibit HDAC activity at the micromolar level. Apicidin is a fungal metabolite which possesses broad-spectrum anti-protozoal activity and inhibits HDAC activity at nanomolar concentrations.<sup>39</sup> A depsipeptide isolated from *Chromobacterium violaceum* has HDAC inhibitory activity at micromolar levels.<sup>40</sup> Both trapoxin and depudecin irreversibly bind to HDAC and inhibit its activity at nanomolar and micromolar concentrations respectively.<sup>41,42</sup> Trapoxin contains the Aeo moiety, and the reactive functional group within this region has shown to be the epoxide group, by which a covalent bond is formed with the enzyme.<sup>43</sup>



**Figure 8** Key characteristics of hydroxamic acid-based HDAC inhibitors

For most hydroxamic acid type HDAC inhibitors, certain functional groups contained within the inhibitor are common, as shown in figure 8; some of these key functional units confer the potency of HDAC inhibition.

The important regions are the terminal hydrophobic moiety, followed by a polar group, then a spacer moiety (a saturated and/or unsaturated carbon chain), succeeded by a second polar site, and finally a hydroxamic acid group. Such a generalization of functionalities has gathered credence from various structure-activity relationships studies.<sup>44,45</sup> Substitution of the hydroxamic acid with an oxime or carboxylic acid results in inactive compounds. The hydrophobic ring (benzene) can be modified in the *meta*- or *para*-positions with no loss of activity. The length of the lipophilic chain is considered crucial, and until recently a length of six carbon atoms was considered optimal,<sup>31</sup> with five or seven carbon units decreasing the activity of the inhibitor. However, a recent study (2001)<sup>46</sup> stated that the optimal length of the spacer unit was five-carbon atoms, as shown in the Table 1.

Compound Structure	No. of carbon units in the spacer	HDAC (IC <sub>50</sub> ) nM
	5	3.0
	6	63
	4	510

**Table 1** Effect of spacer group on the inhibition of HDAC1<sup>46</sup>

As well as the X-ray crystallography showing TSA interactions with histone deacetylase, a deacetylase core homologue was identified from a gene superfamily in the hyperthermophilic bacterium *Aquifex aeolicus* (HLDP), which was used for X-ray crystallography studies. The analysis from the X-ray crystallography of HLDP showed the active site formed as a tubular pocket, containing a zinc-binding site and two asparagine-histidine charge-relay systems. The hydroxamic acid of suberoylanilide hydroxamic acid (SAHA) binds to the zinc in the tubular pocket and



the benzene ring projects out of the pocket over the surface of the protein, as shown in figure 9.<sup>31</sup>

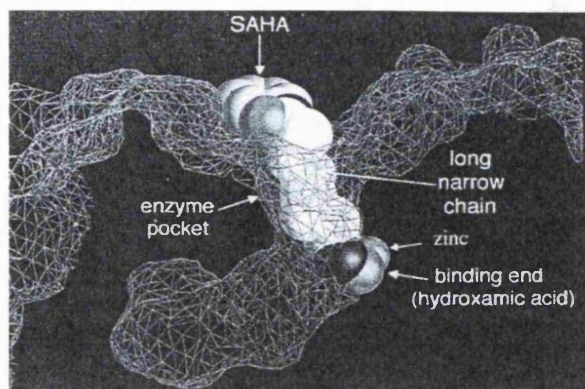


**Figure 9** SAHA binding to HDLP<sup>31</sup>

### 5.7 *In vitro* activity of histone deacetylase inhibitors

In the 1980s various groups reported the inhibition of Friend murine erythroleukaemia (MEL) cells by trichostatins acting at nanomolar concentrations.<sup>47</sup> Further work showed that TSA causes specific cell arrest of rat fibroblasts in both G<sub>1</sub> and G<sub>2</sub> phases by inhibiting histone deacetylation.<sup>48</sup> Human carcinoma cell lines (T24 and HeLa) gave similar results; TSA blocked cell cycle progression at the G<sub>1</sub> phase in the HeLa cell lines and at G<sub>1</sub> and G<sub>2</sub> in the T24 cell lines.<sup>49</sup> Treatment with TSA changed the morphology of cell lines and produced actin stress fibres, indicating that TSA induces the expression of new genes that lead to *de novo* protein synthesis.<sup>49</sup>

Other hydroxamic acid-based inhibitors such as SAHA inhibit partially purified HDAC1 and HDAC3 at micromolar concentrations.<sup>44</sup> HDAC inhibitors can induce growth arrest, differentiation and/or apoptotic in a variety of transformed cells, including neuroblastoma, melanoma, and leukaemia cells and also cells from breast, prostate, lung, ovary and colon cancers.<sup>33,42,50,51,39,52</sup> For example SAHA induces terminal cell differentiation in MEL, T24 and MCF-7 (human breast adenocarcinoma) cell lines.<sup>33</sup> SAHA also induces apoptosis of human multiple myeloma cells (ARP-1), human prostate cell lines (LNCaP) and myelomonocytic leukaemia cells (U937).<sup>31</sup>

It has been reported that the action of HDAC inhibitors on gene expression is very selective.<sup>53</sup> Cells that have been incubated with TSA show only 2% change in expressed genes compared with untreated cells.<sup>53</sup> One gene in particular, p21<sup>WAF1</sup> is known to be induced by a wide variety of HDAC inhibitors.<sup>54</sup> The implications of upregulation of this gene has already been discussed; increased p21<sup>WAF1</sup> gene expression has also been observed in human bladder carcinoma cells (T24).<sup>55</sup>

### **5.8 *In vivo* activity of histone deacetylase inhibitors**

The only therapeutic application so far reported of HDAC inhibitors in human beings is the butyrate analogue sodium phenylbutyrate, which has been shown to be moderately effective in inhibiting growth of solid tumours and leukaemia. However, activity is only observed at relatively high concentrations.<sup>56</sup> There is a well-known case of a 13 year old girl with relapsed APML (type t (11:17) who was clinically resistant to treatment with only all-*trans*-retinoic acid. After 23 days of a combined treatment with all-*trans*-retinoic acid and phenylbutyrate, the girl achieved complete clinical remission.<sup>57</sup> This lasted seven months, before relapsing and eventually becoming resistant to the treatment. It was noticed that the acetylation of histones in her mononuclear blood cells was elevated during the period in which phenylbutyrate was administered. Four other patients were given the same treatment, but no remissions occurred in their cases.<sup>58</sup> TSA has been shown not to be active against human melanoma xenografts in nude mice owing to metabolism in the liver and kidney.<sup>51</sup> Thus although established as a potent *in vitro* inhibitor, metabolically stable analogues may be required to achieve useful *in vivo* activity. However, Professor Coombes' group reported in 2001<sup>59</sup> that TSA is active *in vivo* in carcinogen-induced rat mammary cancer models. Indeed TSA had pronounced anti-tumour activity at 500 µg/kg by injection daily, (showing no toxicity), in which 12 of 16 rats had tumour regression compared with only 1 in 14 rats in the control (untreated) mammary induced carcinomas and a reduction in the mean carcinoma volume of 48%.<sup>59</sup> The histology of the tumours treated with TSA was also examined showing changes to cell structure, as shown in figure 10. Some induction of differentiation was inferred and hence this was proposed as a possible mode of anti-tumour activity.

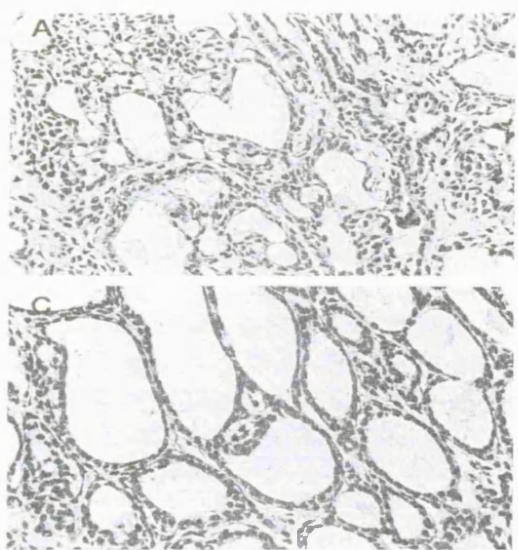
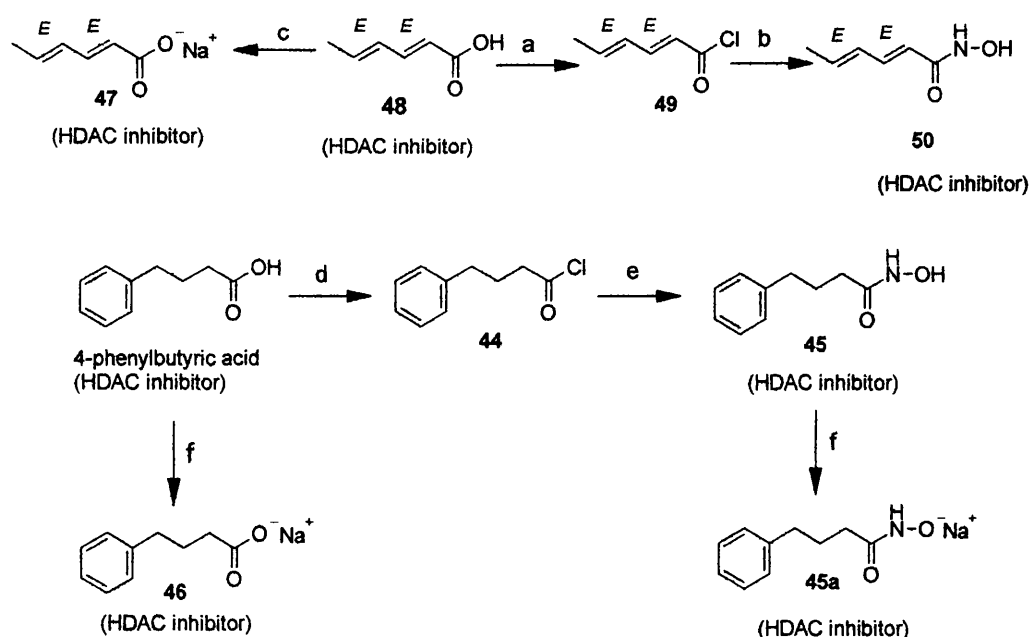


**Figure 10** Histology of carcinogen-induced rat mammary carcinomas<sup>59</sup> Slide A cribriform/papillary carcinoma in a control animal. Slide B, Benign carcinoma tumour that responded to TSA

Although potent *in vitro*, trapoxin showed only very weak activity in animal models.<sup>60</sup> The weak activity probably results from the chemical instability of the epoxyketone group in blood. Suberoylanilide hydroxamic acid (SAHA) was used to treat rats with *N*-methylnitrosourea-induced (NMU) mammary carcinomas; it was observed that the incidence of mammary tumours was reduced by 40% and that the mean tumour volume was reduced by 78% without serious side effects.<sup>61</sup>

### **5.9 Histone deacetylase inhibitors prepared for a non-isotopic enzyme activity (HPLC assay)**

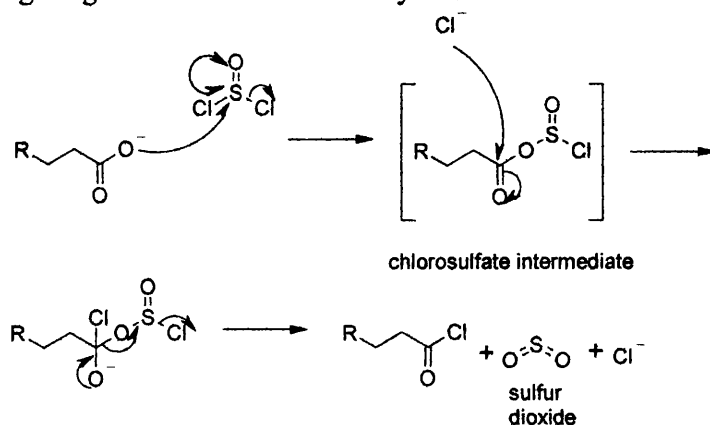
In Scheme 5, the seven compounds prepared as simple known and potential HDAC inhibitors, are shown. Butyric acid and 4-phenylbutyric acid are available commercially from the Aldrich Co.



Reagents: (a) thionyl chloride, (b) HO.NH<sub>3</sub>Cl, (c) NaHCO<sub>3</sub>, (d) thionyl chloride, (e) HO.NH<sub>3</sub>Cl, (f) NaHCO<sub>3</sub>

### Scheme 1 Preparation of known and potential HDAC inhibitors for HPLC assay

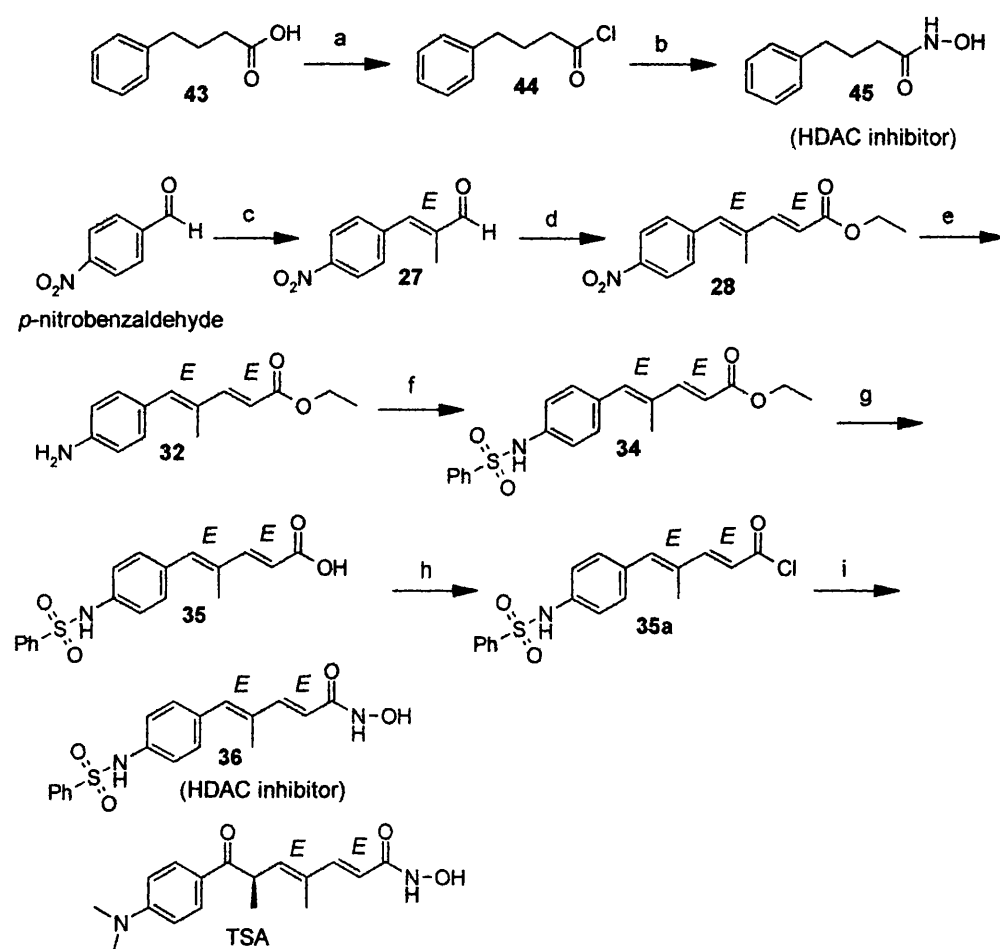
From the corresponding carboxylic acids, chlorination with thionyl chloride, gave (in high yields), the respective carboxylic acid chlorides **44** and **49** (94% and 94%), *via* a chlorosulfate intermediate, (shown in scheme 2). The hydroxamic acids (**45** and **50**) were prepared from the respective carboxylic acid chlorides in moderate yields (57% and 71%) with hydroxylamine hydrochloride and potassium carbonate. The sodium salts (**45a**, **46** and **47**) were prepared in a facile process from their respective carboxylic and hydroxamic acids in quantitative yields with 1 mole equivalent of sodium hydrogen carbonate and the 'acid' in water. The water was removed by 'freeze-drying' to give the sodium salts as crystalline white solids.



Scheme 2 Mechanism of formation of acid chloride

### 5.10 HDAC inhibitors produced with structural features of trichostatin A (TSA)

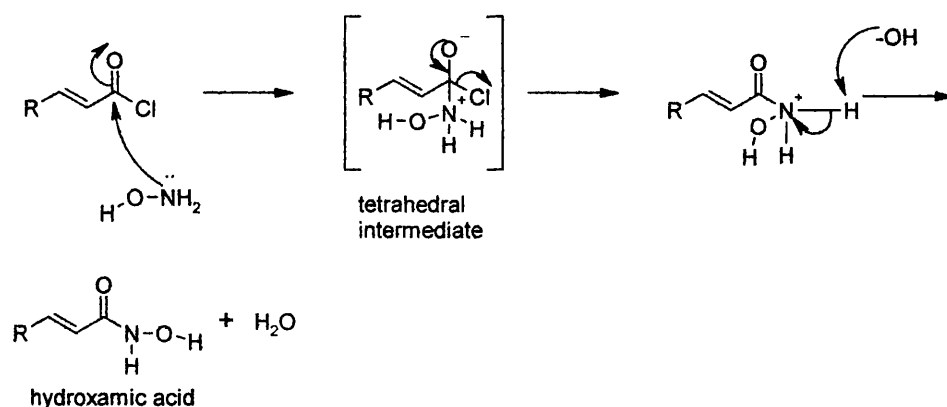
Following from figure 8, (the key characteristics of a potent histone deacetylase inhibitor); several compounds were attempted which contain these key structural features, of which TSA is the lead compound. In Scheme 3, the preparation of HDAC inhibitors **45** and **36** are shown with the structure of TSA for comparison.



**Scheme 3** Synthesis of HDAC inhibitors **36** and **45**

Preparation of *N*-hydroxy-4-phenylbutyramide (**45**) involved treatment chlorination of the carboxylic acid with thionyl chloride (94%) and subsequent reaction of the carboxylic acid chloride with a solution of hydroxylamine hydrochloride and potassium carbonate to give hydroxamic acid **45** in a moderate yield of 57%.

Visualisation of hydroxamic acid products on thin-layer chromatography (TLC) used a ferric sulfate developing solution, the hydroxamic acid moiety formed a dark blue-red spot, whereas a carboxylic acid unit gives no such stain. This is useful, since often the  $R_f$  values of respective carboxylic and hydroxamic acid compounds are very similar. Synthesis of compound **36** (HDAC inhibitor) was much more elaborate, requiring seven steps in total for a moderate yield of 45%. The first step leading to hydroxamic acid **36** was an Aldol condensation with acetaldehyde giving a 9:1 mixture of (*E*:*Z*) geometric isomers, which upon a single recrystallisation afforded compound **27** in the pure (*E*)-form.<sup>67</sup> A subsequent Wittig reaction with a stabilised ylid gave compound **28** in high yield (92%). A 'smooth' reduction of the nitro unit to the amino moiety with  $\text{Fe}^{2+}$  and ammonia (allowing the double bonds to be retained) yielded compound **32** in a good yield (85%). Successive sulfonylation and hydrolysis afforded carboxylic acid **35** in 84% yield. Reaction with thionyl chloride gave the acid chloride **35a** (94%), which was treated with hydroxylamine hydrochloride solution to give hydroxamic acid **36** with a yield of 45%, (mechanism shown in Scheme 4), which retained the single geometric (*E*)-isomer, as confirmed by  $^1\text{H}$  n.m.r spectroscopy.

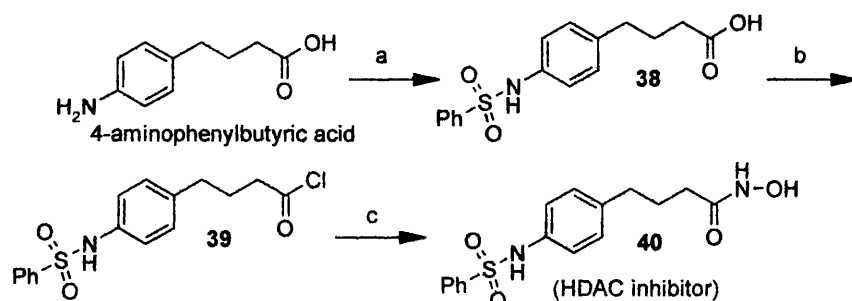


**Scheme 4** Mechanism of formation of hydroxamic acids

Towards the very end of the research period, a method was established by which hydroxamic acid **36** was prepared not *via* the carboxylic acid chloride, but from the diethyl ester **34**. This not only saves two steps in the formation of hydroxamic acid **36**, but also gives an improved yield of 61%. However, this only works for diethyl esters; the corresponding methyl esters were found to react much more slowly and give significantly poorer yields of hydroxamic acids. Therefore, in light of this new

methodology, and since the stabilised ester phosphoranes used, resulted in diethyl esters, this one-step route to hydroxamic acids should now be employed whenever possible.

In Scheme 5, the attempted synthesis of compound **40** (HDAC inhibitor) is shown. The design of hydroxamic acid **40** was considered as a direct comparison to compound **36**, the main difference being the degree of saturation of the lipophilic chain (a potentially key characteristic of a potent HDAC inhibitor) used. In compound **40**, the lipophilic chain is saturated, allowing the lipophilic portion to be more flexible and less constrained than its counterpart in hydroxamic acid **36**, (containing an unsaturated lipophilic chain). Unfortunately, the final step in the synthesis of HDAC inhibitor **40** failed to work. The reasons for this are unknown; especially since 4-phenylbutyric hydroxamic acid having an identical saturated lipophilic portion could be prepared. However, it would be worth trying to prepare HDAC inhibitor **40** from the corresponding diethyl ester, rather than from the acid chloride, with the methodology employed to produce HDAC inhibitor **36** from the diethyl ester, even though it would involve extra steps in the synthesis.

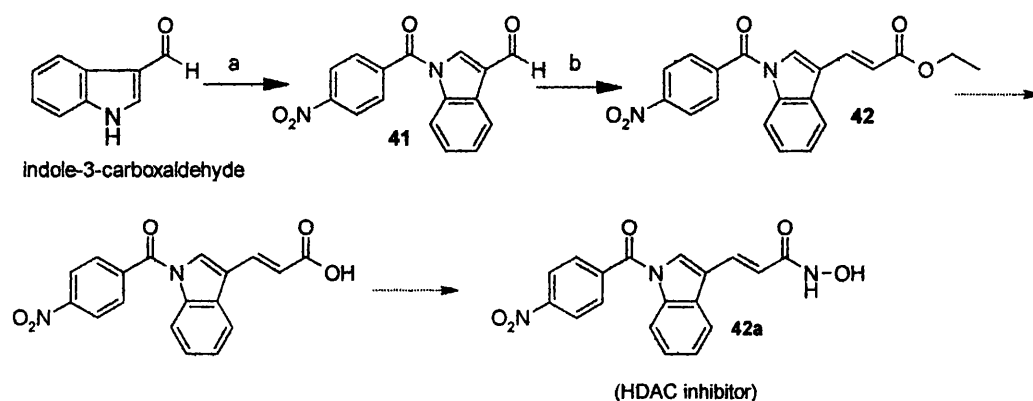


Reagents: (a) benzenesulfonyl chloride, pyridine, (b) thionyl chloride, (c) hydroxylamine hydrochloride, KOH

**Scheme 5** Attempted synthesis of HDAC inhibitor **40**

In Scheme 6, the attempted synthesis of HDAC inhibitor **42a** is shown. The preparation of hydroxamic acid **42a** was contemplated because it has the backbone of TSA (7-atom chain), but lacks the complexity of then chiral centre in TSA. Additionally, while TSA may be subject to cleavage by attack at the C=O group (and displacement of the chain as an enolate), this cannot be the case for HDAC inhibitor **42a** (although it could be subject to peptidase action). Regrettably, neither the

carboxylic acid chloride nor the hydroxamic acid compounds could be produced, even from the diethyl ester corresponding compound **42**. Great difficulty was experienced with the solubility of the compound **42**. Perhaps, if the nitro unit could be converted into the amino moiety, and the latter be sulfonylated, solubility problems may be avoided.

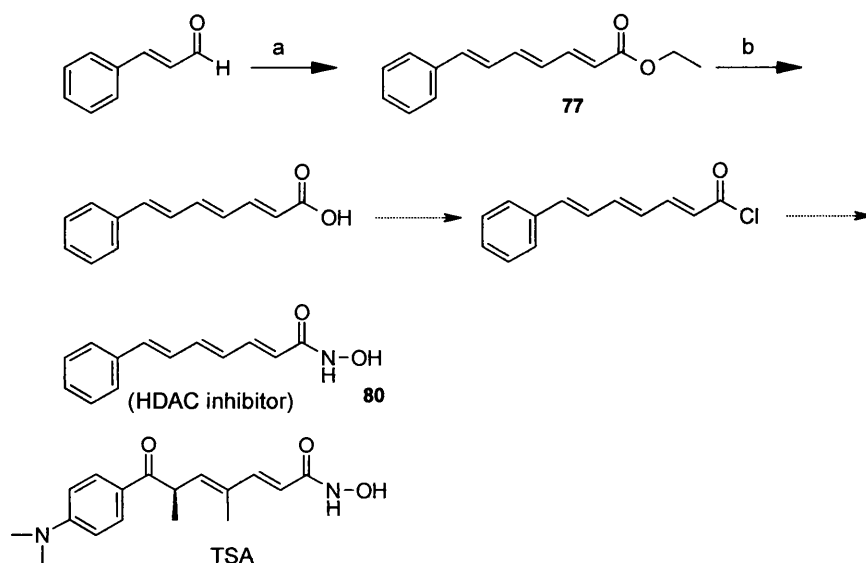


Reagents: (a) sodium acetate, (b) sodium hydride

**Scheme 6** Attempted synthesis of HDAC inhibitor **42a**

In Scheme 7, the attempted preparation of HDAC inhibitor **80** is shown. This particular inhibitor was of interest owing to the similarity in length and degree of unsaturation to the lipophilic chain in TSA. However, hydroxamic acid **80** would not have the complexity of the chiral centre which exists in TSA, and it also lacks the methyl groups on the lipophilic chain, which would allow inferences as to whether such functional units on the lipophilic chain increase/decrease the interaction between the enzyme pocket and the lipophilic chain. Unfortunately, the carboxylic acid chloride and the subsequent hydroxamic acid compound could not be made. With respect to the formation of the acid chloride, 'milder' reagents than thionyl chloride should be used, possibly avoiding any problems involving undesired addition to conjugated double bonds. Also, the methodology used to produce HDAC inhibitor **36** from the corresponding diethyl ester compound, should be employed with compound **77** (the diethyl ester moiety) to yield the subsequent hydroxamic acid (HDAC inhibitor **80**).





Reagents: (a) arsanylidene diethyl ester, (b) LiOH

**Scheme 7** Attempted synthesis of HDAC inhibitor **80**

### 5.11 HPLC assay for determining HDAC inhibition

An important requirement in the identification of HDAC inhibitors is an HPLC (high-performance liquid chromatography) assay that permits rapid determination of HDAC activity in the presence of potential inhibitors. Recently, an isolated enzyme assay was described based on the deacetylation of a fluorescent lysine N-(4-methyl-7-coumarinyl)-N- $\alpha$ -(*tert*-butyloxycarbonyl)-N- $\Omega$ -acetyllysineamide (MAL), as depicted in figure 11.<sup>66</sup> The acetylated (MAL) and deacetylated (ML) species can be easily resolved and quantitated by HPLC analysis.

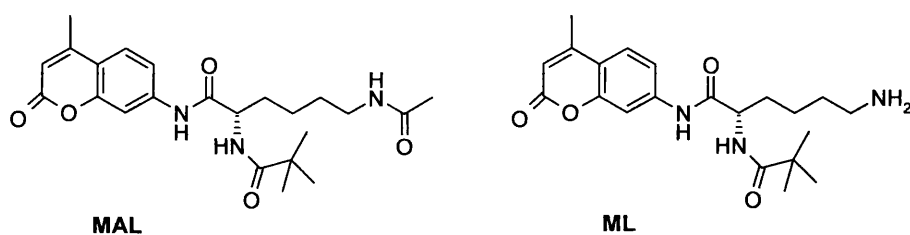


**Figure 11** MAL structure

#### 5.11.1 Data analysis of non-isotopic enzyme activity HDAC assay

MAL and ML were quantitated by fluorescence detection at excitation/emission wavelengths of 330/395 nm respectively. The peak heights of MAL and ML were

used to derive the percentage of MAL in the mixture as the ratio of MAL:MAL+ML. The percentage MAL after a 60 min incubation in the absence of inhibitor was taken as 100% HDAC activity, and the percentage of HDAC activity at higher concentrations derived from  $(100\% \text{ MAL}_{\text{DRUG}}/100\% \text{ MAL}_{\text{NO DRUG}})$ . The data collected (minimum of 4 runs at each concentration for each inhibitor) was fitted to a sigmoidal  $E_{\text{MAX}}$  model (GraphPad Prism, version 2.01),<sup>65</sup> to derive the  $IC_{50}$  concentration for each potential HDAC inhibitor. (See chapter 3, section 3.8.1).

### ***5.12 Evaluation of HPLC assay for determining potential inhibitors of HDAC***

The deacetylated reaction product (ML) was resolved from the substrate peak (MAL) with typical retention times of 2.7 and 3.3 minutes respectively using purified rat liver HDAC. In the absence of enzyme, no conversion of MAL to ML was observed, suggesting a specific enzyme-mediated conversion. In the absence of an inhibitor, the depletion of MAL appeared to plateau after 60 min. Accordingly, subsequent analyses for HDAC activity were based on a single time-point of 60 min incubation. The stability of the enzyme used, (aliquots were frozen and thawed six times, and then analysed for HDAC activity) showed reproducibility observed across all samples used ( $\pm 4.4\%$ ), indicating little, if any, loss of activity.

The HPLC non-isotope activity assay has shown to be simple, rapid and reproducible. A single Sepharose purification of rat liver (40 g) produces sufficient enzyme for approximately 400 individual enzyme reactions; moreover, the enzyme appears to be stable at both 4 °C and -40 °C. The synthetic substrate, MAL, was not deacetylated in the absence of enzyme but acted as a substrate for deacetylation with purified rat liver HDAC. A fairly large number of potential inhibitors could be screened using the purified enzyme, with the assay simplified by the use of a single time point at 60 min to determine activity. The use of a simple synthetic substrate (MAL) also overcomes problems with previous HDAC activity assays that use radio-labelled histones derived from chicken erythrocytes, or synthetic labelled peptides as the substrate, such as danger of exposure of laboratory personal to radiation and disposal of radioactive waste.

The fitted concentration-response curves for each compound used with purified rat liver HDAC are shown in figure 12, with the derived  $IC_{50}$  values displayed in Table 2.

Compounds No./Name	$IC_{50}$ values
Butyric acid	107 mM
46	416 $\mu$ M
45a	3.3 $\mu$ M
TSA	24.4 nM

**Table 2** The  $IC_{50}$  values obtained from known HDAC inhibitors from HPLC assay

Unfortunately, not all compounds prepared (HDAC inhibitors 47, 48, 4-phenylbutyric acid and 45) were used for the HPLC assay owing to the illness of the researcher conducting the HPLC assay in St. Bartholomew's Hospital.

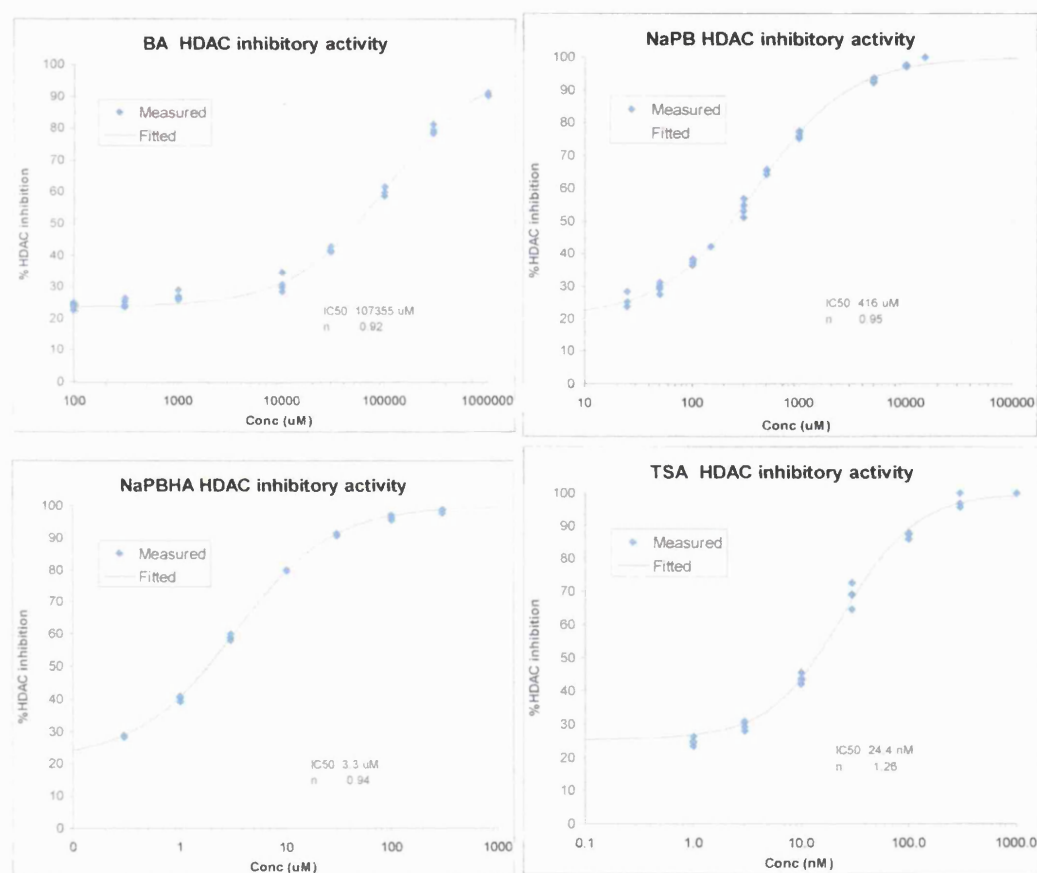


**Figure 12** Concentration-response curves for butyric acid, phenylbutyric acid sodium salt, phenylbutyric hydroxamic acid sodium salt and trichostatin A (left-to-right) with purified rat liver HDAC

Butyric acid is a very weak HDAC inhibitor, with an  $IC_{50}$  in the HPLC assay system of over 100 mM. This molecule has a carboxylic acid in place of the hydroxamic acid as in TSA, lacks an aromatic ring and has a sub-optimal chain length. Addition of an

aromatic ring to this molecule in the form of a phenyl group increased the inhibitory activity by over two log-units for 4-phenylbutyric acid sodium salt ( $IC_{50}$  416  $\mu$ M), while the conversion of the carboxylic acid sodium salt into a hydroxamic acid sodium salt resulted in an additional two log-unit increase in inhibitory activity ( $IC_{50}$  3.3  $\mu$ M). This was still much less than the inhibitory value of TSA ( $IC_{50}$  24 nM) partly because interactions between the side chain of phenylbutyrate hydroxamic acid and the active site residues on the enzyme are sub-optimal. This is shown in a space-filling model of TSA (figure 13)<sup>34</sup> occupying the enzyme pocket of histone deacetylase like-protein (HDLP) derived from the crystal structure.<sup>34</sup> This highlights potentially important characteristics of potent HDAC inhibitors, namely, a cap group to lie on the surface of the enzyme, an aliphatic chain to fit inside the length of the enzyme pocket and a hydroxamic acid moiety to interact with the zinc ion, located near the bottom end of the active site.

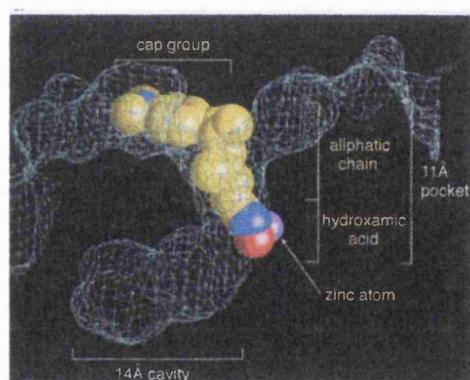


**Figure 13** Space-filling representation of TSA in the active-site pocket of HDLP<sup>34</sup>

### 5.13 *In vitro* [<sup>3</sup>H]acetyl-labelled HDAC assay

Total cellular extracts containing HDAC enzyme were commercially obtained from Life Technologies Inc., Gaithersburg MD and prepared using the methodology by S. Emiliani.<sup>62</sup> The enzyme inhibition assay works using either the natural substrate (acetylated histones, derived from cellular extracts) or synthetic peptides which consist of 24 amino acids, which are derived from the N-termini of certain core histone species (usually H4 histone). The substrate is labelled with [<sup>3</sup>H]acetic acid and the liberation of [<sup>3</sup>H]acetate is measured by scintillation counting giving a measurement on the amount of deacetylation.

### 5.13.1 Determination of IC<sub>50</sub> values

The concentration of TSA and other potential HDAC inhibitors required to inhibit HDAC activity or cell proliferation by 50% (IC<sub>50</sub>) were determined graphically in each case using non-linear regression analysis to fit inhibition data to the appropriate dose-response curve (GraphPad Prism, version 2.0; Graphpad software Inc), as shown in Chapter 3, section 12.1.<sup>64</sup> An example of the data obtained from a HDAC assay obtained using a [<sup>3</sup>H]-acetyl histone H4 peptide for trichostatin A is shown below.

Tube	Inhibitor concentration	Sample	CPM (counts per minute)	CPM minus substrate blank	Percentage of control (inhibitor blank minus substrate blank cpm)
1	0	Enzyme blank	174755		
2	0	Substrate blank	459534	284779	
3	0	Substrate blank	424789	250034	
4	0	Substrate blank	413426	238671	
5	1 nM		358049	183294	71.1
6	10 nM		206109	31354	12.2
7	100 nM		185291	10536	4.1
8	1 $\mu$ M		172738	0	0

**Table 3** The scintillation values obtained for the amount of [<sup>3</sup>H]-labelled histone H4 peptide in the presence of trichostatin A

(Mean  $\pm$ SD 100% of negative substrate control CPM: 257828)

A dose-response curve is drawn with the values of the experiment obtained with trichostatin A as a percentage of the control experiment (inhibitor blank) for the y-axis, and the log concentrations of inhibitor (trichostatin A) used as the x-axis, from which the log IC<sub>50</sub> value can be determined (figure 14).

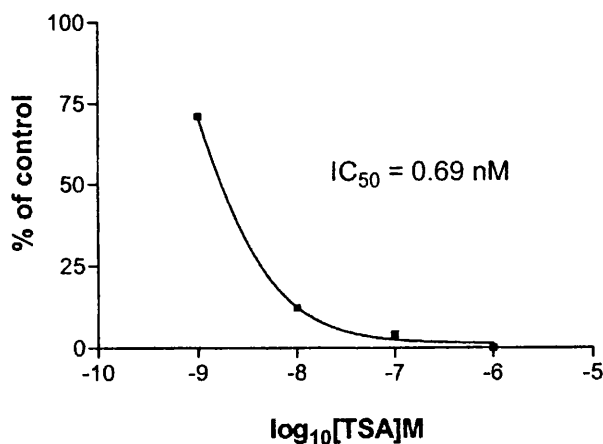


**Figure 14** A sigmoidal dose-response curve of the percentage of CPM for [<sup>3</sup>H]-labelled histone H4 peptide obtained with various concentrations of trichostatin A

From the graph above, the following values were obtained (Table 4).

X values	Y values
Best-fit values	
Bottom	171.3
Top	1.314
LOG IC <sub>50</sub>	-9.157
IC <sub>50</sub>	6.9650 x 10 <sup>-10</sup>
Std Error	
Bottom	69.94
Top	1.643
LOG IC <sub>50</sub>	0.3052
Goodness of fit	
R <sup>2</sup>	0.9986
Absolute sum of squares	4.678

**Table 4** Table of results obtained from the non-linear regression analysis of a sigmoidal dose-response curve for trichostatin A

The results show that the IC<sub>50</sub> value for trichostatin A in terms of histone deacetylase inhibition was 0.69 nM. The accuracy of the IC<sub>50</sub> value was ascertained by the 'goodness of fit' R<sup>2</sup> value (0.9986), where if R<sup>2</sup> = 1.0, then all data points lie exactly on the curve of the graph, minimising the sum-of-squares distance between the line and the data points. The x-axis is expressed in terms of log of concentration, as this would mean the concentrations of the inhibitor used are equally spaced in the log scale, thus the uncertainty of the log IC<sub>50</sub> value is symmetrical (*i.e.* a Gaussian curve

distribution), with the  $IC_{50}$  value obtained simply by taking the anti-log value; whereas the uncertainty of the  $IC_{50}$  values obtained directly from the value of concentration, and not logs of concentration, is unsymmetrical, therefore less Gaussian and more likely to contain larger errors.

#### 5.14 Evaluation of HDAC inhibitors 36 and 45 in an *in vitro* HDAC assay

A set of four compounds (butyric acid, TSA and HDAC inhibitors 36 and 45) was sent to Hammersmith Hospital for *in vitro* HDAC enzyme assays (conducted by Dr. D. M. Vigushin), the results being shown in Table 5.

Compound Name	HDAC $IC_{50}$ value
Butyric acid	5.0 mM
TSA	17.5 nM
HDAC inhibitor 45	6.2 $\mu$ M
HDAC inhibitor 36	172.1 nM

**Table 5** *In vitro* HDAC inhibition values for HDAC inhibitors

Butyric acid was confirmed to be a weak HDAC inhibitor, presumably owing to the lack of an optimal lipophilic chain length and aromatic ring moiety, and the lack of a hydroxamic acid moiety, which is known to confer potent HDAC inhibition. Addition of an aromatic ring, (HDAC inhibitor 45) in the form of a phenyl ring increases HDAC inhibition by over 800-fold ( $IC_{50}$  6.2  $\mu$ M) in comparison to butyric acid ( $IC_{50}$  5.0 mM). The value obtained for HDAC inhibitor 36 was less potent than TSA (the lead HDAC inhibitor) by only a factor of 9.8 ( $IC_{50}$  values of 172.1 nM: 17.5 nM respectively). The fact that the inhibitory value of HDAC inhibitor 36 was slightly less potent than TSA is partly due to the length of the lipophilic chain of HDAC inhibitor 36, causing the interaction between the hydroxamic acid moiety and the zinc ion in the enzyme pocket to be sub-optimal compared to the interaction between the hydroxamic acid of TSA and the zinc ion in the active site of the enzyme. Also, the capping group used in HDAC inhibitor 36 (a sulfonamido unit) may not be the capping group of choice compared with the *p*-dimethyl amino group present in the capping region of TSA.

A hydroxamic acid group is important in conferring potent inhibition of HDAC as it mimics the acetylated lysine within the HDLP active site, and its counterpart HDAC1 enzyme.<sup>34</sup> The deacetylase active site has features of both metallo proteases and serine proteases, consistent with the contacts that TSA makes in the active site, (shown in figure 14). By analogy with zinc proteases,<sup>34</sup> the carbonyl oxygen of the *N*-acetyl amide bond could bind to the zinc ion, the carbonyl group positioning close to a water molecule. The zinc ion could then polarise the carbonyl unit, to make the carbon a better electrophile and also orient the water molecule. The nucleophilicity of the water molecule would be increased by the negative charge of the Asp 166-His 131 charge-relay system to which the water is connected by hydrogen bonds.<sup>34</sup> This nucleophilic attack of water on the carbonyl carbon would result in a tetrahedral carbon, and the oxy-anion intermediate could be stabilised by two zinc-oxygen interactions analogous to the zinc proteases,<sup>34</sup> and possibly by a hydrogen bond from the Tyr 297 hydroxyl group. The final step would involve the break of the carbon-nitrogen bond in the intermediate, and the nitrogen of the scissile bond would accept a proton from the exposed Asp 173-His 132 charge-relay, liberating the acetate and lysine products (as shown in figure 15).<sup>34</sup>

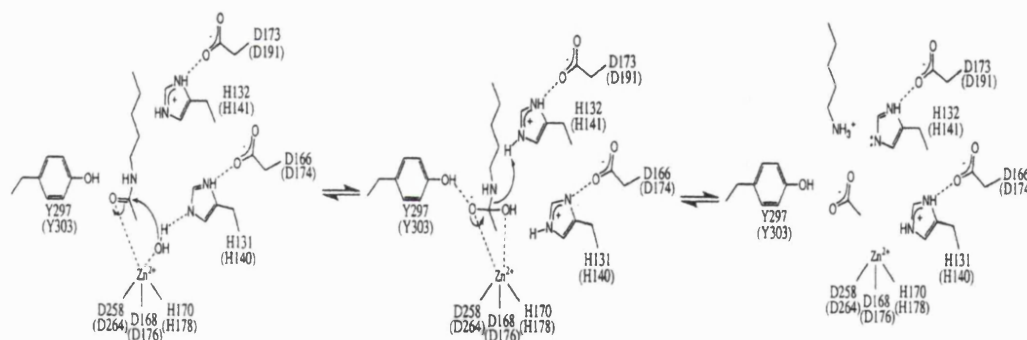


**Figure 15** Proposed catalytic mechanism for the deacetylation of an acetylated lysine in HDLP enzyme pocket<sup>34</sup>

### 5.15 Breast cancer cell line proliferation assay of HDAC inhibitors

A sulforhodamine B (SRB) assay allows rapid *in vitro* analysis of the cytotoxicity of compounds to several different cancerous breast cell lines.<sup>59</sup> The SRB dye binds



electrostatically to macromolecular counter-ions in cells fixed with trichloroacetic acid (TCA), allowing the binding and solubilisation to be controlled by variations in pH.<sup>59</sup> In one pH range, the dyed cells can be quantitatively extracted for measurement of optical density, which correlates in a linear manner with the number of live cells in the cell line culture. Absorbance at 492 nm ( $OD_{492}$ ) for each well was measured on a microtitre plate reader.  $OD_{492}$  values were expressed as the mean  $\pm$ SD for six replicates as a percentage of control (taken as 100%). An example of the linear correlation between the number of live cells and optical density units is shown in figure 16.

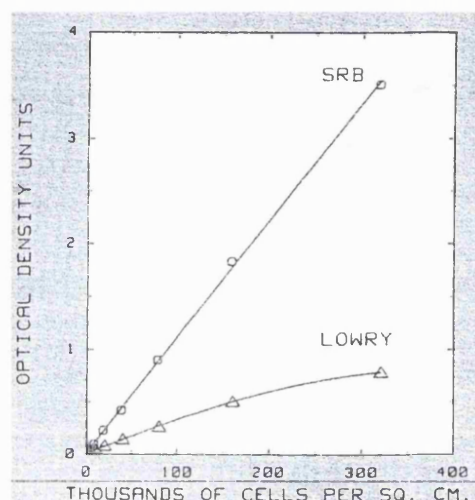


**Figure 16** Calibration of the SRB and Lowry cell proliferation assays *versus* number of cells<sup>59</sup>

### **5.16 Evaluation of the cytotoxic effects of HDAC inhibitor 36 and TSA on various breast cancer cell lines**

Following the results obtained from the *in vitro* [<sup>3</sup>H]acetate-labelled HDAC assay, HDAC inhibitor **36** was selected, along with TSA (the lead HDAC inhibitor), for cancerous cell proliferation assays, conducted by Dr. D. M. Vigushin (at Hammersmith Hospital). The results are shown in Table 6.

Cell Type	Cell proliferation (TSA) IC <sub>50</sub> values	Cell proliferation (HDAC inhibitor 36) IC <sub>50</sub> values	Ratio of in HDAC IC <sub>50</sub> values (36:TSA)
MCF7	27.7 nM	56.1 $\mu$ M	2070
MDA-MB-231	308.1 nM	6.4 $\mu$ M	20.8
T47D	26.4 nM	>100 $\mu$ M	>3800

**Table 6** The cytotoxic IC<sub>50</sub> values for TSA and HDAC inhibitor 8 in various breast cancerous cell lines

The cytotoxic potency of HDAC inhibitor **36** was less than observed for TSA in cancerous cell proliferation, with a difference ranging by a factor of 20 to an excess of 3500. The variation in the difference between the two compounds for each cancerous cell lines is almost certainly dependent on the different types of cancerous cell line used. The results for all the cancerous cell lines show that HDAC inhibitor **36** is not as powerful as TSA, possibly owing to the sub-optimal length of the lipophilic chain and the choice of capping unit for HDAC inhibitor **36**, compared with TSA (as discussed in the section above).

## 5.17 Conclusion

The objective of verifying that an HPLC assay can give reproducible and authentic HDAC inhibition values for known HDAC inhibitors and that novel HDAC inhibitors based on the key characteristics of TSA could be designed have been successfully met. A viable HPLC assay to determine the amount of HDAC inhibition for known HDAC inhibitors was established, allowing simple, rapid and reproducible HDAC assays to be conducted. A HDAC assay conducted *via* HPLC avoids the problems encountered with previous HDAC activity assays that use radio-labelled histones derived from chicken erythrocytes or synthetic labelled peptides, such as the complexity and cost of the assay and of course the unfortunate termination of the chickens involved.

The synthesis of potential HDAC inhibitors thought to contain the key characteristics of TSA (*i.e.* the presence of a hydroxamic moiety at the end of the aliphatic chain, with an aromatic group at the other end of the lipophilic chain and a suitable

lipophilic chain length) which confer optimal binding of TSA to the enzyme and thus inhibition of the enzyme were validated with the values obtained for HDAC inhibitor **36** and **45** for *in vitro* HDAC inhibition assays and cytotoxicity of various breast cancer cell lines.

The aliphatic chain interacts with active amino acid residues at the sides of the enzyme pocket, and also needs to be of a suitable length to allow the aromatic moiety to act as a capping group, making contact with the surface groove at the top of the enzyme pocket. The hydroxamic acid unit is believed to insert at the bottom the enzyme pocket, interacting with the zinc ion that resides there.

## 5.18 References

- 1] Johnson, C. A.; Turner, B. M. *Cell. Div. Biol.*, **1999**, *10*, 179
- 2] Cress. W. D.; Seto, E. *J. Cell. Physiol.*, **2000**, *184*, 1
- 3] Voet, J. in 'Biochemistry', 2<sup>nd</sup> ed, Prentice Hall, **1994**, 23
- 4] Luger, K.; Mader, A. W.; Richmond, R. K.; Sargent, D. F.; Richmond, T. J. *Nature*, **1997**, *389*, 251
- 5] Lee, D. Y.; Hayes, J. J.; Pruss, D.; Wolfee, A. P. *Cell*, **1993**, *72*, 73
- 6] Sun, Z. W.; Hampsey, M. *Genetics*, **1999**, *152*, 921
- 7] Boyes, J.; Byfield, P.; Nakatani, Y.; Ogryzko, V. *Nature*, **1998**, *396*, 594
- 8] Sartorelli, V.; Puri, P. L.; Hamamori, Y.; Ogryzko, V.; Chung, G.; Nakatani, Y.; Wang, J. Y.; Kedes, L. *Mol. Cell*, **1999**, *4*, 725
- 9] Taunton, J.; Hassig, C. A.; Schreiber, S. L. *Science*, **1996**, *272*, 408
- 10] Vidal, M.; Gaber, R. F. *Mol. Cell. Biol.*, **1991**, *11*, 6317
- 11] Yang, W. M.; Inouye, C.; Zeng, Y.; Bearss, D.; Seto, E. *Proc. Natl. Acad. Sci. USA*. **1996**, *93*, 12845
- 12] Dangond, F.; Hafler, D. A.; Tong, J. K.; Randall, J.; Kojima, R.; Utku, N.; Gullans, S. R. *Biochem. Biophys. Res. Commun.*, **1998**, *242*, 648
- 13] Carmen, A. A.; Rundlett, S. E.; Grunstein, M. *J. Biol. Chem.*, **1996**, *271*, 15837
- 14] Rundlett, S. E.; Carmen, A. A.; Kobayashi, R.; Bavkin, S.; Turner, B. M.; Grunstein, M. *Proc. Natl. Acad. Sci. USA*. **1996**, *93*, 14503
- 15] Grozinger, C. M.; Hassig, C. A.; Schreiber, S. L. *Proc. Natl. Acad. Sci. USA*, **1999**, *96*, 4868
- 16] Verdel, A.; Khochbin, S. *J. Biol. Chem.*, **1999**, *274*, 2440
- 17] Lusser, A.; Brosch, G.; Loidl, A.; Haas, H.; Loidl, P. *Science*, **1997**, *277*, 88
- 18] Grunstein, M. *Nature*, **1997**, *389*, 349
- 19] Gu, W.; Roeder, R. G. *Cell*, **1997**, *90*, 595
- 20] Dang, C. V. *Mol. Cell Biol.*, **1999**, *19*, 1
- 21] Li, Y.; Turck, C. M.; Teumer, J. K.; Stavnezer, E. *J. Virol.*, **1986**, *57*, 1065

- 22] Nomura, T.; Khan, M. M.; Kaul, S. C.; Dong, H. D.; Wadhwa, R.; Colmenares, C.; Kohno, I.; Ishii, S. *Genes Dev.*, **1999**, *13*, 412
- 23] Dahl, R.; Kieslinger, M.; Beug, H.; Hayman, M. J. *Proc. Natl. Acad. Sci. USA*, **1998**, *95*, 11187
- 24] Grignani, F.; De Matteis, S.; Nervi, C.; Tomassoni, L.; Gelmetti, V.; Cioce, M.; Fanelli, M.; Ruthardt, M.; Ferrara, F. F.; Zamir, I.; Seiser C.; Lazar, M. A.; Minucci, S.; Pelicci, P. G. *Nature*, **1998**, *391*, 815
- 25] Dr. Joel, S. P. unpublished data
- 26] Wade, P. A.; Jones, P. L.; Vermaak, D.; Wolffe, A. P. *Curr. Biol.*, **1998**, *8*, 843
- 27] Siegfried, Z.; Eden, S.; Mendelsohn, M.; Feng, X.; Tsuberi, B. Z.; Cedar, H. *Nat. Genet.*, **1999**, *22*, 203
- 28] Hendrich, B.; Bird, A. *Mol. Cell Biol.*, **1998**, *18*, 6538
- 29] Nan, X.; Ng, H. H.; Johnson, C. A.; Laherty, C. D.; Turner, B. M.; Eisenman, R. N.; Bird, A. *Nature*, **1998**, *393*, 386
- 30] Archer, S. Y.; Meng, S.; Shei, A.; Hodin, R. A. *Proc. Natl. Acad. Sci. USA*, **1998**, *95*, 6791
- 31] Marks, P. A.; Richon, V. M.; Rifkind, R. A. *J. Natl. Cancer Inst.*, **2000**, *92*, 1210
- 32] Carducci, M.; Bowling, M. K.; Eisenberger, M.; Sinibaldi, V.; Chen, T.; Nor, D. *Anticancer Res.*, **1997**, *17*, 3972
- 33] Tsuji, N.; Kobayashi, M.; Nagashima, K.; Wakisaka, Y.; Koizumi, K. *J. Antibiot.*, **1976**, *29*, 1
- 34] Finnin, M. S.; Donigian, J. R.; Cohen, A.; Richon, V. M.; Rifkind, R. A.; Marks, P. A.; Breslow, R.; Pavietich, N. P. *Nature*, **1999**, *401*, 188
- 35] Torchia, N.; Cress, C.; Rosenfeld, M. G. *Curr. Opin. Cell Biol.*, **1998**, *10*, 373-
- 36] Yoshida, M.; Hoshikawa, Y.; Koseki, K.; Mori, K.; Beppu, T. *J. Antibiot.*, **1990**, *43*, 1101
- 37] Kim, Y. B.; Lee, K. H.; Sugita, K.; Yoshida, M.; Horinouchi, S. *Oncogene*, **1999**, *18*, 2461
- 38] Saito, A.; Yamashita, T.; Mariko, Y.; Nosaka, Y.; Tsuchiya, K.; Ando, T. *Proc. Natl. Acad. Sci. USA*, **1999**, *96*, 4592
- 39] Darkin-Rattray, S. J.; Gurnett, A. M.; Myers, R. W.; Dulski, P. M.; Crumley, T. M.; Allocco, J. J. *Proc. Natl. Acad. Sci. USA*, **1996**, *93*, 13143

- 40] Nakajima, H.; Kim, Y. B.; Terano, H.; Yoshida, M.; Horinouchi, S. *Exp. Cell Res.*, **1998**, *241*, 126
- 41] Kijima, M.; Yoshida, M.; Sugita, K.; Horinouchi, S.; Beppu, T. *J. Biol. Chem.*, **1993**, *268*, 22429
- 42] Kwon, H. J.; Owa, T.; Hassig, C. A.; Shimada, J.; Schreiber, S. L. *Proc. Natl. Acad. Sci. USA*, **1998**, *95*, 3356
- 43] Cluffetti, L. M.; Pope, M. R.; Dunkle, L. D.; Daly, J. M.; Knoche, H. W. *Biochemistry*, **1983**, *22*, 3507
- 44] Richon, V. M.; Emiliani, S.; Verdin, E.; Webb, Y.; Breslow, R.; Rifkind, R. A. *Proc. Natl. Acad. Sci. USA*, **1998**, *95*, 3003
- 45] Breslow, R.; Jursic, B.; Yan, Z. F.; Friedman, E.; Leng, L.; Ngo, L. *Proc. Natl. Acad. Sci. USA*, **1991**, *88*, 5542
- 46] Ayohei, F.; Yasuhiko, K.; Norikazu, N.; Saadi, K.; Minoru, Y.; Sueharu, H. *PNAS*, **2001**, *98*, 87
- 47] Morioka, H.; Ishihara, M.; Takezawa, M.; Shibai, H.; Komoda, Y. *Agric. Biol. Chem.*, **1988**, *52*, 251
- 48] Yoshida, M.; Beppu, T. *Exp. Cell Res.*, **1988**, *177*, 122
- 49] Hoshikawa, Y.; Kwon, H. J.; Yoshida, M.; Horinouchi, S.; Beppu, T. *Exp. Cell Res.*, **1994**, *214*, 189
- 50] Glick, R. D.; Swendeman, S. L.; Coffey, D. C.; Rifkind, R. A.; Marks, P. A.; Richon, V. M. *Cancer Res.*, **1999**, *59*, 4392
- 51] Qui, L.; Kelso, M. J.; Hansen, C.; West, M. L.; Fairlie, D. P.; Parsons, P. G. *Br. J. Cancer*, **1999**, *80*, 1252
- 52] Riggs, M. G.; Whittaker, R. G.; Neumann, J. R.; Ingram, V. S. *Nature*, **1997**, *268*, 462
- 53] Van Lint, C.; Emiliani, S.; Verdin, E. *Gene Expr.*, **1996**, *5*, 245
- 54] Xiao, H.; Hasegawa, T.; Isobe, K. I. *J. Cell Biochem.*, **1999**, *73*, 291
- 55] Richon, V. M.; Sandhoff, T. W.; Rifkind, R. A.; Marks, P. A. *Proc. Am. Assoc. Cancer Res.*, **2000**, *40*, 5131
- 56] Newmark, H. L.; Lupton, J. R.; Young, C. W. *Cancer Lett.*, **1994**, *78*, 1
- 57] Warrell, R. P.; He, L. Z.; Richon, V.; Calleja, E.; Pandolfi, P. P. *J. Natl. Cancer Inst.*, **1998**, *90*, 1621

- 58] Novich, S.; Camacho, L.; Gallagher, R.; Chanel, S.; Ho, R.; Tolentino, T. *Blood*, **1994**, *94*, 61a
- 59] Vigushin, D. M.; Ali, S.; Pace, P. E.; Mirsaidi, N.; Ito, K.; Adcock, I.; Coombes, R. C. *Clin. Cancer Res.*, **2001**, *7*, 971
- 60] Stahelin, H.; Trippmacher, A. *Eur. J. Cancer*, **1974**, *10*, 801
- 61] Cohen, L. A.; Amin, S.; Marks, P. A.; Rifkind, R. A.; Desai, D.; Richon, V. M. *Anticancer Res.*, **1999**, *19*, 4999
- 62] Emiliani, S.; Fischle, W.; Van Lunt, C.; Al-Abed, Y.; Verdin, E. *Proc. Natl. Acad. Sci. USA*, **1998**, *95*, 2795
- 63] Taunton, J.; Hassig, C. A.; Schreiber, S. L. *Science*, **1996**, *272*, 408
- 64] Wilkinson, J. R.; Williams, J. C.; Singh, D.; Goss, P. E.; Easton, D.; Coombes, R. C. *Cancer Res.*, **1986**, *46*, 4862
- 65] Motulsky, H. in 'Analyzing data with GraphPad Prism', **1999**, GraphPad Software Inc., San Diego CA, [www.graphpad.com](http://www.graphpad.com)
- 66] Hoffman, K.; Brosch, G.; Loidl, P.; Jung, M. *Nucleic Acids Res.*, **1999**, *27*, 2057
- 67] Arnold, L. *J. Am. Chem. Soc.*, **1953**, *75*, 5396

## Experimental

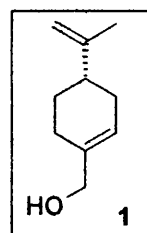
### 6.0 Instrumentation and experimental techniques

*General:* Melting points were determined on a microscope hot-stage apparatus and are uncorrected. The infra-red (I.R.) spectra were recorded on a Perkin-Elmer PE-983 spectrophotometer; absorptions are recorded in wavenumbers ( $\nu_{\max}$  in  $\text{cm}^{-1}$ ).  $^1\text{H}$  spectra and  $^{13}\text{C}$  N.M.R spectra were obtained on a Bruker AC300 (300 MHz), Bruker AC250 (250 MHz) and Bruker AC80 (80 MHz) spectrometer.  $^1\text{H}$  n.m.r spectra are reported in parts per million (ppm,  $\delta$ ), with TMS as the internal standard. Coupling constants ( $J$ ) are given in Hertz (Hz). The following abbreviations are used in signal assignments: s (singlet); bd s (broad singlet); d (doublet); t (triplet); q (quartet); m (multiplet). Mass spectra were recorded on a VG7070H mass spectrometer with Finigan Incos II data system at University College London. High resolution mass spectra (HRMS) were performed by Mr. M. Cocksedge at the London School of Pharmacy using a VGZABSE mass spectrometer. Thin-layer chromatography was performed on Merck 0.2 mm aluminium-backed silica gel 60 F<sub>254</sub> plates and visualised by ultraviolet light or an alkaline  $\text{KMnO}_4$  spray and subsequent heating. Flash column chromatography was performed using Merck 0.040 – 0.063 mm, 230 – 400 mesh silica gel. Petroleum ether (40 – 60 °C fraction) and ethyl acetate were distilled before use; tetrahydrofuran was distilled from sodium and benzophenone; dichloromethane was distilled from calcium hydride. Evaporation refers to the removal of solvent under reduced pressure. Glassware, syringes and needles for moisture-sensitive reactions were pre-dried in an oven (130 °C). Temperatures below 0 °C were obtained from various mixtures of liquid nitrogen and ethyl acetate.

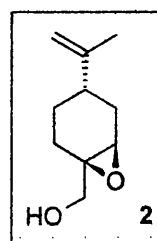


## 6.1 Experimental procedures

**(S)-(-)-Perillyl alcohol (1).** Purchased from Aldrich Co. (96 % pure).

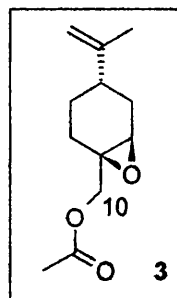


**Epoxy-perillyl alcohol (2).** The Mordini<sup>1</sup> procedure was used. A stirred solution of perillyl alcohol (1) (0.70 g, 4.61 mmol) and vanadyl acetylacetonate (4.1 mg, 0.015 mmol) in benzene (20 mL) was cooled to 0 °C. 6M *tert*-butyl hydroperoxide (0.27 mL, 2.47 mmol) in dichloromethane (15 mL) added dropwise over 30 min. The mixture changed colour from green to red and was allowed to reach 25 °C. The progress of the reaction was monitored by thin-layer chromatographic analysis (developed by KMnO<sub>4</sub> charring). The solution was quenched with saturated aqueous sodium sulfate (2 x 15 mL) and transferred to a separating funnel. The layers were separated and the aqueous layer was extracted with diethyl ether (2 x 15 mL). The combined organic layers were washed with saturated aqueous sodium chloride and dried over anhydrous magnesium sulfate. The solution was filtered through a fluted filter paper and the filtrate was evaporated. The oil was purified by flash column chromatography on silica gel [ethyl acetate-light petroleum ether, 33-66, (v/v); developed by KMnO<sub>4</sub> charring], and the eluent evaporated to give 2 (0.33 g, 80%) as a viscous yellow oil. *R*<sub>F</sub> [ethyl acetate-light petroleum ether, 33-66, (v/v)] 0.41; IR *v*<sub>max</sub> (film) 3457 (OH), 1250 (C-O-C) cm<sup>-1</sup>; <sup>1</sup>H NMR (250 MHz, CDCl<sub>3</sub>)  $\delta$ <sub>H</sub> 8.12 (1H, s, OH), 4.71 (1H, s, =CH<sub>a</sub>), 4.62 (1H, s, =CH<sub>b</sub>), 3.62 (2H, m, CH<sub>2</sub>OH), 3.47 (1H, m, OCH), 2.21 – 2.16 (4H, m, 2 x CH<sub>2</sub> ring), 1.81 (2H, m, CH<sub>2</sub> ring), 1.62 (3H, m, CH<sub>3</sub>), 1.50 (1H, m, =CCH) ppm.

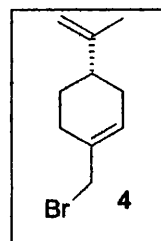


**Acetic acid 4-isopropenyl-7-oxabicyclo[4.1.0] hept-1-yl methyl ester (3).**

To a stirred solution of epoxy-perillyl alcohol (2) (0.29 g, 1.75 mmol) and pyridine (10 mL, 0.12 mmol) was added a solution of 4-dimethylaminopyridine (0.08 g, 0.65 mmol) and acetic anhydride (0.36 mL, 3.82 mmol) at 25 °C. The stirring was continued at 25 °C for 3 h. The progress of the reaction was monitored by thin-layer chromatographic analysis (developed by  $\text{KMnO}_4$  charring). The reaction was quenched by the addition of saturated aqueous hydrogen carbonate (10 mL) and transferred to a separating funnel. The layers were separated and the aqueous layer extracted with dichloromethane (3 x 10 mL). The combined organic layers were washed with saturated aqueous sodium chloride (2 x 5 mL) and dried over anhydrous magnesium sulfate. The solution was filtered through fluted filter paper and the filtrate evaporated. The oil was purified by flash column chromatography on silica gel [ethyl acetate-light petroleum, 1-5, (v,v); developed by  $\text{KMnO}_4$  charring], and the eluent was evaporated to give 3 (0.27g, 73 %) as a clear colourless oil:  $R_F$  [ethyl acetate-light petroleum, 1-5, (v,v)] 0.92; IR  $\nu_{\text{max}}$  (film) 1738 (C=O) and 1237 (C-O-C epoxide)  $\text{cm}^{-1}$ ;  $^1\text{H}$  NMR (250 MHz,  $\text{CDCl}_3$ )  $\delta_{\text{H}}$  4.72 (1H, s, =CH<sub>a</sub>) 4.65 (1H, s, =CH<sub>b</sub>), 4.23 – 3.94 (2H, m, CH<sub>2</sub>(10)), 3.21 (1H, m, epoxy-CH), 2.24 – 2.16 (2H, m, CH<sub>2</sub> ring), 2.08 (3H, s, OCH<sub>3</sub>), 1.97 – 1.82 (4H, m, 2 x CH<sub>2</sub> ring), 1.72 (3H, m, CH<sub>3</sub>), 1.48 (1H, m, =CCH) ppm;  $^{13}\text{C}$  NMR (62 MHz,  $\text{CDCl}_3$ )  $\delta_{\text{C}}$  170.58 (C=O), 148.65 (H<sub>2</sub>C=), 109.33 (H<sub>2</sub>C=C), 69.70 (C-epoxy), 57.64 (C-epoxy), 40.57 (COC=O), 36.44 (CH<sub>2</sub> ring), 30.15 (O=CCH<sub>3</sub>), 26.13 (CH<sub>2</sub> ring), 24.74 (CH<sub>2</sub> ring), 22.58 (=CCH), 20.93 (=CCH<sub>3</sub>) ppm; HRMS<sub>EI</sub> calcd for  $\text{C}_{12}\text{H}_{18}\text{O}_3$  ( $\text{M}^+$ ) 210.1255. Found: 210.1254.

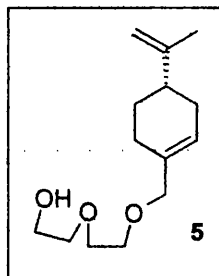
**Perillyl bromide (4).** Based on a procedure used by Buchecker.<sup>2</sup>

To a stirred solution of perillyl alcohol (1), (1.01 mL, 6.5 mmol), in anhydrous diethyl ether (20 mL) at –20 °C under an atmosphere of dry nitrogen was added phosphorus tribromide (0.25 mL, 2.6 mmol) dropwise, by means of a stainless steel needle. The mixture was allowed to warm slowly to 20 °C. Stirring was continued at 20 °C under an atmosphere of dry nitrogen for 5 hours. The progress of the reaction was monitored by thin-layer chromatographic analysis (developed by  $\text{KMnO}_4$  charring). The mixture then quenched by pouring onto crushed ice and transferred to a separating funnel. The



layers were separated and the organic layer washed with water (2 x 5 mL) and saturated aqueous sodium hydrogen carbonate (6.0 mL) and dried over anhydrous sodium sulfate. The solution was filtered through a fluted filter paper and the filtrate evaporated at 1 atmosphere pressure to give **4** (0.31 g, 55 %) as a light yellow oil:  $R_F$  [ethyl acetate-light petroleum, 1-5, (v,v)] 0.92; IR  $\nu_{\max}$  (film) 690 (C-Br)  $\text{cm}^{-1}$ ;  $^1\text{H}$  NMR (80 MHz,  $\text{CDCl}_3$ )  $\delta_H$  5.92 (1H, s, =CH), 4.79 (1H, s, =CH<sub>a</sub>), 4.63 (1H, s, =CH<sub>b</sub>), 4.01 (2H, s, CH<sub>2</sub>Br), 2.26 – 2.04 (6H, m, 3 x CH<sub>2</sub> ring), 1.94 (3H, s, CH<sub>3</sub>), 1.86 (=CCH) ppm.

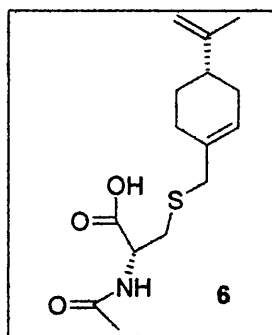
**2-[2-(Isoprenylcyclohex-1-enylmethoxy)-ethanol (5).** To a stirred solution of potassium fluoride (0.81 g, 0.014 mol) and glycol (20 mL, 0.15 mol) was added perillyl bromide (**4**) (1.35 mL, 5.58 mmol) at 25 °C. The reaction temperature was increased to 160 °C and stirring continued at 160 °C for 16 h. The progress of the reaction was monitored by thin-layer



chromatographic analysis (developed by  $\text{KMnO}_4$  charring). The reaction was quenched by pouring onto water (20 mL) and transferred to a separating funnel. The layers were separated and the aqueous layer extracted by diethyl ether (6 x 10 mL). The combined organic layers were dried over anhydrous sodium sulfate. The solution was filtered through fluted filter paper and the filtrate was evaporated. The oil was purified by flash column chromatography on silica gel [ethyl acetate-light petroleum ether, 1-9, (v,v); developed by  $\text{KMnO}_4$  charring], and the eluent was evaporated to give **5** (0.74 g, 55 %) as a colourless viscous oil:  $R_F$  [ethyl acetate-light petroleum ether, 1-4, (v,v)] 0.32; IR  $\nu_{\max}$  (film) 3210 (OH), 1178 (OCCO)  $\text{cm}^{-1}$ ;  $^1\text{H}$  NMR (250 MHz,  $\text{CDCl}_3$ )  $\delta_H$  5.71 (1H, s, =CH), 4.78 (1H, s, =CH<sub>a</sub>), 4.65 (1H, s, =CH<sub>b</sub>), 3.96 (2H, s, =CCH<sub>2</sub>O), 3.71 – 3.49 (8H, m, 4 x CH<sub>2</sub> – diethylene glycol), 3.32 (1H, s, OH), 2.19 – 2.02 (6H, m, 3 x CH<sub>2</sub> ring), 1.64 (3H, m, CH<sub>3</sub>), 1.56 (1H, m, =CCH) ppm;  $^{13}\text{C}$  NMR (62 MHz,  $\text{CDCl}_3$ )  $\delta_C$  149.57 (CC=CH), 134.41 (HC=C), 124.66 (C=CH<sub>2</sub>), 108.65 (H<sub>2</sub>C=C), 75.49 (HOC), 72.61 (CO), 70.39 (OCH<sub>2</sub>), 68.87 (CH<sub>2</sub>O), 61.62 (=CCH<sub>2</sub>O), 41.04 (=CCH), 30.46 (CH<sub>2</sub> ring), 27.42 (CH<sub>2</sub> ring), 26.26 (CH<sub>2</sub> ring), 20.15 (CH<sub>3</sub>) ppm;  $^{13}\text{C}$  NMR<sub>DEPT</sub> confirmed the above assignments above to be correct; HRMS<sub>EI</sub> calcd for  $\text{C}_{14}\text{H}_{24}\text{O}_3$  ( $M^+$ ) 240.1725. Found 240.1725.

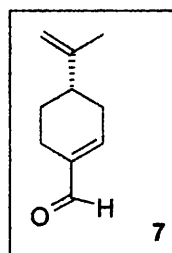
**2-Acetylamino-3-(4-isoprenyl-1-enyl)-propionic acid**

**(6).** To a stirred solution of *N*-acetyl-L-cysteine (0.20 g, 1.23 mmol) in methanol (8.0 mL) and 10 M aqueous sodium hydroxide (2.20 mL) was added a solution of perillyl bromide (**4**) (0.51 mL, 2.30 mmol) in methanol (8.0 mL) at 25 °C. Stirring was continued at 25 °C for 15 min. The progress of the reaction was monitored by thin-

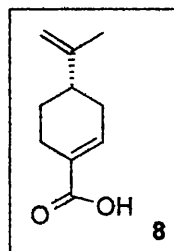


layer chromatographic analysis (developed by  $\text{KMnO}_4$  charring). The mixture was quenched by the addition of water (40 mL), this was transferred to a separating funnel and washed with diethyl ether (3 x 10 mL). The layers were separated and the aqueous layer acidified to pH 1 by conc. hydrochloric acid (5.1 mL) and saturated aqueous sodium chloride (6.0 mL) added. The mixture was transferred to a separating funnel and extracted with dichloromethane (6 x 15 mL). The combined organic layers were dried with anhydrous magnesium sulfate, filtered through a fluted filter paper and the filtrate evaporated to give a solid that was recrystallised from ethyl acetate to give **6** (0.22 g, 60 %) as white needles: mp 140-141 °C;  $R_F$  [ethyl acetate-light petroleum ether, 1-5, (v,v)]; IR  $\nu_{\text{max}}$  (film) 3350 (NH weak), 3230 (OH), 1731 (C=O aldehyde), 1672 (C=O acid), 712 (C-S stretching)  $\text{cm}^{-1}$ ;  $^1\text{H}$  NMR (250 MHz,  $\text{CDCl}_3$ )  $\delta_{\text{H}}$  12.72 (1H, s, OH), 8.20 (1H, d,  $J$  4.8 Hz, NH), 5.61 (1H, s, =CH), 4.76 (1H, s, =CH<sub>a</sub>), 4.62 (1H, s, =CH<sub>b</sub>), 4.43 (1H, m, HNCH), 3.11 (2H, s,  $\text{CH}_2\text{S}$ ), 2.71 (2H, m,  $\text{SCH}_2$ ), 2.52 (2H, m,  $\text{CH}_2$  ring), 2.16 (4H, bs, 2 x  $\text{CH}_2$  ring), 1.84 (3H, s,  $\text{O}=\text{CCH}_3$ ), 1.73 (3H, s, = $\text{CCH}_3$ ), 1.52 (1H, m, =CCH) ppm; Anal. calcd. for  $\text{C}_{15}\text{H}_{23}\text{O}_3\text{S}$  = C, 60.57, H, 7.79, N, 4.70. Found C, 60.59, H, 7.75, N, 4.71 %.

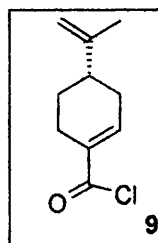
**(S)-(-)-Perillaldehyde (7).** Purchased from Aldrich Co. (92 % pure).



**Perillic acid (8).** Based on a procedure by Wang.<sup>3</sup> To a stirred aqueous solution of silver oxide (1.70 g, 7.34 mmol) was added sodium hydroxide (3.88 g, 97 mmol) at 25 °C. The mixture was warmed to 80 °C, and stirring continued as perillaldehyde (7) (1.20 g, 7.99 mmol) was added dropwise, by means of a stainless steel needle. The reaction continued at 80 °C for 20 min. The progress of the reaction was monitored by thin-layer chromatographic analysis (developed by  $\text{KMnO}_4$  charring). The mixture was filtered with a fluted filter paper and the filtrate transferred to a separating funnel was washed with hot water (5 x 10 mL). The non-aqueous layer was acidified with dilute hydrochloric acid (30 mL) until a pH of 2 was reached. The acidified solution was then extracted with dichloromethane (3 x 10 mL). The combined organic layers were dried over anhydrous magnesium sulfate. The solution was filtered with a fluted filter paper and the filtrate evaporated to give a solid that was purified by flash column chromatography on silica gel eluting with solvents [ethyl acetate-light petroleum ether, 1-3, (v,v); developed by  $\text{KMnO}_4$  charring], and the eluent was evaporated to give **8** (0.74 g, 60 %) as white crystalline platelets: mp 130-132 °C, lit.<sup>3</sup> mp 129-131 °C;  $R_F$  [ethyl acetate-light petroleum ether, 1-3, (v,v)] 0.61; IR  $\nu_{\text{max}}$  (film) 3010 (OH), 1685 (C=O)  $\text{cm}^{-1}$ ;  $^1\text{H}$  NMR (250 MHz,  $\text{CDCl}_3$ )  $\delta_{\text{H}}$  10.04 – 9.32 (1H, bs, OH), 7.02 (1H, m, =CH), 4.77 (1H, s, =CH<sub>a</sub>), 4.65 (1H, s, =CH<sub>b</sub>), 2.46 – 2.21 (4H, m, 2 x CH<sub>2</sub> ring), 2.09 (2H, m, CH<sub>2</sub> ring), 1.64 (3H, s, CH<sub>3</sub>), 1.48 (1H, m, =CCH) ppm;  $^{13}\text{C}$  NMR (62 MHz,  $\text{CDCl}_3$ )  $\delta_{\text{C}}$  169.01 (C=O), 149.66 (C=CH), 139.95 (C=CH<sub>2</sub>), 130.65 (HC=C), 109.46 (H<sub>2</sub>C=C), 40.82 (=CC), 31.64 (CH<sub>2</sub> ring), 27.81 (CH<sub>2</sub> ring), 25.15 (CH<sub>2</sub> ring), 20.77 (CH<sub>3</sub>) ppm.

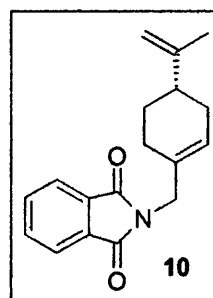


**4-Isopropenylcyclohexene-1-carbonyl chloride (9).** Based on a procedure utilised by Fujita.<sup>4</sup> To a stirred solution of perillic acid (**8**) (0.20 g, 1.20 mmol) in anhydrous dichloromethane (5.0 mL) at 0 °C under an atmosphere of nitrogen was added thionyl chloride (0.15 mL, 2.02 mmol) dropwise by means of a stainless steel needle. The mixture was allowed to warm slowly to 20 °C and continued stirring at 20 °C under an atmosphere of nitrogen for 16 hours. The progress of the reaction was monitored by aliquots taken from the mixture by means of a stainless steel needle and



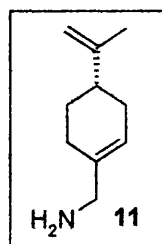
an IR conducted. The mixture was evaporated to give **9** (0.2 g, quantitative yield) as a colourless oil and used immediately *in situ* for the next reaction; IR  $\nu_{\max}$  (film) 1747 (C=O), 745 (C-Cl)  $\text{cm}^{-1}$ .

**Perillyl phthalimide (10).** Based on a procedure used by Sen.<sup>5</sup> To a stirred solution of perillyl alcohol (**1**) (0.62 mL, 3.94 mmol), phthalimide (0.69 g, 5.13 mmol) and triphenylphosphine (1.35 g, 5.13 mmol) in 10 mL of anhydrous tetrahydrofuran at 20 °C under an atmosphere of nitrogen, and in the absence of light, was added diisopropyl azodicarboxylate

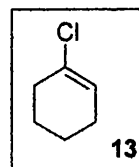


(1.01 mL, 5.13 mmol) dropwise by means of a stainless steel needle. The stirring continued at 20 °C under an atmosphere of dry nitrogen for 4 h. The progress of the reaction was monitored by thin-layer chromatographic analysis (developed by  $\text{KMnO}_4$  charring). The mixture was quenched by the addition of water (30 mL) and transferred to a separating funnel. The layers were separated and the aqueous layer was extracted with light petroleum ether (3 x 30 mL). The combined organic layers were washed with saturated aqueous sodium chloride (20 mL) and dried over anhydrous magnesium sulfate. The solution was filtered through a fluted filter paper and the filtrate evaporated. The oil was purified by flash column chromatography on silica gel [ethyl acetate-light petroleum ether, 1-4, (v,v); developed by  $\text{KMnO}_4$  charring], and the eluent was evaporated to give **10** (0.98 g, 88 %) as a pale yellow oil:  $R_F$  [ethyl acetate-light petroleum ether, 2-5, (v,v)] 0.91; IR  $\nu_{\max}$  (film) 3105 (C=C aromatic stretch), 1718 (C=O)  $\text{cm}^{-1}$ ;  $^1\text{H}$  NMR (270 MHz,  $\text{CDCl}_3$ )  $\delta_{\text{H}}$  7.91 (2H, m, 2 x Ar-H), 7.76 (2H, m, 2 x Ar-H), 5.63 (1H, bs, =CH), 4.65 (2H, bs, =CH<sub>2</sub>), 4.15 (2H, s, CH<sub>2</sub>N), 2.08 (4H, m, 2 x CH<sub>2</sub> ring), 1.82 (2H, m, CH<sub>2</sub> ring), 1.54 (3H, m, CH<sub>3</sub>), 1.42 (1H, m, =CCH) ppm;  $^{13}\text{C}$  NMR (67 MHz,  $\text{CDCl}_3$ )  $\delta_{\text{C}}$  168.24 (C=O), 149.62 (C=CH), 133.93 (C=CH<sub>2</sub>), 132.13 (C=CH), 131.82 (C-Ar), 123.60 (C-Ar), 123.29 (C-Ar), 108.75 (=CH<sub>2</sub>), 43.29 (CH<sub>2</sub>N), 40.79 (=CCH), 30.39 (CH<sub>2</sub> ring), 27.34 (CH<sub>2</sub> ring), 27.12 (CH<sub>2</sub> ring), 20.73 (CH<sub>3</sub>) ppm.

**Perillylamine (11).** Based on procedure by Sen.<sup>5</sup> A solution of perillyl phthalimide (**10**) (0.52 g, 1.85 mmol) in 0.3 M methanolic hydrazine hydrate (19.8 mL) at 25 °C was stirred for 30 min. To this was added 5 % dilute hydrochloric acid (11 mL) and stirring continued at 25 °C for 12 h. The progress of the reaction was monitored by thin-layer chromatographic analysis (developed by  $\text{KMnO}_4$  charring). The mixture was filtered through a fluted filter paper and the filtrate was diluted with an equal amount of water, acidified with dilute hydrochloric acid until a pH of 2 was reached and then transferred to a separating funnel. The aqueous layer was washed with diethyl ether (3 x 8 mL). The aqueous layer was basified with solid potassium hydroxide (0.43 g, 11.0 mmol) until a pH of 10 or above was reached. This was transferred to a separating funnel and the aqueous layer extracted with diethyl ether (3 x 10 mL). The combined organic layers were washed with saturated aqueous sodium chloride (2 x 10 mL) and dried over anhydrous magnesium sulfate. The solution was filtered through a fluted filter paper and the filtrate was evaporated. The oil was purified by flash column chromatography on silica gel [methanol-chloroform, 3-97, (v,v); developed by  $\text{KMnO}_4$  charring], and the eluent was evaporated to give **11** (0.24 g, 86 %) as a pale yellow oil:  $R_F$  [methanol-chloroform, 1-49, (v,v)] 0.61; IR  $\nu_{\text{max}}$  (film) 3345 ( $\text{NH}_2$ )  $\text{cm}^{-1}$ ;  $^1\text{H}$  NMR (300 MHz,  $\text{CDCl}_3$ )  $\delta_{\text{H}}$  5.62 (1H, s, =CH), 4.75 (1H, s, =CH<sub>a</sub>), 4.63 (1H, s, =CH<sub>b</sub>), 3.09 (2H,  $\text{CH}_2\text{N}$ ), 2.08 – 1.88 (4H, m, 2 x  $\text{CH}_2$  ring), 1.84 (2H, m,  $\text{CH}_2$  ring), 1.62 (2H, s,  $\text{NH}_2$ ), 1.57 (3H, s,  $\text{CH}_3$ ), 1.40 (1H, m, =CCH) ppm;  $^{13}\text{C}$  NMR (75 MHz,  $\text{CDCl}_3$ )  $\delta_{\text{C}}$  149.72 ( $\text{C}=\text{CH}$ ), 136.12 ( $\text{C}=\text{CH}_2$ ), 122.31 ( $\text{C}=\text{CH}$ ), 108.72 ( $\text{C}=\text{CH}_2$ ), 47.14 ( $\text{CH}_2\text{N}$ ), 41.07 (=CCH), 30.54 ( $\text{CH}_2$  ring), 27.17 ( $\text{CH}_2$  ring), 26.69 ( $\text{CH}_2$  ring), 20.80 ( $\text{CH}_3$ ) ppm;  $^{13}\text{C}$  NMR<sub>DEPT</sub> showed the above assignments above to be correct.

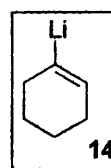


**1-Chlorocyclohexene (13).** Based on a procedure by Baird.<sup>6</sup> Cyclohexene (11.8 mL, 0.11 mol) was added dropwise over 2 h, by means of a stainless steel needle, to phosphorus pentachloride (18.7 g, 0.09 mol) at 0 °C. The mixture was continued at 0 °C and stirred for 24 h. The progress of the reaction was monitored by thin-layer chromatographic analysis (developed by  $\text{KMnO}_4$  charring). The mixture was quenched by water (10 mL). This solution was transferred to a separating funnel and was then extracted with

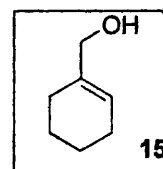


dichloromethane (4 x 5 mL). The combined organic layers were dried over anhydrous calcium chloride. The solution was filtered through a fluted filter paper and concentrated under 1 atmosphere pressure. The oil was purified by fractional distillation through a vigreux unit to give **13** (1.00 g, 9.5%) as a clear, colourless oil and was used immediately in the next reaction: bp 78 - 79 °C/2 mmHg, lit<sup>6</sup> bp 78 - 80 °C;  $R_F$  [ethyl acetate-light petroleum ether, 1-4, (v,v)] 0.32; IR  $\nu_{\max}$  (film) 1644 (C=C), 775 (C-Cl).

**1-Lithiocyclohexene (14).** Based on methodology conducted by Braude.<sup>7</sup> To a stirred suspension of lithium metal (7.32 g, 1.05 mol) flattened with a hammer and cut into 1 mm x 2 mm x 1 cm strips, and two broken pasteur pipettes in anhydrous diethyl ether (50 mL) at 25 °C under an atmosphere of nitrogen was added 1-chlorocyclohexene (**13**) (6.02 mL, 0.05 mol,) in one portion by means of a stainless steel needle. Stirring was continued at 25 °C under an atmosphere of nitrogen for 12 h. The progress of the reaction was monitored by thin-layer chromatographic analysis (thin-layer chromatography was developed by  $Ce_2(SO_4)_3$  charring). A grey/green suspension was formed. An aliquot of suspension was taken by means of a stainless steel needle and an IR run: IR  $\nu_{\max}$  (film) 1640 (C=C), and a complete absence of C-Cl (775)  $cm^{-1}$ ;  $R_F$  [ethyl acetate-light petroleum ether, 1-4, (v,v)] 0.08 The suspension **14** (2.32 g, 50%) was used immediately *in situ* for the next reaction.



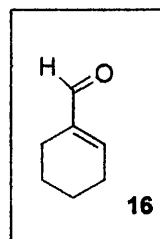
**1-Cyclohexenyl-1-methanol (15).** Based on a procedure by Arnold.<sup>8</sup> To a stirred suspension of 1-lithiocyclohexene (**14**) (2.32 g, 0.026 mol) at 25 °C under an atmosphere of nitrogen was added dropwise by means of a stainless steel needle, a solution of paraformaldehyde (1.23 g, 0.041 mol) in anhydrous diethyl ether (40 mL). The mixture was heated at reflux for 1.5 h. The progress of the reaction was monitored by thin-layer chromatographic analysis (thin-layer chromatography was developed by  $Ce_2(SO_4)_3$  charring). The mixture was cooled to -10 °C and quenched by the addition





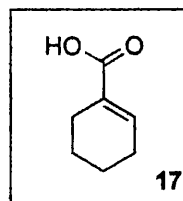
dropwise, by the means of a stainless steel needle, of pre-cooled saturated aqueous ammonium chloride (35 mL). The mixture was allowed to slowly reach 25 °C and then transferred to a separating funnel. The layers were separated and the aqueous layer extracted with dichloromethane (5 x 20 mL). The combined organic layers were dried over anhydrous magnesium sulfate. The solution was filtered through a fluted filter paper and the filtrate concentrated to give an oil that was purified by flash column chromatography on silica gel [ethyl acetate-light petroleum ether, 1-4, (v,v); thin-layer chromatography was developed by cerium sulfate charring], and the eluent was evaporated to give **15** (1.49 g, 51%) as a pale yellow oil:  $R_F$  [ethyl acetate-light petroleum ether, 2-5, (v,v)] 0.56; IR  $\nu_{\max}$  (film) 3420 (OH), 1650 (C=C)  $\text{cm}^{-1}$ ;  $^1\text{H}$  NMR (250 MHz,  $\text{CDCl}_3$ )  $\delta_H$  5.17 (1H, m, =CH), 3.99 (2H, m,  $\text{CH}_2\text{O}$ ), 2.48 (1H, bs, OH), 2.11 (4H, m, 2 x  $\text{CH}_2$  ring), 1.64 (4H, m, 2 x  $\text{CH}_2$  ring) ppm;  $^{13}\text{C}$  NMR (62 MHz,  $\text{CDCl}_3$ )  $\delta_C$  137.49 (C=CH), 122.42 (C=CH), 67.02 ( $\text{CH}_2\text{OH}$ ), 25.55 ( $\text{CH}_2$  ring), 24.91 ( $\text{CH}_2$  ring), 22.56 ( $\text{CH}_2$  ring), 22.50 ( $\text{CH}_2$  ring) ppm.

**1-Cyclohexene-1-carboxaldehyde (16).** Based on a procedure by Braude.<sup>7</sup> To a stirred suspension of 1-lithiocyclohexene (**14**) (4.00 g, 0.045 mol) in anhydrous diethyl ether (10 mL) at 25 °C under an atmosphere of nitrogen was added dimethylformamide (4.70 mL, 0.061 mol) dropwise, by means of a stainless steel needle. The



mixture continued to be stirred at 25 °C under an atmosphere of nitrogen for 2 h. The progress of the reaction was monitored by thin-layer chromatographic analysis (developed by  $\text{KMnO}_4$  charring). The mixture was quenched by the addition of water (10 mL) and transferred to a separating funnel. The aqueous layer was extracted by diethyl ether (6 x 15 mL). The combined organic layers were dried over anhydrous sodium sulfate. The solution was filtered through a fluted filter paper and the filtrate was evaporated. The oil was purified by flash column chromatography on silica gel eluting with [ethyl acetate-light petroleum ether, 1-4, (v,v); developed by  $\text{KMnO}_4$  charring]. The eluent was evaporated to give **16** (1.98 g, 40%) as a pale yellow oil:  $R_F$  [ethyl acetate-light petroleum ether, 2-5, (v,v)] 0.36; IR  $\nu_{\max}$  (film) 1705 (C=O conjugated)  $\text{cm}^{-1}$ ;  $^1\text{H}$  NMR (80 MHz,  $\text{CDCl}_3$ )  $\delta_H$  9.41 (1H, s, CHO), 6.82 (1H, m, =CH), 2.34 (4H, m, 2 x  $\text{CH}_2$  ring), 1.80 (4H, m, 2 x  $\text{CH}_2$  ring) ppm.

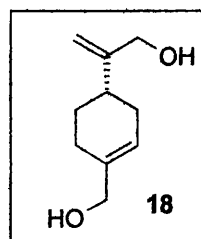
**1-Cyclohexene-1-carboxylic acid (17).** Based on a procedure by Hayashi.<sup>9</sup> To a stirred solution of 1-cyclohexene-1-carboxaldehyde (16) (1.20 g, 0.011 mol) in acetone (18 mL) at 0 °C was added Jones reagent (12 mL, 0.03 mol) dropwise over 30



min, by means of a stainless steel needle. The mixture was allowed to warm slowly to 25 °C and stirring was continued at 25 °C for 2 h. The progress of the reaction was monitored by thin-layer chromatographic analysis (developed by  $\text{KMnO}_4$  charring). The mixture was quenched by the addition of isopropyl alcohol (3.5 mL) and the solution concentrated to one-quarter of its total volume. The residual solution was diluted with saturated aqueous sodium hydrogen carbonate (5.0 mL) and transferred to a separating funnel. The solution was extracted with diethyl ether (2 x 5 mL). The combined organic layers were extracted with saturated aqueous hydrogen carbonate (10 mL). This aqueous layer was then acidified to pH 1 with concentrated hydrochloric acid (4.5 mL) and transferred to a separating funnel. The aqueous layer was then extracted with diethyl ether (3 x 10 mL). The combined organic layers were washed with saturated aqueous sodium chloride (2 x 10 mL) and dried over anhydrous magnesium sulfate. The solution was filtered through a fluted filter paper and the filtrate evaporated. The oil was purified by fractional distillation [bp 102–104 °C/4 mmHg] to give 17 (0.96 g, 69%) as a white crystalline solid: mp 39–40 °C, lit<sup>9</sup> mp 37–38 °C;  $R_F$  [ethyl acetate-light petroleum ether, 1-4, (v,v)] 0.12; IR  $\nu_{\text{max}}$  (film) 3010 (OH carboxylic acid), 1700 (C=O), 1660 (C=C)  $\text{cm}^{-1}$ ;  $^1\text{H}$  NMR (80 MHz,  $\text{CDCl}_3$ )  $\delta_{\text{H}}$  10.45 (1H, bs, COOH), 6.94 (1H, s, =CH), 2.31 (4H, m, 2 x  $\text{CH}_2$  ring), 1.84 (4H, m, 2 x  $\text{CH}_2$  ring) ppm.

**3-(4-Hydroxymethylcyclohex-3-enyl)-but-3-en-1-ol (18).**

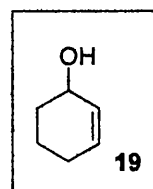
Based on a procedure by Suemune.<sup>10</sup> To a stirred suspension of sodium hydride (0.32 g, 0.013 mol) in anhydrous light petroleum ether (5.0 mL) at 5 °C was added perillyl alcohol (1) (0.80 g, 5.26 mmol), dropwise, by means of a stainless steel



needle. The mixture was heated to 50 °C and stirring continued at 50 °C for 1 h. The mixture was then cooled to -60 °C and stirred under an oxygen atmosphere. The

mixture was warmed slowly to 0 °C over 1 h. The reaction was quenched with the addition of *tert*-butanol (5.0 mL). The mixture was diluted with water (50 mL), ethyl acetate (30 mL) and 25 % sodium sulfite solution (10 mL) and the mixture stirred at 25 °C for 24 h. The solution was transferred to a separating funnel and the organic layer separated. The aqueous layer was with ethyl acetate (3 x 15 mL). The combined organic layers were washed with saturated aqueous brine (10 mL) and dried over anhydrous sodium sulfate. The solution was filtered through a fluted filter paper and the filtrate evaporated. The oil was purified by flash column chromatography [acetone-light petroleum ether, 1-5, (v,v); developed by KMnO<sub>4</sub> charring]. The eluent was evaporated to give **18** (0.21 g, 22%) as a colourless oil: *R*<sub>F</sub> [acetone-light petroleum ether, 1-5, (v,v)] 0.29; IR *v*<sub>max</sub> (film) 3340 (OH), 1650 (C=C) cm<sup>-1</sup>; <sup>1</sup>H NMR (250 MHz, CDCl<sub>3</sub>) δ<sub>H</sub> 5.71 (1H, s, C=CH ring), 5.08 (1H, d, *J* 1.5 Hz, C=CH<sub>a</sub>), 4.92 (1H, d, *J* 1.5 Hz, C=CH<sub>b</sub>), 4.13 (2H, s, C=CCH<sub>2</sub>OH), 3.99 (2H, s, H<sub>2</sub>C=CCH<sub>2</sub>OH), 2.40 – 2.01 (4H, m, 2 x CH<sub>2</sub> ring), 1.69 (2H, m, CH<sub>2</sub> ring), 1.54 (1H, m, =CCH ring) ppm; <sup>13</sup>C NMR (62 MHz, CDCl<sub>3</sub>) δ<sub>C</sub> 153.32 (C=CH), 137.36 (C=CH<sub>2</sub>), 122.24 (C=CH), 108.31 (C=CH<sub>2</sub>), 67.16 (=CCH<sub>2</sub>OH), 65.19 (=CCH<sub>2</sub>OH), 37.01 (=CCH), 31.01 (CH<sub>2</sub> ring), 27.83 (CH<sub>2</sub> ring), 26.13 (CH<sub>2</sub> ring) ppm.

**2-Cyclohexen-1-ol (19).** Procedure based on methodology by Barnier.<sup>11</sup> To a stirred solution of calcium chloride (0.88 g, 7.93 mmol) in methanol (8.0 mL) was added a solution of 2-cyclohexen-1-one (0.38 g, 3.95 mmol) in methanol (8.0 mL). The resulting clear

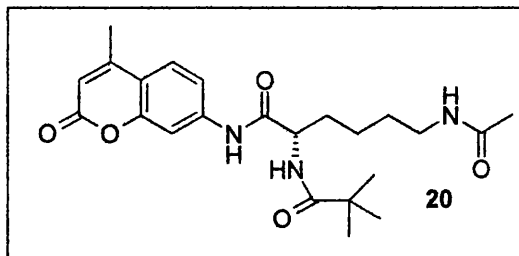


solution was stirred for 30 min at 25 °C. The reaction was cooled to 0 °C and sodium hydroborohydride (0.22 g, 5.82 mmol) was added carefully with stirring. The mixture was warmed to 25 °C and stirring continued for 1 hr. After which, 1M hydrochloric acid (30 mL) was added and the mixture was transferred to a separatory funnel and extracted with ethyl acetate (3 x 10 mL). The combined organic layers were dried with anhydrous sodium sulfate. The solution was filtered through a fluted filter paper and the filtrate evaporated. The oil was purified by flash column chromatography [acetone-light petroleum ether, 1-5, (v,v); developed by KMnO<sub>4</sub> charring]. The eluent was evaporated to give **19** (0.32 g, 83%) as a yellow oil; *R*<sub>F</sub> [acetone-light petroleum ether, 1-5, (v,v)] 0.34; IR *v*<sub>max</sub> (film) 3310 (OH), 1675 (C=C) cm<sup>-1</sup>; <sup>1</sup>H NMR (80

MHz,  $\text{CDCl}_3$ )  $\delta_{\text{H}}$  6.01-5.78 (1H, m,  $\text{HC}=\text{CH}$ ), 4.81-4.62 (1H, m,  $\text{HC}=\text{CH}$ ), 2.56 (1H, m,  $\text{CHOH}$ ), 2.09-1.15 (6H, m, 3 x  $\text{CH}_2$ ).

***N*-[5-Acetylamino-1-(4-methyl-2-oxo-2H-chromen-7-ylcarbamoyl)-pentyl]-2,2-dimethylpropionamide (20).**

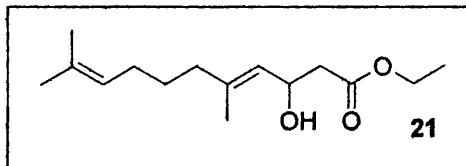
Based on a procedure by Hoffmann.<sup>12</sup> To a stirred solution of *Boc*-protected lysine-(Ac)-alcohol



(0.30 g, 1.10 mmol) and 7-amino-4-methylcoumarin (0.19 g, 1.10 mmol) in anhydrous pyridine (8.0 mL) at  $-15^\circ\text{C}$  under an atmosphere of nitrogen was added phosphorus oxychloride (0.11 mL, 1.18 mmol) dropwise by means of a stainless steel needle. Stirring continued at  $-15^\circ\text{C}$  for 30 min. The progress of the reaction was monitored by thin-layer chromatographic analysis (developed by  $\text{KMnO}_4$  charring). The reaction was quenched by the addition of crushed ice/water (15 mL) and the solution was transferred to a separating funnel. The aqueous layer was extracted with ethyl acetate (3 x 15 mL) and the combined organic layers were washed with saturated aqueous sodium hydrogen carbonate (2 x 15 mL) and then washed with saturated aqueous sodium chloride (2 x 15 mL). The organic layer was dried over anhydrous sodium sulfate and filtered through a fluted filter paper. The filtrate was evaporated and then co-evaporated with toluene, ethyl acetate and methanol successively to give **20** (0.10 g, 21%) as a clear yellow oil:  $R_{\text{F}}$  [ethyl acetate-light petroleum ether, 1-4, (v,v)] 0.31; IR  $\nu_{\text{max}}$  (film) 3010 (C-H aromatic stretching), 1711 ( $\text{C}=\text{O}$ )  $\text{cm}^{-1}$ ;  $^1\text{H}$  NMR (250 MHz,  $\text{CDCl}_3$ )  $\delta_{\text{H}}$  9.72 (1H, bs, NH), 8.60 (1H, bs, NH), 7.69 (1H, s, Arom-H), 7.40 (2H, m, 2 x Arom-H), 6.47 (1H, s,  $\text{CHCO}$ ), 5.69 (1H, d,  $J$  5.1 Hz,  $\text{OCC}(\text{H})\text{NH}$ ), 4.41 (1H, bs, NH), 3.20 (2H, m,  $\text{CH}_2$ ), 2.39 (3H, s,  $=\text{CCH}_3$  ring), 1.98 (3H, s,  $\text{OCC}(\text{CH}_3)_3$  chain), 1.62 (6H, m, 3 x  $\text{CH}_2$  ring), 1.50 (9H, m, 3 x  $\text{CH}_3$ ,  $\text{OCC}(\text{CH}_3)_3$  ppm;  $^{13}\text{C}$  NMR (62 MHz,  $\text{CDCl}_3$ )  $\delta_{\text{C}}$  172.01 ( $\text{OCO}$  ring), 170.94 ( $\text{OCC}(\text{CH}_3)_3$ ), 165.43 ( $\text{OCC}(\text{H})\text{NH}$ ), 161.50 ( $\text{HNCO}$ ), 154.10 ( $\text{OC}=\text{C}$ ), 152.86 ( $=\text{CNH}$  ring), 147.43 ( $=\text{CCH}_3$ ), 145.21 ( $\text{C}=\text{C}$  arom), 141.87 ( $\text{H}_3\text{CC}=\text{CH}$ ), 125.20 ( $\text{C}=\text{CH}$  arom), 115.93 ( $\text{C}=\text{CH}$  arom), 107.27 ( $\text{C}=\text{CH}$  arom), 55.27 ( $\text{OCC}(\text{H})\text{NH}$ ), 50.11 ( $\text{OCC}(\text{CH}_3)_3$ ), 39.06 ( $\text{CH}_2$  chain), 32.06 ( $\text{CH}_2$  chain), 29.05 ( $\text{CH}_2$  chain), 28.52 ( $\text{CH}_2$

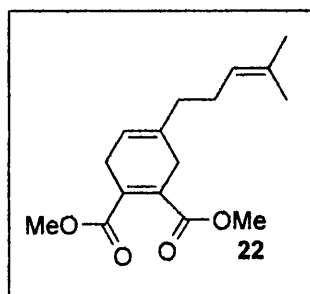
chain), 23.39 (CH<sub>3</sub> boc), 22.93 (CH<sub>3</sub> boc), 18.70 (CH<sub>3</sub> boc), 16.43 (=CCH<sub>3</sub>), 14.91 (=CCH<sub>3</sub> ring) ppm.

**(*E*)-3-Hydroxy-5,10-dimethylundeca-4,9-dienoic acid ethyl ester (21).** Based on a procedure by Bortolussi.<sup>13</sup> A stirred solution of citral (0.40 g, 2.63 mmol)



and 2-bromoethyl acetate (0.57 g, 3.41 mmol) in tetrahydrofuran (1.5 mL) was added to zinc/silver couple (0.59 g, 3.41 mmol) at 25 °C dropwise by means of a stainless steel needle. During the addition of the solution to the zinc/silver couple, the mixture was heated at reflux (75 °C) and maintained for 30 min. The progress of the reaction was monitored by thin-layer chromatographic analysis (developed by KMnO<sub>4</sub> charring). The mixture was cooled and the reaction quenched by the addition of cold saturated aqueous ammonium chloride (5.0 mL). The solution was transferred to a separating funnel and extracted with diethyl ether (2 x 10 mL). The combined organic layers were dried over anhydrous magnesium sulfate. The solution was filtered through a fluted filter paper and evaporated. The oil was purified by flash column chromatography on silica gel with [ethyl acetate-light petroleum ether, 2-3, (v,v); thin-layer chromatography was developed by KMnO<sub>4</sub> charring]. The eluent was evaporated to give **21** (0.31 g, 46%) as a colourless oil: R<sub>F</sub> [acetone-light petroleum ether, 1-2, (v,v)] 0.51; IR ν<sub>max</sub> (film) 3310 (OH), 1711 (C=O), 1631 (C=C) cm<sup>-1</sup>; <sup>1</sup>H NMR (250 MHz, CDCl<sub>3</sub>) δ<sub>H</sub> 5.15 (1H, t, *J* 5.0 Hz, (CH<sub>3</sub>)<sub>2</sub>=CH), 5.01 (1H, d, *J* 4.8 Hz, H<sub>3</sub>CC=CH), 4.70 (1H, m, =CCHOH), 4.03 (2H, q, *J* 7.5 Hz, OCH<sub>2</sub>), 2.48 (2H, m, CH<sub>2</sub>CO), 2.00 (4H, m, 2 x CH<sub>2</sub>), 1.61 (6H, s, 2 x =CH<sub>3</sub>), 1.54 (3H, s, =CCH<sub>3</sub>), 1.19 (3H, t, *J* 7.5 Hz, OCH<sub>2</sub>CH<sub>3</sub>) ppm.

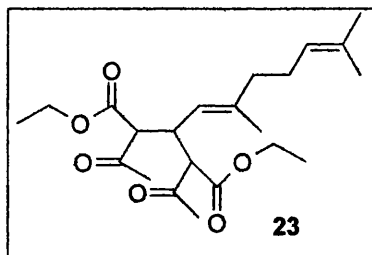
**4-(4-Methylpent-3-enyl)-cyclohexa-1,4-diene-1,2-dicarboxylic acid dimethyl ester (22).** Based on a procedure by Mehta.<sup>14</sup> A suspension of freshly distilled γ-myrcene (2.40 g, 0.018 mol), dimethyl acetylenedicarboxylate (2.22 mL, 0.018 mol) and hydroquinone (0.10 g, 0.91 mmol) was contained inside



a sealed tube under an atmosphere of nitrogen. This mixture was placed in an oven and heated to 55 °C left for 96 h. The sealed tube was broken and the oil was purified by flash column chromatography on silica gel with [ethyl acetate-light petroleum ether, 1-5, (v,v); developed by KMnO<sub>4</sub> charring]. The eluent was evaporated to give **22** (3.95 g, 78%) as a yellow oil: *R<sub>F</sub>* [ethyl acetate-light petroleum ether, 2-5, (v,v)] 0.29; IR  $\nu_{\text{max}}$  (film) 1724 (C=O), 1691 (C=O conjugated) cm<sup>-1</sup>; <sup>1</sup>H NMR (250 MHz, CDCl<sub>3</sub>)  $\delta_{\text{H}}$  5.43 (1H, m, HC=C ring), 5.17 (1H, m, HC=C chain), 3.78 (6H, s, 2 x CH<sub>3</sub>O), 3.10 – 2.84 (4H, m, 2 x CH<sub>2</sub> chain), 2.19 – 2.00 (4H, m, 2 x CH<sub>2</sub> ring), 1.69 (3H, s, =CCH<sub>3</sub>), 1.59 (3H, s, =CCH<sub>3</sub>) ppm; <sup>13</sup>C NMR (62 MHz, CDCl<sub>3</sub>)  $\delta_{\text{C}}$  168.06 (C=O), 133.31 (HC=C ring), 132.50 (C=C ring), 132.39 (C=C ring), 131.58 (HC=C chain), 123.61 (HC=C ring), 116.24 (HC=C chain), 51.77 (OCH<sub>3</sub>), 36.43 (CH<sub>2</sub> ring), 30.50 (CH<sub>2</sub> ring), 28.36 (CH<sub>3</sub>), 25.72 (CH<sub>2</sub> chain), 25.41 (CH<sub>2</sub> chain), 17.44 (CH<sub>3</sub>) ppm.

**2,4-Diacetyl-3-((*E*)-2,6-dimethylhepta-1,5-dienyl)-pentanedioic acid diethyl ester (**23**).**

Based on a procedure by Knoevenagel.<sup>15</sup> To a stirred suspension of freshly distilled ethyl acetoacetate (10.2 mL, 0.080 mol) and citral (6.86 mL, 0.040 mol) at –5 °C was added

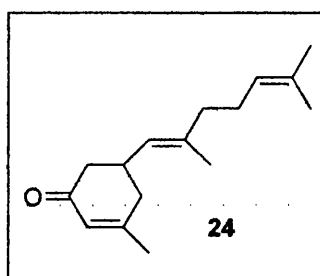


piperidine (0.34 mL, 3.41 mmol), dropwise, by means of a stainless steel needle. The stirring mixture was continued at –5 °C for 48 h. The progress of the reaction was monitored by thin-layer chromatographic analysis (thin-layer chromatography was developed by KMnO<sub>4</sub> charring). The mixture was allowed to warm slowly to 25 °C and left to stand for 72 h. The crude crystalline product formed was filtered through a sintered glass funnel. This solid was purified by recrystallisation from light petroleum ether to give **23** (8.72 g, 55%) as white crystalline needles: mp 63 – 64 °C, lit<sup>15</sup> mp 63 – 64 °C; *R<sub>F</sub>* [ethyl acetate-light petroleum ether, 1-4, (v,v)] 0.34; IR  $\nu_{\text{max}}$  (film) 1745 (C=O), 1735 (C=O carboxylic esters) cm<sup>-1</sup>; <sup>1</sup>H NMR (300 MHz, CDCl<sub>3</sub>)  $\delta_{\text{H}}$  5.12 (1H, m, HC=CCH<sub>3</sub>CH<sub>3</sub>), 5.06 (1H, d, *J* 10 Hz, HC=C chain), 4.19 (4H, 2q, *J* 4.7 Hz, 2 x OCH<sub>2</sub>), 3.21 (1H, d, *J* 10 Hz, =CCH), 2.72 (2H, d, *J* 10 Hz, CHCO<sub>2</sub>Et), 2.67 (1H, d, *J* 10 Hz, CHCO<sub>2</sub>Et), 2.07 (4H, m, 2 x CH<sub>2</sub> chain), 1.79 (3H, s, =CCH<sub>3</sub> ring), 1.71 (3H,

s, =CCH<sub>3</sub>), 1.68 (3H, s, =CCH<sub>3</sub>), 1.42 – 1.27 (9H, m, =CCH<sub>3</sub> chain and 2 x OCH<sub>2</sub>CH<sub>3</sub>) ppm; <sup>13</sup>C NMR (75 MHz, CDCl<sub>3</sub>) δ<sub>C</sub> 201.83 (O=CCH<sub>3</sub>), 186.21 (O=CCH<sub>3</sub>), 174.65 (OC=O), 168.61 (OC=O), 140.95 (=CCH<sub>3</sub>), 132.11 (=CCH<sub>3</sub>CH<sub>3</sub>), 124.04 (HC=C), 122.79 (HC=C(CH<sub>3</sub>)<sub>2</sub>), 62.68 (O=CCH), 61.53 (OCH<sub>2</sub>), 56.27 (O=C-CH), 52.89 (OCH<sub>2</sub>), 40.13 (=CCH<sub>3</sub>CH<sub>2</sub>), 39.02 (=CCH<sub>3</sub>), 29.01 (OCH<sub>2</sub>CH<sub>3</sub>), 27.05 (CH<sub>2</sub>C= chain), 25.96 (OCH<sub>2</sub>CH<sub>3</sub>), 18.00 (=CCH<sub>3</sub>), 16.85 (=CCH<sub>3</sub> chain), 14.58 (=CCH<sub>3</sub>CH<sub>3</sub> chain), 14.51 (=CCH<sub>3</sub>CH<sub>3</sub> chain) ppm; <sup>13</sup>C NMR<sub>DEPT</sub> confirmed the above assignments.

#### 5-((*E*)-4,8-Dimethylnona-3,7-dienyl)-3-

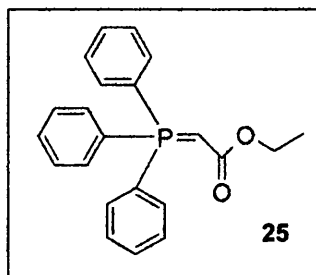
methylocyclohex-2-enone (**24**). Based on a procedure by Knoevenagel.<sup>15</sup> To a stirred solution of 2,4-diacetyl-3-((*E*)-2,6-dimethylhepta-1,5-dienyl)-pentanedioic acid diethyl ester (**23**) (0.5 g, 1.27 mmol) in ethanol (0.46 mL) at -5 °C was added a solution of 4M potassium



hydroxide (0.31 g) in ethanol (1.38 mL). The mixture was then heated at vigorous reflux (85 °C) for 4 h. The progress of the reaction was monitored by thin-layer chromatographic analysis (developed by KMnO<sub>4</sub> charring). After cooling to 25 °C, the mixture was acidified with 10 % dilute hydrochloric acid until just acidic (pH 5-6). The solution was then concentrated until complete removal of ethanol. The resulting solution was transferred to a separating funnel, and after allowing the temperature to reach 25 °C, was extracted with diethyl ether (3 x 7 mL). The combined organic layers were dried over anhydrous sodium sulfate. The solution was filtered through a fluted filter paper and the filtrate evaporated. The oil was purified by fractional distillation [197-199 °C/15 mmHg] to give **24** (0.20 g, 68%) as a clear, colourless oil: bp 197-199 °C, lit<sup>15</sup> bp 197 – 198 °C; R<sub>F</sub> [ethyl acetate-light petroleum ether, 1-4, (v,v)] 0.34; IR ν<sub>max</sub> (film) 1670 (C=O ketone) cm<sup>-1</sup>; <sup>1</sup>H NMR (300 MHz, CDCl<sub>3</sub>) δ<sub>H</sub> 5.92 (1H, s, HC=C ring), 5.03 (2H, d, *J* 10.2 Hz, 2 x HC=C chain), 3.20 (1H, m, O=CCH<sub>2</sub>CH ring), 2.24 – 2.07 (4H, m, 2 x CH<sub>2</sub> chain), 1.97 – 1.83 (4H, m, 2 x CH<sub>2</sub> ring), 1.63 (3H, m, =CH<sub>3</sub> ring), 1.56 (3H, m, =CH<sub>3</sub>CH<sub>3</sub> chain), 1.50 (3H, m, =CH<sub>3</sub>CH<sub>3</sub> chain), 1.26 (3H, m, =CH<sub>3</sub> chain) ppm; <sup>13</sup>C NMR (75 MHz, CDCl<sub>3</sub>) δ<sub>C</sub> 199.47 (C=O), 138.85 (=CCH<sub>3</sub> ring), 138.70 (=CCH<sub>3</sub> chain), 131.96 (=CCH<sub>3</sub>CH<sub>3</sub> chain), 128.60 (HC=C ring), 124.11 (HC=C chain), 116.89 (HC=CH<sub>3</sub>CH<sub>3</sub> chain),

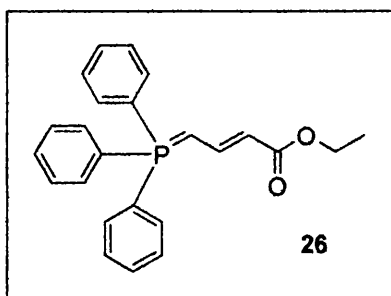
53.87 (O=CCH<sub>2</sub>CH ring), 39.87 (CH<sub>2</sub> ring), 37.78 (CH<sub>2</sub> ring), 23.57 (CH<sub>2</sub> chain), 22.90 (CH<sub>2</sub> chain), 20.52 (=CH<sub>3</sub> ring), 18.00 (=CH<sub>3</sub> chain), 14.62 (=CCH<sub>3</sub>CH<sub>3</sub> chain), 14.51 (=CCH<sub>3</sub>CH<sub>3</sub> chain) ppm; <sup>13</sup>C NMR<sub>DEPT</sub> confirmed the above assignments.

**(Triphenyl- $\gamma^5$ -phosphanylidene)-acetic acid ethyl ester (25).** Based on a procedure by Cappon.<sup>16</sup> To a stirred solution of (triphenyl- $\gamma^5$ -phosphanylidene)-acetic acid ethyl ester bromine salt (5.2 g, 0.012 mol) in water (70 mL) at 0 °C was added a solution of aqueous 2M sodium hydroxide (10 mL,) dropwise, by



means of a stainless steel needle until a pH of 10 or above was reached. The solution was transferred to a separating funnel and extracted with dichloromethane (3 x 25 mL). The combined organic layers were dried over anhydrous sodium sulfate. The solution was filtered through a fluted filter paper and the filtrate was evaporated to give **25** (2.78 g, 67%) as white platelets: mp 167 – 168 °C, lit<sup>16</sup> 126 – 127 °C; IR  $\nu_{\text{max}}$  (film) 3070 (aromatic C-H stretch), 1750 (C=O ester) cm<sup>-1</sup>; <sup>1</sup>H NMR (250 MHz, CDCl<sub>3</sub>)  $\delta_{\text{H}}$  7.71 – 7.39 (15H, m, 3 x 5 Ar-H), 3.97 (2H, bs, OCH<sub>2</sub>), 2.94 (1H, s, P=CH), 1.14 (3H, bs, OCH<sub>2</sub>CH<sub>3</sub>) ppm.

**(E)-4-(Triphenyl- $\gamma^5$ -phosphanylidene)-but-2-enoic acid ethyl ester (26).** Based on a procedure by Bredenkamp.<sup>17</sup> To a stirred solution of (triphenyl- $\gamma^5$ -phosphanylidene)-acetic acid ethyl ester (**25**) (2.0 g, 4.40 mmol) in water (80 mL) at 0 °C was added a solution of aqueous 2M sodium hydroxide (9.0 mL)



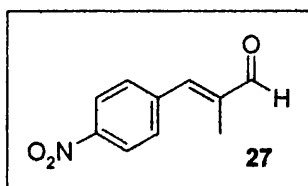
dropwise, by means of a stainless steel needle. The mixture was allowed to warm slowly to 25 °C and stirring was continued at 25 °C for 16 h. The progress of the reaction was monitored by thin-layer chromatographic analysis (developed by KMnO<sub>4</sub> charring). The resulting precipitate was filtered through a fluted filter paper. The solid was adsorbed onto silica gel and was purified by flash column



chromatography on silica gel with [ethyl acetate-light petroleum ether, 1-4, (v,v); thin-layer chromatography was developed by KMnO<sub>4</sub> charring]. The eluent was evaporated to give **26** (1.37 g, 83%) as crystalline yellow platelets: mp 185-186 °C, lit<sup>17</sup> mp 186 – 188 °C; R<sub>F</sub> [ethyl acetate-light petroleum ether, 1-5, (v,v)] 0.43; IR  $\nu_{\max}$  (film) 3060 (aromatic C-H stretch), 1740 (C=O ester), 1625 (C=C conjugation) cm<sup>-1</sup>; <sup>1</sup>H NMR (300 MHz, CDCl<sub>3</sub>)  $\delta_{\text{H}}$  7.93 – 7.73 (15H, m, 3 x 5 Ar-H), 7.32 (1H, s, =CHCH=C), 6.74 (1H, m, P=CH), 5.36 (1H, m, =CH-CO), 4.12 (2H, q, *J* 8.5 Hz, OCH<sub>2</sub>), 1.21 (3H, t, *J* 8.5 Hz, OCH<sub>2</sub>CH<sub>3</sub>) ppm; <sup>13</sup>C NMR (75 MHz, CDCl<sub>3</sub>)  $\delta_{\text{C}}$  165.51 (C=O), 135.67 (C=C arom), 132.78 (C=C arom), 131.30 (C=C arom), 130.98 (C=C arom), 128.72 (P=C), 118.47 (P=CC=), 117.32 (=CC=O), 61.19 (OCH<sub>2</sub>), 14.50 (OCH<sub>2</sub>CH<sub>3</sub>) ppm.

**(*E*)-2-Methyl-3-(4-nitrophenyl)-propenal (27).**

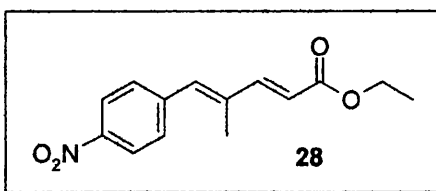
Based on a procedure by Boyle.<sup>18</sup> To a stirred solution of 4-nitrobenzaldehyde (5.5 g, 0.036 mol) in 220 mL of 50 % aqueous ethanol and



propionaldehyde (2.7 mL, 0.037 mol) at 25 °C was added a solution of aqueous sodium hydroxide (0.40 g, 0.010 mol) in water (10 mL), dropwise by means of a stainless steel needle. Stirring was continued at 25 °C for 30 min. The progress of the reaction was monitored by thin-layer chromatographic analysis (developed by KMnO<sub>4</sub> charring). The precipitate formed was filtered through a fluted filter paper, and the solid was purified by recrystallisation from ethanol to give **27** (6.01 g, 87%) as pale yellow platelets: mp 112-114 °C, lit<sup>18</sup> mp 110-112 °C; R<sub>F</sub> [ethyl acetate-light petroleum ether, 1-4, (v,v)] 0.26; IR  $\nu_{\max}$  (film) 3040 (aromatic C-H stretch), 1750 (C=O aldehyde) cm<sup>-1</sup>; <sup>1</sup>H NMR (300 MHz, CDCl<sub>3</sub>)  $\delta_{\text{H}}$  9.62 (1H, s, CHO), 8.23 (2H, d, *J* 8.5 Hz, 2 x Ar-H), 7.61 (2H, d, *J* 8.5 Hz, 2 x Ar-H), 7.26 (1H, s, HC=C), 2.07 (3H, s, =CCH<sub>3</sub>) ppm; <sup>13</sup>C NMR (75 MHz, CDCl<sub>3</sub>)  $\delta_{\text{C}}$  195.19 (C=O), 148.12 (Ar-H), 146.53 (Ar-NO<sub>2</sub>), 145.81 (*Ar*-C=), 141.69 (HC=CCH<sub>3</sub>), 130.85 (Ar-H), 124.28 (HC=C), 11.48 (=CCH<sub>3</sub>) ppm.

**(2*E*,4*E*)-4-Methyl-5-(4-nitrophenyl)-penta-2,4-dienoic acid ethyl ester (28).**

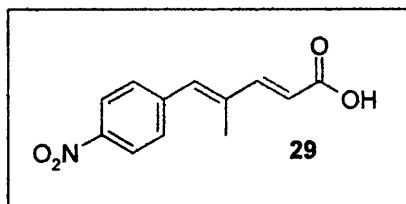
To a stirred solution of (*E*)-2-methyl-3-(4-nitrophenyl)-propenal (27) (1.00 g, 5.24



mmol) in toluene (6.0 mL) was added (triphenyl- $\gamma^5$ -phosphanylidene)-acetic acid ethyl ester (25) (2.76 g, 7.93 mmol) at 25 °C. The mixture was heated to 40 °C and stirring was continued at 40 °C for 4 h. The progress of the reaction was monitored by thin-layer chromatographic analysis (developed by KMnO<sub>4</sub> charring). The mixture was evaporated to one-third its original volume and the solid was purified by flash column chromatography on silica gel eluting with [ethyl acetate-light petroleum ether, 1-3, (v,v); developed by KMnO<sub>4</sub> charring]. The eluent was evaporated to give **28** (1.26 g, 92%) as crystalline yellow platelets: mp 124-125 °C; *R*<sub>F</sub> [ethyl acetate-light petroleum ether, 1-4, (v,v)] 0.56; IR  $\nu_{\max}$  (film) 1712 (C=O ester), 1625 (C=C conjugated), 1519 (NO<sub>2</sub>) cm<sup>-1</sup>; <sup>1</sup>H NMR (300 MHz, CDCl<sub>3</sub>)  $\delta_{\text{H}}$  8.18 (2H, d, *J* 8.0 Hz, *ortho* to NO<sub>2</sub>), 7.47 (2H, d, *J* 8.0 Hz, *meta* to NO<sub>2</sub>), 7.41 (1H, d, *J* 15 Hz, CH=CHCO<sub>2</sub>Et), 7.39 (1H, s, Ar-CH=C), 6.79 (1H, s, =CHC=O), 6.03 (1H, d, *J* 15 Hz, =CCH=C), 4.14 (2H, q, *J* 7.8 Hz, OCH<sub>2</sub>), 2.00 (3H, s, =CCH<sub>3</sub>), 1.23 (3H, t, *J* 7.8 Hz, OCH<sub>2</sub>CH<sub>3</sub>) ppm; <sup>13</sup>C NMR (75 MHz, CDCl<sub>3</sub>)  $\delta_{\text{C}}$  167.23 (C=O), 148.69 (Ar-H), 147.18 (Ar-NO<sub>2</sub>), 143.64 (*Ar*-C=), 137.85 (=CCH<sub>3</sub>), 136.08 (Ar-H), 130.40 (HC=CCCH<sub>3</sub>), 124.00 (=CHC=O), 120.18 (HC=CH), 60.94 (OCH<sub>2</sub>), 14.67 (OCH<sub>2</sub>CH<sub>3</sub>), 14.30 (=CCH<sub>3</sub>) ppm; <sup>13</sup>C NMR<sub>DEPT</sub> showed the assignments above to be correct; Anal. calcd. for C<sub>14</sub>H<sub>15</sub>NO<sub>4</sub> = C, 64.37, H, 5.79, N, 5.36. Found C, 64.33, H, 5.76, N, 5.39 %.

**(2*E*,4*E*)-4-Methyl-5-(4-nitrophenyl)-penta-**

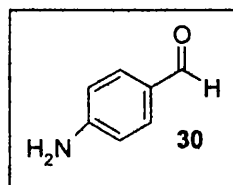
**2,4-dienoic acid (29).** To a stirred solution of (2*E*,4*E*)-4-methyl-5-(4-nitrophenyl)-penta-2,4-dienoic acid ethyl ester (**28**) (0.30 g, 1.15 mmol)



in tetrahydrofuran (5.0 mL) and water (5.0 mL) was added lithium hydroxide (0.14 g, 5.83 mmol). The mixture was heated to 80 °C and stirring continued at 80 °C for 5 h. The progress of the reaction was monitored by thin-layer chromatographic analysis (developed by KMnO<sub>4</sub> charring). The mixture was transferred to a separating funnel.

The aqueous layer was washed with diethyl ether (3 x 10 mL). The aqueous layer was then acidified with 10 % hydrochloric acid to pH 2, and the acidified solution was transferred to a separating funnel. The aqueous layer was then extracted with diethyl ether (3 x 10 mL). The combined organic layers were dried over anhydrous magnesium sulfate. The solution was filtered through a fluted filter paper and the filtrate evaporated to give **29** (0.24 g, 90%) as pale yellow needles: mp 141–143 °C,  $R_F$  [methanol-chloroform, 1-19, (v,v)] 0.16; IR  $\nu_{\max}$  (film) 3030 (OH acid), 1700 (C=O acid), 1620 (C=C conjugated), 1340 (NO<sub>2</sub>) cm<sup>-1</sup>; <sup>1</sup>H NMR (250 MHz, CDCl<sub>3</sub>)  $\delta_H$  8.29 (2H, d,  $J$  9.0 Hz, *ortho* to NO<sub>2</sub>), 7.50 (2H, d,  $J$  9.0 Hz, *meta* to NO<sub>2</sub>), 7.48 (1H, d,  $J$  15 Hz, CH=CHCO<sub>2</sub>H), 6.86 (1H, s, Ar-CH=), 6.08 (1H, d,  $J$  15 Hz, =CHCO), 2.14 (3H, s, =CCH<sub>3</sub>) ppm; <sup>13</sup>C NMR (62 MHz, CDCl<sub>3</sub>)  $\delta_c$  193.53 (C=O), 155.95 (Ar-H), 147.11 (Ar-NO<sub>2</sub>), 142.76 (Ar-C=), 137.69 (=CCH<sub>3</sub>), 137.41 (Ar-H), 130.21 (HC=CCH<sub>3</sub>), 129.91 (HC=CCO), 123.78 (=CHCO), 14.14 (=CCH<sub>3</sub>) ppm; <sup>13</sup>C NMR<sub>DEPT</sub> confirmed the above assignments; Anal. calcd. for C<sub>12</sub>H<sub>11</sub>NO<sub>4</sub> = C, 61.79, H, 4.75, N, 6.00. Found C, 61.81, H, 4.72, N, 6.06 %.

**4-Aminobenzaldehyde (30).** To a stirred solution of 4-nitrobenzaldehyde (1.00 g, 6.62 mmol) in ethanol (20 mL) at 65 °C was added a hot solution of iron(II) sulfate heptahydrate (10.80 g, 0.039 mol) in water (25 mL) and

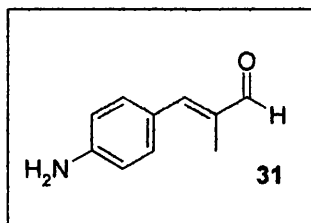


concentrated ammonia (15 mL). The mixture was heated at 80 °C and continued stirring at 80 °C for 15 min. The progress of the reaction was monitored by thin-layer chromatographic analysis (developed by KMnO<sub>4</sub> charring). The mixture was transferred to a separating funnel and extracted with dichloromethane (3 x 15 mL). The combined organic layers were dried over anhydrous calcium chloride, and filtered through a fluted filter paper and evaporated. The solid was purified by recrystallisation from ethanol to give **30** (0.69 g, 86%) as orange coloured platelets: mp 99–101 °C, lit<sup>19</sup> mp 98–100 °C;  $R_F$  [ethyl acetate-light petroleum ether, 1-5, (v,v)] 0.38; IR  $\nu_{\max}$  (film) 3340 (aromatic NH<sub>2</sub> stretch), 1711 (C=O aldehyde) cm<sup>-1</sup>; <sup>1</sup>H NMR (250 MHz, CDCl<sub>3</sub>)  $\delta_H$  9.65 (1H, s, CHO), 7.62 (2H, d,  $J$  8.5 Hz, *meta* to NH<sub>2</sub>), 6.60 (2H, d,  $J$  8.5 Hz, *ortho* to NH<sub>2</sub>), 2.98 (2H, s, NH<sub>2</sub>) ppm; <sup>13</sup>C NMR (62 MHz,

$\text{CDCl}_3$ )  $\delta_{\text{C}}$  190.18 (C=O), 154.40 ( $\text{H}_2\text{N-Ar}$ ), 131.93 ( $\text{Ar-CHO}$ ), 125.11 (Ar-H), 111.03 (Ar-H) ppm.

**(*E*)-3-(4-Aminophenyl)-2-methylpropenal (31).**

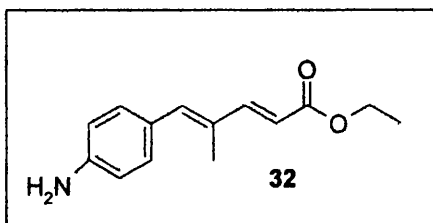
Based on the procedure utilized by Hirata.<sup>20</sup> To a stirred solution of (*E*)-2-methyl-3-(4-nitrophenyl)-propenal (27) (0.89 g, 4.66 mmol) in ethanol (20 mL) at 65 °C was added a hot solution of iron(II) sulfate



heptahydrate (7.92 g, 0.027 mol) in water (25 mL) and concentrated ammonia (15 mL). The mixture was heated at 80 °C and continued stirring at 80 °C for 15 min. The progress of the reaction was monitored by thin-layer chromatographic analysis (developed by  $\text{KMnO}_4$  charring). The mixture was transferred to a separating funnel and extracted with dichloromethane (3 x 15 mL). The combined organic layers were dried over anhydrous calcium chloride, and filtered through a fluted filter paper and evaporated. The solid was purified by recrystallisation from ethanol to give 31 (0.65 g, 87%) as deep orange coloured platelets: mp 178-180 °C, lit<sup>20</sup> mp 178-180 °C;  $R_{\text{F}}$  [ethyl acetate-light petroleum ether, 1-5, (v,v)] 0.38; IR  $\nu_{\text{max}}$  (film) 3300 (aromatic  $\text{NH}_2$  stretch), 1700 (C=O aldehyde)  $\text{cm}^{-1}$ ;  $^1\text{H}$  NMR (300 MHz,  $\text{CDCl}_3$ )  $\delta_{\text{H}}$  9.42 (1H, s, CHO), 7.34 (2H, d,  $J$  8.5 Hz, *meta* to  $\text{NH}_2$ ), 7.03 (1H, s,  $\text{HC}=\text{C}$ ), 6.69 (2H, d,  $J$  8.5 Hz, *ortho* to  $\text{NH}_2$ ), 3.99 (2H, bs,  $\text{NH}_2$ ), 2.07 (3H, s,  $=\text{CCH}_3$ ) ppm;  $^{13}\text{C}$  NMR (62 MHz,  $\text{CDCl}_3$ )  $\delta_{\text{C}}$  196.07 (C=O), 151.22 (Ar-H), 148.59 ( $\text{H}_2\text{N-Ar}$ ), 134.95 ( $\text{Ar-C}=\text{C}$ ), 132.81 ( $=\text{CCH}_3$ ), 125.97 (Ar-H), 115.08 ( $\text{HC}=\text{CCH}_3$ ), 11.41 ( $=\text{CCH}_3$ ) ppm.

**(2*E*,4*E*)-5-(4-Aminophenyl)-4-methylpenta-2,4-dienoic acid ethyl ester (32).**

To a stirred solution of iron(II) sulfate heptahydrate (18.3 g, 0.066 mol) in water (140 mL) and concentrated ammonia (70

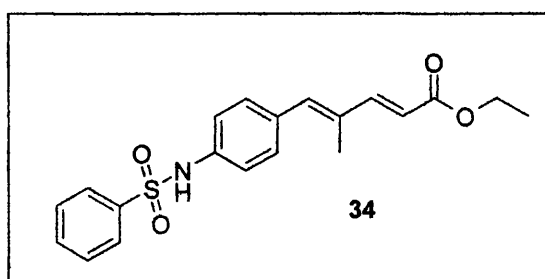


mL) at 60 °C was added a solution of (2*E*,4*E*)-4-methyl-5-(4-nitrophenyl)-penta-2,4-dienoic ethyl ester (28) (3.00 g, 0.011 mol) in ethanol (100 mL) by means of a stainless steel needle. The mixture was warmed to 80 °C and stirring was continued at

80 °C for 10 min. The progress of the reaction was monitored by thin-layer chromatographic analysis (developed by  $\text{KMnO}_4$  charring). After allowing the mixture to cool, it was then transferred to a separating funnel. The mixture was extracted with diethyl ether (4 x 15 mL). The combined organic layers were dried over anhydrous sodium sulfate, then the solution was filtered through a fluted filter paper, and the filtrate evaporated. The oil was purified by flash column chromatography on silica gel [ethyl acetate-light petroleum ether, 1-4, (v,v); developed by  $\text{KMnO}_4$  charring], and the eluent was evaporated to give **32** (2.15 g, 85%) as a clear yellow oil:  $R_F$  [ethyl acetate-light petroleum ether, 1-5, (v,v)] 0.34; IR  $\nu_{\text{max}}$  (film) 1720 (C=O ester), 1530 (C=C conjugated)  $\text{cm}^{-1}$ ;  $^1\text{H}$  NMR (250 MHz,  $\text{CDCl}_3$ )  $\delta_{\text{H}}$  7.50 (1H, d,  $J$  15 Hz,  $\text{CH}=\text{CHCO}_2\text{Et}$ ), 7.19 (2H, d,  $J$  9.0 Hz, *meta* to  $\text{NH}_2$ ), 6.73 (1H, s,  $\text{CCH}_3\text{-CH=}$ ), 6.65 (2H, d,  $J$  9.0 Hz, *ortho* to  $\text{NH}_2$ ), 5.90 (1H, d,  $J$  15 Hz,  $=\text{CHCO}_2\text{Et}$ ), 4.24 (2H, q,  $J$  7.0 Hz,  $\text{OCH}_2$ ), 3.87 (2H, bs,  $\text{NH}_2$ ), 2.02 (3H, s,  $\text{CH}_3$ ), 1.36 (3H, t,  $J$  7.0 Hz,  $\text{OCH}_2\text{CH}_3$ ) ppm;  $^{13}\text{C}$  NMR (62 MHz,  $\text{CDCl}_3$ )  $\delta_{\text{C}}$  168.04 (C=O), 151.16 (Ar-H), 147.03 ( $\text{H}_2\text{N-Ar}$ ), 143.57 ( $\text{Ar-C=}$ ), 137.79 ( $=\text{CCH}_3$ ), 136.19 (Ar-H), 131.58 (Ar-CH=), 123.91 ( $=\text{CHCO}$ ), 115.02 ( $\text{CH}=\text{CHCO}$ ), 60.51 ( $\text{OCH}_2$ ), 14.66 ( $\text{OCH}_2\text{CH}_3$ ), 14.18 ( $=\text{CCH}_3$ ) ppm;  $^{13}\text{C}$  NMR<sub>DEPT</sub> confirmed the above assignments; Anal. calcd. for  $\text{C}_{14}\text{H}_{17}\text{NO}_2$  = C, 72.70, H, 7.40, N, 6.05. Found C, 72.65, H, 7.45, N, 6.00 %.

**(2E,4E)-5-(4-**

**Benzenesulfonylaminophenyl)-4-methylpenta-2,4-dienoic acid ethyl ester (34).** To a stirred solution of (2E,4E)-5-(4-aminophenyl)-4-methylpenta-2,4-



dienoic acid ethyl ester (**32**) (0.35 g, 1.52 mmol) in pyridine (8.0 mL) at 25 °C was added benzenesulfonyl chloride (0.39 mL, 3.04 mmol) by means of a stainless steel needle. The mixture was warmed to 90 °C and stirring was continued at 90 °C for 2 h. The progress of the reaction was monitored by thin-layer chromatographic analysis (developed by  $\text{KMnO}_4$  charring). The reaction was quenched by the addition of crushed ice (2.5 mL). The resulting suspension was filtered through a sintered-glass

funnel, and the precipitate was purified by recrystallisation from ethanol to give **34** (0.41 g, 73%) as dark yellow platelets: mp 134-136 °C;  $R_F$  [ethyl acetate-light petroleum ether, 1-3, (v,v)] 0.37; IR  $\nu_{\max}$  (film) 3070 (C-H aromatic stretch), 1724 (C=O ester), 1170 (sulfonamide)  $\text{cm}^{-1}$ ;  $^1\text{H}$  NMR (300 MHz,  $\text{CDCl}_3$ )  $\delta_H$  8.19 (2H, d,  $J$  8.5 Hz, *meta* to NHAr), 7.82 (1H, d,  $J$  15 Hz,  $\text{CH}=\text{CHCO}_2\text{Et}$ ), 7.77 (2H, d,  $J$  10.2 Hz, *ortho* to NHAr), 7.56 (3H, m, 3 x Ar-H), 7.21 (2H, m, aryl), 7.04 (1H, s,  $=\text{CHCO}$ ), 6.25 (1H, s, Ar-CH=), 4.45 (2H, q,  $J$  15 Hz,  $\text{OCH}_2$ ), 2.23 (3H, s,  $=\text{CCH}_3$ ), 1.91 (1H, bs, NH), 1.56 (3H, t,  $J$  15 Hz,  $\text{OCH}_2\text{CH}_3$ ) ppm;  $^{13}\text{C}$  NMR (62 MHz,  $\text{CDCl}_3$ )  $\delta_C$  169.41 (C=O), 149.41 (*meta* to NH), 146.74 (HN-Ar), 142.14 (Ar-C=), 139.88 ( $=\text{CCH}_3$ ), 137.30 (*ortho* to NH), 136.15 (Ar-S), 134.39 (Ar-H), 131.84 (Ar-H), 130.55 (Ar-H), 129.41 (Ar-CH=), 128.97 ( $=\text{CHCO}$ ), 119.07 ( $\text{CH}=\text{CHCO}$ ), 60.82 ( $\text{OCH}_2$ ), 14.70 ( $\text{OCH}_2\text{CH}_3$ ), 14.21 ( $=\text{CCH}_3$ ) ppm;  $^{13}\text{C}$  NMR<sub>DEPT</sub> confirmed the above assignments; Anal. calcd. for  $\text{C}_{20}\text{H}_{21}\text{NO}_4\text{S}$  = C, 64.66, H, 5.69, N, 3.77. Found C, 64.62, H, 5.72, N, 3.70%

#### (2*E*,4*E*)-5-(4-

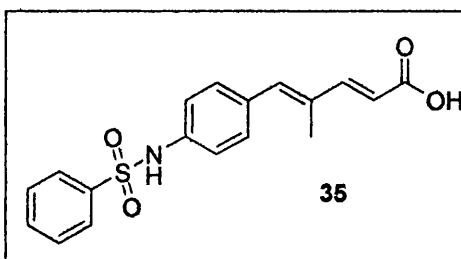
#### Benzenesulfonylaminophenyl)-4-

#### methylpenta-2,4-dienoic acid (**35**). To a

stirred solution of (2*E*,4*E*)-5-

#### (4benzenesulfonylaminophenyl)-4-

#### methylpenta-2,4-dienoic acid ethyl ester (**34**)

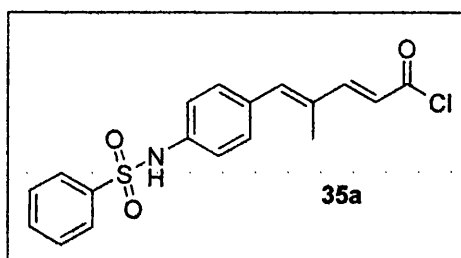


(0.40 g, 1.08 mmol) in tetrahydrofuran (5.0 mL) and water (5.0 mL) was added lithium hydroxide (0.15 g, 6.25 mmol). The mixture was heated at 80 °C and stirring continued at 80 °C for 5 h. The progress of the reaction was monitored by thin-layer chromatographic analysis (developed by  $\text{KMnO}_4$  charring). The mixture was transferred to a separating funnel. The aqueous layer was washed with diethyl ether (3 x 10 mL). The aqueous layer was then acidified with 10 % hydrochloric acid (2.4 mL) to pH 2, and the acidified solution was transferred to a separating funnel. The aqueous layer was then extracted with diethyl ether (3 x 10 mL). The combined organic layers were dried over anhydrous magnesium sulfate. The solution was filtered through a fluted filter paper and the filtrate evaporated to give **35** (0.31 g, 84%) as bright orange platelets: mp 162-163 °C;  $R_F$  [methanol-chloroform, 1-49, (v,v)] 0.19; IR  $\nu_{\max}$  (film) 3040 (C-H aromatic stretch), 1705 (C=O acid), 1150 (sulfonamide)  $\text{cm}^{-1}$ ;  $^1\text{H}$  NMR

(250 MHz,  $\text{CDCl}_3$ )  $\delta_{\text{H}}$  7.94 (2H, m, *ortho* to  $\text{SO}_2\text{NHAr}$ ), 7.79 (2H, m, 2 x *Ar-H*), 7.72 (1H, d,  $J$  15 Hz,  $\text{CH}=\text{CHCO}$ ), 7.49 (3H, m, aryl), 7.19 (2H, m, *ortho* to  $\text{NHAr}$ ), 6.78 (1H, d,  $J$  15 Hz,  $=\text{CHCO}$ ), 6.02 (1H, s, *Ar-CH*), 2.01 (3H, s,  $=\text{CCH}_3$ ), 1.34 (1H, s, NH) ppm;  $^{13}\text{C}$  NMR (62 MHz,  $\text{CDCl}_3$ )  $\delta_{\text{C}}$  178.28 ( $\text{C}=\text{O}$ ), 152.41 ( $\text{HN-Ar-H}$ ), 150.78 ( $\text{NH-Ar}$ ), 145.02 ( $\text{Ar-C}=\text{C}$ ), 143.99 ( $=\text{CCH}_3$ ), 143.90 ( $\text{HN-Ar-H}$ ), 137.47 ( $\text{Ar-S}$ ), 136.14 ( $\text{Ar-H}$ ), 132.48 ( $\text{Ar-H}$ ), 131.47 ( $\text{Ar-H}$ ), 128.11 ( $\text{Ar-CH}=\text{C}$ ), 124.02 ( $=\text{CHCO}$ ), 122.74 ( $\text{HC}=\text{CHCO}$ ), 12.47 ( $\text{CH}_3$ ) ppm; Anal. Calcd. for  $\text{C}_{18}\text{H}_{17}\text{NO}_4\text{S}$  = C, 62.95, H, 4.98, N, 4.07. Found C, 62.99, H, 4.96, N, 4.01 %.

**(2*E*,4*E*)-5-(4-Benzenesulfonylamino-phenyl)-4-methylpenta-2,4-dienoyl chloride (35a).**

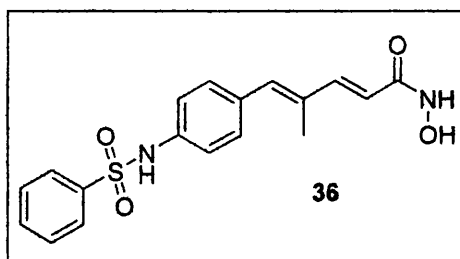
To a stirred solution of (2*E*,4*E*)-5-(4-benzenesulfonylamino-phenyl)-4-methylpenta-2,4-dienoic acid (**35**) (0.45 g,



1.31 mmol) in anhydrous dichloromethane (6.0 mL) at 0 °C under an atmosphere of nitrogen was added thionyl chloride (0.26 mL, 3.53 mmol) dropwise by means of a stainless steel needle. The mixture was allowed to warm slowly to 20 °C and continued stirring at 20 °C under an atmosphere of nitrogen for 16 h. The progress of the reaction was monitored by aliquots taken from the mixture by means of a stainless steel needle and an IR conducted. The mixture was evaporated to give **35a** (0.45 g, quantitative yield) as a colourless oil and used immediately *in situ* for the next reaction; IR  $\nu_{\text{max}}$  (film) 1740 ( $\text{C}=\text{O}$ ), 1376 (O-S-O stretching) 762 ( $\text{C-Cl}$ )  $\text{cm}^{-1}$ .

**(2*E*,4*E*)-5-(4-Benzenesulfonylamino-phenyl)-4-methylpenta-2,4-dienoic acid hydroxamide (36).**

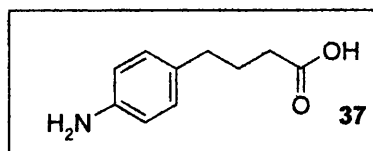
To a stirred solution of hydroxylamine hydrochloride (0.56 g, 8.06



mmol) in methanol (4.0 mL) at 40 °C was added a solution of potassium hydroxide (0.45 g, 8.06 mmol) in methanol (4.0 mL). The solution was cooled to 0 °C and the suspension filtered through a sintered glass funnel. To the filtrate with stirring was

added (2*E*,4*E*)-5-(4-benzenesulfonylamino-phenyl)-4-methylpenta-2,4-dienoic acid ethyl ester (**34**) (0.30 g, 0.81 mmol) at 25 °C. Stirring was continued at 25 °C whilst potassium hydroxide (0.20 g, 3.57 mmol) was added portionwise over 30 min. The solution was stirred at 25 °C for 4 h. The progress of the reaction was monitored by thin-layer chromatographic analysis (thin-layer chromatography was developed by ferric sulfate charring). The reaction was quenched by the addition of water (4.0 mL) and the solution made slightly acidic by 0.5 M hydrochloric acid and the solution then transferred to a separating funnel. The solution was washed with ethyl acetate (2 x 5 mL). The aqueous layer was basified with potassium hydroxide (0.11 g, 1.96 mmol) and the solution transferred to a separating funnel and the solution extracted with ethyl acetate (2 x 5 mL). The combined organic layers were dried over anhydrous magnesium sulfate and filtered through a fluted filter paper. The filtrate was evaporated to give a solid. This was purified by recrystallisation with benzene to give **36** (0.20 g, 61%) as bright orange crystals: mp 137-139 °C; IR  $\nu_{\max}$  (film) 3010 (C-H aromatic stretch), 1689 (C=O acid), 1123 (sulfonamide)  $\text{cm}^{-1}$ ;  $^1\text{H}$  NMR (250 MHz,  $\text{DMSO}_6$ )  $\delta_{\text{H}}$  10.60 (1H, bs, NH), 10.02 (1H, bs, NHOH), 7.82 (2H, d,  $J$  7.5 Hz, *ortho* to  $\text{SO}_2$ ), 7.70 – 7.50 (3H, m, *meta* to  $\text{SO}_2$  and *para* to  $\text{SO}_2$ ), 7.30 (2H, d,  $J$  7.5 Hz, *meta* to NHAr), 7.22 (1H, d,  $J$  16 Hz,  $\text{CH}=\text{CHCO}$ ), 7.14 (2H, d,  $J$  7.5 Hz, *ortho* to NHAr), 6.76 (1H, s, Ar-CH=), 5.94 (1H, d,  $J$  16 Hz,  $\text{CH}=\text{CHCO}$ ), 1.96 (3H, s,  $=\text{CCH}_3$ ) ppm;  $^{13}\text{C}$  NMR (62 MHz,  $\text{DMSO}_6$ )  $\delta_{\text{C}}$  164.38 (C=O), 143.86 (HN-Ar-H), 139.87 (NH-Ar), 137.16 (Ar-C=), 135.91 ( $=\text{CCH}_3$ ), 133.45 (HN-Ar-H), 133.13 (Ar-S), 132.56 (Ar-H), 130.46 (Ar-H), 129.46 (Ar-H), 126.69 (Ar-CH=), 119.72 ( $=\text{CHCO}$ ), 118.25 ( $\text{HC}=\text{CHCO}$ ), 13.95 ( $\text{CH}_3$ ) ppm; Anal. calcd. for  $\text{C}_{18}\text{H}_{18}\text{N}_2\text{O}_4\text{S}$  = C, 60.32; H, 5.06; N, 7.81; Found: C, 60.37; H, 5.10; N, 7.79 %.

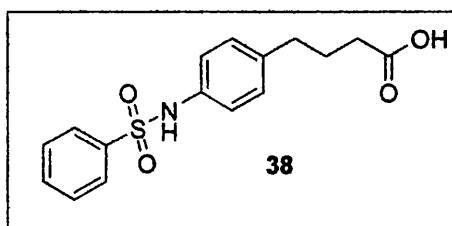
**4-(4-Aminophenyl)butyric acid (37).** Purchased from Aldrich Co. (95 % pure).





**5-(4-Benzenesulfonylamino-phenyl)-**

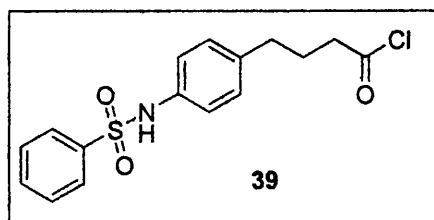
**pentanoic acid (38).** To a stirred solution of 4-(4-aminophenyl)butyric acid (37) (0.30 g, 1.68 mmol) in 2M aqueous sodium hydroxide (2.5 mL) at 25 °C was added



benzenesulfonyl chloride (0.42 mL, 3.28 mmol) dropwise, by means of a stainless steel needle, over 1 h. Stirring was continued at 25 °C for 3 h, with the periodic addition of 10 M aqueous sodium hydroxide (3.6 mL) to keep the pH above 10. The progress of the reaction was monitored by thin-layer chromatographic analysis (developed by KMnO<sub>4</sub> charring). The mixture was acidified with 1 M hydrochloric acid to pH 4.5 and the resulting precipitate was filtered through a fluted filter paper. The pale pink solid was washed with 1 M hydrochloric acid (3 x 15 mL) and water (3 x 15 mL) and dried under vacuum in the desiccator to give **38** (0.23 g, 43%) as pale white crystals: mp 134–135 °C; R<sub>F</sub> [methanol-chloroform, 1-49, (v,v)] 0.21; IR  $\nu_{\max}$  (film) 1725 (C=O acid), 1350 (O-S-O stretching) cm<sup>-1</sup>; <sup>1</sup>H NMR (250 MHz, DMSO<sub>6</sub>)  $\delta_{\text{H}}$  7.76 (2H, d, *J* 7.5 Hz, *ortho* to SO<sub>2</sub>), 7.55 (1H, t, *J* 7.5 Hz, SO<sub>2</sub>Ar), 7.44 (2H, t, *J* 7.5 Hz, *meta* to SO<sub>2</sub>Ar), 7.07 (2H, d, *J* 8.0 Hz, *meta* to NH), 6.97 (2H, d, *J* 8.0 Hz, *ortho* to NH), 2.60 (2H, t, *J* 7.5 Hz, Ar-CH<sub>2</sub>), 2.48 (1H, bs, NH), 2.33 (2H, t, *J* 7.5 Hz, CH<sub>2</sub>CO), 2.28 (1H, bs, OH), 1.92 (2H, pentet, *J* 7.5 Hz, CH<sub>2</sub>CH<sub>2</sub>CH<sub>2</sub>) ppm; <sup>13</sup>C NMR (62 MHz, DMSO<sub>6</sub>)  $\delta_{\text{C}}$  174.45 (C=O), 157.09 (*ortho* to SO<sub>2</sub>NHAr), 139.95 (SO<sub>2</sub>NH-Ar), 137.00 (Ar-CH<sub>2</sub>), 135.02 (*meta* to SO<sub>2</sub>NHAr), 133.00 (Ar-S), 129.42 (*ortho* to SO<sub>2</sub>Ar), 126.90 (*meta* to SO<sub>2</sub>Ar), 120.91 (*para* to SO<sub>2</sub>Ar), 33.91 (Ar-CH<sub>2</sub>), 33.31 (CH<sub>2</sub>CO), 26.42 (CH<sub>2</sub>-CH<sub>2</sub>-CH<sub>2</sub>) ppm; Anal. calcd. for C<sub>16</sub>H<sub>17</sub>NO<sub>4</sub> = C, 60.17, H, 5.36, N, 4.38. Found C, 60.13, H, 5.33, N, 4.39 %.

**5-(4-Benzenesulfonylamino-phenyl)-**

**pentanoyl chloride (39).** To a stirred solution of 5-(4-benzenesulfonylamino-phenyl)-pentanoic acid (**38**) (0.40 g, 1.25 mmol) in

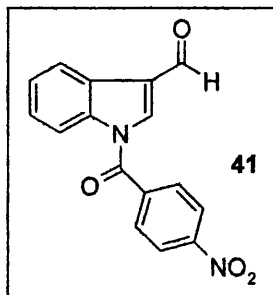


anhydrous dichloromethane (5.0 mL) at 0 °C under an atmosphere of nitrogen was added thionyl chloride (0.18 mL, 2.50 mmol) dropwise, by means of a stainless steel needle. The mixture was allowed to warm slowly to 20 °C and continued stirring at 20

°C under an atmosphere of nitrogen for 16 h. The progress of the reaction was monitored by aliquots taken from the mixture by means of a stainless steel needle and an IR conducted. The mixture was evaporated to give **39** (0.40 g, quantitative yield) as a colourless oil and used immediately *in situ* for the next reaction; IR  $\nu_{\max}$  (film) 1747 (C=O), 1325 (O-S-O stretching) 745 (C-Cl)  $\text{cm}^{-1}$ .

**1-[1-(4-Nitrophenyl)-methanoyl]-1*H*-indole-3-**

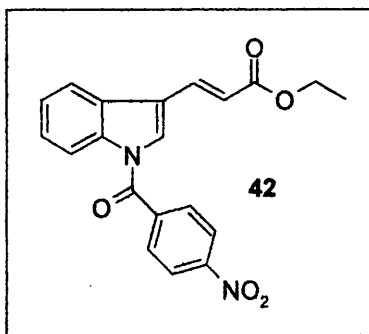
**carboxaldehyde (41).** Based on a procedure by El-Ezbawy.<sup>21</sup> A stirred solution of indole-3-carboxaldehyde (3.00 g, 0.021 mol), *p*-nitrobenzoyl chloride (5.58 g, 0.030 mol), sodium acetate (5.49 g, 0.067 mol) in acetic acid (83.2 mL) and pyridine (20.8 mL) at 25 °C was heated at reflux (90 °C) for 4 h. The progress of the reaction was monitored



by thin-layer chromatographic analysis (developed by  $\text{KMnO}_4$  charring). The solid was filtered with a fluted filter paper and washed with water (2 x 10 mL). The solid was recrystallised from ethanol to give **41** (2.21 g, 36%) as pale cream-coloured platelets: mp 169-170 °C, lit<sup>21</sup> mp 168-169 °C;  $R_f$  [ethyl acetate-light petroleum ether, 1-5, (v,v)] 0.34; IR  $\nu_{\max}$  (film) 3080 (C-H aromatic stretching), 1732 (C=O conjugated aldehyde), 1377 (C=C), 875 (Ar- $\text{NO}_2$  stretching)  $\text{cm}^{-1}$ ;  $^1\text{H}$  NMR (250 MHz,  $\text{CDCl}_3$ )  $\delta_{\text{H}}$  10.11 (1H, s, CHO), 8.63 (2H, m, *ortho* to  $\text{NO}_2$ ), 8.48 – 8.16 (4H, m, 4 x Aryl-H), 7.45 (3H, m, *meta* to  $\text{NO}_2$  and =CHN) ppm;  $^{13}\text{C}$  NMR (62 MHz,  $\text{CDCl}_3$ )  $\delta_{\text{C}}$  206.18 (C=O), 186.57 (CHO), 170.33 (Ar-C=), 166.19 (Ar-N), 151.36 (Ar- $\text{NO}_2$ ), 149.69 (Ar-CO), 138.72 ( $\text{O}_2\text{N-Ar-H}$ ), 131.58 (=CCHO), 126.90 ( $\text{O}_2\text{N-Ar-H}$ ), 125.61 (Ar-H), 124.25 (Ar-H), 122.26 (Ar-H), 117.02 (=CH-N) ppm;  $^{13}\text{C}$  NMR<sub>DEPT</sub> confirmed the above assignments.

**(*E*)-3-{[1-(4-Nitrophenyl)-methanoyl]-1*H*-**

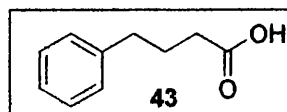
**indol-3-yl}-acrylic acid ethyl ester (42).** To a stirred suspension of sodium hydride (0.20 g, 8.33 mmol) in anhydrous ethylene glycol dimethyl ether (6.3 mL) at 25 °C under an atmosphere of nitrogen was added a solution of triethyl phosphonoacetate (0.81 g, 3.61 mmol)



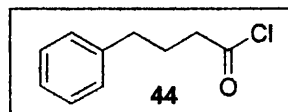
in

anhydrous ethylene glycol dimethyl ether dropwise, by means of a stainless steel needle. The mixture continued to be stirred at 25 °C under an atmosphere of nitrogen for 30 min. A solution of 1-[1-(4-nitrophenyl)-methanoyl]-1*H*-indole-3-carboxaldehyde (**41**) (1.00 g, 3.40 mmol) in anhydrous ethylene glycol dimethyl ether (4.3 mL) was added dropwise, by means of a stainless steel needle to the stirring mixture. The mixture was then heated at reflux (98 °C) and continued for 3 h. The progress of the reaction was monitored by thin-layer chromatographic analysis (developed by KMnO<sub>4</sub> charring). The mixture was quenched by pouring onto an ice-water mixture (35 mL) and transferred to a separating funnel. The layers were separated and the aqueous layer was extracted with dichloromethane (3 x 15 mL). The combined organic extracts were washed with 20 % aqueous potassium carbonate (4.2 mL) and dried over anhydrous sodium sulfate. The solution was filtered through a fluted filter paper and the filtrate evaporated. The oil was purified by flash column chromatography on silica gel [ethyl acetate-light petroleum ether, 2-5, (v,v); developed by KMnO<sub>4</sub> charring], and the eluent evaporated to give **42** (0.81 g, 65%) as pale orange platelets: mp 184-185 °C; R<sub>F</sub> [ethyl acetate-light petroleum ether, 1-4, (v,v)] 0.24; IR ν<sub>max</sub> (film) 3053 (C-H aromatic stretch), 1714 (C=O ester), 1635 (C=O), 1261 (C=C conjugated), 748 (Ar-NO<sub>2</sub> stretching) cm<sup>-1</sup>; <sup>1</sup>H NMR (250 MHz, DMSO<sub>6</sub>) δ<sub>H</sub> 8.75 (2H, m, *ortho* to NO<sub>2</sub>), 7.90 (3H, m, *meta* to NO<sub>2</sub> and =CHN), 7.42 (2H, m, 2 x Aryl-H), 7.39 (3H, m, 2 x Aryl-H and =CHCO), 6.50 (2H, d, *J* 13.6 Hz, CH=CHCO), 4.35 (2H, q, *J* 7.0 Hz, OCH<sub>2</sub>), 1.39 (3H, t, *J* 7.0 Hz, OCH<sub>2</sub>CH<sub>3</sub>) ppm; <sup>13</sup>C NMR (62 MHz, DMSO<sub>6</sub>) δ<sub>C</sub> 204.18 (C=O), 168.50 (C=O ester), 165.42 (*Ar*-C=), 163.78 (*Ar*-N), 144.49 (*Ar*-NO<sub>2</sub>), 138.36 (*Ar*-CO), 137.21 (*ortho* to NO<sub>2</sub>), 128.89 (=CCH=), 125.41 (*meta* to NO<sub>2</sub>), 123.41 (Ar-H), 121.57 (Ar-H), 120.54 (Ar-H), 113.68 (=CHCO), 113.52 (CH=CHCO), 111.88 (=CHN), 60.24 (OCH<sub>2</sub>), 14.51 (OCH<sub>2</sub>CH<sub>3</sub>) ppm; <sup>13</sup>C NMR<sub>DEPT</sub> confirmed the above assignments; Anal. calcd. for C<sub>20</sub>H<sub>16</sub>N<sub>2</sub>O<sub>5</sub> = C, 65.92, H, 4.42, N, 7.68. Found C, 65.95, H, 4.39, 7.67 %.

**4-Phenylbutyric acid (43).** Purchased from Aldrich Co. (99 % pure).

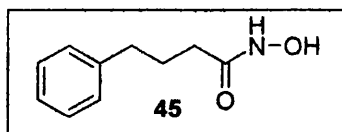


**4-Phenylbutyryl chloride (44).** Based on a procedure by Brumer.<sup>22</sup> To a stirred solution of 4-phenylbutyric acid (43) (1.50 g, 9.15 mmol) in anhydrous



dichloromethane (7.0 mL) at 0 °C under an atmosphere of nitrogen was added thionyl chloride (1.66 mL, 0.02 mol), dropwise, by means of a stainless steel needle. The mixture was allowed to warm slowly to 20 °C and continued stirring at 20 °C under an atmosphere of nitrogen for 16 h. The progress of the reaction was monitored by aliquots taken from the mixture by means of a stainless steel needle and an IR conducted. The mixture was evaporated to give **44** (1.48 g, quantitative yield) as a colourless oil and used immediately *in situ* for the next reaction; IR  $\nu_{\max}$  (film) 3028 (C-H aromatic stretch), 1773 (C=O), 754 (C-Cl)  $\text{cm}^{-1}$ .

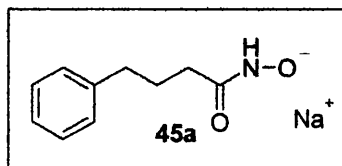
**N-Hydroxy-4-phenylbutyramide (45).** To a stirred ice-cold solution of hydroxylamine hydrochloride (4.26 g, 61.3 mmol) and potassium carbonate (11.41



g, 82.6 mmol) in water (12 mL) and chloroform (12 mL) was added a solution of 4-phenylbutyryl chloride (**44**) (1.40 g, 7.67 mmol) in chloroform (7.0 mL) dropwise, by means of a stainless steel needle. The mixture was warmed slowly to 25 °C and stirring was continued at 25 °C for 24 h. The progress of the reaction was monitored by thin-layer chromatographic analysis (thin-layer chromatography was developed by ferric sulfate charring). The mixture was acidified by the addition of 10 % aqueous hydrochloric acid (8.0 mL) and transferred to a separating funnel. The layers were separated and the aqueous layer extracted with chloroform (3 x 10 mL). The combined organic layers were dried over anhydrous magnesium sulfate. The solution was filtered through fluted filter paper and the filtrate evaporated. The solid was recrystallised from benzene to give **45** (0.78 g, 57%) as white crystalline platelets: mp 76-77 °C, lit<sup>23</sup> 76-77 °C;  $R_F$  [methanol-chloroform, 1-5, (v,v)] 0.62; IR  $\nu_{\max}$  (film) 3025 (aromatic C-H stretching), 1690 (C=O)  $\text{cm}^{-1}$ ;  $^1\text{H}$  NMR (300 MHz,  $\text{DMSO}_d6$ )  $\delta_H$  10.16 (1H, bs, NH), 8.89 (1H, bs, OH), 7.22 (5H, m, 5 x Aryl-H), 2.59 (2H, t,  $J$  7.5 Hz, Ar-CH<sub>2</sub>), 2.10 (2H, t,  $J$  7.5 Hz, CH<sub>2</sub>CO), 1.94 (2H, pentet,  $J$  7.5 Hz, ArCH<sub>2</sub>CH<sub>2</sub>)

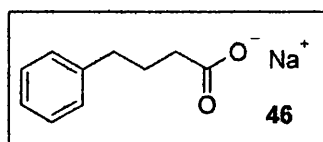
ppm;  $^{13}\text{C}$  NMR (75 MHz,  $\text{DMSO}_6$ )  $\delta_{\text{C}}$  176.81 (C=O), 146.12 (*Ar*-CH<sub>2</sub>), 133.47 (*Ar*-H), 133.11 (*Ar*-H), 131.08 (*Ar*-H), 39.94 (*Ar*-CH<sub>2</sub>), 37.19 (CH<sub>2</sub>CO), 31.89 (CH<sub>2</sub>CH<sub>2</sub>CH<sub>2</sub>) ppm; Anal. calcd. for  $\text{C}_{10}\text{H}_{13}\text{NO}_2$  = C, 67.02; H, 7.31; N, 7.82; Found: C, 66.75; H, 7.39; N, 7.89%.

**Sodium 4-phenylbutyrohoxamate (45a).** To a stirred solution of sodium hydrogen carbonate (0.16 g, 2.79 mmol) in water (6.0 mL) at 70 °C was added *N*-hydroxy-4-phenylbutyramide (45) (0.50 g, 2.79



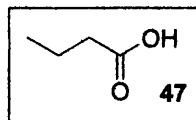
mmol). The mixture was stirred at 70 °C for 10 min until a clear solution is formed. The solution was then cooled to – 70 °C by liquid nitrogen and placed in the freeze-dryer and left for 24 h under vacuum. The solid was collected with a fluted filter paper and placed in a desiccator for a further 24 h to give 45a (0.48 g, quantitative yield) as white crystals: IR  $\nu_{\text{max}}$  (film) 1690 (C=O acid salt  $\text{cm}^{-1}$ );  $^1\text{H}$  NMR (250 MHz,  $\text{D}_2\text{O}$ )  $\delta_{\text{H}}$  7.49 (5H, m, 5 x Aryl-H), 2.81 (2H, t, *J* 7.5 Hz, *Ar*-CH<sub>2</sub>), 2.46 (2H, t, *J* 7.5 Hz, CH<sub>2</sub>CO), 2.10 (2H, pentet, *J* 7.5 Hz, CH<sub>2</sub>CH<sub>2</sub>CH<sub>2</sub>) ppm;  $^{13}\text{C}$  NMR (62 MHz,  $\text{D}_2\text{O}$ )  $\delta_{\text{C}}$  174.58 (C=O), 144.98 (*Ar*-CH<sub>2</sub>), 131.95 (*Ar*-H), 131.60 (*Ar*-H), 129.10 (*Ar*-H), 37.11 (*Ar*-CH<sub>2</sub>), 34.83 (CH<sub>2</sub>CO), 29.71 (CH<sub>2</sub>CH<sub>2</sub>CH<sub>2</sub>) ppm.

**Sodium phenylbutyrate salt (46).** To a stirred solution of sodium hydrogen carbonate (0.17 g, 2.79 mmol) in water (6.0 mL) at 70 °C was added 4-

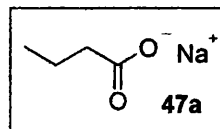


phenylbutyric acid (43) (0.50 g, 3.05 mmol). The mixture was stirred at 70 °C for 10 min until a clear solution is formed. The solution was then cooled to – 70 °C by liquid nitrogen and placed in the freeze-dryer and left for 24 h under vacuum. The solid was collected with a fluted filter paper and placed in a desiccator for a further 24 h to give 46 (0.48 g, quantitative yield) as white crystals: IR  $\nu_{\text{max}}$  (film) 1675 (C=O acid salt  $\text{cm}^{-1}$ );  $^1\text{H}$  NMR (250 MHz,  $\text{D}_2\text{O}$ )  $\delta_{\text{H}}$  7.44 (5H, m, 5 x Aryl-H), 2.75 (2H, t, *J* 7.5 Hz, *Ar*-CH<sub>2</sub>), 2.44 (2H, t, *J* 7.5 Hz, CH<sub>2</sub>CO), 2.13 (2H, pentet, *J* 7.5 Hz, CH<sub>2</sub>CH<sub>2</sub>CH<sub>2</sub>) ppm;  $^{13}\text{C}$  NMR (62 MHz,  $\text{D}_2\text{O}$ )  $\delta_{\text{C}}$  173.45 (C=O), 146.56 (*Ar*-CH<sub>2</sub>), 132.67 (*Ar*-H), 129.60 (*Ar*-H), 129.01 (*Ar*-H), 38.34 (*Ar*-CH<sub>2</sub>), 35.63 (CH<sub>2</sub>CO<sub>2</sub>), 28.94 (CH<sub>2</sub>CH<sub>2</sub>CH<sub>2</sub>) ppm.

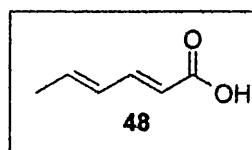
**Butyric acid (47).** Commercially available from Aldrich Co. (99% pure).



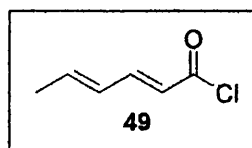
**Sodium butyrate (47a).** Procured from Aldrich Co. (98% pure).



**(2E,4E)-Hexa-2,4-dienoic acid (48).** Purchased from Aldrich Co. (99 % pure).

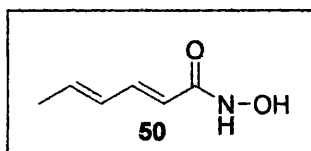


**(2E,4E)-Hexa-2,4-dienoyl chloride (49).** Based on a procedure by Staudinger.<sup>24</sup> To a stirred solution of (2E,4E)-hexa-2,4-dienoic acid (**48**) (4.00 g, 0.036 mol) in anhydrous dichloromethane (7.0 mL) at 0 °C under an atmosphere of nitrogen was added thionyl chloride (5.55 mL, 0.076 mol) dropwise, by means of a stainless steel needle. The mixture was allowed to warm slowly to 20 °C and continued stirring at 20 °C under an atmosphere of nitrogen for 16 h. The progress of the reaction was monitored by aliquots taken from the mixture by means of a stainless steel needle and an IR conducted. The mixture was evaporated to give **44** (1.48 g, quantitative yield) as a colourless oil and used immediately *in situ* for the next reaction; IR  $\nu_{\text{max}}$  (film) 3028 (C-H aromatic stretching), 1748 (C=O), 778 (C-Cl)  $\text{cm}^{-1}$ .



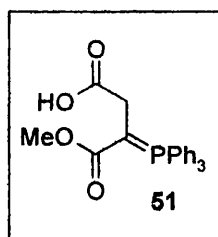
**(2E,4E)-Hexa-2,4-dienoic acid hydroxyamide (50).**

Based on methodology utilized by Steinberg.<sup>25</sup> To a stirring ice-cold solution of hydroxylamine hydrochloride (15.99 g, 0.23 mol) and sodium carbonate (32.86 g, 0.31 mol) in water (40 mL) and chloroform (40 mL) was added a solution of (2E,4E)-hexa-2,4-dienoyl chloride (**49**) (4.00 g, 0.031 mol) in chloroform (15 mL) dropwise, by means of a stainless steel needle. The mixture was warmed



slowly to 25 °C and stirring was continued at 25 °C for 24 h. The progress of the reaction was monitored by thin-layer chromatographic analysis (thin-layer chromatography was developed by ferric sulfate charring). The mixture was acidified by the addition of 10 % aqueous hydrochloric acid (22 mL) and transferred to a separating funnel. The layers were separated and the aqueous layer extracted with ethyl acetate (3 x 18 mL). The combined organic layers were dried over anhydrous magnesium sulfate. The solution was filtered through fluted filter paper and the filtrate evaporated. The solid was recrystallised from ethyl acetate to give **50** (2.78 g, 71%) as white needles: mp 130-132 °C, lit<sup>25</sup> mp 131-133 °C;  $R_F$  [methanol-chloroform, 1-4, (v,v)] 0.56; IR  $\nu_{\max}$  (film) 1690 (C=O), 1321 (C=C conjugation), 1110 (C-N stretch)  $\text{cm}^{-1}$ ;  $^1\text{H}$  NMR (300 MHz,  $\text{DMSO}_6$ )  $\delta_{\text{H}}$  7.31 (1H, m,  $\text{CH}=\text{CHCO}$ ), 6.16 (2H, m,  $=\text{CHCH}=\text{CHCO}$ ), 5.80 (1H, m,  $\text{CH}=\text{CHCH}=\text{CHCO}$ ), 1.91 (3H, m,  $\text{H}_3\text{CCH}=\text{CH}$ ) ppm;  $^{13}\text{C}$  NMR (75 MHz,  $\text{DMSO}_6$ )  $\delta_{\text{C}}$  174.09 (C=O), 144.84 ( $=\text{CHCO}$ ), 139.38 ( $\text{CH}=\text{CHCO}$ ), 130.04 ( $\text{H}_3\text{CCH}=\text{CH}$ ), 120.16 ( $\text{H}_3\text{CCH}=\text{CH}$ ), 18.68 ( $\text{H}_3\text{CCH}=\text{CH}$ ) ppm.

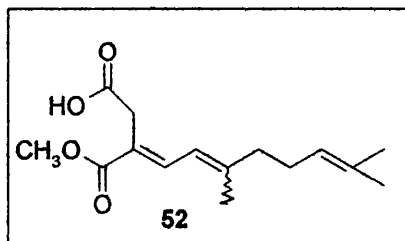
**2-(Triphenyl- $\gamma^5$ -phosphanylidene)-succinic acid 1-methyl ester (**51**).** Procedure used was based on methodology by Fulcrand.<sup>26</sup> A solution of 3-(triphenyl- $\gamma^5$ -phosphanylidene)-dihydrofuran-2,5-dione (5.50g, 0.015 mol) was dissolved in methanol (50 mL) at 25 °C and stirring continued at 25 °C for



24 h. The progress of the reaction was monitored by thin-layer chromatographic analysis (developed by  $\text{KMnO}_4$  charring). The solution was evaporated and the solid was filtered to give **51** (4.51 g, 80%) as pale yellow crystals, which were used immediately: mp 148-149 °C, lit<sup>26</sup> mp 150-152 °C;  $R_F$  [ethyl acetate-light petroleum ether, 1-4, (v,v)] 0.45; IR  $\nu_{\max}$  (film) 3040 (C-H aromatic stretching), 1731 (C=O ester), 1699 (C=O acid)  $\text{cm}^{-1}$ ;  $^1\text{H}$  NMR (300 MHz,  $\text{CDCl}_3$ )  $\delta_{\text{H}}$  7.57 (15H, m, 3 x 5 Ar-H), 5.50 (1H, bs, OH), 3.29 (3H, s,  $\text{OCH}_3$ ), 2.78 (2H, d,  $J$  15 Hz,  $\text{OCCH}_2$ ) ppm;  $^{13}\text{C}$  NMR (75 MHz,  $\text{CDCl}_3$ )  $\delta_{\text{C}}$  173.53 (C=O acid), 171.19 (C=O ester), 134.19 (Ar-P), 133.74 (Ar-H), 130.68 (Ar-H), 128.78 (Ar-H), 120.00 ( $\text{P}=\text{CCO}$ ), 52.06 ( $\text{OCH}_3$ ), 35.53 ( $\text{OCCH}_2\text{C}=\text{P}$ ) ppm.

**2-((E)-3,7-Dimethylocta-2,6-dienylidene)-**

**succinic acid 1-methyl ester (52).** To a stirred solution of 2-(triphenyl- $\gamma^5$ -phosphanylidene)-succinic acid 1-methyl ester (**51**) (3.50 g, 8.93 mmol) in toluene (15 mL) at 25 °C was added citral (3.82 mL, 0.02 mol) by means of a stainless

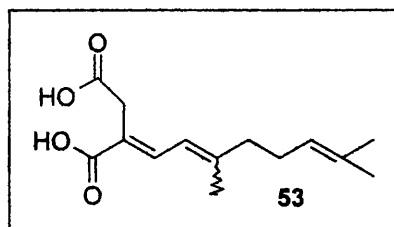


steel needle. Stirring continued at 25 °C for 120 h. The progress of the reaction was monitored by thin-layer chromatographic analysis (developed by  $\text{KMnO}_4$  charring). The solution was evaporated and the oil was purified by flash column chromatography on silica gel [ethyl acetate-light petroleum ether, 1-7, (v,v); developed by  $\text{KMnO}_4$  charring], and the eluent was evaporated to give **52** (2.00 g, 84%) as a clear yellow oil:  $R_F$  [ethyl acetate-light petroleum ether, 1-5, (v,v)] 0.31; IR  $\nu_{\text{max}}$  (film) 2940 (OH), 1745 (C=O ester) 1705 (C=O acid)  $\text{cm}^{-1}$ ;  $^1\text{H}$  NMR (300 MHz,  $\text{CDCl}_3$ )  $\delta_{\text{H}}$  7.59 (1H, m,  $\text{COC}=\text{CH}$ ), 6.03 (1H, d,  $J$  10 Hz,  $\text{CH}=\text{CCH}_3$ ), 5.01 (1H, m,  $\text{CH}=\text{CCH}_3$ ), 3.69 (3H, s,  $\text{OCH}_3$ ), 3.39 (2H, s,  $\text{COCH}_2\text{C}=\text{}$ ), 2.06 (4H, m, 2 x  $\text{CH}_2$ ), 1.89 (3H, s,  $=\text{CCH}_3$ ), 1.60 (3H, s,  $=\text{CCH}_3\text{CH}_3$ ), 1.56 (3H, s,  $=\text{CCH}_3\text{CH}_3$ ) ppm;  $^{13}\text{C}$  NMR (75 MHz,  $\text{CDCl}_3$ )  $\delta_{\text{C}}$  177.47 (C=O acid), 168.45 (C=O ester), 151.55 ( $\text{OCCH}_2\text{C}=\text{}$ ), 140.17 ( $=\text{CCH}_3$ ), 132.39 ( $=\text{CCH}_3$ ), 123.65 ( $=\text{CHCH}=\text{}$ ), 122.18 ( $\text{HC}=\text{CCH}_3$ ), 121.05 ( $\text{HC}=\text{CCH}_3$ ), 52.14 ( $\text{OCH}_3$ ), 40.98 ( $\text{OCCH}_2\text{C}=\text{}$ ), 32.37 ( $\text{CCH}_3\text{CH}_2$ ), 32.30 ( $\text{H}_2\text{CCH}_2\text{CH}=\text{}$ ), 25.82 ( $=\text{CCH}_3$  isomer 3:1), 17.83 ( $=\text{CCH}_3\text{CH}_3$ ), 17.74 ( $=\text{CCH}_3\text{CH}_3$ ) ppm;  $\text{HRMS}_{\text{EI}}$  calcd. for  $\text{C}_{15}\text{H}_{22}\text{O}_4$  ( $\text{M}^+$ ) 266.1518. Found 266.1518.

**2-((E)-3,7-Dimethylocta-2,6-dienylidene)-**

**succinic acid (53).** To a stirred solution of 2-((E)-3,7-dimethylocta-2,6-dienylidene)-

succinic acid 1-methyl ester (**52**) (0.30 g, 1.13 mmol) in a mixture of tetrahydrofuran (3.0



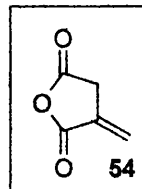
mL) and water (3.0 mL) at 25 °C was added lithium hydroxide (0.054 g, 2.25 mmol).

The mixture was heated to 55 °C and stirring continued at 55 °C for 4 h. The progress of the reaction was monitored by thin-layer chromatographic analysis (developed by

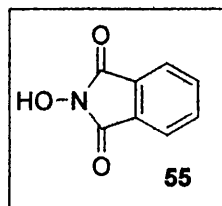


KMnO<sub>4</sub> charring). The mixture was then acidified by the addition of 1M hydrochloric acid (4.5 mL) until a pH of 1 was reached. The acidified solution was transferred to a separating funnel and extracted with ethyl acetate (3 x 8 mL). The combined organic layers are dried over anhydrous magnesium sulfate and the filtrate evaporated. The solid was purified by flash column chromatography on silica gel [methanol-chloroform, 1-49, (v,v); developed by KMnO<sub>4</sub> charring], and the eluent was evaporated to give **53** (0.23 g, 81%) as pale orange platelets: mp 176-178 °C; R<sub>F</sub> [methanol-chloroform, 1-49, (v,v)] 0.29; IR  $\nu_{\text{max}}$  (film) 1745 (C=O acid), 1483 (C=C conjugated) cm<sup>-1</sup>; <sup>1</sup>H NMR (300 MHz, CDCl<sub>3</sub>)  $\delta_{\text{H}}$  7.72 (1H, m, OCC=CH), 6.03 (1H, d, *J* 9.3 Hz, OCC=CHCH=), 5.00 (1H, m, HC=CCH<sub>3</sub>), 3.39 (2H, s, OCCH<sub>2</sub>C=), 2.11 (4H, m, 2 x CH<sub>2</sub>), 1.87 (3H, s, =CCH<sub>3</sub>), 1.60 (3H, s, =CCH<sub>3</sub>CH<sub>3</sub>), 1.56 (=CCH<sub>3</sub>CH<sub>3</sub>) ppm; <sup>13</sup>C NMR (75 MHz, CDCl<sub>3</sub>)  $\delta_{\text{C}}$  177.74 (C=O conjugated) 173.75 (C=O), 153.27 (OCC=), 132.78 (=CCH<sub>3</sub>), 130.19 (=CCH<sub>3</sub>CH<sub>3</sub>), 123.61 (OCC=CH), 120.75 (HC=CCH<sub>3</sub>), 120.26 (HC=CCH<sub>3</sub>CH<sub>3</sub>), 41.21 (OCCH<sub>2</sub>C=), 32.42 (=CCH<sub>3</sub>CH<sub>2</sub>), 26.74 (CH<sub>2</sub>CH<sub>2</sub>C=), 25.99 (=CCH<sub>3</sub> 3:1 isomer), 18.29 (=CCH<sub>3</sub>CH<sub>3</sub>), 18.09 (=CCH<sub>3</sub>CH<sub>3</sub>) ppm; <sup>13</sup>C NMR<sub>DEPT</sub> confirmed the above assignments; Anal. calcd. for C<sub>14</sub>H<sub>20</sub>O<sub>4</sub> = C, 66.64; H, 7.98; Found: C, 66.68; H, 7.99%.

**3-Methylenedihydrofuran-2,5-dione (54).** Purchased from Aldrich Co. (99 % pure).

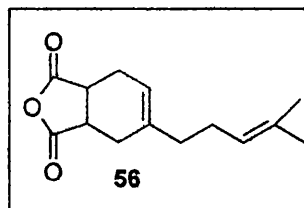


**2-Hydroxyisoindole-1,3-dione (55).** Purchased from Aldrich Co.



**5-(4-Methylpent-3-enyl)-3a,4,7,7a-**

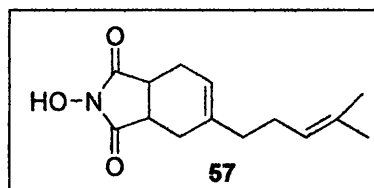
**tetrahydroisobenzofuran-1,3-dione (56).** To a stirred solution of maleic anhydride (0.98 g, 10.0 mmol) in anhydrous benzene (14 mL) at 25 °C was added  $\gamma$ -myrcene (9.6 mL, 20.0 mmol) dropwise by



means of a stainless steel needle. The solution was heated at reflux (80 °C), and stirring continued at 80 °C for 18 h. The progress of the reaction was monitored by thin-layer chromatographic analysis (developed by  $\text{KMnO}_4$  charring). The solution was evaporated, and the oil was purified by kugelrohr (100 °C/0.1 mmHg) to give a colourless oil, which upon cooling formed **56** (1.22 g, 52%) as white leaflets: mp 22–23 °C, lit<sup>27</sup> mp 22 °C;  $R_F$  [ethyl acetate–light petroleum ether, 1–9, (v,v)] 0.34; IR  $\nu_{\text{max}}$  (film) 1865 (C=O cyclic anhydride) and 1782 (C=O cyclic anhydride), 1632 (C=C)  $\text{cm}^{-1}$ ;  $^1\text{H}$  NMR (300 MHz,  $\text{CDCl}_3$ )  $\delta_{\text{H}}$  5.88 (1H, m,  $\text{CH}_2\text{CH}=\text{ring}$ ), 5.26 (1H, s,  $\text{CH}_2$  ring), 3.64 (2H, m, 2 x  $\text{COCH}$ ), 2.95 – 2.75 (2H, m,  $\text{CH}_2$  ring), 2.52 (2H, m,  $=\text{CCH}_2\text{CH}_2$ ), 2.32 (4H, s,  $\text{CH}_2\text{CH}_2\text{C}=\text{}$ ), 1.92 (3H, s,  $=\text{CCH}_3\text{CH}_3$ ), 1.85 (3H, s,  $=\text{CCH}_3\text{CH}_3$ ), ppm;  $^{13}\text{C}$  NMR (75 MHz,  $\text{CDCl}_3$ )  $\delta_{\text{C}}$  174.92 (C=O), 174.73 (C=O), 141.00 (HC=C ring), 132.72 ( $=\text{CCH}_3\text{CH}_3$ ), 123.67 (HC=C ring), 120.41 (HC=C $\text{CH}_3\text{CH}_3$ ), 40.67 (OCCH), 40.14 (OCCH), 37.60 (OCCH $\text{CH}_2$ ), 27.94 (OCCH $\text{CH}_2$ ), 26.29 ( $=\text{CCH}_2\text{CH}_2$ ), 26.12 ( $=\text{CCH}_3\text{CH}_3$ ), 24.41 ( $\text{CH}_2\text{CH}_2\text{C}=\text{}$ ), 18.17 ( $=\text{CCH}_3\text{CH}_3$ ) ppm; LRMS<sub>EI</sub> mass calcd for  $\text{C}_{14}\text{H}_{19}\text{O}_3$  ( $\text{M}^+$ ) 235. Found 235 ( $\text{M}^+$ , 15 %), 181 (16), 78 (40), 69 (100)%.

**2-Hydroxy-5-(4-methylpent-3-enyl)-3a,4,7,7a-**

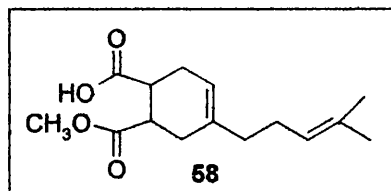
**tetrahydroisindole-1,3-dione (57).** To a stirred solution of hydroxylamine hydrochloride (0.18 g, 2.59 mmol) and 5-(4-methylpent-3-enyl)-



**3a,4,7,7a-tetrahydroisobenzofuran-1,3-dione (56)** (0.15 g, 0.64 mmol) in toluene (4.0 mL) at 25 °C was added pyridine (0.3 mL, 3.71 mmol) dropwise, by means of a stainless steel needle. The mixture was heated at reflux (120 °C), and stirring continued at 120 °C for 15 min. The progress of the reaction was monitored by thin-layer chromatographic analysis (developed by  $\text{KMnO}_4$  charring). The mixture was quenched by the addition of saturated aqueous ammonium chloride (4.0 mL) and

transferred to a separating funnel. The aqueous layer was extracted with toluene (3.0 mL) and the combined organic layers were dried over anhydrous magnesium sulfate. The solution was filtered through a fluted filter paper and the filtrate evaporated to give an oil which was purified by flash column chromatography on silica gel [ethyl acetate-light petroleum ether, 1-3, (v,v); developed by  $\text{KMnO}_4$  charring]. The eluent was evaporated to give **57** (0.13 g, 82%) as white crystals: mp 35-36 °C;  $R_F$  [ethyl acetate-light petroleum ether, 1-3, (v,v)] 0.21; IR  $\nu_{\text{max}}$  (film) 3270 (HO-N), 1725 (N-C=O stretching)  $\text{cm}^{-1}$ ;  $^1\text{H}$  NMR (300 MHz,  $\text{CDCl}_3$ )  $\delta_{\text{H}}$  6.52 (1H, bs, OH), 5.45 (1H, s, HC=C ring), 4.92 (1H, s,  $\text{HC}=\text{CCH}_3\text{CH}_3$ ), 2.98 (2H, s, 2 x CH ring), 2.38 (2H, m,  $=\text{CCH}_2\text{CH}_2$ ), 2.19 (2H, m,  $\text{CH}_2\text{CH}_2\text{C}=\text{}$ ), 1.89 (4H, s, 2 x  $\text{CH}_2$  ring), 1.69 (3H, s,  $=\text{CCH}_3\text{CH}_3$ ), 1.56 (3H, s,  $=\text{CCH}_3\text{CH}_3$ ) ppm;  $^{13}\text{C}$  NMR (75 MHz,  $\text{CDCl}_3$ )  $\delta_{\text{C}}$  174.41 (C=O), 173.89 (C=O), 139.22 (HC=C ring) 130.99 ( $=\text{CCH}_3\text{CH}_3$ ), 122.48 (HC=C ring), 118.71 (HC= $\text{CCH}_3\text{CH}_3$ ), 36.21 ( $\text{CH}_2$  ring), 35.96 (OCCH), 35.63 (OCCH), 26.21 ( $\text{CH}_2$  ring), 24.94 ( $=\text{CCH}_2\text{CH}_2$ ), 24.66 ( $=\text{CCH}_3\text{CH}_3$ ), 22.72 ( $\text{CH}_2\text{CH}_2\text{C}=\text{}$ ), 16.71 ( $=\text{CCH}_3\text{CH}_3$ ) ppm;  $^{13}\text{C}$  NMR<sub>DEPT</sub> confirmed the above assignments; Anal. calcd. for  $\text{C}_{14}\text{H}_{19}\text{NO}_3$  = C, 67.44; H, 7.68; N, 5.61. Found: C, 67.48; H, 7.66; N, 5.62%.

**4-(4-Methylpent-3-enyl)-cyclohex-4-ene-1,2-dicarboxylic acid 2-methyl ester (58).** To a stirred solution of 5-(4-methylpent-3-enyl)-3a,4,7,7a-tetrahydroisobenzofuran-1,3-dione (**56**) (0.30 g, 1.28 mmol) in methanol (6.0 mL)

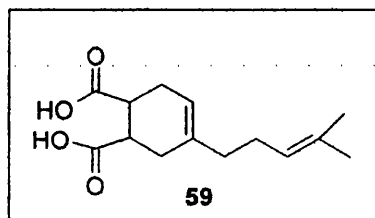


at 25 °C was added potassium carbonate (0.18 g, 1.28 mmol). Stirring continued at 25 °C for 18 h. The progress of the reaction was monitored by thin-layer chromatographic analysis (developed by  $\text{KMnO}_4$  charring). The solution was neutralised by the addition of 1M aqueous hydrochloric acid (3.5 mL) and transferred to a separating funnel. The solution was extracted with ethyl acetate (3 x 6 mL) and the combined organic layers were dried over anhydrous magnesium sulfate. The solution was filtered through a fluted filter paper and the filtrate was evaporated. The oil was purified by flash column chromatography on silica gel [ethyl acetate-light petroleum ether, 2-3, (v,v); developed by  $\text{KMnO}_4$  charring], and the eluent was evaporated to give **58** (0.20 g, 59%) as a clear, colourless oil:  $R_F$  [ethyl acetate-light

petroleum ether, 1-3, (v,v)] 0.25; IR  $\nu_{\max}$  (film) 1765 (C=O acid), 1735 (C=O ester)  $\text{cm}^{-1}$ ;  $^1\text{H}$  NMR (300 MHz,  $\text{CDCl}_3$ )  $\delta_{\text{H}}$  10.15 (1H, bs, OH), 5.23 (1H, s,  $\text{HC}=\text{C}$  ring), 4.93 (1H, s,  $\text{H}=\text{CCH}_3\text{CH}_3$ ), 3.68 (3H, s,  $\text{OCH}_3$ ), 2.98 (2H, s, 2 x  $\text{OCCH}$ ), 2.39 (2H, m,  $=\text{CCH}_2\text{CH}_2$ ), 2.20 (2H, m,  $=\text{CCH}_2\text{CH}_2$ ), 1.97 (2H, m,  $\text{CH}_2$  ring), 1.90 (2H, m,  $\text{CH}_2$  ring), 1.59 (3H, s,  $=\text{CCH}_3\text{CH}_3$ ), 1.50 (3H, s,  $=\text{CCH}_3\text{CH}_3$ ) ppm;  $^{13}\text{C}$  NMR (75 MHz,  $\text{CDCl}_3$ )  $\delta_{\text{C}}$  179.85 (C=O acid), 174.12 (C=O ester), 136.39 (C= $\text{CCH}_2$ ), 131.76 ( $=\text{CCH}_3\text{CH}_3$ ), 124.29 (HC=C ring), 119.13 (HC= $\text{CCH}_3\text{CH}_3$ ), 52.13 ( $\text{OCH}_3$ ), 40.46 ( $\text{CH}_2$  ring), 39.90 ( $\text{OCCH}$ ), 39.74 ( $\text{OCCH}$ ), 29.01 ( $\text{CH}_2$  ring), 28.86 ( $=\text{CCH}_2\text{CH}_2$ ), 26.51 ( $=\text{CCH}_3\text{CH}_3$ ), 25.94 ( $=\text{CCH}_2\text{CH}_2$ ), 17.93 ( $=\text{CCH}_3\text{CH}_3$ ) ppm; HRMS<sub>EI</sub> calcd for  $\text{C}_{15}\text{H}_{22}\text{O}_4$  ( $\text{M}^+$ ) 266.1518. Found: 266.1510.

#### 4-(4-Methylpent-3-enyl)-cyclohex-4-ene-1,2-

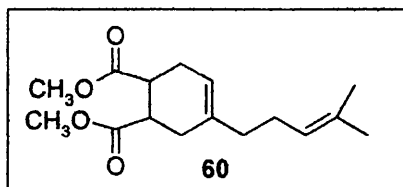
**dicarboxylic acid (59).** Based on a procedure utilised by Sutherland.<sup>28</sup> To a stirred solution of 5% aqueous potassium hydroxide (9.0 mL) at 25 °C was added 5-(4-methylpent-3-enyl)-3a,4,7,7a-



tetrahydroisobenzofuran-1,3-dione (**56**) (0.31 g, 1.32 mmol). The solution was heated to 45 °C and stirring continued at 45 °C for 50 min. The progress of the reaction was monitored by thin-layer chromatographic analysis (developed by  $\text{KMnO}_4$  charring). The solution was transferred to a separating funnel and extracted with diethyl ether (2 x 4 mL). The combined organic layers were acidified to pH 1 by the addition of 1M aqueous hydrochloric acid (6.0 mL). The acidified solution was transferred to a separating funnel and extracted with diethyl ether (2 x 4 mL). The combined organic layers were dried over anhydrous magnesium sulfate and filtered through a fluted filter paper. The filtrate was evaporated to give **59** (0.26 g, 78%) as white prisms: mp 120-121 °C, lit<sup>28</sup> mp 121-122 °C;  $R_{\text{F}}$  [methanol-chloroform, 1-49, (v,v)] 0.29; IR  $\nu_{\max}$  (film) 1755 (C=O acid), 1290 (C=C)  $\text{cm}^{-1}$ ;  $^1\text{H}$  NMR (300 MHz,  $\text{CDCl}_3$ )  $\delta_{\text{H}}$  11.0 – 9.86 (2H, bs, 2 x OH), 5.29 (1H, s, HC=C ring), 5.01 (1H, m,  $\text{HC}=\text{CCH}_3\text{CH}_3$ ), 3.00 (2H, m, 2 x  $\text{OCCH}$ ), 2.49 (2H, m,  $\text{CH}_2$  ring), 2.20 (2H, m,  $\text{CH}_2$  ring), 1.93 (2H, m,  $=\text{CCH}_2\text{CH}_2$ ), 1.88 (2H, m,  $=\text{CCH}_2\text{CH}_2$ ), 1.56 (3H, s,  $=\text{CCH}_3\text{CH}_3$ ), 1.45 (3H, s,  $=\text{CCH}_3\text{CH}_3$ ) ppm;  $^{13}\text{C}$  NMR (75 MHz,  $\text{CDCl}_3$ )  $\delta_{\text{C}}$  180.87 (C=O), 180.74 (C=O), 136.54 (HC=C ring), 132.18 (HC= $\text{CCH}_3\text{CH}_3$ ), 124.37 (HC=C ring), 119.15

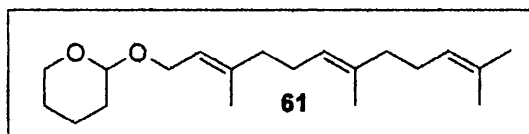
(HC=CCH<sub>3</sub>CH<sub>3</sub>), 40.35 (CH<sub>2</sub> ring), 39.79 (OCCH), 37.74 (OCCH), 28.95 (CH<sub>2</sub> ring), 26.67 (=CCH<sub>2</sub>CH<sub>2</sub>), 26.17 (=CCH<sub>3</sub>CH<sub>3</sub>), 26.07 (=CCH<sub>2</sub>CH<sub>2</sub>), 18.19 (=CCH<sub>3</sub>CH<sub>3</sub>) ppm; Anal. calcd. for C<sub>14</sub> H<sub>20</sub> O<sub>4</sub> = C, 66.64; H, 7.98. Found: C, 66.61; H, 7.92%.

**4-(4-Methylpent-3-enyl)-cyclohex-4-ene-1,2-dicarboxylic acid dimethyl ester (60).**



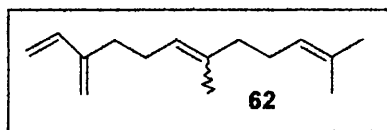
Procedure utilised based on methodology used by West.<sup>29</sup> To a stirred solution of 5-(4-methylpent-3-enyl)-3a,4,7,7a-tetrahydroisobenzofuran-1,3-dione (**56**) (0.20 g, 0.85 mmol) in methanol (5.0 mL) at 25 °C was added potassium carbonate (0.102 g, 0.75 mmol). The mixture was heated at reflux (80 °C) and stirring continued at 80 °C for 23 h. The progress of the reaction was monitored by thin-layer chromatographic analysis (developed by KMnO<sub>4</sub> charring). The solution was neutralised by the addition of 1M aqueous hydrochloric acid (3.0 mL) and transferred to a separating funnel. The solution was extracted with ethyl acetate (3 x 5 mL) and the combined organic layers were dried over anhydrous magnesium sulfate. The solution was filtered through a fluted filter paper and the filtrate was evaporated. The oil was purified by flash column chromatography on silica gel [ethyl acetate-light petroleum ether, 2-3, (v,v); developed by KMnO<sub>4</sub> charring], and the eluent was evaporated to give **60** (0.23 g, 68%) as a clear, colourless oil: bp 23-25 °C/3 mmHg, lit<sup>29</sup> bp 23-25 °C/3 mmHg; R<sub>F</sub> [ethyl acetate-light petroleum ether, 1-3, (v,v)] 0.22; IR ν<sub>max</sub> (film) 1725 (C=O ester), 1735 (C=O ester) cm<sup>-1</sup>; <sup>1</sup>H NMR (300 MHz, CDCl<sub>3</sub>) δ<sub>H</sub> 5.45 (1H, s, =CH ring), 5.05 (1H, s, HC= chain), 3.73 (3H, s, OCH<sub>3</sub>), 3.67 (3H, s, OCH<sub>3</sub>), 3.05 (2H, m, OCCH), 2.50 – 2.30 (4H, m, 2 x CH<sub>2</sub> ring), 2.15 – 2.00 (4H, m, CH<sub>2</sub>CH<sub>2</sub>), 1.43 (=CCH<sub>3</sub>CH<sub>3</sub>), 1.39 (=CCH<sub>3</sub>CH<sub>3</sub>) ppm; <sup>13</sup>C NMR (75 MHz, CDCl<sub>3</sub>) δ<sub>C</sub> 174.47 (C=O ester) 174.09 (C=O ester), 133.30 (HC=C ring), 131.87 (HC=CCH<sub>3</sub>CH<sub>3</sub>), 128.54 (HC=C ring), 126.71 (HC=CCH<sub>3</sub>CH<sub>3</sub>), 52.11 (OCH<sub>3</sub>), 52.02 (OCH<sub>3</sub>), 33.97 (CH<sub>2</sub> ring), 31.45 (OCCH), 31.28 (OCCH), 30.91 (CH<sub>2</sub> ring), 27.52 (=CCH<sub>2</sub>CH<sub>2</sub>), 25.98 (=CCH<sub>3</sub>CH<sub>3</sub>), 22.98 (=CCH<sub>2</sub>CH<sub>2</sub>), 19.47 (=CCH<sub>3</sub>CH<sub>3</sub>) ppm; HRMS<sub>EI</sub> calcd for C<sub>16</sub>H<sub>24</sub>O<sub>4</sub> (M<sup>+</sup>) 280.1674. Found 280.1679.

**3-((2*E*,6*E*)-3,7,11-Trimethyldodeca-2,6,10-trienyloxy)-tetrahydropyran (61).**



Procedure according to Schwartzapfel.<sup>30</sup> To a stirred solution of farnesol (2.25 mL, 9.00 mmol) in dichloromethane (10 mL) at 25 °C was added 3,4-dihydro-2*H*-pyran (1.2 mL, 13.0 mmol) and pyridinium *p*-toluenesulfonate (0.004 g, 0.016 mmol). Stirring continued at 25 °C for 12 h. The progress of the reaction was monitored by thin-layer chromatographic analysis (developed by KMnO<sub>4</sub> charring). The solution was transferred to a separating funnel and extracted with ethyl acetate (3 x 5 mL) and the combined organic layers were dried over anhydrous magnesium sulfate. The solution was filtered through a fluted filter paper and the filtrate was evaporated. The oil was purified by flash column chromatography on silica gel [ethyl acetate-light petroleum ether, 1-3, (v,v); developed by KMnO<sub>4</sub> charring], and the eluent was evaporated to give **61** (2.15 g, 78%) as a clear, colourless oil: bp 176-178 °C/3 mmHg; R<sub>F</sub> [ethyl acetate-light petroleum ether, 1-3, (v,v)] 0.17; IR ν<sub>max</sub> (film) 1725 (C-O-C ether), 1321 (C=C stretch) cm<sup>-1</sup>; <sup>1</sup>H NMR (300 MHz, CDCl<sub>3</sub>) δ<sub>H</sub> 5.30 (1H, t, *J* 7.0 Hz, =CHCH<sub>2</sub>O), 5.02 (2H, m, 2HC=C), 4.57 (1H, distorted t, OCHO ring), 4.18 (1H, dd, *J* 12 and 6.0 Hz, =CHCH<sub>a</sub>H<sub>b</sub>O), 3.95 (1H, dd, *J* 12 and 7.0 Hz, =CHCH<sub>a</sub>H<sub>b</sub>O), 3.84 (1H, m, CHOCH<sub>a</sub>H<sub>b</sub>), 3.75 (1H, m, CHOCH<sub>a</sub>H<sub>b</sub>), 2.15 – 1.90 (8H, m, 2 x CH<sub>2</sub>CH<sub>2</sub> chain), 1.85 – 1.40 (6H, m, OCH<sub>2</sub>CH<sub>2</sub>CH<sub>2</sub>CH<sub>2</sub> ring), 1.66 (6H, s, 2 x =CCH<sub>3</sub>), 1.54 (6H, =C(CH<sub>3</sub>)<sub>2</sub> ppm; <sup>13</sup>C NMR (75 MHz, CDCl<sub>3</sub>) δ<sub>C</sub> 140.49 (=CCH<sub>3</sub>), 135.77 (=C(CH<sub>3</sub>)<sub>2</sub>), 131.53 (=CCH<sub>3</sub>), 124.24 (HC=CCH<sub>3</sub>), 124.09 (HC=CH<sub>3</sub>), 120.99 (HC=C(CH<sub>3</sub>)<sub>2</sub>), 63.73 (OCH<sub>2</sub> ring), 62.42 (OCH<sub>2</sub> chain), 40.27 (OCHO ring), 31.02 (CH<sub>2</sub>), 26.95 (CH<sub>2</sub>), 26.52 (CH<sub>2</sub>), 26.02 (CH<sub>2</sub>), 25.83 (CH<sub>2</sub>), 23.71 (CH<sub>2</sub>), 20.09 (CH<sub>2</sub>), 19.96 (=CCH<sub>3</sub>), 17.96 (CCH<sub>3</sub>), 16.33 (CCH<sub>3</sub>CH<sub>3</sub>), 14.53 (CCH<sub>3</sub>CH<sub>3</sub>) ppm.

**(*E*)-7,11-Dimethyl-3-methylenedodeca-1,6,10-triene (62).** Based on a procedure by Djahanbini.<sup>31</sup> To a stirred solution of 3-

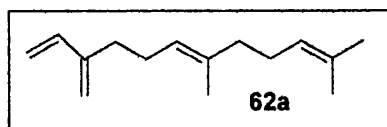


((2*E*,6*E*)-3,7,11-trimethyldodeca-2,6,10-trienyloxy)-tetrahydropyran (**61**) (0.30 g,

0.94 mmol) in anhydrous tetrahydrofuran (7.0 mL) under an atmosphere of dry nitrogen at 25 °C was added potassium *tert*-butoxide (1.13 g, 10.0 mmol) and 18-crown-6 (0.60 g, 2.27 mmol). The mixture was heated to reflux (80 °C) and stirring continued at 80 °C for 2 h. The progress of the reaction was monitored by thin-layer chromatographic analysis (developed by KMnO<sub>4</sub> charring). After allowing to cool to 25 °C, the mixture was diluted with water (4.0 mL) and transferred to a separating funnel. The solution was extracted with benzene (3 x 11 mL) and the combined organic layers were washed with saturated aqueous sodium chloride (6.0 mL) and dried over anhydrous potassium carbonate. The solution was filtered through a fluted filter paper and the filtrate evaporated. The oil was purified by flash column chromatography on silica gel [benzene-light petroleum ether, 1-9, (v,v); developed by KMnO<sub>4</sub> charring], and the eluent was evaporated to give **62** (0.14 g, 73%) as a clear yellow oil: *R*<sub>F</sub> [benzene-light petroleum ether, 1,9, (v,v)] 0.12; IR *v*<sub>max</sub> (film) 1298 (C=C conjugated) cm<sup>-1</sup>; <sup>1</sup>H NMR (300 MHz, CDCl<sub>3</sub>) δ<sub>H</sub> 6.32 (1H, dd, *J* 17 and 10 Hz, H<sub>2</sub>C=CHC=CH<sub>2</sub>), 5.12 (4H, m, H<sub>2</sub>C=C-C=CH<sub>2</sub>), 5.01 (1H, m, HC=C(CH<sub>3</sub>)<sub>2</sub>), 3.89 (HC=CCH<sub>3</sub>), 2.10 (4H, m, CH<sub>2</sub>CH<sub>2</sub>), 1.69 (4H, m, CH<sub>2</sub>CH<sub>2</sub>), 1.27 (3H, s, HC=CCH<sub>3</sub>), 0.78 (6H, m, HC=C(CH<sub>3</sub>)<sub>2</sub>) ppm; <sup>13</sup>C NMR (75 MHz, CDCl<sub>3</sub>) δ<sub>C</sub> 141.45 (C=CH<sub>2</sub>), 137.96 (H<sub>2</sub>C=CHC=CH<sub>2</sub>), 134.36 (=CCH<sub>3</sub>), 127.30 (=C(CH<sub>3</sub>)<sub>2</sub>), 123.31 (HC=C(CH<sub>3</sub>)<sub>2</sub>), 122.98 (HC=CCH<sub>3</sub>), 114.72 (H<sub>2</sub>C=CHC=CH<sub>2</sub>), 112.02 (H<sub>2</sub>C=CCH=CH<sub>2</sub>), 38.67 (=CCH<sub>2</sub>CH<sub>2</sub>C=), 30.35 (=CCH<sub>2</sub>CH<sub>2</sub>C=), 28.68 (=CCH<sub>2</sub>CH<sub>2</sub>C=), 25.67 (=CCH<sub>2</sub>CH<sub>2</sub>C=), 24.68 (=CCH<sub>3</sub>CH<sub>3</sub>), 16.66 (=CCH<sub>3</sub>CH<sub>3</sub>), 14.99 (=CCH<sub>3</sub> 3:1 isomer), 13.78 (=CCH<sub>3</sub>) ppm; <sup>13</sup>C NMR<sub>DEPT</sub> (75 MHz; CDCl<sub>3</sub>) verified the above carbon assignment.

**(*E*)-7,11-Dimethyl-3-methylenedodeca-**

**1,6,10-triene (62a).** The procedure was carried out as described above, except all-*trans*-farnesol

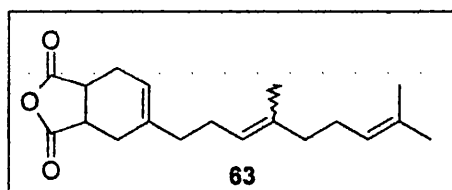


was used instead of the mixture of isomers. The oil was purified by flash column chromatography on silica gel [benzene-light petroleum ether, 1-9, (v,v); developed by KMnO<sub>4</sub> charring], and the eluent was evaporated to give **62a** (0.15 g, 79%) as a clear yellow oil: *R*<sub>F</sub> [benzene-light petroleum ether, 1,9, (v,v)] 0.12; IR *v*<sub>max</sub> (film) 1310

(C=C conjugated)  $\text{cm}^{-1}$ ;  $^1\text{H}$  NMR (300 MHz,  $\text{CDCl}_3$ )  $\delta_{\text{H}}$  6.29 (1H, m,  $\text{H}_2\text{C}=\text{CHC}=\text{CH}_2$ ), 5.13 (4H, m,  $\text{H}_2\text{C}=\text{CC}=\text{CH}_2$ ), 5.08 (1H, m,  $\text{HC}=\text{C}(\text{CH}_3)_2$ ), 3.84 (1H, m,  $\text{HC}=\text{CCH}_3$ ), 2.10 (4H, m,  $\text{CH}_2\text{CH}_2$ ), 1.70 (4H, m,  $\text{CH}_2\text{CH}_2$ ), 1.22 (3H, s,  $\text{HC}=\text{CCH}_3$ ), 0.98 (6H, m,  $\text{HC}=\text{C}(\text{CH}_3)_2$ ) ppm;  $^{13}\text{C}$  NMR (75 MHz,  $\text{CDCl}_3$ )  $\delta_{\text{C}}$  142.21 ( $\text{C}=\text{CH}_2$ ), 138.16 ( $\text{H}_2\text{C}=\text{CHC}=\text{CH}_2$ ), 136.63 ( $=\text{CCH}_3$ ), 127.99 ( $=\text{C}(\text{CH}_3)_2$ ), 124.11 ( $\text{HC}=\text{C}(\text{CH}_3)_2$ ), 122.68 ( $\text{HC}=\text{CCH}_3$ ), 116.45 ( $\text{H}_2\text{C}=\text{CHC}=\text{CH}_2$ ), 112.76 ( $\text{H}_2\text{C}=\text{CCH}=\text{CH}_2$ ), 39.32 ( $=\text{CCH}_2\text{CH}_2\text{C}=\text{C}$ ), 31.39 ( $=\text{CCH}_2\text{CH}_2\text{C}=\text{C}$ ), 30.12 ( $=\text{CCH}_2\text{CH}_2\text{C}=\text{C}$ ), 25.98 ( $=\text{CCH}_2\text{CH}_2\text{C}=\text{C}$ ), 24.87 ( $=\text{CCH}_3\text{CH}_3$ ), 18.99 ( $=\text{CCH}_3\text{CH}_3$ ), 15.82 ( $=\text{CCH}_3$ ) ppm;  $^{13}\text{C}$  NMR<sub>DEPT</sub> (75 MHz;  $\text{CDCl}_3$ ) verified the above carbon assignment.

**5-((E)-4,8-Dimethylnona-3,7-dienyl)-**

**3a,4,7,7a-tetrahydroisobenzofuran-1,3-dione (63).** To a stirred solution of maleic anhydride (0.30 g, 3.06 mmol) in

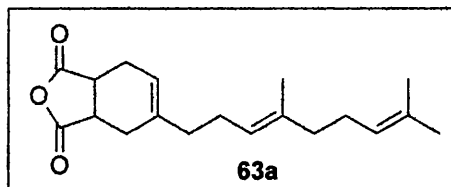


anhydrous benzene (10 mL) at 25 °C was added  $\beta$ -farnesene (3:1 6E:6Z isomer) (**62**) (1.25 g, 6.13 mmol) dropwise, by means of a stainless steel needle. The solution was heated at reflux (80 °C), and stirring continued at 80 °C for 16 h. The progress of the reaction was monitored by thin-layer chromatographic analysis (developed by  $\text{KMnO}_4$  charring). The solution was evaporated, and the oil was purified by kugelrohr (125 °C/0.1 mmHg) to give a colourless oil, which upon cooling formed **63** (0.46 g, 50%) as white prisms: mp 42- 45 °C;  $R_{\text{F}}$  [ethyl acetate-light petroleum ether, 1-5, (v,v)] 0.41; IR  $\nu_{\text{max}}$  (film) 1699 ( $\text{C}=\text{O}$  cyclic anhydride) and 1631 ( $\text{C}=\text{O}$  cyclic anhydride), 1423 ( $\text{C}=\text{C}$ )  $\text{cm}^{-1}$ ;  $^1\text{H}$  NMR (300 MHz,  $\text{CDCl}_3$ )  $\delta_{\text{H}}$  5.60 (1H, m,  $\text{HC}=\text{C}$  ring), 5.02 (2H, m, 2 x  $\text{HC}=\text{C}$  chain), 3.31 (2H, m, 2 x  $\text{OCCH}$ ), 2.64 (2H, m,  $\text{CH}_2$  ring), 2.19 (2H, m,  $\text{CH}_2$  ring), 1.86 (8H, m, 4 x  $\text{CH}_2$  chain), 1.72 (3H, s,  $=\text{CCH}_3$ ), 1.54 (3H, s,  $=\text{CCH}_3\text{CH}_3$ ), 1.51 (3H, s,  $\text{CCH}_3\text{CH}_3$ ) ppm;  $^{13}\text{C}$  NMR (75 MHz,  $\text{CDCl}_3$ )  $\delta_{\text{C}}$  173.47 ( $\text{C}=\text{O}$ ), 173.29 ( $\text{C}=\text{O}$ ), 139.62 ( $\text{HC}=\text{C}$  ring), 134.88 ( $=\text{CCH}_3$ ), 130.35 ( $=\text{CCH}_3\text{CH}_3$ ), 123.23 ( $\text{HC}=\text{C}$  ring), 122.08 ( $\text{HC}=\text{CCH}_3$ ), 119.03 ( $\text{HC}=\text{CCH}_3\text{CH}_3$ ), 39.20 ( $\text{OCCH}$ ), 38.65 ( $\text{OCCH}$ ), 38.59 ( $\text{CH}_2$  ring), 36.19 ( $\text{CH}_2$  ring), 26.51 ( $\text{CH}_2$  chain), 25.59 ( $\text{CH}_2$  chain), 24.74 ( $=\text{CCH}_3$  3:1 isomer), 18.09 ( $\text{CH}_2$  chain), 18.04



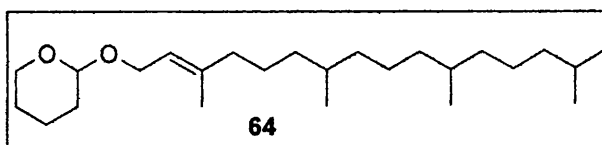
(=CCH<sub>3</sub>CH<sub>3</sub>), 16.44 (CH<sub>2</sub> chain), 14.47 (=CCH<sub>3</sub>CH<sub>3</sub>) ppm; Anal. calcd. for C<sub>19</sub>H<sub>26</sub>O<sub>3</sub> = C, 75.46; H, 8.66. Found: C, 75.51; H, 8.70%.

**5-((E)-4,8-Dimethylnona-3,7-dienyl)-3a,4,7,7a-tetrahydroisobenzofuran-1,3-dione (63a).** To a stirred solution of maleic anhydride (0.15 g, 1.53 mmol) in



anhydrous benzene (14 mL) at 25 °C was added β-farnesene (**62a**) (0.62 g, 3.04 mmol) dropwise, by means of a stainless steel needle. The solution was heated at reflux (80 °C), and stirring continued at 80 °C for 14 h. The progress of the reaction was monitored by thin-layer chromatographic analysis (developed by KMnO<sub>4</sub> charring). The solution was evaporated, and the oil was purified by kugelrohr (124 °C/0.1 mmHg) to give a colourless oil, which upon cooling formed **63a** (0.24 g, 52%) as white prisms: mp 75-75 °C; R<sub>F</sub> [ethyl acetate-light petroleum ether, 1-5, (v,v)] 0.41; IR ν<sub>max</sub> (film) 1690 (C=O cyclic anhydride) and 1642 (C=O cyclic anhydride), 1434 (C=C) cm<sup>-1</sup>; <sup>1</sup>H NMR (300 MHz, CDCl<sub>3</sub>) δ<sub>H</sub> 5.59 (1H, m, HC=C ring), 5.01 (2H, m, 2 x HC=C chain), 3.30 (2H, m, 2 x OCCH), 2.54 (2H, m, CH<sub>2</sub> ring), 2.23 (2H, m, CH<sub>2</sub> ring), 1.91 (8H, m, 4 x CH<sub>2</sub> chain), 1.69 (3H, s, =CCH<sub>3</sub>), 1.57 (3H, s, =CCH<sub>3</sub>CH<sub>3</sub>), 1.54 (3H, s, CCH<sub>3</sub>CH<sub>3</sub>) ppm; <sup>13</sup>C NMR (75 MHz, CDCl<sub>3</sub>) δ<sub>C</sub> 174.93 (C=O), 174.71 (C=O), 136.83 (HC=C ring), 134.54 (=CCH<sub>3</sub>), 131.28 (=CCH<sub>3</sub>CH<sub>3</sub>), 128.23 (HC=C ring), 121.42 (HC=CCH<sub>3</sub>), 113.52 (HC=CCH<sub>3</sub>CH<sub>3</sub>), 35.31 (OCCH), 35.02 (OCCH), 34.12 (CH<sub>2</sub> ring), 33.30 (CH<sub>2</sub> ring), 31.23 (CH<sub>2</sub> chain), 29.74 (CH<sub>2</sub> chain), 24.52 (=CCH<sub>3</sub>), 22.93 (CH<sub>2</sub> chain), 19.54 (=CCH<sub>3</sub>CH<sub>3</sub>), 18.21 (CH<sub>2</sub> chain), 11.71 (=CCH<sub>3</sub>CH<sub>3</sub>) ppm; Anal. calcd. for C<sub>19</sub>H<sub>26</sub>O<sub>3</sub> = C, 75.46; H, 8.66. Found: C, 75.40; H, 8.62%.

**3-((E)-3,7,11,15-Tetramethylhexadec-2-enyloxy)-tetrahydropyran (64).** To a stirred solution of

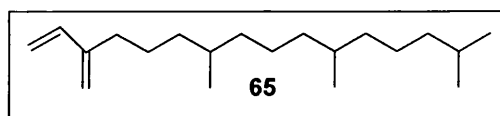


phytol (2.35 mL, 6.74 mmol) in dichloromethane (10 mL) at 25 °C was added 3,4-

dihydro-2*H*-pyran (0.33 mL, 3.70 mmol) and pyridinium *p*-toluenesulfonate (0.004 g, 0.016 mmol). Stirring was continued at 25 °C for 12 h. The progress of the reaction was monitored by thin-layer chromatographic analysis (developed by KMnO<sub>4</sub> charring). The solution was transferred to a separating funnel and extracted with ethyl acetate (3 x 5 mL) and the combined organic layers were dried over anhydrous magnesium sulfate. The solution was filtered through a fluted filter paper and the filtrate was evaporated. The oil was purified by flash column chromatography on silica gel [ethyl acetate-light petroleum ether, 1-3, (v,v); developed by KMnO<sub>4</sub> charring], and the eluent was evaporated to give **64** (1.15 g, 82%) as a clear, colourless oil: bp 188-190 °C/3 mmHg, lit<sup>32</sup> bp 185 – 188 °C; *R*<sub>F</sub> [ethyl acetate-light petroleum ether, 1-3, (v,v)] 0.13; IR  $\nu_{\text{max}}$  (film) 1735 (C-O-C ether), 1311 (C=C stretch) cm<sup>-1</sup>; <sup>1</sup>H NMR (300 MHz, CDCl<sub>3</sub>)  $\delta_{\text{H}}$  5.23 (1H, m, C=CH chain), 4.61 (1H, bs, CHCH<sub>3</sub>), 4.19 (1H, m, CHCH<sub>3</sub>), 3.92 (1H, m, CHCH<sub>3</sub>), 3.82 (1H, m, OCHO ring), 3.47 (2H, m, OCH<sub>2</sub> ring), 1.97 (2H, m, OCH<sub>2</sub> chain), 1.64-1.52 (18H, m, 9 x CH<sub>2</sub> chain), 1.32 (3H, s, =CCH<sub>3</sub>), 1.07 (6H, m, 3 x CH<sub>2</sub> ring), 0.81 (6H, m, 2 x CHCH<sub>3</sub>), 0.81 (6H, CHCH<sub>3</sub>CH<sub>3</sub>) ppm; <sup>13</sup>C NMR (75 MHz, CDCl<sub>3</sub>)  $\delta_{\text{C}}$  141.41 (C=CCH<sub>3</sub>), 121.60 (HC=CCH<sub>3</sub>), 63.97 (OCH<sub>2</sub> ring), 62.44 (OCH<sub>2</sub> chain), 40.32 (OCHO ring), 37.80 (CH<sub>2</sub>), 37.76 (CH<sub>2</sub>), 37.69 (CH<sub>2</sub>), 37.66 (CH<sub>2</sub>), 33.15 (CH<sub>2</sub>), 33.13 (CH<sub>2</sub>), 33.05 (CH<sub>2</sub>), 31.08 (CH<sub>2</sub>), 28.34 (CH<sub>2</sub>), 25.90 (CH<sub>2</sub>), 25.45 (CH<sub>2</sub>), 25.18 (CH<sub>2</sub>), 23.09 (=CCH<sub>3</sub>), 20.04 (CHCH<sub>3</sub>), 20.00 (CHCH<sub>3</sub>), 19.91 (CCH<sub>3</sub>CH<sub>3</sub>), 16.67 (CCH<sub>3</sub>CH<sub>3</sub>) ppm.

### 7,11,15-Trimethyl-3-

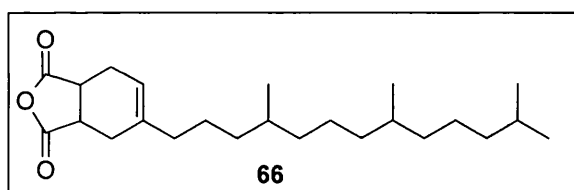
**methylenehexadec-1-ene (65).** Based on a procedure utilised by Grossi.<sup>33</sup> To a



stirred solution of 3-((*E*)-3,7,11,15-tetramethylhexadec-2-enyloxy)-tetrahydropyran (**64**) (2.00 g, 5.26 mmol) in anhydrous tetrahydrofuran (12 mL) under an atmosphere of dry nitrogen at 25 °C was added Bu<sup>t</sup>OK (5.60 g, 0.05 mol) and 18-crown-6 (2.90 g, 0.011 mol). The mixture was heated at reflux (80 °C) and stirring continued at 80 °C for 2 h. The progress of the reaction was monitored by thin-layer chromatographic analysis (thin-layer chromatography was developed by KMnO<sub>4</sub> charring). After allowing to cool to 25 °C, the mixture was diluted with water (7.0 mL) and transferred

to a separating funnel. The solution was extracted with benzene (3 x 14 mL) and the combined organic layers were washed with saturated aqueous sodium chloride (8.0 mL) and dried over anhydrous potassium carbonate. The solution was filtered through a fluted filter paper and the filtrate evaporated. The oil was purified by flash column chromatography on silica gel [benzene-light petroleum ether, 1-9, (v,v); thin-layer chromatography was developed by  $\text{KMnO}_4$  charring], and the eluent was evaporated to give **65** (1.05 g, 72%) as a clear yellow oil:  $R_F$  [benzene-light petroleum ether, 1,9, (v,v)] 0.11; IR  $\nu_{\text{max}}$  (film) 1298 ( $\text{C}=\text{C}$  conjugated)  $\text{cm}^{-1}$ ;  $^1\text{H}$  NMR (300 MHz,  $\text{CDCl}_3$ )  $\delta_H$  6.12 (2H, m,  $\text{C}=\text{CH}_2$ ), 5.63 (2H, m,  $\text{HC}=\text{CH}_2$ ), 5.00 (1H, m,  $\text{H}_2\text{C}=\text{CH}$ ), 2.10 (2H, m, 2 x  $\text{CHCH}_3$ ), 1.80 (1H, m,  $\text{CH}(\text{CH}_3)_2$ ), 1.31-1.24 (18H, 9 x  $\text{CH}_2$ ), 0.81 (6H, m, 2 x  $\text{CHCH}_3$ ), 0.73 (6H, m,  $\text{CHCH}_3\text{CH}_3$ ) ppm;  $^{13}\text{C}$  NMR (75 MHz,  $\text{CDCl}_3$ )  $\delta_C$  145.43 ( $\text{H}_2\text{C}=\text{C}$ ), 136.84 ( $\text{H}_2\text{C}=\text{CH}$ ), 134.97 ( $\text{H}_2\text{C}=\text{CH}$ ), 124.00 ( $\text{H}_2\text{C}=\text{C}$ ), 38.41 ( $\text{CH}_2$ ), 36.45 ( $\text{CH}_2$ ), 36.37 ( $\text{CH}_2$ ), 36.35 ( $\text{CH}_2$ ), 36.21 ( $\text{CH}_2$ ), 36.13 ( $\text{CH}_2$ ), 36.11 ( $\text{CH}_2$ ), 36.08 ( $\text{CH}_2$ ), 36.04 ( $\text{CHCH}_3$ ), 31.81 ( $\text{CHCH}_3$ ), 31.73 ( $\text{CH}_2$ ), 31.70 ( $\text{CH}_2$ ), 30.71 ( $\text{CH}_2$ ), 27.01 ( $\text{CHCH}_3$ ), 24.62 ( $\text{CH}_2$ ), 23.88 ( $\text{CH}_2$ ), 23.60 ( $\text{CH}_2$ ), 23.58 ( $\text{CH}_2$ ), 23.52 ( $\text{CH}_2$ ), 22.56 ( $\text{CH}_2$ ), 21.73 ( $\text{CH}_2$ ), 21.63 ( $\text{CHCH}_3$ ), 18.74 ( $\text{CH}_2$ ), 18.67 ( $\text{CHCH}_3$ ), 12.58 ( $\text{CHCH}_3\text{CH}_3$ ), 11.05 ( $\text{CHCH}_3\text{CH}_3$ ) ppm.

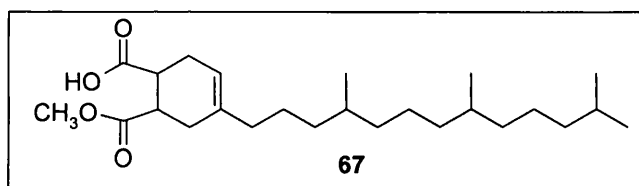
**5-(4,8,12-Trimethyltridecyl)-  
3a,4,7,7a-  
tetrahydroisobenzofuran-1,3-  
dione (66).** To a stirred solution



of maleic anhydride (0.30 g, 3.06 mmol) in anhydrous benzene (14 mL) at 25 °C was added neophytadiene (**65**) (1.66 g, 5.90 mmol) dropwise by means of a stainless steel needle. The solution was heated to reflux (80 °C), and stirring continued at 80 °C for 20 h. The progress of the reaction was monitored by thin-layer chromatographic analysis (thin-layer chromatography was developed by  $\text{KMnO}_4$  charring). The solution was evaporated, and the oil was purified by kughlrohr (164 °C/0.1 mmHg) to give a colourless oil, which upon cooling formed **66** (0.70 g, 71%) as white prisms:

mp 89-90 °C, lit<sup>34</sup> mp 90 °C;  $R_F$  [ethyl acetate-light petroleum ether, 1-4, (v,v)] 0.29; IR  $\nu_{\max}$  (film) 1676 (C=O cyclic anhydride) and 1641 (C=O cyclic anhydride), 1431 (C=C)  $\text{cm}^{-1}$ ;  $^1\text{H}$  NMR (300 MHz,  $\text{CDCl}_3$ )  $\delta_{\text{H}}$  5.56 (1H, m, HC=C ring), 3.32 (2H, m, 2 x OCCH), 2.50 (2H, m,  $\text{CH}_2$  ring), 2.17 (2H, m,  $\text{CH}_2$  ring), 1.97 (2H, t,  $J = 8\text{ Hz}$ , exocyclic  $\text{CH}_2$ ), 1.47 (1H, octet,  $J = 7.0\text{ Hz}$ , internal chain methine), 1.40 – 0.90 (18H, m, 8 x  $\text{CH}_2$  chain and 2 x  $\text{CHCH}_3$ ), 0.81 (3H, s,  $\text{CH}_3$ ), 0.78 (6H, s, 2 x  $\text{CH}_3$ ), 0.76 (3H, s,  $\text{CH}_3$ ) ppm;  $^{13}\text{C}$  NMR (75 MHz,  $\text{CDCl}_3$ )  $\delta_{\text{C}}$  175.01 (C=O), 174.83 (C=O), 141.47 (HC=C ring), 120.12 (HC=C ring), 40.62 (OCCH), 40.19 (OCCH), 39.21 ( $\text{CH}_2$  ring), 37.92 ( $\text{CH}_2$  ring), 37.78 ( $\text{CH}_2$  chain), 33.17 ( $\text{CH}_2$  chain), 33.15 ( $\text{CH}_2$  chain), 28.65 ( $\text{CCH}_3\text{CH}_2$ ), 28.36 ( $\text{CH}_2$  chain), 27.82 ( $\text{CH}_2$  chain), 25.20 ( $\text{CCH}_3\text{CH}_2$ ), 25.00 ( $\text{CCH}_3\text{CH}_2\text{CH}_2$ ), 24.86 ( $\text{CH}_2$  chain), 24.84 ( $\text{CH}_3$ ), 24.44 ( $\text{CH}_3$ ), 23.13 ( $\text{CHCH}_3$ ), 23.03 ( $\text{CH}_3$ ), 20.14 ( $\text{CHCH}_3$ ), 20.07 ( $\text{CH}_3$ ) ppm; Anal. calcd. for  $\text{C}_{24}\text{H}_{40}\text{O}_3$  = C, 76.54; H, 10.70. Found: C, 76.50; H, 10.76%.

**4-(4,8,12-Trimethyltridecyl)-cyclohex-4-ene-1,2-dicarboxylic-2-methyl**

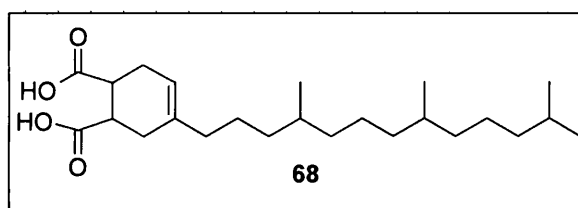


**ester (67).** To a stirred solution of 5-(4,8,12-trimethyltridecyl)-3a,4,7,7a-tetrahydroisobenzofuran-1,3-dione (**66**) (0.20 g, 0.53 mmol) in methanol (4.0 mL) at 25 °C was added potassium carbonate (0.073 g, 0.53 mmol). Stirring continued at 25 °C for 18 h. The progress of the reaction was monitored by thin-layer chromatographic analysis (thin-layer chromatography was developed by  $\text{KMnO}_4$  charring). The solution was neutralised by the addition of 1M aqueous hydrochloric acid (2.5 mL) and transferred to a separating funnel. The solution was extracted with ethyl acetate (3 x 5 mL) and the combined organic layers were dried over anhydrous magnesium sulfate. The solution was filtered through a fluted filter paper and the filtrate was evaporated. The oil was purified by flash column chromatography on silica gel [ethyl acetate-light petroleum ether, 1-3, (v,v); thin-layer chromatography was developed by  $\text{KMnO}_4$  charring], and the eluent was evaporated to give **67** (0.19 g, 88%) as a clear, colourless oil:  $R_F$  [ethyl acetate-light petroleum ether, 1-3, (v,v)] 0.28; IR  $\nu_{\max}$  (film) 1765 (C=O acid), 1735 (C=O ester)  $\text{cm}^{-1}$ ;  $^1\text{H}$  NMR (300 MHz,

CDCl<sub>3</sub>)  $\delta_H$  5.34 (1H, s, HC=C ring), 3.65 (3H, s, OCH<sub>3</sub>), 2.98 (2H, m, 2 x OCCH), 2.40 (2H, m, CH<sub>2</sub> ring), 2.21 (2H, t, *J* 8.0 Hz, exocyclic CH<sub>2</sub>), 1.82 (2H, m, 2 x HCCH<sub>3</sub>), 1.40 (1H, octet, *J* 7.0 Hz, internal chain methine), 1.32 – 1.01 (16H, m, 8 x CH<sub>2</sub> chain), 0.82 (3H, s, CH<sub>3</sub>), 0.81 (3H, s, CH<sub>3</sub>), 0.79 (3H, s, CCH<sub>3</sub>CH<sub>3</sub>), 0.78 (3H, s, CCH<sub>3</sub>CH<sub>3</sub>) ppm; <sup>13</sup>C NMR (75 MHz, CDCl<sub>3</sub>)  $\delta_C$  180.30 (C=O acid), 174.67 (C=O ester), 136.38 (HC=C), 128.31 (HC=C ring), 60.40 (OCH<sub>3</sub>), 39.87 (CH<sub>2</sub> chain), 39.35 (CH<sub>2</sub> chain), 37.41 (OCCH), 37.38 (OCCH), 37.32 (CH<sub>2</sub> ring) 37.28 (CH<sub>2</sub> ring), 36.63 (=CCH<sub>2</sub>), 32.78 (CCH<sub>3</sub>CH<sub>2</sub>), 32.60 (CH<sub>2</sub> chain), 28.29 (CH<sub>2</sub> chain), 27.96 (CCH<sub>3</sub>CH<sub>2</sub>), 24.79 (CH<sub>2</sub> chain), 24.47 (CH<sub>2</sub> chain), 22.71 (CHCH<sub>3</sub>), 22.61 (CHCH<sub>3</sub>), 19.72 (CH<sub>3</sub>), 19.65 (CH<sub>3</sub>), 14.34 (CH<sub>3</sub>), 14.18 (CH<sub>3</sub>) ppm; HRMS<sub>EI</sub> calcd. for C<sub>25</sub>H<sub>42</sub>O<sub>4</sub> (M<sup>+</sup>) 408.3239. Found 408.3242.

**4-(-4,8,12-Trimethyltridecyl)-cyclohex-4-ene-1,2-**

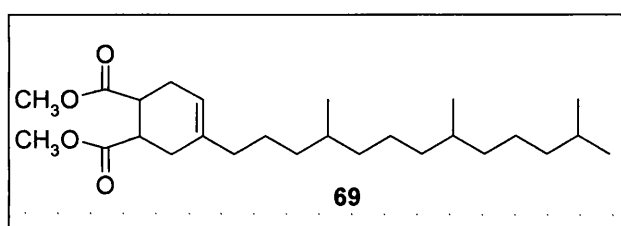
**dicarboxylic acid (68).** To a stirred solution of 5% aqueous



potassium hydroxide (9.0 mL) at 25 °C was added 5-(4,8,12-trimethyltridecyl)-3a,4,7,7a-tetrahydroisobenzofuran-1,3-dione (**66**) (0.47 g, 1.25 mmol). The solution was heated at 45 °C and stirring continued at 45 °C for 1 hr. The progress of the reaction was monitored by thin-layer chromatographic analysis (thin-layer chromatography was developed by KMnO<sub>4</sub> charring). The solution was transferred to a separating funnel and extracted with diethyl ether (2 x 4 mL). The combined organic layers were acidified to pH 1 by the addition of 1M aqueous hydrochloric acid (6.0 mL). The acidified solution was transferred to a separating funnel and extracted with diethyl ether (2 x 4 mL). The combined organic layers were dried over anhydrous magnesium sulfate and filtered through a fluted filter paper. The filtrate was evaporated to give **68** (0.32 g, 65%) as white prisms: mp 121-123 °C, lit<sup>34</sup> mp 121-122 °C; R<sub>F</sub> [methanol-chloroform, 1-49, (v,v)] 0.21; IR  $\nu_{\max}$  (film) 1750 (C=O acid), 1290 (C=C) cm<sup>-1</sup>; <sup>1</sup>H NMR (300 MHz, CDCl<sub>3</sub>)  $\delta_H$  10.54 – 9.71 (2H, bs, 2 x OH), 5.34 (1H, s, HC=C ring), 3.02 (2H, d, *J* 8.0 Hz ring junction), 2.61 (2H, m CH<sub>2</sub> ring), 2.21 (2H, m, CH<sub>2</sub> ring), 1.82 (2H, t, *J* 8.0 Hz, exocyclic CH<sub>2</sub>), 1.32 (1H, octet, *J* 7.0 Hz, internal chain methine), 1.29 – 1.01 (16H, m, 8 x CH<sub>2</sub>), 0.94 (2H, m, 2 x HCCH<sub>3</sub>),

0.80 (3H, s, CH<sub>3</sub>), 0.78 (3H, s, CCH<sub>3</sub>CH<sub>3</sub>), 0.76 (CCH<sub>3</sub>CH<sub>3</sub>), 0.74 (3H, s, CH<sub>3</sub>) ppm; <sup>13</sup>C NMR (75 MHz, CDCl<sub>3</sub>) δ<sub>C</sub> 179.46 (2 x C=O), 135.38 (HC=C), 117.78 (HC=C ring), 38.97 (CH<sub>2</sub> ring), 38.86 (OCCH), 38.34 (OCCH), 36.72 (CH<sub>2</sub> ring), 36.66 (=C-CH<sub>2</sub>), 36.63 (CH<sub>2</sub> chain), 36.37 (CH<sub>2</sub> chain), 36.27 (CH<sub>2</sub> chain), 31.77 (CH<sub>2</sub> chain), 31.59 (CH<sub>2</sub> chain), 26.99 (CCH<sub>2</sub>CH<sub>2</sub>), 26.95 (CH<sub>2</sub> chain), 23.89 (CH<sub>2</sub> chain), 23.79 (CHCH<sub>3</sub>), 23.46 (CHCH<sub>3</sub>), 21.70 (CH<sub>3</sub>), 21.61 (CH<sub>3</sub>), 18.68 (CH<sub>3</sub>), 18.66 (CH<sub>3</sub>) ppm; Anal. calcd. for C<sub>24</sub>H<sub>42</sub>O<sub>4</sub> = C, 73.05; H, 10.72. Found: C, 73.09; H, 10.68%.

**4-(4,8,12-trimethyltridecyl)-cyclohex-4-ene-1,2-dicarboxylic acid dimethyl ester (69).** To a stirred

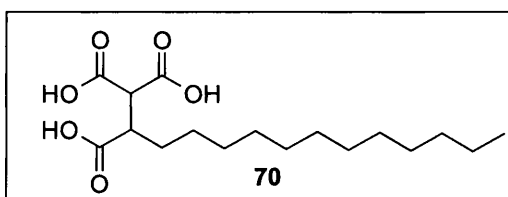


solution of 5-(4,8,12-trimethyltridecyl)-3a,4,7,7a-tetrahydroisobenzofuran-1,3-dione (**66**) (0.45 g, 1.21 mmol) in methanol (4.0 mL) at 25 °C was added potassium carbonate (0.17 g, 1.21 mmol). The mixture was heated at reflux (80 °C) and stirring continued at 80 °C for 23 h. The progress of the reaction was monitored by thin-layer chromatographic analysis (thin-layer chromatography was developed by KMnO<sub>4</sub> charring). The solution was neutralised by the addition of 1M aqueous hydrochloric acid (3.2 mL) and transferred to a separating funnel. The solution was extracted with ethyl acetate (3 x 8 mL) and the combined organic layers were dried over anhydrous magnesium sulfate. The solution was filtered through a fluted filter paper and the filtrate was evaporated. The oil was purified by flash column chromatography on silica gel [ethyl acetate-light petroleum ether, 1-4, (v,v); thin-layer chromatography was developed by KMnO<sub>4</sub> charring], and the eluent was evaporated to give **69** (0.37 g, 74%) as a clear, colourless oil: R<sub>F</sub> [ethyl acetate-light petroleum ether, 1-3, (v,v)] 0.22; IR ν<sub>max</sub> (film) 1740 (C=O ester), 1725 (C=O ester) cm<sup>-1</sup>; <sup>1</sup>H NMR (300 MHz, CDCl<sub>3</sub>) δ<sub>H</sub> 5.23 (1H, s, HC=C ring), 3.79 (3H, s, OCH<sub>3</sub>), 3.54 (3H, s, OCH<sub>3</sub>), 2.98 (2H, m, 2 x OCCH), 2.70 (2H, m, CH<sub>2</sub> ring), 2.37 (2H, m, CH<sub>2</sub> ring), 1.83 (2H, t, *J* 8.0 Hz, exocyclic CH<sub>2</sub>), 1.59 (1H, octet, *J* 7.0 Hz, internal chain methine), 1.48 – 1.04 (16H, m, 8 x CH<sub>2</sub>), 0.95 (2H, m, 2 x CHCH<sub>3</sub>), 0.92 (3H, s, CH<sub>3</sub>), 0.89 (3H, s, CCH<sub>3</sub>CH<sub>3</sub>), 0.85 (CCH<sub>3</sub>CH<sub>3</sub>), 0.71 (3H, s, CH<sub>3</sub>) ppm; <sup>13</sup>C NMR (75 MHz, CDCl<sub>3</sub>) δ<sub>C</sub>

172.83 (2 x C=O), 135.43 (HC=C ring), 117.50 (HC=C ring), 50.76 (OCH<sub>3</sub>), 50.75 (OCH<sub>3</sub>), 38.70 (OCCH), 38.34 (OCCH), 37.25 (CH<sub>2</sub> ring), 36.67 (CH<sub>2</sub> ring), 36.37 (=CCH<sub>2</sub>), 36.27 (CH<sub>2</sub> chain), 35.69 (CH<sub>2</sub> chain), 35.59 (CH<sub>2</sub> chain), 31.75 (CH<sub>2</sub> chain), 31.64 (CH<sub>2</sub> chain), 27.60 (CH<sub>2</sub> chain), 24.82 (CH<sub>2</sub> chain), 23.92 (CH<sub>2</sub> chain), 23.78 (CH<sub>3</sub>), 23.46 (CH<sub>3</sub>), 21.70 (CH), 21.60 (CH), 21.32 (CH<sub>3</sub>), 18.72 (CH<sub>3</sub>) ppm; HRMS<sub>EI</sub> calcd for C<sub>26</sub>H<sub>46</sub>O<sub>4</sub> (M<sup>+</sup>) 422.3395. Found 422.3388.

**Tetradecane-1,1,2-tricarboxylic acid**

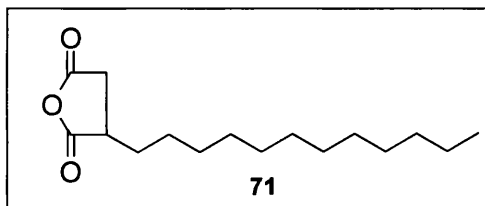
**(70).** Based on a procedure by Nargund.<sup>35</sup> To a stirred solution of sodium ethoxide (0.18 g, 2.65 mmol)



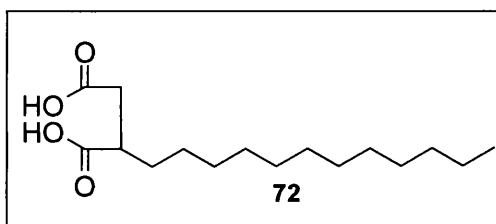
in ethanol (1.76 mL) and diethyl malonate (0.98 mL, 6.43 mmol) at 25 °C was added ethyl 2-bromomyristate (1.88 mL, 5.96 mmol) dropwise, by means of a stainless steel needle. The mixture was heated at reflux (85 °C) and stirring continued at 85 °C for 2 h. The solution is allowed to cool to 25 °C, to which was added a solution of sodium hydroxide (0.47 g, 0.012 mol) in 50% aqueous ethanol (2.34 mL) by means of a stainless steel needle. The solution was heated at reflux (90 °C) and stirring continued at 90 °C for 6 h. The progress of the reaction was monitored by thin-layer chromatographic analysis (thin-layer chromatography was developed by KMnO<sub>4</sub> charring). The solution was evaporated to remove all traces of alcohol, and the addition of water (2.0 mL) followed. The solution was acidified by the addition of concentrated hydrochloric acid (1.2 mL) to produce a pale yellow mass, which was filtered through a sintered glass funnel. The solid was purified by recrystallisation from dilute acetic acid to give **70** (0.65 g, 74%) as pale white needles: mp 133-135 °C, lit<sup>35</sup> mp 134 °C; R<sub>F</sub> [methanol-chloroform, 1-49, (v,v)] 0.19; IR ν<sub>max</sub> (film) 3210 (OH stretching), 1712 (C=O acid) cm<sup>-1</sup>; <sup>1</sup>H NMR (300 MHz, CDCl<sub>3</sub>) δ<sub>H</sub> 8.89 (2H, bs, 2 x OH), 4.03 (2H, m, OCCHCH<sub>2</sub>), 3.72 (1H, d, *J* 10 Hz, OCCHCO), 3.19 (1H, m, OCCHCH<sub>2</sub>), 1.55 (2H, m, CH<sub>2</sub>CH<sub>3</sub>), 1.20 (18H, s, OCCHCH<sub>2</sub>(CH<sub>2</sub>)<sub>18</sub>CH<sub>2</sub>CH<sub>3</sub>), 0.89 (3H, m, CH<sub>2</sub>CH<sub>3</sub>) ppm; <sup>13</sup>C NMR (75 MHz, CDCl<sub>3</sub>) δ<sub>C</sub> 174.20 (C=O), 173.11 (C=O), 172.82 (C=O), 53.70 (OCCH), 44.69 (OCCH), 43.11 (OCCHCH<sub>2</sub>), 41.98 (CH<sub>2</sub>), 37.21 (CH<sub>2</sub>), 32.28 (CH<sub>2</sub>), 30.27 (CH<sub>2</sub>), 29.99 (CH<sub>2</sub>), 29.88 (CH<sub>2</sub>), 29.71 (CH<sub>2</sub>), 26.90 (CH<sub>2</sub>), 23.04 (CH<sub>2</sub>), 14.44 (CH<sub>2</sub>CH<sub>3</sub>), 14.35 (CH<sub>2</sub>CH<sub>3</sub>) ppm.

**Dodecenylsuccinic anhydride (71).**

Purchased from Aldrich Co. (90 % pure).



**Dodecylsuccinic acid (72).** Based on a procedure by Barry.<sup>36</sup> To a stirred solution of 5% aqueous potassium hydroxide (9.0 mL) at 25 °C was added dodecylsuccinic anhydride (71) (0.30 g,

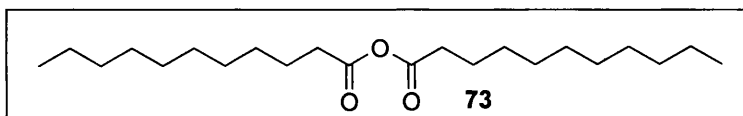


1.13 mmol). The solution was heated at 45 °C and stirring continued at 45 °C for 1 hr. The progress of the reaction was monitored by thin-layer chromatographic analysis (thin-layer chromatography was developed by  $\text{KMnO}_4$  charring). The solution was transferred to a separating funnel and extracted with diethyl ether (2 x 4 mL). The combined organic layers were acidified to pH 1 by the addition of 1M aqueous hydrochloric acid (6.0 mL). The acidified solution was transferred to a separating funnel and extracted with diethyl ether (2 x 4 mL). The combined organic layers were dried over anhydrous magnesium sulfate and filtered through a fluted filter paper. The filtrate was evaporated to give **72** (0.23 g, 72%) as white prisms: mp 119-120 °C, lit<sup>36</sup> 118-120 °C;  $R_F$  [methanol-chloroform, 1-49, (v,v)] 0.24; IR  $\nu_{\text{max}}$  (film) 1750 (C=O acid), 1711 (C=O acid)  $\text{cm}^{-1}$ ;  $^1\text{H}$  NMR (300 MHz,  $\text{CDCl}_3$ )  $\delta_{\text{H}}$  2.72 (2H, m,  $\text{OCCH}_2$ ), 2.69 (1H, dd,  $J$  16 and 10 Hz,  $\text{CH}_3\text{CH}_2\text{CO}$ ), 1.57 (2H, m,  $\text{OCCHCH}_2$ ), 1.19 (20H, s,  $\text{CH}_2(\text{CH}_2)_{10}$ ), 0.89 (3H, m,  $\text{CH}_2\text{CH}_3$ ) ppm;  $^{13}\text{C}$  NMR (75 MHz,  $\text{CDCl}_3$ )  $\delta_{\text{C}}$  179.90 (C=O), 174.16 (C=O), 59.67 ( $\text{OCCH}_2$ ), 40.36 ( $\text{OCCH}$ ), 40.06 ( $\text{OCCHCH}_2$ ), 34.80 ( $\text{CH}_2$ ), 30.93 ( $\text{CH}_2$ ), 30.65 ( $\text{CH}_2$ ), 28.66 ( $\text{CH}_2$ ), 28.57 ( $\text{CH}_2$ ), 28.55 ( $\text{CH}_2$ ), 28.40 ( $\text{CH}_2$ ), 25.85 ( $\text{CH}_2$ ), 24.17 ( $\text{CH}_2$ ), 14.08 ( $\text{CH}_2\text{CH}_3$ ), 13.13 ( $\text{CH}_2\text{CH}_3$ ) ppm.

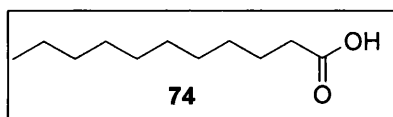


**Lauric anhydride**

(73). Purchased from Aldrich Co. (98 % pure).

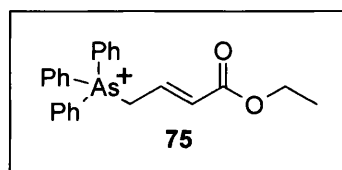


**Lauric acid (74).** Purchased from Aldrich Co. (98 % pure).



**(E)-4-(Triphenyl- $\gamma^5$ -arsanyl)-but-2-enoic acid ethyl ester (75).** Based on a procedure by Huang.<sup>37</sup>

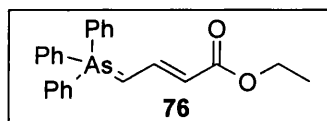
To a stirred solution of triphenylarsine (3.0 g, 9.80 mmol) in benzene (1.6 mL) at 25 °C was added



ethyl 4-bromocrotonate (1.79 mL, 0.013 mol) dropwise by means of a stainless steel needle. The mixture was heated at reflux 80 °C and stirring was continued at 80 °C for 2 h. The progress of the reaction was monitored by thin-layer chromatographic analysis (thin-layer chromatography was developed by  $\text{KMnO}_4$  charring). The solution was left to stand for 168 h at 25 °C and the solid formed was filtered with a sintered glass funnel. The solid was purified by recrystallisation with ethyl acetate to give **75** (4.04 g, 83%) as pale white leaflets: mp 151-152 °C, lit<sup>37</sup> mp 151-152 °C;  $R_F$  [ethyl acetate-light petroleum ether, 1-4, (v,v)] 0.67; IR  $\nu_{\text{max}}$  (film) 3040 (C-H aromatic stretch), 1742 (C=O conjugated ester)  $\text{cm}^{-1}$ ;  $^1\text{H}$  NMR (300 MHz,  $\text{CDCl}_3$ )  $\delta_H$  7.83 – 7.52 (15H, m, 5 x Ar-H), 6.84 (1H, m,  $\text{CH}_2\text{CH}=\text{CH}$ ), 6.41 (1H, d,  $J$  16 Hz,  $\text{CH}_2\text{CH}=\text{CH}$ ), 5.29 (2H, d,  $J$  8.5 Hz,  $\text{CH}_2\text{CH}=\text{CH}$ ), 4.20 (2H, q,  $J$  7.5 Hz,  $\text{OCH}_2$ ), 1.21 (3H, t,  $J$  7.5 Hz,  $\text{OCH}_2\text{CH}_3$ ) ppm;  $^{13}\text{C}$  NMR (75 MHz,  $\text{CDCl}_3$ )  $\delta_C$  165.40 (C=O), 134.73 (Ar-As), 133.85 (Ar-H), 131.35 (Ar-H), 130.70 (Ar-H), 128.71 ( $\text{CH}_2\text{CH}=\text{CH}$ ), 120.90 ( $\text{CH}_2\text{CH}=\text{CH}$ ), 61.18 ( $\text{OCH}_2$ ), 30.14 ( $\text{CH}_2\text{CH}=\text{CH}$ ), 14.51 ( $\text{OCH}_2\text{CH}_3$ ) ppm.

**(E)-4-(Triphenyl- $\gamma^5$ -arsanylidene)-but-2-enoic acid ethyl ester (76).** Based on a procedure by Huang.<sup>37</sup>

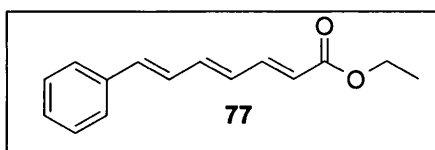
A solution of sodium ethoxide (0.27 g, 4.01 mmol in



1.85 mL of ethanol) was evaporated and a solution of (*E*)-4-(triphenyl- $\gamma^5$ -arsanyl)-but-2-enoic acid ethyl ester (**75**) (2.00 g, 4.01 mmol) in ether (11.36 mL) was added at 0 °C. The mixture was warmed to 25 °C and stirring continued at 25 °C for 30 min. The progress of the reaction was monitored by thin-layer chromatographic analysis (thin-layer chromatography was developed by KMnO<sub>4</sub> charring). The precipitate was filtered through a fluted filter paper and washed with ice-cold water (0 °C, 3 x 3 mL) until a neutral pH was obtained to give **76** (1.16 g, 69%) as pale orange leaflets: mp 130-131 °C, lit<sup>37</sup> mp 131-133 °C, R<sub>F</sub> [ethyl acetate-light petroleum ether, 1-5, (v,v)] 0.45; IR  $\nu_{\max}$  (film) 3020 (C-H aromatic stretching), 1731 (C=O conjugated ester), 1248 (C=C conjugated) cm<sup>-1</sup>; <sup>1</sup>H NMR (300 MHz, CDCl<sub>3</sub>)  $\delta_{\text{H}}$  7.80 – 7.10 (18H, m, aryl and vinylic), 7.23 (2H, d, *J* 17 Hz, CHCO), 4.08 (2H, m, OCH<sub>2</sub>CH<sub>3</sub>), 1.12 (3H, t, *J* 6.5, OCH<sub>2</sub>CH<sub>3</sub>) ppm; <sup>13</sup>C NMR (75 MHz, CDCl<sub>3</sub>)  $\delta_{\text{C}}$  163.34 (C=O ester), 139.98 (Ar-As), 134.10 (Ar-H), 133.13 (Ar-H), 132.69 (Ar-H), 130.26 (=CHCH=CHCO), 129.04 (=CHCH=CHCO), 128.85 (=CHCH=CHCO), 61.05 (OCH<sub>2</sub>), 14.58 (OCH<sub>2</sub>CH<sub>3</sub>) ppm.

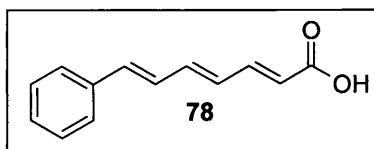
**(2*E*,4*E*,6*E*)-7-Phenylhepta-2,4,6-trienoic acid ethyl ester (**77**).**

Based on a procedure by Huang.<sup>37</sup> To a stirred solution of (*E*)-4-(triphenyl- $\gamma^5$ -arsanylidene)-but-2-enoic acid ethyl ester (**76**) (0.70 g, 1.67 mmol) in diethyl ether (6.3 mL) at 25 °C was added *trans*-cinnamaldehyde (0.21 mL, 1.67 mmol) dropwise, by means of a stainless steel needle. Stirring continued at 25 °C for 4 h. The progress of the reaction was monitored by thin-layer chromatographic analysis (thin-layer chromatography was developed by KMnO<sub>4</sub> charring). The precipitate was filtered with a sintered glass funnel and partially dissolved with diethyl ether (3 x 5 mL). The combined diethyl ether layers were filtered through a fluted filter paper. The filtrate was evaporated to give a solid which was purified by recrystallisation from ethanol to give **77** (0.27 g, 71%) as pale yellow crystals: mp 90-91 °C, lit<sup>37</sup> mp 90-92 °C, R<sub>F</sub> [ethyl acetate-light petroleum ether, 1-4, (v,v)] 0.45; IR  $\nu_{\max}$  (film) 3020 (C-H aromatic stretch), 1739 (C=O conjugated ester), 1212 (C=C conjugated) cm<sup>-1</sup>; <sup>1</sup>H NMR (300 MHz, CDCl<sub>3</sub>)  $\delta_{\text{H}}$  7.67 (5H, m, 5 x Ar-H), 6.98 (1H, m, Ar-CH=CH), 6.82 (1H, m, Ar-CH=CHCH), 6.78 (1H, m, Ar-CH=CHCH=CH),



6.60 (Ar-CH=CHCH=CHCH), 6.29 (1H, t,  $J$  4.9, Ar-CH=CHCH=CHCH=CH), 6.04 (1H, m, =CHCO), 4.31 (2H, q,  $J$  7.0 Hz, OCH<sub>2</sub>), 1.32 (3H, t,  $J$  7.0 Hz, OCH<sub>2</sub>CH<sub>3</sub>) ppm; <sup>13</sup>C NMR (75 MHz, CDCl<sub>3</sub>)  $\delta_c$  167.50 (C=O ester), 141.19 (Ar-CH=), 137.73 (Ar-H), 137.09 (Ar-H), 136.99 (Ar-H), 129.18 (Ar-CH=), 128.83 (=CHCO), 128.40 (Ar-CH=CH), 127.43 (Ar-CH=CHCH), 124.11 (Ar-CH=CHCH=CH), 117.50 (Ar-CH=CHCH=CHCH=), 60.66 (OCH<sub>2</sub>), 14.78 (OCH<sub>2</sub>CH<sub>3</sub>) ppm.

**(2E,4E,6E)-7-Phenylhepta-2,4,6-trienoic acid (78).** To a stirred solution of (2E,4E,6E)-7-phenylhepta-2,4,6-trienoic acid ethyl ester (77)



(0.40 g, 1.75 mmol) in tetrahydrofuran (3.0 mL) and water (3.0 mL) was added lithium hydroxide (0.19 g, 7.88 mmol). The mixture was heated at 40 °C and stirring continued at 40 °C for 5 h. The progress of the reaction was monitored by thin-layer chromatographic analysis (thin-layer chromatography was developed by KMnO<sub>4</sub> charring). The mixture was transferred to a separating funnel. The aqueous layer was washed with diethyl ether (3 x 10 mL). The aqueous layer was then acidified with 10% hydrochloric acid (2.6 mL) to pH 2, and the acidified solution was transferred to a separating funnel. The aqueous layer was then extracted with diethyl ether (3 x 10 mL). The combined organic layers were dried over anhydrous magnesium sulfate. The solution was filtered through a fluted filter paper and the filtrate evaporated to give **78** (0.27 g, 77%) as pale yellow needles: mp 190-191 °C, lit<sup>38</sup> mp 191 °C,  $R_F$  [methanol-chloroform, 1-19, (v,v)] 0.25; IR  $\nu_{max}$  (film) 3010 (C-H aromatic stretch), 1690 (C=O conjugated acid), 1356 (C=C conjugated) cm<sup>-1</sup>; <sup>1</sup>H NMR (300 MHz, CDCl<sub>3</sub>)  $\delta_H$  7.60 – 7.15 (6H, CH=CHCO and 5 Aryl-H) 6.90 – 6.60 (3H, m, vinylic), 6.39 (1H, m, vinylic), 5.85 (1H, d,  $J$  16 Hz, CH=CHCO), 1.20 (1H, bs, OH) ppm; <sup>13</sup>C NMR (75 MHz, CDCl<sub>3</sub>)  $\delta_c$  172.13 (C=O acid), 147.09 (Ar-CH=), 142.34 (Ar-H), 137.86 (Ar-H), 136.89 (Ar-H), 130.34 (Ar-CH=), 129.19 (=CHCO), 128.99 (Ar-CH=CH), 128.24 (Ar-CH=CHCH=CH), 127.30 (Ar-CH=CHCH=CH), 120.10 (Ar-CH=CHCH=CHCH=) ppm.

## 6.2 *In vitro* [ $^3\text{H}$ ]-labelled prenyl-protein transferase enzyme inhibition assay methodology<sup>39</sup>

Recombinant human farnesyl-protein transferase and geranylgeranyl-protein transferase I were a generous gift from Dr. M. Seabra (Imperial College of Science, Technology and Medicine, London, UK). Stock solutions of each inhibitor were prepared in dimethyl sulfoxide (DMSO; Sigma) at one hundred times the desired final assay concentrations. Working solutions were prepared by diluting stock solutions (1:20) in prenyl-protein transferase assay buffer (PFT buffer; 50 mM Tris-HCl; 20  $\mu\text{M}$   $\text{ZnCl}_2$ ; 20 mM KCl; 5 mM dithiothreitol (DTT); 0.2% (w/v) *n*-octyl- $\beta$ -D-glucopyranoside (sigma), pH 7.5). Cofactor/substrate solutions were prepared in sufficient quantity for 20 assays by mixing 19  $\mu\text{L}$  of 13  $\mu\text{M}$  [ $^3\text{H}$ ]FPP or 4  $\mu\text{L}$  of 60  $\mu\text{M}$  [ $^3\text{H}$ ]GGPP, 2.5  $\mu\text{L}$  of 1M  $\text{MgCl}_2$ , 100  $\mu\text{L}$  of double strength PFT buffer, and double-distilled, deionised water to a final volume of 200  $\mu\text{L}$ . The standard reaction mixture (25  $\mu\text{L}$ ) contained the following components in silanised 2 mL microcentrifuge tubes (Anachem Ltd., Bedfordshire, UK): 7.5  $\mu\text{M}$  of wild-type (*rh*) H-Ras or CVLL peptide in 5  $\mu\text{L}$  of PFT buffer; 0.5  $\mu\text{M}$  of [ $^3\text{H}$ ] FPP or [ $^3\text{H}$ ] GGPP in 10  $\mu\text{L}$  pf cofactor/substrate solution; 5  $\mu\text{L}$  of inhibitor at five times the desired final concentration in PFT buffer/5% (v/v) DMSO. Reactions were initiated by the addition of 0.5 pmol FPTase or GGPTase-I in 5  $\mu\text{L}$  of PFT buffer, mixed by vortex for 10 seconds, and incubated in a 37 °C water bath for 60 min. The reactions were then quenched by the addition of 0.5 mL 4% (w/v) sodium dodecyl sulfate (SDS), and proteins precipitated with 0.5 mL of 30% (w/v) trichloroacetic acid (TCA). After mixing by vortex for 30 seconds, tubes were incubated upright and undisturbed for 15 min at room temperature. 1.5 mL of 6% (w/v) TCA/2% (w/v) SDS was added to each tube and the mixture filtered onto 25 mm-diameter glass-fibre filter discs (Type APFC; Millipore (UK) Ltd, Hertfordshire, UK), using a vacuum filtration manifold (Millipore). Filters were washed with 1.5 mL 6% (w/v) TCA/2% (w/v) SDS, tubes rinsed twice with the same buffer and the residues passed over the same filters. Each filter was then washed five times with 6% (w/v) TCA, dried, transferred to 20 mL polyethylene scintillation vials (Canberra-Packard LTd., Berkshire, UK) and after addition of 10 mL Hionic-Fluor scintillant (Canberra-Packard), counted by liquid scintillation counting. The amount of [ $^3\text{H}$ ] FPP or [ $^3\text{H}$ ] GGPP transferred to native or chimaeric H-Ras, respectively, for each concentration of inhibitor was expressed as a

proportion of control incubations without inhibitor. Each value represented a single incubation, except for control values (taken as 100%) which were the mean of three determinations. A blank value, determined in a parallel reaction not containing substrate, was subtracted from each measurement.

The quantities of reagents needed to conduct both FPTase and GGPTase enzyme inhibition assays are shown below:

#### FPTase assay

x100 stock dilutions in DMSO		x5 working dilutions in PFT/5% DMSO		Final [ ] Reaction Volume 25µl	
100 mM		5 mM		1 mM	
10 mM		500 µM		100 µM	
1 mM		50 µM		10 µM	
100 µM		5 µM		1 µM	
Substrate					
rh-H-Ras		Source	Stock [ ]	Dilution	Reaction Constituents
WT		PanVera	40µg/8µl	1:8 (8+56)	5µl 3.5µg 7µM
[ <sup>3</sup> H]-Farnesylpyrophosphate					
Source		Specific Radioactivity	Diluent		Reaction Constituents
Amersham		7.4kBq/µl	[ <sup>3</sup> H]FPP 20µl 1M MgCl <sub>2</sub> 2.5µl x2 PFT 100µl dH <sub>2</sub> O 77.5µl		10µl 0.5µM cpm
Farnesyltransferase Enzyme					
Source			Stock [ ]	Dilution	Reaction Constituents
rh FTase (Miguel Seabra)			0.5µg/0.25µl	1:250 (0.25 +62.8µl )	5µl 42ng 0.5pmol

**Table 1** The quantities of the various reagents necessary for a FPTase enzyme inhibition assay

The PFT solution in which the potential inhibitors, the substrate and prenyl-protein transferase enzyme are diluted with is comprised of the following:

<b>X1 PFT</b>	5 mL
<b>X5 PFT</b>	1000 $\mu$ L
<b>Distilled H<sub>2</sub>O</b>	3,975 $\mu$ L
<b>1M DTT</b>	25 $\mu$ L

**Table 2** The composition X1 PFT stock buffer solution

The X5 PFT stock solution (30 mL) consists of:

<b>X5 PFT stock</b>	20 mL
1M Tris-HCl pH 7.5	5 mL
100 mM ZnCl <sub>2</sub>	20 $\mu$ L
1M KCl	2 mL
10% (w/v) <i>n</i> -octyl- $\beta$ -D-glucopyranoside	2 mL
Distilled H <sub>2</sub> O	20 mL

**Table 3** Constituents of X5 PFT stock buffer solution

All of the above quantities for X1 and X5 PFT solutions are exactly the same for the GGPTase enzyme inhibition assay.

### GGPTase assay

x100 stock dilutions in DMSO		x5 working dilutions in PFT/5% DMSO		Final [    ] Reaction Volume 25µl
100 mM		5 mM		1 mM
10 mM		500 µM		100 µM
1 mM		50 µM		10 µM
100 µM		5 µM		1 µM
Substrate				
rh-H-Ras	Source	Stock [    ]	Dilution in PFT	Reaction Constituents
CVLL	PanVera	50 µg/16 µl	1:4 (16+ 48 µl)	5µl 3.9 µg 7.8 µM
<sup>[3]H</sup> -Geranylgeranylpyrophosphate				
Source	Specific Radioactivity	Diluent		Reaction Constituents
Amersham	7.4 kBq/µl	<sup>[3]H</sup> -GGPP 8 µl 1M MgCl <sub>2</sub> 2.5 µl x2 PFT 100 µl dH <sub>2</sub> O 89.5µl		10 µl 0.5 µM cpm
Geranylgeranyltransferase I Enzyme				
Source		Stock [    ]	Dilution in PFT	Reaction Constituents
rhGGTase I (Miguel Seabra)		0.25 µg/0.2 µl	1:300 (0.2+ 59.8 µl)	5 µl 17 ng 0.2 pmol

**Table 4** The quantities of the various reagents necessary for a GGPTase enzyme inhibition assay

### **6.3 *In vitro* [<sup>3</sup>H]acetyl-labelled HDAC assay methodology<sup>40</sup>**

The total cellular extract was prepared from T-47D breast cancer cell line. At 4 °C,  $\sim 2.5 \times 10^6$  cells were washed with DPBS, and suspended in 200  $\mu$ L of lysis buffer, which consists of NaCl (120 mM), Tris (50 mM, 7.5 pH) EDTA (5 mM) and NP40 (0.5% (v/v)). Also present in the lysis buffer are protease inhibitors [apoptinin (2  $\mu$ g/mL), chymostatin (10  $\mu$ g/mL) leupeptin (1  $\mu$ g/mL), pepstatin A (1  $\mu$ g/mL) and PMSF (0.5 mM). After a brief sonification, total cell lysates were cleared by two series of centrifugation ( $\times$  15,000 rpm for 10 minutes), and the supernatants were stored at  $-80$  °C. Then 20  $\mu$ L of cell extract ( $\sim 2.5 \times 10^5$  cells), in the presence of varying concentrations of TSA and other potential HDAC inhibitors in 0.1% (v/v) ethanol or 0.1% (v/v) ethanol as a control, were incubated for 60 minutes at 25 °C with 1  $\mu$ L of [<sup>3</sup>H]acetyl-labelled histone H4 peptide substrate (NH<sub>2</sub>-terminal residues 2-20) that had been acetylated with [<sup>3</sup>H]acetic acid, sodium salt (3.7 GBq/mmol). Each reaction (200  $\mu$ L) was quenched by the addition of 1M HCl/0.16 M acetic acid (50  $\mu$ L) and extracted with ethyl acetate (600  $\mu$ L), and released [<sup>3</sup>H]acetate was quantified by scintillation counting.

### **6.4 *Methodology for using a non-isotopic enzyme activity assay (HPLC)*<sup>12</sup>**

Histone deacetylase (HDAC) was isolated from rat liver. The supernatant obtained from the high-speed centrifugation of the rat liver homogenates was purified on a Q-Sepharose column using a sodium chloride gradient (10 – 500 mM), with a Tris (15 mM), EDTA (0.25 mM) and glycerol (10%) buffer at pH 7.9. The fractions containing HDAC activity were collated and stored at  $-40$  °C. The assay buffer contained Tris-HCl (10 mM), NaCl (10 mM), MgCl<sub>2</sub> (15 mM), EDTA (0.1 mM), 10% (v/v) glycerol and mercaptoethanol (0.007%). HDAC inhibitors were made up in Hepes buffer (50 mM, pH 7.4). The substrate MAL, was diluted with Hepes buffer to a concentration of 5  $\mu$ g/mL. Stock solutions of each HDAC inhibitor were prepared by dissolving the compounds in Hepes (50 mM) at a concentration of 1 mg/mL. Further serial dilution with Hepes buffer achieved the desired concentrations for each

compound. TSA (1 mg/mL) was dissolved in ethanol before diluting with Hepes buffer owing to the reduced solubility of TSA in Hepes buffer.

HDAC activity was determined from a solution of purified HDAC (100  $\mu$ L), 5  $\mu$ g/mL MAL (100  $\mu$ L), inhibitor (100  $\mu$ L) and Hepes assay buffer (100  $\mu$ L). This mixture was incubated for 60 minutes at 37 °C. The enzymatic reaction was quenched by the addition of acetonitrile (100  $\mu$ L), the mixtures centrifuged ( $\times$  10,000 rpm/ 10 min) and then placed on ice until HPLC analysis could be performed. The chromatographic separation of MAL and ML was performed on a 15 cm Apex ODS 5 $\mu$  column, with an acetonitrile/distilled H<sub>2</sub>O (40:60), 2% TFA (v/v) mobile phase at a flow rate of 1.2 mL per minute. MAL and ML were quantitated by fluorescence detection at excitation/emission wavelengths of 330/395 nm respectively.

## **6.5 Methodology for sulforhodamine B cell proliferation assay<sup>40</sup>**

Stock solutions of breast cancer cell lines MDA MB231, and T47D (American Type Culture, Rockville, MD, USA) were grown in 75 cm<sup>2</sup> flasks (Becton-Dickinson, Lincoln Park, NJ, USA) in Dulbecco's Eagle's Medium (DMEM) containing 10% (v/v) foetal calf serum (FCS), 2 mM L-glutamine, 100 units/mL penicillin and 100  $\mu$ g/mL streptomycin. Flasks were incubated at 37 °C in 5% CO<sub>2</sub> atmosphere. Cells were counted in a haemocytometer after detachment using 0.25% (w/v) trypsin in Dulbecco's Phosphate Buffered Saline (DPBS) without Ca<sup>2+</sup> or Mg<sup>2+</sup> (Sigma) containing 0.02% (w/v) EDTA. Viability was determined by Trypan blue exclusion. For each cell line, cells were seeded in 96-well microtitre plates at optimal densities determined in prior experiments to ensure exponential growth for the duration of the assay. After a 24 h pre-incubation, growth medium was replaced with experimental medium containing test compound at final concentrations ranging from 10<sup>-8</sup> M to 10<sup>-4</sup> M in half-log dilutions and 0.05% (v/v) DMSO, or growth medium containing 0.05% (v/v) DMSO as a control. After 48 hr incubation, cells were fixed by gently layering 100  $\mu$ L of ice-cold 50% (w/v) TCA on the surface of the culture medium in each well and incubated at 4 °C for 60 min. After washing in tap water for 5 min, 100  $\mu$ L of 0.4% (w/v) sulforhodamine B (Sigma) in 1% (v/v) acetic acid was added to each well and plates were incubated at room temperature for 30 min. Plates were then air-dried



overnight before bound dye was solubilised with 100  $\mu$ L 10 mM Tris base for 15 min on a gyratory shaker. Absorbance at 492 nm for each well was measured on a microtitre plate reader.

---

## 6.6 References

- 1] Mordini, A.; Pecchi, S.; Caozzi, G.; Capperucci, A. *J. Org. Chem.*, **1994**, *59*, 4784
- 2] Buchecker, R.; Marti, U.; Eugster, C. H. *Helv. Chim. Acta.*, **1982**, *3*, 896
- 3] Wang, Q.; Fan, S. Y.; Wong, H. N. C.; Li, Z.; Fung, B. M. *Tetrahedron*, **1993**, *49*, 619
- 4] Fujita, T.; Nakayama, M. *Phytochemistry*, **1993**, *6*, 1545
- 5] Sen, S. E.; Roach, S. L. *Synthesis*, **1995**, 756
- 6] Baird, M. S.; Nethercott, W.; Slowey, P. D. *J. Chem. Res. Miniprint*, **1985**, *12*, 3815
- 7] Braude, E. *J. Chem. Soc.*, **1995**, *45*, 3334
- 8] Arnold, L. *J. Chem. Soc.*, **1953**, *75*, 5396
- 9] Hayashi, M.; Terashima, S.; Koga, K. *Tetrahedron*, **1981**, *16*, 2797
- 10] Suemune, H.; Iwasaki, G.; Ueno, K.; Sakai, K. *Chem. Pharm. Bull. Japan*, **1984**, *32*, 4632
- 11] Barnier, J-P.; Morrisson, V.; Volle, I.; Blanco, L. *Tetrahedron Asymm.*, **1999**, *10*, 1107
- 12] Hoffmann, K.; Brosch, G.; Loidl, P.; Jung, M. *Nuc. Acids Research*, **1999**, *27*, 2058
- 13] Bortolussi, M.; Seydenpenne, J. *Synth. Commun.*, **1989**, *19*, 2355
- 14] Mehta, G. *Indian J. Chem.*, **1969**, *7*, 835
- 15] Knoevenagel, E. *J. Prakt. Chem.*, **1918**, 331
- 16] Cappon, J. J.; Boart, J.; Walle, G. A. M.; Lugtenburg, J. *Recl. Trav. Chim. Pays-Bas.*, **1991**, *5*, 158
- 17] Bredenkamp, M. W.; Lesch, J. S.; Malherbe, J. J.; Molnar, E. M.; Schneider, D. F. *Tetrahedron Lett.*, **1980**, *21*, 4199
- 18] Boyle, P. H. *J. Chem. Soc., Perkin Trans. 1*, **1972**, 1617
- 19] Singh, A. K.; Das, J.; Majumder, N. *J. Am. Chem. Soc.*, **1996**, *26*, 6185
- 20] Hirata, X.; Nakata, H.; Yamada, K.; Okuhara, K.; Naito, T. *Chem. Abstr.*, **1961**, *79*, 6461
- 21] El-Ezbawy, S. R.; Abdel-Wahab, A. A. *Phosphorous, Sulfur, Silicon, Relat. Elem.*, **1989**, *44*, 285
- 22] Brunner, H.; Schmidt, P. *Eur. J. Org. Chem.*, **2000**, *11*, 2119
- 23] Gouriay, R. I.; Kirby, G. W. *J. Chem. Res. Miniprint*, **1997**, *5*, 1001

- 24] Staudinger, S. *Chem. Ber.*, **1923**, 56, 710
- 25] Steinberg, B. *J. Org. Chem.*, **1956**, 21, 660
- 26] Doulut, S.; Dubuc, I.; Rodriguez, M.; Vecchini, F.; Fulorand, H. *J. Med. Chem.*, **1993**, 10, 1369
- 27] *Justus Liebigs Ann. Chem.*, **1929**, 81
- 28] Gallagher, M. J.; Sutherland, M. D. *Aust. J. Chem.*, **1960**, 13, 367
- 29] West, A.; *J. Chem. Soc.*, **1941**, 140
- 30] Schvartzapel, A. J.; Zhang, L.; Docampo, R.; Rodriguez, J. B.; Gros, E. G. *J. Med. Chem.*, **1997**, 40, 2314
- 31] Djahanbini, D.; Cazes, B.; Gore, J. *Tetrahedron*, **1984**, 19, 3645
- 32] Schmid, M.; Gerber, F.; Hirth, G. *Helv. Chim. Acta.*, **1982**, 684
- 33] Grossi, V.; Rontani, J-F. *Tetrahedron Lett.*, **1995**, 18, 3141
- 34] Rowland, R.; *J. Am. Chem. Soc.*, **1957**, 79, 5007
- 35] Nargund, K. S.; Prasad, K.; Thakur, M. M. *J. Indian. Chem. Soc.*, **1978**, LV, 497
- 36] Barry, T. *Chem. Abstr.*, **1947**, 51B, 4454
- 37] Huang, Y.; Yanchang, S.; Zheng, J.; Zhang, S. *Synthesis*, **1985**, 1, 57
- 38] Meisters, W. *Austr. J. Chem.*, **1966**, 19, 1215
- 39] Reiss, Y.; Seabra, M. C.; Goldstein, J. L.; Brawn, M. S. in 'Methods', **1991**, San Diego, 1, 241
- 40] Vigushin, D. M.; Ali, S.; Pace, P. E.; Mirsaidi, N.; Ito, K.; Adcock, I.; Coombes, R. C. *Clin. Cancer Res.*, **2001**, 7, 971

